

**Modulating the eIF4E–eIF4G Protein–Protein Interaction in Human Disease**

by

Erin E. Gallagher

A dissertation submitted in partial fulfillment  
of the requirements for the degree of  
Doctor of Philosophy  
(Medicinal Chemistry)  
in the University of Michigan  
2019

Doctoral Committee:

Assistant Professor Amanda Garner  
Professor Scott Larsen  
Professor Henry Mosberg  
Professor Nouri Neamati

Erin E. Gallagher

[eribeth@med.umich.edu](mailto:eribeth@med.umich.edu)

ORCID ID: 0000-0002-6020-9418

© Erin E. Gallagher 2019

## **Acknowledgments**

I would like to thank my advisor, Dr. Amanda Garner for all her help throughout the years. I also am indebted to Arya Menon, who tirelessly performed many cell assays for me without (much) complaint, and to Dr. Lauren Mishra, who trained me when I was new to chemistry. I must also thank Dr. Tanpreet Kaur, who was always happy to discuss any problem I might encounter and provide assistance wherever she could. I also acknowledge Dr. James Song, who worked closely with me throughout the years. Additionally, Kirsten Deprey and the Kritzer lab have been very helpful by running the cell penetration assay.

I also must thank my friends at the University of Michigan who made the last five years at worst bearable and at best fun. I am missing many of you already, and I am sad to leave everyone else behind. I would not have made it this far without the Saturday football games, drinks at Grotto, or days spent on the river.

I owe my parents a lot of gratitude for listening to me ramble on about research, sympathizing when things weren't going well, and offering to help in any way they could. Even when you couldn't help, I still appreciated the offer.

Finally, I must thank Brandt for his friendship and relative sanity throughout the years. I am excited for the next steps in life, and I'm glad I don't have to take them alone.

## Table of Contents

ACKNOWLEDGMENTS .....	ii
LIST OF TABLES .....	v
LIST OF FIGURES .....	vii
LIST OF APPENDICES .....	x
LIST OF ACRONYMS .....	xi
ABSTRACT .....	xiii
CHAPTER	
<b>1. Cap-Dependent Translation and its Relevance to Disease .....</b>	<b>1</b>
1.1 The PI3K pathway and its relation to cancer .....	1
1.2 Efforts at targeting mTORC1 .....	4
1.3 Cap-dependent translation and its relation to cancer .....	5
1.4 Efforts at targeting cap-dependent translation .....	8
1.5 Research objective .....	10
<b>2. An Investigation into the Binding Mechanism of 4E-BP and eIF4G Peptides</b> .....	<b>11</b>
2.1 Intrinsically disordered proteins, their role in signaling pathways, and their potential as drug targets .....	11
2.2 Helical propensity and inhibitory potential of 4E-BP1 and eIF4G peptides .....	17

2.3 Kinetic analysis of 4E-BP1 and eIF4G peptides .....	20
2.4 Consideration of binding mechanism in designing IDP mimetics.....	25
2.5 Cell penetration and activity of HCS peptides.....	28
2.6 Conclusions .....	30
2.7 Materials and methods .....	31
<b>3. Designing a Stapled Peptide to Probe the eIF4E–eIF4G PPI .....</b>	<b>39</b>
3.1 Stapled peptides.....	39
3.2 Structure activity relationships of linear 4E-BP1 and eIF4G peptides.	42
3.3 Structure activity relationships of stapled 4E-BP1 peptides.....	45
3.4 Kinetic analysis of 4E-BP1 stapled peptides.....	52
3.5 Cell activity of 4E-BP1 stapled peptides .....	54
3.6 Cell penetration of lactam stapled peptides .....	55
3.7 Conclusions .....	58
3.8 Materials and methods .....	60
<b>4. Future Directions.....</b>	<b>63</b>
4.1 Additional structural modifications for lactam stapled peptides.....	63
4.2 Pharmacokinetic studies of lactam stapled peptides .....	66
4.3 Pulldown experiments with stapled peptides .....	67
4.4 Relationship between staple type and cell penetration.....	70
4.5 Development of a functionalized staple .....	72
4.6 Conclusions .....	74
APPENDICES .....	76
REFERENCES.....	152

## List of Tables

Table 2.1 – Sequences, IC <sub>50</sub> s, and helicities of linear peptides.....	18
Table 2.2 – Kinetic binding data for linear peptides determined by SPR.....	20
Table 2.3 – Sequences, IC <sub>50</sub> s, and helicities of 4E-BP1 and eIF4G stapled peptides .....	26
Table 2.4 – Kinetic binding data for stapled peptides determined by SPR.....	28
Table 3.1 – Series of linear 4E-BP1 based peptides and their IC <sub>50</sub> s obtained with cat- ELCCA and their helicities determined with circular dichroism.....	42
Table 3.2 – eIF4G based peptides with IC <sub>50</sub> s determined using cat-ELCCA and helicities from circular dichroism .....	44
Table 3.3 – Series of mHCS peptides .....	48
Table 3.4 – Comparison between early (E) and late (L) isomers for certain mHCS peptides.....	49
Table 3.5 – Series of OAISer and HCS peptides.....	50
Table 3.6 – Series of lactam stapled peptides, LacA and LacB .....	52
Table 3.7 – Binding kinetics of the mHCS and OAISer peptides determined by SPR .....	53
Table 3.8 – Binding kinetics for the HCS and lactam stapled peptides .....	54
Table 4.1 – Potential replacements for the unstable cysteine and methionine residues .....	64

Table 4.2 – Potential staple positions and types for cell penetration experiments71

Table A2.1 – Kinetic binding data at a variety of temperatures for linear peptides  
determined by SPR .....85

Table A2.2 – Kinetic binding data at a variety of salt concentrations for linear peptides  
determined by SPR .....85

## List of Figures

Figure 1.1 – Signaling the eIF4E–4E-BP PPI and cap-dependent translation.....	2
Figure 1.2 – FDA approved Rapalogs for targeting certain cancers.....	5
Figure 1.3 – The 5' cap of mRNA.....	5
Figure 1.4 – The cap-dependent translation pre-initiation complex.....	6
Figure 1.5 – Reported ligands on the surface of eIF4E.....	7
Figure 1.6 – Inhibitors of eIF4E.....	9
Figure 2.1 – Overlay of 4E-BP1 and eIF4G bound to eIF4E.....	16
Figure 2.2 – Bound structure of the linear 4E-BP1 and eIF4G peptides that we intend to use for our studies.....	16
Figure 2.3 – Percent helicity of the linear 4E-BP1 and eIF4G peptides in buffer and with the helicity inducer, trifluoroethanol.....	19
Figure 2.4 – The kinetics of binding of the 4E-BP1 and eIF4G peptides in response to increasing temperature as determined by SPR.....	21
Figure 2.5 – The kinetics of binding of 4E-BP1 and eIF4G peptides in response to increasing ionic strength.....	22
Figure 2.6 – The effect of temperature and salt on the conformation of the peptides.....	24
Figure 2.7 – eIF4E CD spectra across temperatures tested in SPR.....	25



Figure 2.8 – Circular dichroism spectra for the stapled peptides in phosphate buffer and with the addition of 40% TFE .....	27
Figure 2.9 – Confocal imaging of FITC labeled peptides inside the cell .....	29
Figure 2.10 – eIF4E pulldown data for 4E-BP1 (G <sup>49</sup> -N <sup>64</sup> ) and HCS 4E-BP1 .....	29
Figure 2.11 – Typical coomassie gel of His10 eIF4E purification .....	35
Figure 3.1 – Crystal structure of the linear 4E-BP1 peptide bound to eIF4E .....	43
Figure 3.2 Aggregation of mHCS-1 visualized by dynamic light scattering .....	46
Figure 3.3 – Comparing IC <sub>50</sub> curves for linear and stapled peptides .....	47
Figure 3.4 – Comparison of IC <sub>50</sub> curves between 4E-BP1-1, mHCS-1, and HCS-1 .....	51
Figure 3.5 – Pulldown data for LacA-1 and LacB-1 in Tamoxifen resistant MCF-7 and MDA-MB-231 cells .....	55
Figure 3.6 – Concentration dependence in pulldown assay for LacB-1 in MCA-MB-231 cells .....	55
Figure 3.7 – Cell penetration of lactam stapled peptides, as determined using the CAPA assay .....	57
Figure 3.8 – Percent uptake of peptide at 0.74 μM, as determined by CAPA .....	57
Figure 4.1 – Chymotrypsin cleavage sites in LacB-1 .....	65
Figure 4.2 – The effect of peptide treatment on 4E-BP1 phosphorylation and S6K phosphorylation .....	68
Figure 4.3 – Cell viability measured by a Cell Titer Glo assay after treatment with sTIP-04, HCS 4E-BP1, and HCS 4E-BP1 LM->AA. An LDH assay indicates that sTIP-04 does not cause membrane leakage .....	70

Figure 4.4 – Unsuccessful attempts towards designing an arginine functionalized stapled peptide .....72

Figure 4.5 – Proposed scheme for the synthesis of a functionalized staple in solution .....73

Figure 4.6 – Proposed scheme for the incorporation of the solution synthesized functionalized staple into the resin-bound peptide .....73

## List of Appendices

Appendix A.....	76
IC <sub>50</sub> Curves for Peptides.....	76
CD Curves for Peptides.....	80
SPR Curves for Peptides.....	83
Appendix B.....	101
Compound Characterization.....	101
IC <sub>50</sub> Curves for Peptides.....	119
CD Curves for Peptides.....	131
SPR Curves for Peptides.....	144

## **List of Acronyms**

mTOR – mechanistic Target of Rapamycin

mTORC1 – mechanistic Target of Rapamycin Complex 1

eIF4E – eukaryotic Initiation Factor 4E

4E-BP – 4E Binding Protein

eIF4G – eukaryotic Initiation Factor 4G

PPI – Protein-Protein Interaction

CD – Circular Dichroism

SPR – Surface Plasmon Resonance

Cat ELCCA – Catalytic Enzyme Linked Click Chemistry Assay

CAPA – Chloroalkane Penetration Assay

HCS – Hydrocarbon Stapled

PI3K – Phosphoinositide 3-Kinase

EGFR – Epidermal Growth Factor Receptor

HER2 – Human Epidermal Growth Factor Receptor 2

PTEN – Phosphatase and Tensin Homolog

Akt – Protein Kinase B

TSC – Tuberous Sclerosis Protein

Rheb – Ras Homolog Enriched in Brain

S6K – Ribosomal Protein S6 Kinase Beta-1

Deptor – DEP Domain-Containing mTOR-Interacting Protein

mLST8 – Mammalian Lethal with SEC13 Protein 8

Raptor – Regulatory-Associated Protein of mTOR

PRAS40 – Proline-Rich AKT1 Substrate 1

eIF4A – eukaryotic Initiation Factor 4A

eIF4F – eukaryotic Initiation Factor 4F

ATF4 – Activating Transcription Factor 4

SREBP – Sterol Regulatory Element-Binding Protein

MAPK – Mitogen Activated Protein Kinase

Bcl-xl – B-Cell Lymphoma - Extra Large

SAR – Structure Activity Relationship

PAINS – Pan Assay Interfering Compounds

HINT – Histidine Triad Nucleotide-Binding Protein

CPP – Cell Penetrating Peptide

IDP – Intrinsically Disordered Protein

IDR – Intrinsically Disordered Regions

mHCS – mono-Hydrocarbon Stapled

TFE –Trifluoroethanol

IC<sub>50</sub> – Half Maximal Inhibitory Concentration

FITC – Fluoresceine Isothiocyanate

GnRH – Gonadotropin Releasing Hormone

HPLC – High Pressure Liquid Chromatography

## **Abstract**

Dysregulation of the mTORC1 pathway has been linked to several human diseases, particularly cancer; but attempts to target mTORC1 directly have been mostly unsuccessful due to observed drug resistance. Most mechanisms of resistance result in dysregulation of cap-dependent translation, and thus, perpetuation of a cancerous phenotype. eIF4E is a downstream effector of mTORC1 signaling and the rate-limiting factor in cap-dependent translation. Cellular eIF4E activity is regulated by the 4E-BPs, which act as gatekeepers of eIF4E by binding and sequestering the protein to prevent cap-dependent translation initiation. Hyperphosphorylation of the 4E-BPs by mTORC1 decreases their affinity for eIF4E and allows it to bind eIF4G and ultimately initiate cap-dependent translation of oncogenes, growth factors, and survival factors. The aim of this work is to develop an inhibitor of the eIF4E–eIF4G PPI using eIF4G and 4E-BP1 peptides as models.

eIF4G and 4E-BP share the same binding site on the surface of eIF4E. Both proteins are intrinsically disordered or have intrinsically disordered regions in solution but adopt a short helix upon binding to eIF4E. Peptide versions of each of the proteins which encompass the crystalized binding sites were purchased and analyzed by CD and SPR. It was found that, while both peptides share a near identical binding motif, their structures in solution and their kinetics of binding are quite different. The 4E-BP peptide is somewhat helical in solution, demonstrates little temperature dependence of

its on-rate ( $k_a$ ), off-rate ( $k_d$ ), and binding constant ( $K_D$ ), and has a slower  $k_d$  and stronger  $K_D$  with increasing ionic strength. Conversely, the eIF4G peptide is not helical in solution, has a faster  $k_d$  with increasing temperature, and a weaker  $K_D$  with increasing ionic strength. The  $k_a$  of eIF4G was faster under all circumstances than the  $k_a$  of 4E-BP, but the 4E-BP peptide had a much slower  $k_d$  and therefore a stronger  $K_D$ . Taken together, this data indicates that while eIF4G associates much more quickly with eIF4E, its binding motif is much less stable. We hypothesize that the differences are due to different binding mechanisms adopted by each peptide, in which eIF4G favors an induced fit binding mode, but 4E-BP likely adopts a combination of induced fit and conformational selection.

We next synthesized hydrocarbon stapled peptide based on the eIF4G and 4E-BP peptide sequences. While the helicity of the 4E-BP stapled peptide (HCS 4E-BP1) was much higher than the linear peptide, the eIF4G stapled peptide (HCS eIF4G) was still barely helical in solution. Additionally, the binding constant for the 4E-BP peptide improved from 26 nM to 4 nM upon stapling, whereas the binding constant for the eIF4G peptide lost activity (29 nM to 90 nM). The constraint of the staple appears to be preventing its preferred association mechanism, and its loss in affinity is entirely due to a decreased  $k_a$ . We hypothesize that this is because HCS eIF4G still favors an induced fit binding mechanism. We also analyzed linear and stapled versions of sTIP-04, an eIF4E binding stapled peptide from the literature.<sup>1</sup> This peptide is based on the eIF4G sequence, but has been mutated to favor the bound structure. Interestingly, the linear peptide behaved very similarly to the linear eIF4G peptide at different temperatures, but behaved more similarly to the linear 4E-BP peptide at different salt concentrations. The

stapled peptide, sTIP-04, behaved similarly to HCS 4E-BP1. We suspect that this sequence is able to bind through multiple mechanisms, and therefore its association rate is less penalized by the constraint of the staple.

While the hydrocarbon stapled 4E-BP peptide demonstrated excellent activity *in vitro* and in cell based assays, it still suffered from poor solubility, poor reproducibility, and a tendency to aggregate. Thus, efforts were made to construct a stapled peptide with better properties in solution. While modifications to the peptide side chains did not improve the peptides *in vitro* activity, changing the staple type from hydrocarbon to a lactam staple of similar length significantly improved solubility and behavior while maintaining activity. This new lead peptide has similar structural properties as HCS 4E-BP1 (lactam staple = 40% helical, HCS = 44% helical) and similar affinity for eIF4E (lactam staple = 2 nM, HCS = 4 nM). Additionally, the lactam stapled peptide is highly cell permeable, as demonstrated with CAPA performed by the Kritzer lab. We solved the NMR structure of this peptide in solution and found that it forms a compact structure in phosphate buffer and hypothesize that this structure is critical for cell penetration.

Future directions on this project will focus on optimizing this peptide for use as a probe for the eIF4E–eIF4G PPI. First, there are two unstable residues (methionine and cysteine) which have a tendency to oxidize. Further work will be done to replace these residues to improve the shelf life of the peptide. Next, we are currently getting information about the stability of the peptide when exposed to proteases and other metabolizing enzymes *in vitro*. This information will be used to block the most metabolically labile sites to improve the half-life of the peptide *in vivo*. We will also further investigate the effects of staple length, type, and orientation on the activity and



cell penetrability of the peptide. Finally, we will explore options for good models to use the optimized peptide to validate the eIF4E–eIF4G PPI *in vivo*.

## Chapter 1

### Cap-Dependent Translation and its Relevance to Disease

#### 1.1 The PI3K pathway and its relation to cancer

Cancerous cells increase their evolutionary advantage over healthy cells by hijacking normally innocent cell processes and manipulating them for more insidious purposes. DNA mutations, dysregulation of transcription, post transcriptional and translational modifications, and altered translation are all used to dysregulate the general order of the cell to promote excessive growth, avoid apoptosis, promote angiogenesis, and ultimately metastasize. Traditional chemotherapeutic drugs focus on targeting the excessive growth of cancer cells using DNA binding and damaging agents. However, these treatments are harmful to fast replicating healthy cells and many cancers develop resistance mechanisms, limiting the effectiveness of these treatments. This has led to the search for other targets which are dysregulated in cancer cells in hopes of finding a more effective treatment.

One such pathway which is highly mutated in cancer cells is the phosphoinositol 3-kinase (PI3K) pathway (**Figure 1.1**). The PI3K pathway is one of the few pathways in which mutations have been found in every major element over a broad range of cancers.<sup>2</sup> PI3K is activated by receptor tyrosine kinases, amplification of which leads to overactivation of PI3K and a cancerous cell phenotype. Many different receptor

tyrosine kinases are implicated in cancer through this mechanism: for example, EGFR is closely linked to non-small cell lung cancer<sup>3</sup> and HER2 to breast cancer.<sup>4</sup> *PIK3CA*, the gene which encodes the p110 $\alpha$  catalytic subunit of PI3K, is also often mutated or amplified in cancer cells, and mutations in the downstream effector Akt and loss of the negative regulator of PI3K, PTEN, have both been seen in clinical isolates. The result of any one of these aberrations is upregulation of the PI3K pathway, which leads to a cancerous phenotype.<sup>2</sup>

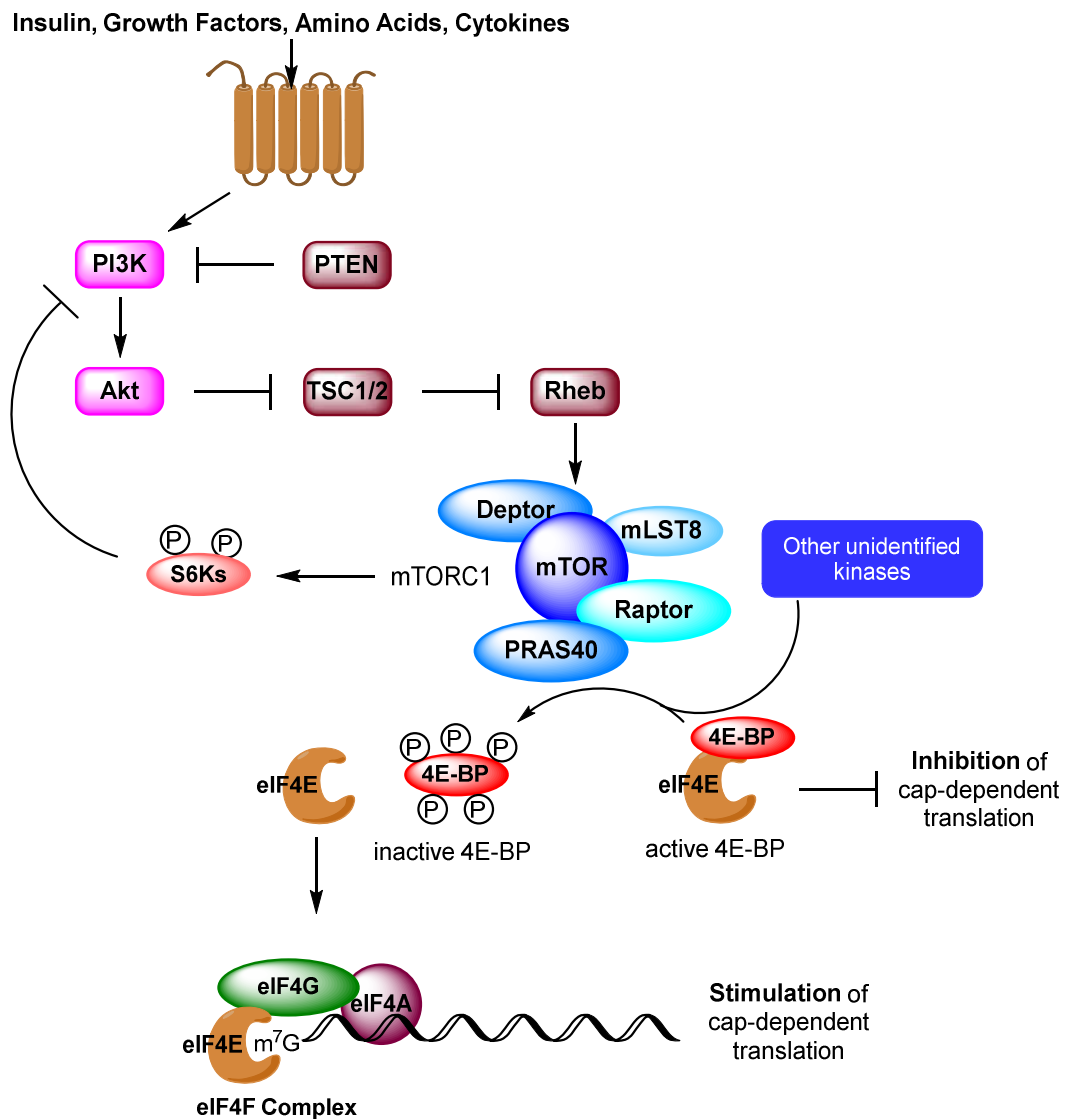


**Figure 1.1 - Signaling the eIF4E-4E-BP PPI and cap-dependent translation.**

PI3K inhibitors have been developed in an attempt to modulate this pathway. These inhibitors bind in the ATP binding site of PI3K. Pan inhibitors (such as wortmannin) of PI3K are sometimes used in life-threatening diseases in which their side effects on the glucose pathway and the immune system can be tolerated short term. Isoform specific PI3K inhibitors, some of which have recently been FDA approved<sup>5</sup>, are much more useful in the treatment of cancers in which aberrant PI3K pathways are known to exist. Currently, many isoform specific PI3K inhibitors are in clinical trials.<sup>6</sup>

### **mTORC1 is a key downstream effector in the PI3K pathway**

Activation of PI3K leads to the activation of the downstream kinase complex mTORC1. mTORC1 senses the cell environment to indicate when the cell should grow and when growth should be arrested. The presence of certain amino acids, oxygen, and growth factors all activate mTORC1 and induce cell growth, whereas lack of energy, hypoxic environments, and stress inhibit mTORC1. mTORC1 induces translation of mRNA through activation of S6K and deactivation of 4EBP1. Activation of mTORC1 also encourages metabolism through induction of nucleotide synthesis through the activation of the transcription factor ATF4 and S6K, induces lipid synthesis through the activation of transcription factor SREBP, and inhibits autophagy, lysosome biogenesis, and proteasome assembly.<sup>7</sup>

There are many mTORC1 related processes that are linked to tumorigenesis, and mTORC1 functions as a downstream effector of many frequently mutated oncogenic pathways. For instance, mutations in the PI3K/Akt pathway and the MAPK pathway both result in mTORC1 hyperactivation in many cancers.<sup>7</sup> Dysregulation of the mTORC1 pathway has been linked to several human diseases including cancer,

obesity, insulin resistance, and autism.<sup>8-10</sup> However, the most critical process linked to mTORC1's tumorigenesis is its impact on the eIF4E/4EBP pathway, which regulates cap-dependent translation.<sup>11-14</sup> This will be further discussed in section 1.4.

## 1.2 Efforts at targeting mTORC1

While attempts have been made to target mTORC1 directly using rapamycin, rapalogs, and active site inhibitors, these therapies have been mostly unsuccessful due to resistance mechanisms observed in many cancers<sup>15-23</sup> leading to overactivation of the upstream effector Akt,<sup>24-27</sup> upregulation of eIF4E,<sup>28,29</sup> or downregulation of 4E-BP.<sup>30,31</sup> The rapalogs have also been linked to a negative feedback loop, in which inhibition of mTORC1 prevents phosphorylation of S6K, leading to overstimulation of the PI3K pathway. These events result in dysregulation of cap-dependent translation, causing an overall increase in the translation of oncogenic mRNAs and a cancerous phenotype.<sup>32</sup> Two of the rapalogs, everolimus and temsirolimus shown in **Figure 1.2**, have been approved to treat some cancers, including renal cell carcinoma, but for many cancers they are ineffective, potentially due to their failure to completely inhibit phosphorylation of 4E-BP1.<sup>33</sup> Dual mTOR/PI3K inhibitors have been tried to overcome the negative feedback loop which ultimately overcomes active-site mTOR inhibitors, but concerns have been raised over their toxicity in early clinical trials. Attempts have also been made to link ATP competitive inhibitors with rapalogs in order to better fight mTOR resistance mechanisms.<sup>33</sup> Resistance to mTOR targeted drugs has been observed through mTOR-independent 4E-BP1 phosphorylation,<sup>34</sup> incomplete inhibition of 4E-BP1 phosphorylation,<sup>35</sup> downregulation of 4E-BP1 expression,<sup>30,31</sup> and amplification of

eIF4E.<sup>28,29</sup>

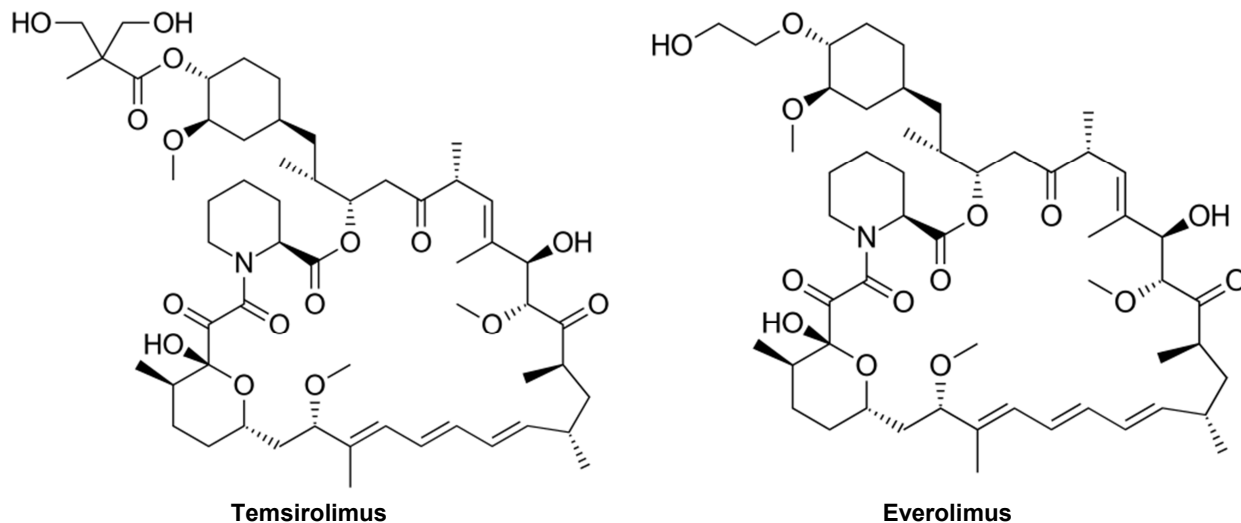
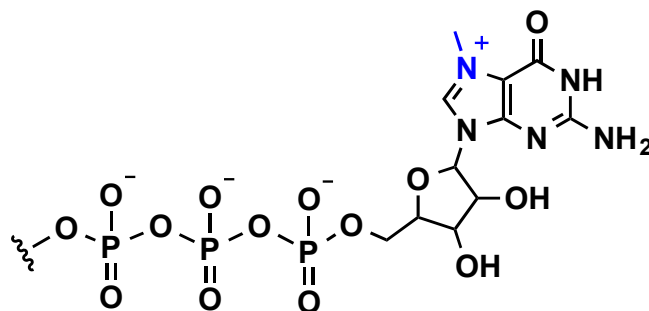


**Figure 1.2 - FDA approved Rapalogs for targeting certain cancers.**

### 1.3 Cap-dependent translation and its relation to cancer

Hyperactivation of the PI3K pathway and mTORC1 leads to overactivation of cap-dependent translation. An increase in cap-dependent translation does not cause an increase in overall protein expression; rather, it selectively enhances the translation of mRNAs encoding for oncoproteins in addition to growth and survival factors.<sup>36-39</sup>



**7-Methylguanosine  
(m<sup>7</sup>G) Cap**

**Figure 1.3 - The 5' cap of mRNA.**

mTORC1 modulates cap-dependent translation by controlling the availability of eIF4F, which binds to the mRNA 5' cap, shown in **Figure 1.3**.<sup>40</sup> eIF4F is composed of the scaffolding protein eIF4G, the DEAD-box helicase eIF4A, and the rate limiting m<sup>7</sup>GpppX-cap-binding translation initiation factor eIF4E.<sup>41</sup> Assembly of the eIF4F complex on the 5' cap of mRNA leads to recruitment of the 40S small ribosomal subunit as well as eukaryotic initiation factors 2 and 3. This process, shown in **Figure 1.4**, begins the assembly of the ribosome and leads to translation of the mRNA.

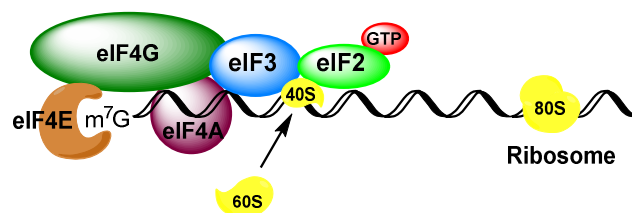


**Figure 1.4 - The cap-dependent translation pre-initiation complex.**

eIF4E is elevated in approximately 30% of cancers<sup>37,38,40,42-45</sup> and its link to cancer has been confirmed through knockdown and knockout studies.<sup>46,47,56-58,48-55</sup> Breast, colorectal, lung, and prostate cancers, glioblastoma, and hematological malignancies have all been shown to have increased levels of eIF4E.<sup>37,38,40,42-45</sup> Over-expression of eIF4E has been shown to correlate with poor prognosis and cause increased expression of eIF4E-sensitive mRNAs which encode for proliferation and survival promoting proteins like the cyclins, cMyc, and Bcl-xl.<sup>37,38,40,42-45</sup>

Cellular eIF4E activity is highly regulated through eIF4E expression,<sup>59,60</sup> phosphorylation,<sup>61,62</sup> and by the 4E-BPs, which act as gatekeepers of eIF4E by binding and sequestering the protein to prevent the formation of the eIF4F translation initiation complex and translation.<sup>41,63-68</sup> 4E-BP activity is regulated by mTORC1 phosphorylation in which hypophosphorylated 4E-BP binds to eIF4E whereas

hyperphosphorylated 4E-BP releases eIF4E to initiate mRNA translation.<sup>69-73</sup> Hyperphosphorylation of 4E-BP is a biomarker for malignancy and patient survival,<sup>74-79</sup> ectopic expression of 4E-BP1 has been shown to suppress tumorigenicity in vitro and in vivo,<sup>22,80-85</sup> and eIF4E/4E-BP stoichiometry has been shown to directly correlate with the sensitivity of cancer cells and tumors to mTOR/PI3K-targeted therapies.<sup>32,35,86</sup>

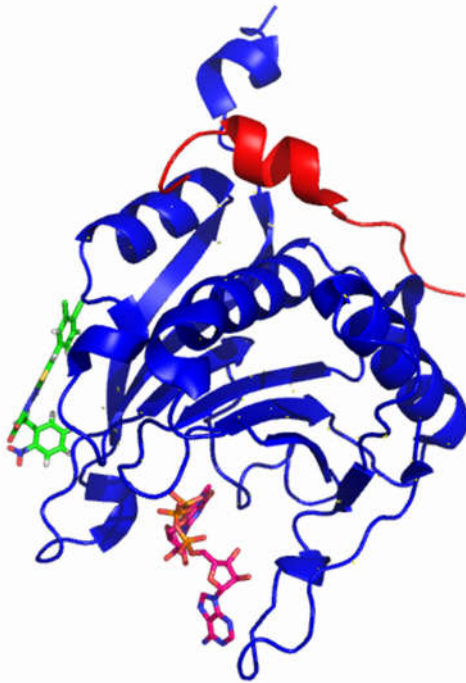


**Figure 1.5 – Reported ligands on the surface of eIF4E (in blue).** The binding site of the 4E-BPs and eIF4G is shown in red, the cap-binding pocket is shown in pink, and the allosteric binding site is in green (pictured here is 4EGI-1).

When eIF4E is free from the 4E-BPs, it interacts with eIF4G as part of the eIF4F complex. The eIF4E-eIF4G interaction site is made up of only 15 amino acids and is an important target in translational control.<sup>41</sup> The 4E-BP suppressors share the binding site of eIF4G, and crystal structures indicate that both proteins form a small  $\alpha$ -helix upon binding. This binding site, along with the m<sup>7</sup>GTP binding site and an allosteric binding site shown in **Figure 1.5**, have all been targeted as an attempt to inhibit cap-dependent



translation, which will be discussed in the next section.

#### 1.4 Efforts at targeting cap-dependent translation

Two small molecules, 4E1Rcat and 4EGI-1, have been identified to purportedly target the eIF4E-eIF4G interaction (**Figure 1.6**).<sup>48,87,88</sup> While both compounds show anti-proliferative effects, evidence indicates that this is not due solely to their inhibition of the eIF4E-4E-BP interaction and cap-dependent translation.<sup>48,49,58,89,50–57</sup> 4EGI-1 induces several phenotypes not associated with eIF4E knockdown or knockout<sup>48,49,58,50–57</sup> and its *in vitro* IC<sub>50</sub> of ~25 μM is not consistent with the cellular apoptosis data.<sup>48,57,58,90,91</sup> This indicates that 4EGI-1's effects on cancer cell growth are due to several off-target effects in addition to inhibition of the eIF4E-4E-BP interaction. Additionally, both 4EGI-1 and 4E1Rcat have been shown through X-ray co-crystal structures to act through allosteric mechanisms rather than acting as 4E-BP mimetics.<sup>92</sup> From a medicinal chemistry standpoint, neither compound is ideal for drug development. 4EGI-1 is known to produce toxic and reactive metabolites and 4E1Rcat has been linked to the inhibition of many different systems aside from eIF4E. Additionally, both compounds demonstrate flat SAR, have no conclusive target identification, and have been identified as pan assay interference compounds (PAINS).<sup>89,93–95</sup> This evidence indicates that these compounds are not suited for validation of the eIF4E-eIF4G PPI as a therapeutic target in human disease.<sup>96–98</sup>

m<sup>7</sup>G-cap analogues have also been explored as eIF4E antagonists (**Figure 1.6**),<sup>99</sup> but these compounds suffer from poor permeability.<sup>100</sup> An exception is the analogue 4EI-1, which contains a histidine triad nucleotide binding protein (HINT)-dependent protecting group, but this compound is only active at concentrations ≥50 μM

and shows cell-type-dependent activity.<sup>101,102</sup> The antiviral drug, ribavirin, has also been reported as an inhibitor of the eIF4E–m<sup>7</sup>G-cap interaction,<sup>103</sup> but this has been called into question,<sup>104</sup> no cellular target identification analyses have been described, and this compound has failed to show efficacy in >100 antitumor screens.<sup>39</sup>

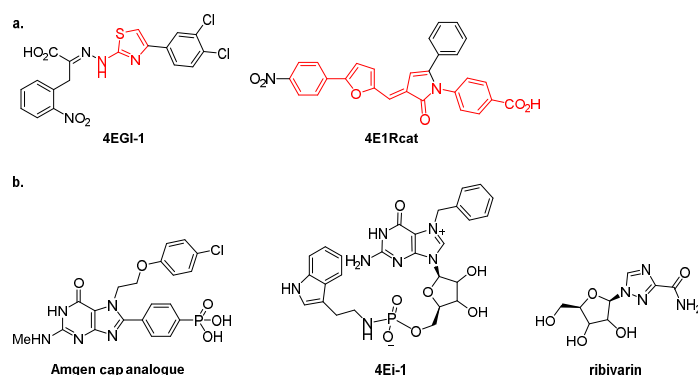


**Figure 1.6 – Inhibitors of eIF4E (a.)** Known inhibitors of the eIF4E-4E-BP PPI. PAINS motifs are shown in red. **(b.)** Inhibitors of m<sup>7</sup>G cap binding.

Previously it has been shown that delivery of the 4E-BP1 protein has anti-cancer properties in lung cancer mouse models,<sup>105</sup> and peptides designed around the sequence of 4E-BP are able to bind to eIF4E, inhibit the growth of cancer cells, and in some cases induce cell death.<sup>106–108</sup> Peptides designed around the eIF4G sequence have also been developed, but these compounds are less efficacious than the 4E-BP peptides.<sup>109</sup> While computational simulations of stapling of an eIF4G peptide showed an increase in binding affinity,<sup>1</sup> no stapled peptides have been published in relationship to this system with any cellular data. However, the use of helix inducers and mutations which encourage alpha helices in the eIF4G peptide have been successful in increasing the peptide's potency.<sup>109,110</sup> While initial experiments involving the 4E-BP and eIF4G peptides have shown success, they suffer from poor cell permeability and in every case require conjugation to cell-penetrating peptides (CPPs), such as penetratin or TAT, or conjugation to a hormone to encourage active uptake of the peptides.<sup>106–108,110</sup>

## 1.5 Research objective

The objective of this thesis is to investigate the eIF4E protein-protein interactions with 4E-BP and eIF4G and to design inhibitors which are active *in vitro* and *in cellulo*. Chapter 2 will detail efforts to investigate the binding mechanism of the peptide versions of 4E-BP and eIF4G via kinetic studies at varying temperatures and ionic strengths. This information will guide the design of stapled peptides based on their binding mechanism. Chapter 3 will describe efforts to improve our first generation stapled peptides through mutations to the sequence and staple of the 4E-BP peptides. Chapter 4 will outline future investigations into the chemical and metabolic stability of the peptides, as well as attempted identification of alternative targets, investigation of cellular uptake dependence on staple type, and the synthesis of a functionalized staple.

## Chapter 2

### An Investigation into the Binding Mechanism of 4E-BP and eIF4G Peptides

#### 2.1 Intrinsically disordered proteins, their role in signaling pathways, and their potential as drug targets

The most well-known and simplest explanation for the structure of proteins originates from Dr. Christian Anfinsen, whose “thermodynamic hypothesis” stated that the three-dimensional structure of a protein in its native physiological environment is the one in which the system has the lowest Gibbs free energy. Van der Waals forces, hydrophobic and charge-charge interactions, and solvent expulsion all play a part in determining which structure is the thermodynamic minimum. Further implied in Anfinsen’s hypothesis is that each amino acid sequence has only one structure, and that structure evolved to best perform one biological function.<sup>111,112</sup>

We now know that the relationship between protein sequence, structure, and function is not nearly so simple. NMR and computational studies have shown that protein sequences have considerable structural plasticity, and this flexibility has been shown to be critical for the protein’s biological function.<sup>113</sup> Some proteins interconvert between two equally favored thermodynamic minima, others have one primary structure but perform multiple seemingly unrelated functions, and still others have no low energy state whatsoever, rapidly interconverting between many partially folded states.<sup>112,114</sup>

This last group of proteins, known as intrinsically disordered proteins (IDPs), lack a high density of bulky, hydrophobic amino acids, and are therefore unable to form a hydrophobic core. These proteins are key players in numerous crucial cell functions,<sup>115</sup> and prediction algorithms indicate that 33.0% of the eukaryotic proteome either is an IDP or contains significant Intrinsically Disordered Regions (IDRs) as opposed to only 2.0% of archaeon proteins and 4.2% of eubacterial proteins.<sup>116</sup>

The flexibility of IDPs and IDRs allows them to bind a diverse range of macromolecules and other proteins to respond to a variety of physiological needs.<sup>117–119</sup> Additionally, they can interact through mechanisms that are disfavored or even impossible for globular proteins.<sup>120,121</sup> Disorder is commonly seen in proteins that regulate the function of multiple binding partners and promote the assembly of multi-molecular complexes.<sup>115,122–125</sup> For instance, hub proteins, which interact with 10 or more binding partners, have been shown to be significantly more disordered than end proteins, which interact with only one partner, and in general proteins involved in regulation, transcription, and development annotations are enriched in disorder.<sup>124</sup>

Disordered proteins typically have a “kinetic advantage” over ordered alternatives; they are often able to recognize their partner very quickly and exhibit very fast on-rates, although this is not always the case.<sup>126</sup> This kinetic advantage is associated with a process known as “fly-casting,” in which disordered proteins possess a larger capture radius which allows them to collide more rapidly with their partner.<sup>127</sup> The specifics of this interaction vary from system to system. In general, IDPs bind through a process known as “coupled folding and binding,” in which the protein folds upon binding to its partner.<sup>128–130</sup> The order of this process is often described as an

“induced fit” mechanism, in which the protein binds through an initial non-specific interaction and then folds to the final bound state, or a “conformational selection” mechanism, in which the protein folds into the preferred conformation and then binds in a single event.<sup>131</sup> However, it is likely that IDP mechanisms of interaction are much more complex. The “dock and coalesce” mechanism, in which the initial interaction catalyzes the binding of the remaining segments,<sup>132</sup> formation of “fuzzy complexes,” in which the IDP remains disordered even after binding,<sup>133</sup> and multistep mechanisms with multiple parallel pathways<sup>134</sup> have all been used to describe interactions made by various IDPs. Additionally, it is important to remember that these mechanisms are observed *in vitro*, and the true method of association likely varies based on environmental conditions, competition, compartmentalization, and reactant concentrations.

Determining the binding mechanism of disordered interactions is quite challenging due to the complexity of the many weak, non-covalent interactions, but structural, kinetic, and dynamics data can be used to figure out some details.<sup>131</sup> Observing the helicity of the IDP can provide information about binding properties, but does not necessarily inform about the mechanism, since a correlation between helicity and association constant could be explained as an increased rate of binding of the folded helix or a stabilization of the transition state for folding after binding.<sup>135–137</sup> However, one can observe binding kinetics under pseudo-first order experiments with respect to each ligand to differentiate between induced fit and conformational selection.<sup>138</sup> Comparing rate constants at different temperatures and solvent conditions can also provide information about the binding mechanism.<sup>139</sup> While in many cases the

mechanism cannot be definitively proven with these methods, they can be used to understand more about the protein interactions and how to perturb them.

Given the prevalence of disordered proteins in key cellular processes, as well as their ability to participate in a wide variety of interactions, it should come as no surprise that disordered proteins have been associated with cancer<sup>140,141</sup> and neurodegenerative disorders and are now being investigated as potential drug targets.<sup>142,143</sup> However, disordered proteins are challenging drug targets due to their lack of tertiary structure, the dynamic or transient nature of what structure they do have, and the many potential mechanisms of binding. Early efforts to target IDPs include the use of small molecules to bind partially folded regions of the protein,<sup>144,145</sup> the inhibition of PPIs between disordered and ordered proteins in which the inhibitor binds to the ordered partner (for instance, nutlins, which inhibit the p53-MDM2 PPI),<sup>146</sup> and the use of compounds to induce structure formation, leading to loss of function of the IDP.<sup>147</sup> Computational methods have also been helpful in trying to target IDPs, although more work is necessary to optimize computational tools for disorder-based drug design.<sup>148</sup>

The focus of this thesis is primarily to inhibit the eIF4E-eIF4G protein-protein interaction. However, eIF4G and the 4E-BPs, which both bind in the same site on the surface of eIF4E, are disordered proteins. In fact, nearly 75% of the residues in eIF4G are classified as disordered, and eIF4G is predicted to have 18 disordered binding sites.<sup>149</sup> The 4E-BPs are completely unstructured in solution, but their eIF4E binding site has been shown to have high helical propensity. Interestingly, the 4E-BP2 protein still maintains some disorder after complexing with eIF4E, forming a somewhat “fuzzy” complex.<sup>150,151</sup> Phosphorylation by mTORC1 or other kinases decreases the helical

propensity at the binding site, which causes the 4E-BPs to favor an unfolded (or incorrectly folded) state which cannot bind to eIF4E.<sup>152,153</sup>

In order to inhibit this interaction, it was important to consider other methods for inhibiting intrinsically disordered interactions. In the work to be presented, the probe will be binding to eIF4E, which is a mostly ordered protein; however, the peptide binding surface of eIF4E is quite planar, lacking any distinctive feature to recognize eIF4G or 4E-BP1.<sup>1</sup> A small molecule approach (which has been tried before, and is described in Chapter 1) seemed unlikely to succeed. Since the eIF4E interacting residues of eIF4G and 4E-BP1 are structural mimics of each other, forming a short helix once bound,<sup>67</sup> we decided to attempt to mimic the disordered proteins which bind to eIF4E's surface. Thus, the goal of this chapter was to use, to the best of our ability, the methods described in the literature to compare the binding mechanisms of eIF4G and 4E-BP1 peptides to eIF4E, and to use that information to discern the best way to target this pathway through the use of 4E-BP1 and eIF4G peptides.

While there is some information available concerning the binding mechanism of the full-length 4E-BP proteins, there is less information regarding the 4E-BP or eIF4G peptides. The full-length 4E-BP and eIF4G proteins interact via a bipartite mode, which involves the canonical binding sequence as well as a second binding site shown in **Figure 2.1.**<sup>150,154</sup> The binding of 4E-BP1 peptides, which contain only the canonical binding site, is 2–3 fold weaker than that of the full-length 4E-BP1 protein.<sup>155,156</sup> Additionally, it has been suggested that 4E-BP1 must first bind in the second, non-canonical binding site in order to displace eIF4G and repress translation.<sup>157</sup>



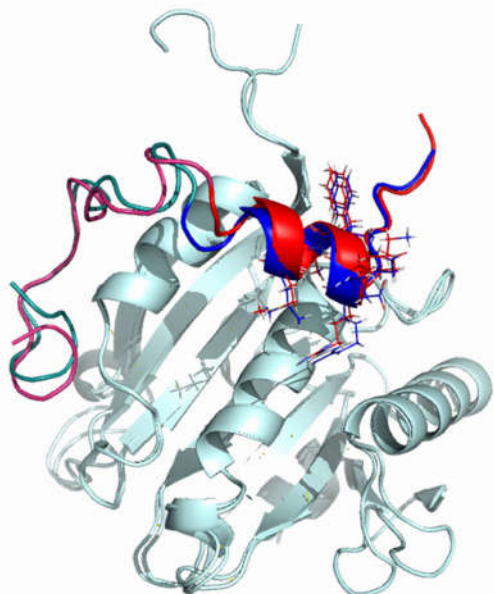


**Figure 2.1 – Overlay of 4E-BP1 (red/purple) and eIF4G (blue/teal) bound to eIF4E.** The residues of the canonical binding site are shown. The secondary binding site is shown in purple for 4E-BP1 and teal for eIF4G. PDB ID 4UED and 5T46.

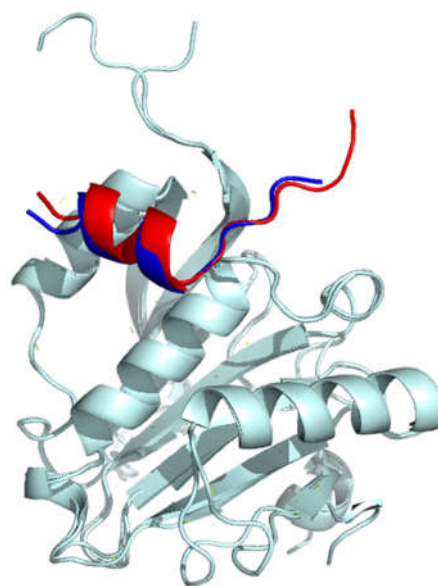


**Figure 2.2 – Bound structure of the linear 4E-BP1 (red) and eIF4G (blue) peptides that we intend to use for our studies.**

We were interested in developing mimics of the eIF4G or 4E-BP proteins in order to better probe the system, validate eIF4E as a target, and ultimately aid in the development of a cancer therapeutic. It therefore made sense to use only the canonical binding site (plus some flanking amino acids) for our studies, which consists of 16 amino acids for 4E-BP1 and 14 amino acids for eIF4G (**Figure 2.2**). We were unsure of the effect of truncation on the binding mechanism of these short peptides and what that would mean for our attempts to use them as inhibitors of the eIF4E–eIF4G protein-protein interaction. Additionally, while constraining peptides through stapling or cyclization has been used in the past (and will be discussed in Chapter 3) to improve their drug-like properties, we did not know how this technique would apply to disordered peptides. The aim of this chapter was to explore the binding mechanism of the 4E-BP1

and eIF4G peptides and to apply that information to the development of a probe for cap-dependent translation, but along the way, we also learned about larger implications involving mimicking IDPs.

## 2.2 Helical propensity and inhibitory potential of 4E-BP1 and eIF4G peptides

We compared several peptides based around the sequences for 4E-BP1 and eIF4G (**Table 2.1**). Our longest peptide, 4E-BP1 (G<sup>49</sup>-N<sup>64</sup>), was chosen based on the crystal structure of a peptide containing the canonical binding sequence bound to eIF4E. The eIF4G peptide also encompasses the canonical binding site (eIF4G K<sup>608</sup>-F<sup>622</sup>), although it is slightly shorter (only 14 amino acids as opposed to 16) because we wanted both peptides to have the same total charge, and extending the eIF4G peptide to include all 16 residues would add two additional glutamate residues.<sup>67</sup> We therefore also tested a slightly truncated 4E-BP1 peptide, 4E-BP1 (R<sup>51</sup>-N<sup>64</sup>), in order to confirm that the differences we observed were not only due to sequence length. We also examined a linear version of sTIP-04, which is a stapled eIF4G peptide previously described in the literature, eIF4G (K<sup>608</sup>-F<sup>620</sup>, D<sup>613</sup>S, F<sup>616</sup>Q, F<sup>620</sup>L).<sup>1</sup> sTIP-04 will be discussed in more detail in Chapter 3. Finally, we tested a 4E-BP1/eIF4G hybrid peptide, 4E-BP1 (R<sup>51</sup>-N<sup>64</sup>, R<sup>51</sup>K, I<sup>52</sup>K, I<sup>53</sup>R).

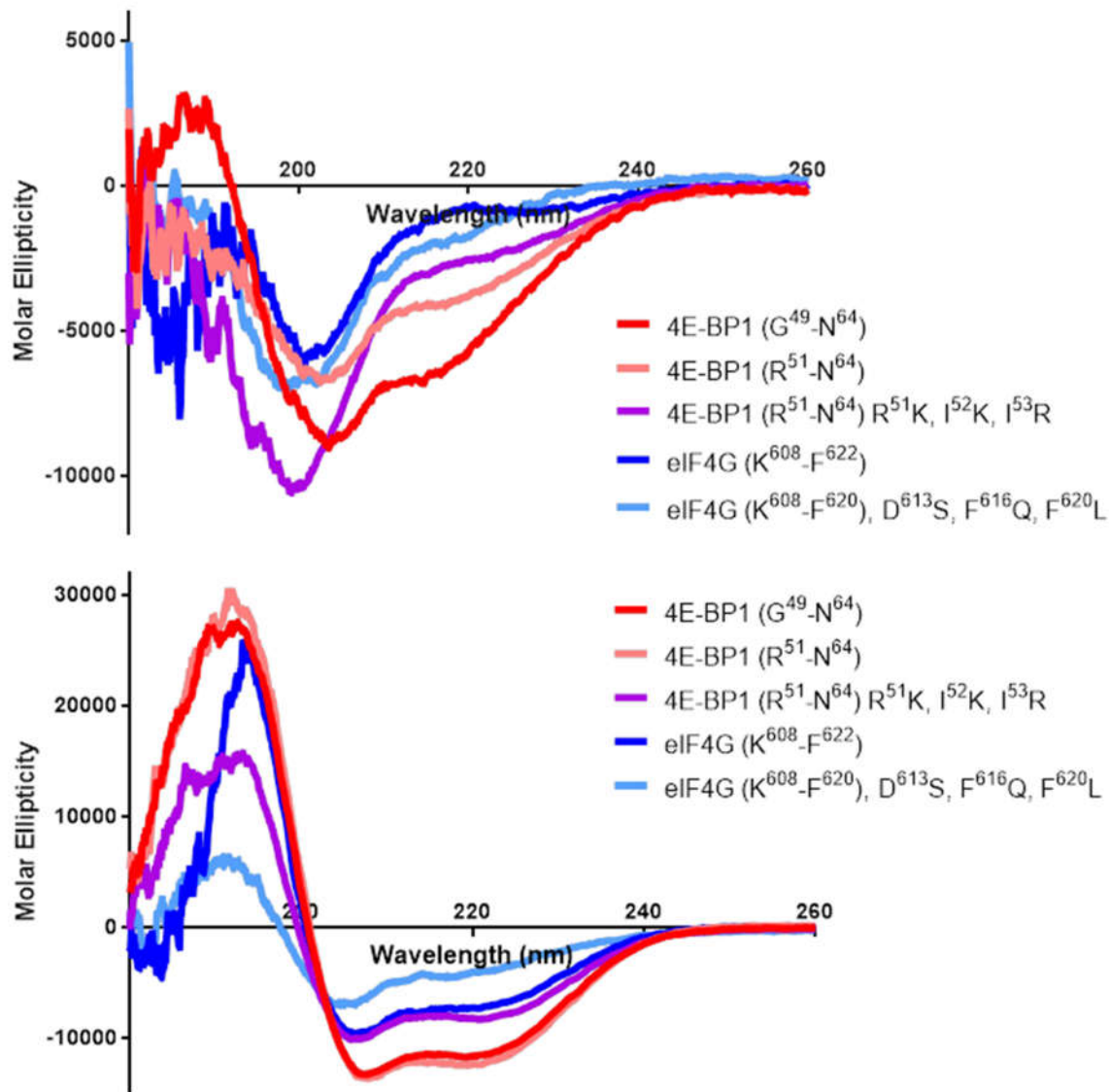
We found that the 4E-BP1 peptides had much better IC<sub>50</sub>s (curves for all peptides are in Chapter 2 – Supplemental Information - IC<sub>50</sub>s) than their eIF4G analogues. Interestingly, the 4E-BP1/eIF4G hybrid peptide significantly lost activity (10-fold reduction over the native 4E-BP1 sequence) with the introduction of the KKR on the N-terminus. This hybrid peptide was actually 3-fold worse than the eIF4G peptide, indicating that the addition was definitely not beneficial to activity. Also, the

linear version of sTIP-04 had a worse IC<sub>50</sub> than the un-mutated eIF4G sequence, which was surprising because that sequence was optimized by Phage display, and its stapled version has a very high affinity for eIF4E (this will be discussed later in this chapter).

**Table 2.1 – Sequences, IC<sub>50</sub>s, and helicities of linear peptides.** IC<sub>50</sub>s were measured using cat-ELCCA and curves are shown in Supplemental Information 2.1.

	Y X X X X L φ	IC <sub>50</sub> (nM)	%Helicity	% Helicity (40% TFE)
4E-BP1 (G <sup>49</sup> -N <sup>64</sup> )	G T R I I Y D R K F L M E C R N	70 ± 20	16	37
4E-BP1 (R <sup>51</sup> -N <sup>64</sup> )	R I I Y D R K F L M E C R N	41 ± 9	14	46
4E-BP1 (R <sup>51</sup> -N <sup>64</sup> ), R <sup>51</sup> K, I <sup>52</sup> K, I <sup>53</sup> R	K K R Y D R K F L M E C R N	420 ± 98	8	28
eIF4G (K <sup>602</sup> -F <sup>622</sup> )	K K R Y D R E F L L G F Q F	160 ± 30	3	24
eIF4G (K <sup>602</sup> -F <sup>620</sup> ), D <sup>613</sup> S, F <sup>616</sup> Q, F <sup>620</sup> L	K K R Y S R E Q L L G L	500 ± 100	4	13

The 4E-BP1 peptides were also more helical than the eIF4G peptides, although all of the peptides were still mostly unstructured (**Figure 2.3**). We also tested helicity in the presence of trifluoroethanol (TFE), which induces helicity, in order to observe the propensity for helicity. We found that the 4E-BP1 peptides had a greater helical propensity, the hybrid peptide averaged the helicities of the 4E-BP1 and eIF4G peptides, and the linear version of sTIP-04 had the least potential for helicity. Curves for all peptides are in Chapter 2 – Supplemental Information – CD.



	Phosphate Buffer	Phosphate Buffer + 40% TFE
4E-BP1 (G <sup>49</sup> -N <sup>64</sup> )	16%	37%
4E-BP1 (R <sup>51</sup> -N <sup>64</sup> )	12%	41%
4E-BP1 (R <sup>51</sup> -N <sup>64</sup> ) R <sup>51</sup> K, I <sup>52</sup> K, I <sup>53</sup> R	8%	28%
eIF4G (K <sup>608</sup> -F <sup>622</sup> )	3%	24%
eIF4G (K <sup>608</sup> -F <sup>620</sup> ) D <sup>613</sup> S, F <sup>616</sup> Q, F <sup>620</sup> L	4%	13%

**Figure 2.3 – Percent helicity of the linear 4E-BP1 and eIF4G peptides in buffer (top) and with the helicity inducer, trifluoroethanol (bottom).**

### 2.3 Kinetic analysis of 4E-BP1 and eIF4G peptides

**Table 2.2 – Kinetic binding data for linear peptides determined by SPR.**

	$K_a$ ( $M^{-1}s^{-1}$ )	$K_d$ ( $s^{-1}$ )	$K_D$ (nM)
4E-BP1 (G <sup>49</sup> –N <sup>64</sup> )	$0.82 \pm 0.3 \times 10^6$	$2.1 \pm 0.4 \times 10^{-2}$	$26 \pm 6$
4E-BP1 (R <sup>51</sup> –N <sup>64</sup> )	$1.10 \pm 0.01 \times 10^6$	$1.92 \pm 0.03 \times 10^{-2}$	$17.5 \pm 0.3$
4E-BP1 (R <sup>51</sup> –N <sup>64</sup> ), R <sup>51</sup> K, I <sup>52</sup> K, I <sup>53</sup> R	$2.0 \pm 0.9 \times 10^6$	$15 \pm 2 \times 10^{-2}$	$77 \pm 7$
eIF4G (K <sup>602</sup> –F <sup>622</sup> )	$1.7 \pm 0.3 \times 10^6$	$4.8 \pm 0.9 \times 10^{-2}$	$29 \pm 6$
eIF4G (K <sup>602</sup> –F <sup>620</sup> ), D <sup>613</sup> S, F <sup>616</sup> Q, F <sup>620</sup> L	$1.99 \pm 0.06 \times 10^6$	$12.3 \pm 0.8 \times 10^{-2}$	$62 \pm 4$

In order to further elucidate the mechanism, we measured the  $k_a$ ,  $k_d$ , and  $K_D$  values for each linear peptide at room temperature using Surface Plasmon Resonance (SPR) spectroscopy (**Table 2.2**). We found that the eIF4G peptides exhibited much faster  $k_a$ s than the 4E-BP peptides. We hypothesized that this could be due to the KKR sequence on the N-terminus of the eIF4G peptides, which is known to contribute to the “fly-casting” ability of many intrinsically disordered proteins. Indeed, the 4E-BP1 peptide with the mutated KKR N-terminus also has a faster (almost 2-fold) association rate than the un-mutated 4E-BP1 peptides. The hybrid 4E-BP1/eIF4G peptide had the worst dissociation rate of all, which likely explains its significantly worse  $IC_{50}$ . The 4E-BP1 peptides had slower off-rates than the eIF4G peptides, and generally had stronger binding constants. While we suspected that these differences could be explained by a difference in binding mechanism of the two peptide sequences, more experiments were required to support our hypothesis. Sensorgrams for all peptides are in Chapter 2 – Supplemental Information – SPR.

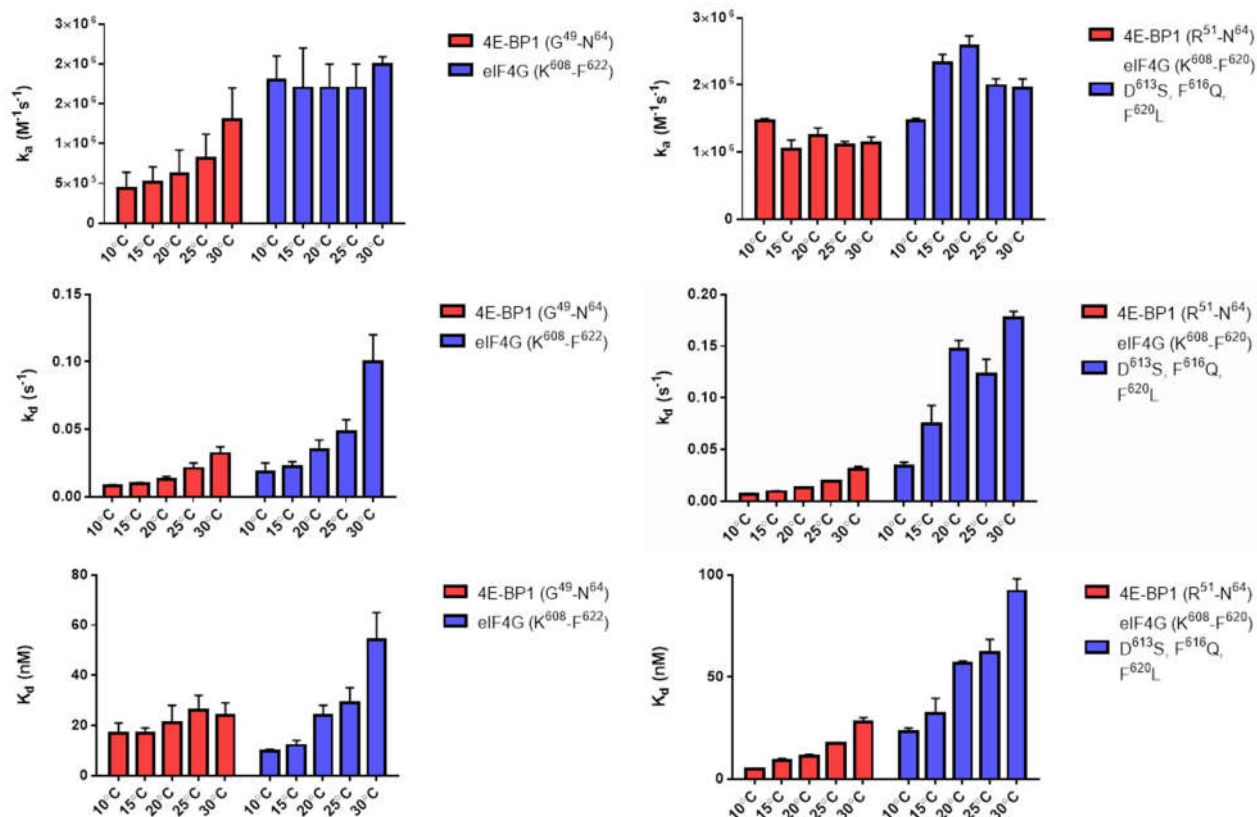


**Figure 2.4 – The kinetics of binding of the 4E-BP1 and eIF4G peptides in response to increasing temperature as determined by SPR.** The full length peptides 4E-BP1 (red) and eIF4G (blue) peptides are on the left series of graphs, and the truncated 4E-BP1 (red) and mutated eIF4G (blue) peptides are on the right series of graphs. The y-axis from top to bottom is the  $k_a$ ,  $k_d$ , and  $K_D$ .

As discussed in section 4.1, IDPs and IDRs have been shown to be affected by temperature, so we next analyzed the binding kinetics of the peptides between 10°C and 30°C (**Figure 2.4**). 4E-BP1 (G<sup>49</sup>–N<sup>64</sup>) had an increased on-rate and off-rate with increasing temperature, but ultimately only a very small increase in the binding constant. The truncated 4E-BP1 (R<sup>51</sup>–N<sup>64</sup>) peptide had an on-rate unaffected by temperature, an increase in off-rate, and an increase in the binding constant. This was surprising, because we expected these two very similar peptides to behave the same. Since the truncated 4E-BP1 peptide is slightly less ordered than the full-length peptide, it is possible that some preordering of this sequence is required for the initial

interaction. eIF4G (K<sup>608</sup>-F<sup>622</sup>) had an unchanged on-rate and a significant increase in off-rate with increasing temperature, leading to a significantly higher binding constant. This looks more similar to the behavior of the shorter 4E-BP1 peptide, and the decreased helicity of the eIF4G peptide correlates with its much weaker binding overall. The mutated linear peptide based off the sequence of sTIP-04 followed the same trends as eIF4G, but, as expected, the overall binding of this peptide was weaker.

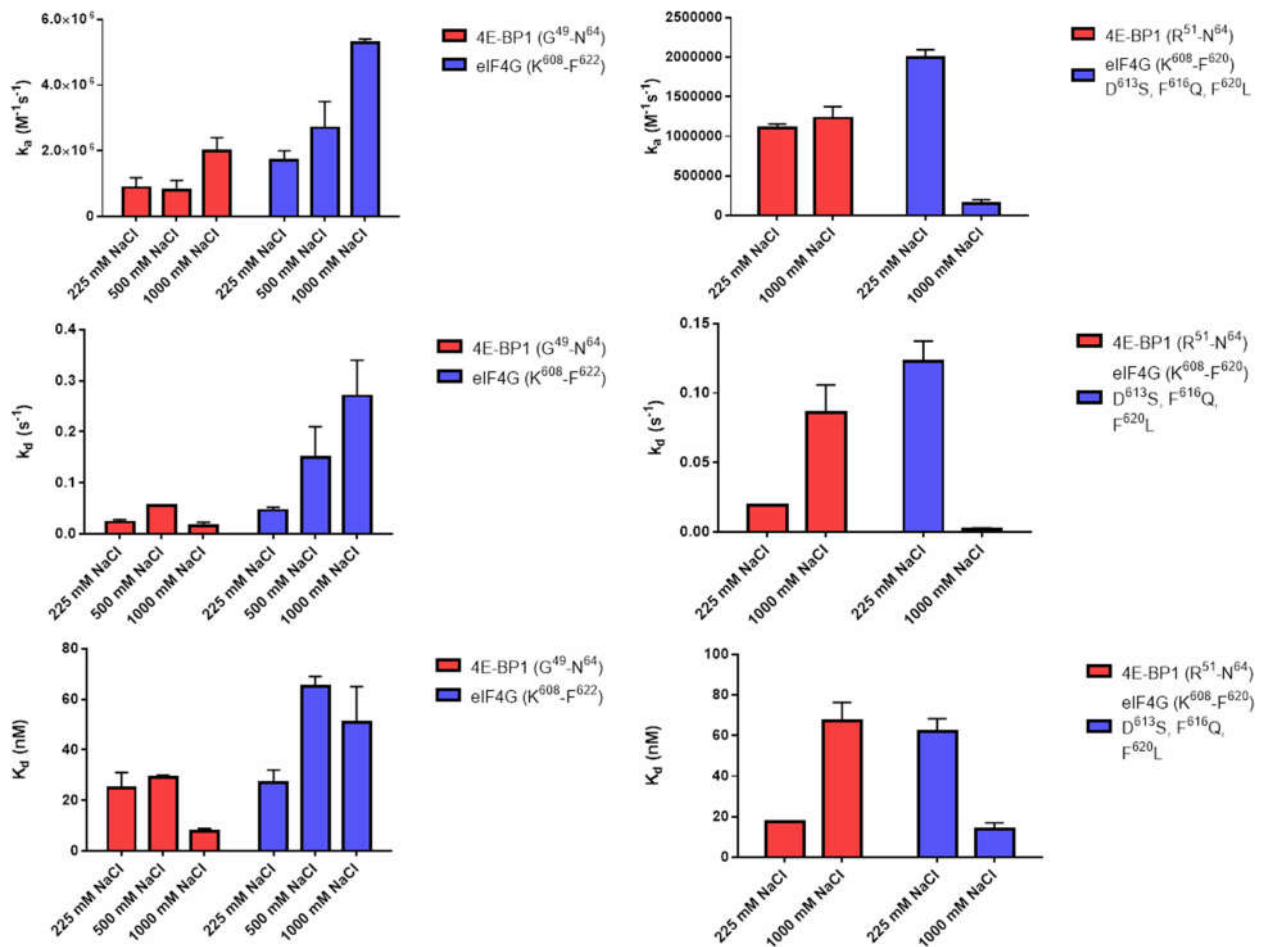


**Figure 2.5 – The kinetics of binding of 4E-BP1 and eIF4G peptides in response to increasing ionic strength.** The left series of graphs compares the full length, unmutated 4E-BP1 (red) and eIF4G (blue) peptides. The right series compares the truncated 4E-BP1 (red) and mutated eIF4G (blue). From top to bottom, the y-axis is  $k_a$ ,  $k_d$ , and  $K_D$ . Note that eIF4G (K<sup>608</sup>-F<sup>620</sup>), D<sup>613</sup>S, F<sup>616</sup>Q, F<sup>620</sup>L has two sets of kinetic data at 1000 mM NaCl from its two binding events.

To further probe the binding mechanism of the peptides, we measured the binding kinetics at 225 mM, 500 mM, and 1000 mM sodium chloride (**Figure 2.5**). We found that the 4E-BP1 (G<sup>49</sup>-N<sup>64</sup>) peptide had a slightly increased on-rate, an unchanged off-rate, and an improved binding constant in response to increasing salt concentrations. This trend was reversed in the case of the shorter 4E-BP1 peptide, in which the off-rate and binding constant increased with ionic strength. eIF4G (K<sup>608</sup>-F<sup>622</sup>) had a larger increase in on-rate, a corresponding increase in off-rate, and an overall weaker binding constant in response to increasing salt concentrations. The mutated eIF4G peptide had a much slower on-rate and off-rate at high ionic strength. This is surprising, as it appears to behave more similarly to the 4E-BP1 peptide, although the decrease in on-rate is unique. This indicates that the mutated eIF4G peptide has changed its mechanism of interaction in some way with increasing ionic strength.

We next considered if the observed differences were due to changes in peptide or eIF4E stability across temperatures or salt concentrations (**Figure 2.6**). The peptides appeared to have the same conformation over all temperatures tested. A slight change in conformation was observed at 1 M sodium chloride versus 0 M. Sodium chloride distorts the spectrum significantly below 200 nm, which is why we only reported wavelengths between 200–260 nm. The differences in the spectra are only observed at less than 210 nm, so it is possible that the salt itself, rather than a change in conformation, is responsible for the low UV shift. However, it is also possible that the peptides in 1 M sodium chloride have less “random coil” character than those without salt. In any case, the salt does not appear to affect the helicity of



the peptides (seen around 222 nm). We also found that eIF4E was stable at the temperatures tested in SPR for at least 20 min, which is the length of the assay (Figure 2.7).

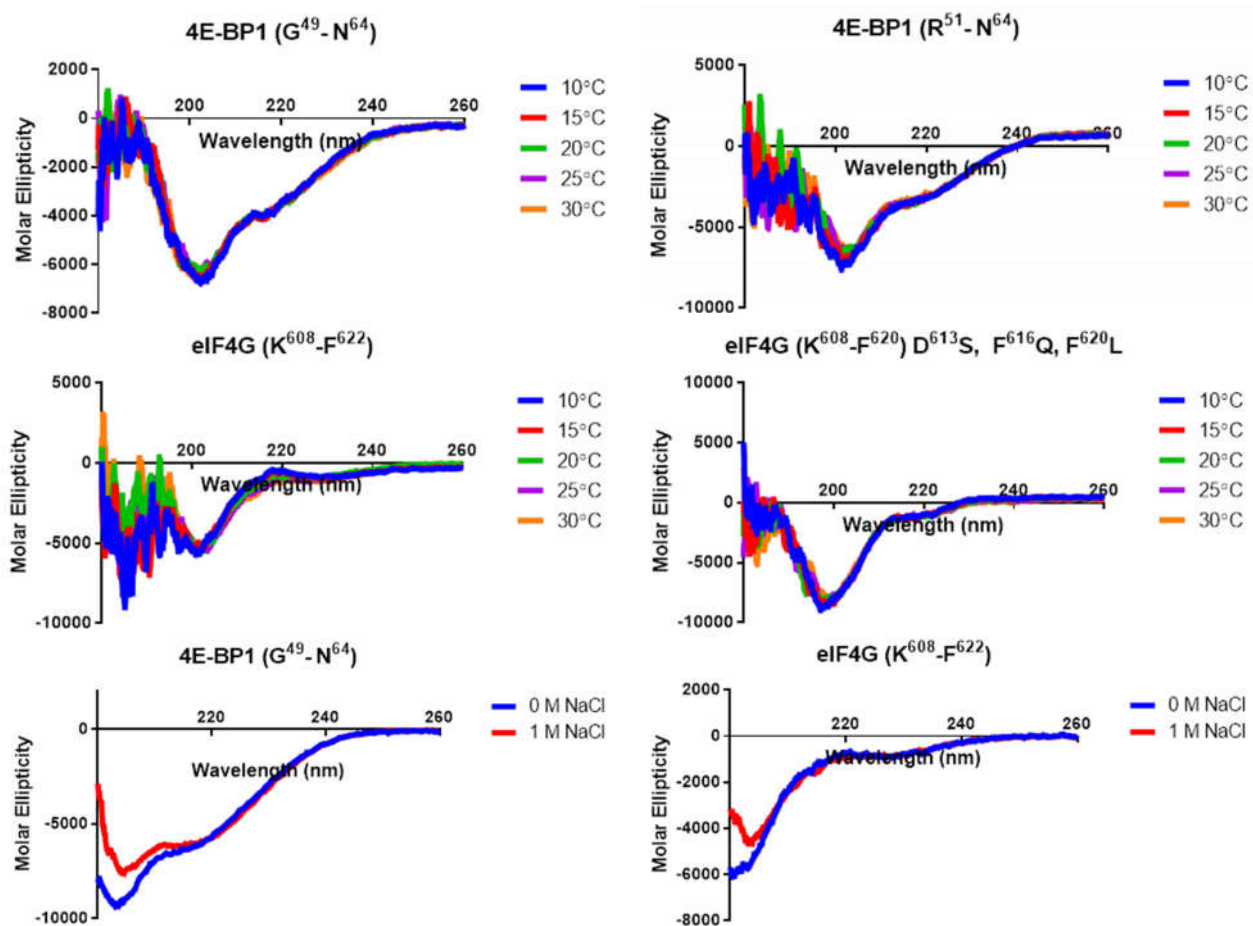


**Figure 2.6 – The effect of temperature (top four images) and salt (bottom two images) on the conformation of the peptides.**

Based on this data, we hypothesize that the eIF4G peptide binds through an induced fit mechanism. Its fast on-rate and the KKR sequence on the N-terminus are consistent with a peptide binding through the fly casting mechanism. Additionally, it appears to form a less stable complex with eIF4E (as opposed to the 4E-BP1 peptide). This is evidence by its increased off-rate in the presence of increased temperature and higher ionic strength. We propose that eIF4G forms a very quick initial interaction, but

is much slower to fold into its final helical form. 4E-BP1, on the other hand, has both a slower on-rate and off-rate compared to the eIF4G peptide. Additionally, its binding constant is unaffected by increasing temperature and actually improved by increasing ionic strength. We hypothesize that the 4E-BP1 peptide binds via a conformational selection mechanism, in which it first forms a helix in solution and then binds to eIF4E. This could explain the greater stability of the eIF4E–4E-BP1 complex, because the peptide has already folded into the appropriate helix upon binding. However, it appears that the mechanism of interaction is highly sequence dependent, because we observe differences in kinetics with only a short truncation in the case of 4E-BP1 and a few mutations (and additional truncation) in the case of eIF4G.

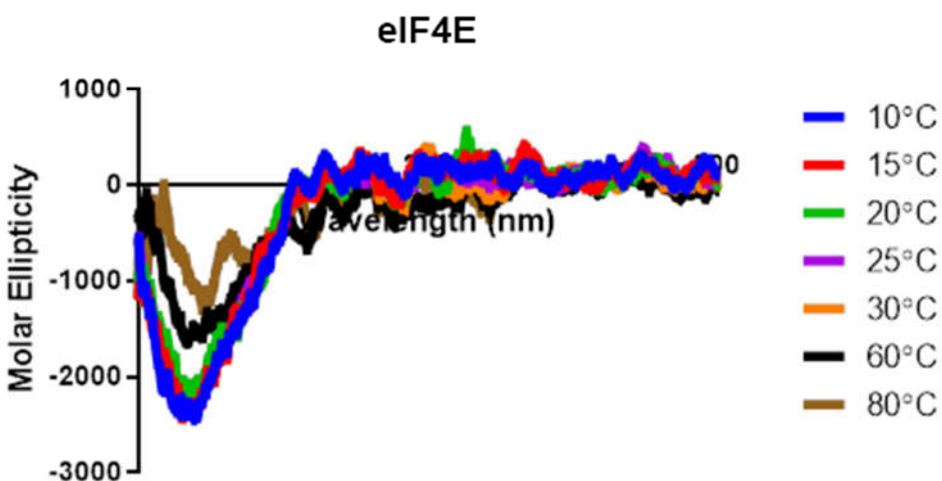


**Figure 2.7 – eIF4E CD spectra across temperatures tested in SPR.** We also observed the spectra at 60 and 80 degrees to indicate the expected change in spectra with denaturation.

#### 2.4 Consideration of binding mechanism in designing IDP mimetics

In order to see how our observation of peptide kinetics would affect our efforts to make a constrained peptide probe, we made a series of stapled peptides and compared their activity versus eIF4E. Dr. James Song synthesized a hydrocarbon

stapled 4E-BP1 (G<sup>49</sup>-N<sup>64</sup>), hereafter referred to as HCS 4E-BP1. Dr. Song also made the sTIP-04 peptide from the literature, and a hydrocarbon stapled 4E-BP1 negative control, HCS-4E-BP1 (G<sup>49</sup>-N<sup>64</sup>), L<sup>59</sup>A, M<sup>60</sup>A, hereafter referred to as HCS 4E-BP1 LM->AA. Alyah Chmiel made a hydrocarbon stapled eIF4G (K<sup>608</sup>-F<sup>620</sup>), referred to as HCS eIF4G. The sequences and IC<sub>50</sub>s of these peptides are shown in **Table 2.3**.

**Table 2.3 – Sequences, IC<sub>50</sub>s, and helicities of 4E-BP1 and eIF4G stapled peptides. X = pentenyl alanine.**

	Y X X X X L φ	IC <sub>50</sub> (nM)	%Helicity	% Helicity (40% TFE)
HCS 4E-BP1	G T R I I Y D R X F L M X C R N	5 ± 2	44	83
HCS 4E-BP1 LM->AA	G T R I I Y D R X F A A X C R N	8000 ± 7000	35	64
HCS eIF4G	K K R Y D R X F L L X F	6000 ± 1000	5	19
sTIP-04	K K R Y S R X Q L L X L	24 ± 7	38	58

The stapled 4E-BP1 peptide showed a significant improvement in IC<sub>50</sub>, as one might expect based on stapled peptide literature. However, HCS eIF4G actually showed a significant loss of potency; the linear eIF4G peptide had an IC<sub>50</sub> of 29 nM, but upon stapling the IC<sub>50</sub> increased to 6 μM. Interestingly, sTIP-04, which has been mutated to favor a helical conformation, has an IC<sub>50</sub> of 24 nM. The IC<sub>50</sub>s of the stapled peptides correlate reasonably well with helicity (**Figure 2.8**), in which the two best peptides, HCS 4E-BP1 and sTIP-04, are quite helical, whereas HCS eIF4G is not helical at all. A notable exception is HCS 4E-BP1 LM->AA, which is 35% helical but lacks activity. Interestingly, even the addition of TFE to HCS eIF4G does not cause it to form an alpha helix. The curve lacks distinct dips at 222 and 208 nm, which can be clearly seen in the spectra for the other three peptides. This indicates that HCS eIF4G not only lacks intrinsic helicity, but also lacks the propensity for helicity.

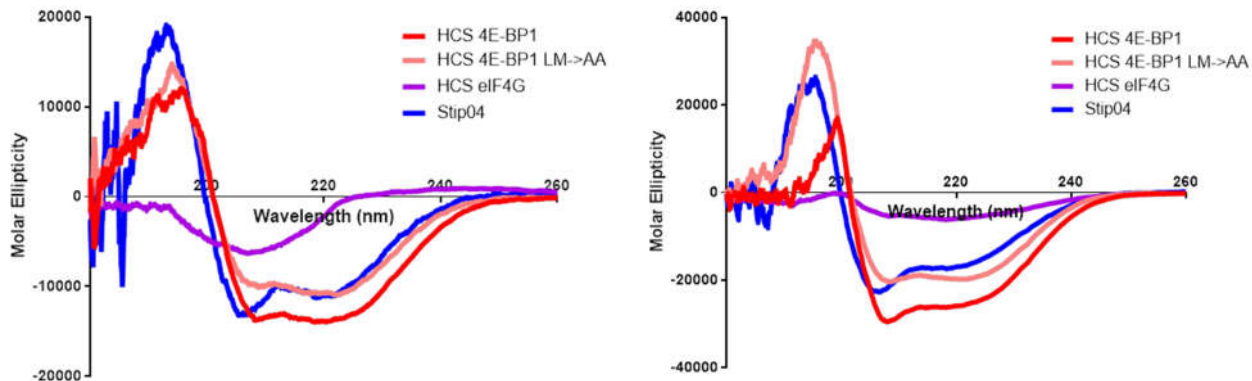


**Figure 2.8 – Circular dichroism spectra for the stapled peptides in phosphate buffer (left) and with the addition of 40% TFE (right).**

We next tested the stapled peptides for kinetic binding (**Table 2.4**). We did not test HCS 4E-BP1 LM->AA due to its weak activity which would be difficult to observe by SPR. The HCS 4E-BP1 peptide had an improved on-rate and off-rate over its linear counterpart, leading to an improved binding constant of 4 nM. HCS eIF4G also had an improved off-rate, but its on-rate was significantly slower than the linear eIF4G peptide, which is what led to its overall loss in affinity. This could be explained by its decreased propensity for helicity. Interestingly, the sTIP-04 peptide also had a slower on-rate relative to the linear peptide, but its off-rate was improved enough to lead to a stronger binding peptide. Constraining the peptides improved the dissociation constant in all cases, but only improved the association constant for the 4E-BP1 sequence. This appears to support our hypothesis that the 4E-BP1 sequence binds through a conformational selection type mechanism, whereas the eIF4G sequence binds through induced fit. Constraining (or ordering) the eIF4G peptides reduces the association rate, likely because they now lack the kinetic advantage lent by their disorder. The 4E-BP1 sequence, however, seems to require a helical conformation to bind in the first place, so stapling lowers the barrier for that first step.

**Table 2.4 – Kinetic binding data for stapled peptides determined by SPR.**

	$K_a$ ( $M^{-1}s^{-1}$ )	$K_d$ ( $s^{-1}$ )	$K_D$ (nM)
HCS 4E-BP1	$1.5 \pm 0.2 \times 10^6$	$5 \pm 4 \times 10^{-3}$	$4 \pm 3$
HCS eIF4G	$0.33 \pm 0.01 \times 10^6$	$30 \pm 4 \times 10^{-3}$	$90.0 \pm 0.3$
sTIP-04	$0.83 \pm 0.05 \times 10^6$	$5.2 \pm 0.1 \times 10^{-3}$	$6.3 \pm 0.4$

## 2.5 Cell penetration and activity of HCS peptides

To confirm that the peptides entered the cell, we used FITC labeled stapled peptides and observed cell penetration using confocal imaging. These imaging studies were performed by Arya Menon, and the results are shown in **Figure 2.9**. All three of the peptides entered the cell. Videos of the cells (not shown) indicate that the fluorescent blobs are inside the cell and not stuck to the surface. Surprisingly, the peptides are clustered in blobs inside the cell. It is possible that the peptides aggregated once inside the cells, that they are localizing to stress granules,<sup>158</sup> or that they have localized to different cellular compartment. The physical properties of the peptide are altered with the introduction of the FITC tag, so it is unclear if the untagged peptide would behave the same. Going forward, we use a different type of cell penetration assay, which will be described in Chapter 3.

To determine if the peptides were effective in cancer cells, we used an eIF4E pulldown assay which was performed by Arya Menon. The cells were treated with peptide for 6 hours and then lysed.  $M^7$ GDP immobilized on resin was added to the cell lysate in order to bind eIF4E. The resin was washed, boiled, and the proteins were run on a gel to be analyzed by Western Blot. We used eIF4E as a normalization control, and looked for a decrease in pulldown of eIF4G and 4E-BP1 proteins in the presence of peptide. The results are shown in **Figure 2.10**.

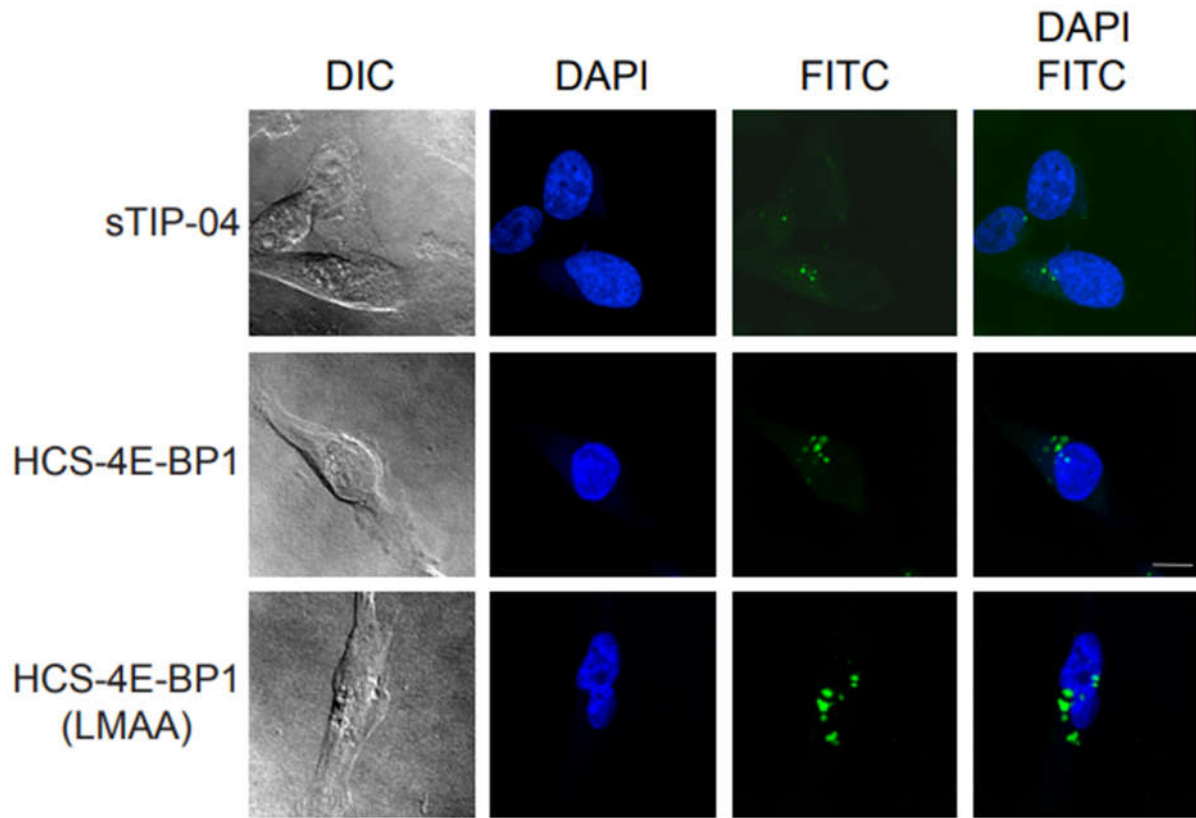


**Figure 2.9 – Confocal imaging of FITC labeled peptides inside the cell.**

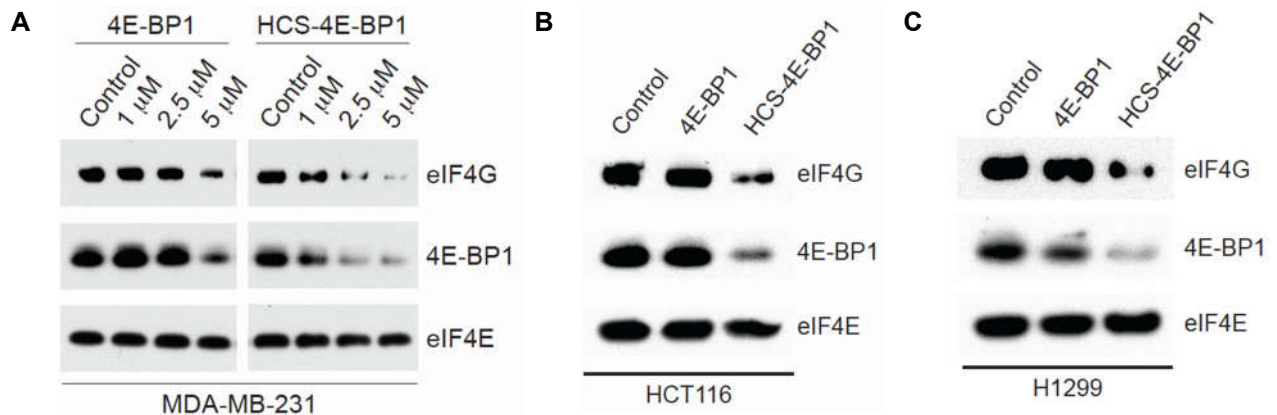


**Figure 2.10 – eIF4E pulldown data for 4E-BP1 (G<sup>49</sup>-N<sup>64</sup>) and HCS 4E-BP1 in (A) MDA-MB-231 cells, (B) HCT116 cells, and (C) H1299 cells (both HCT116 and H1299 were treated with 2.5 μM peptide).**

We found that HCS 4E-BP1 partially inhibited the pulldown of both eIF4G and 4E-BP1 in all cell lines. The linear 4E-BP1 peptide was not active at 2.5 μM and was

less active at 5  $\mu$ M when compared with the stapled peptide. We see activity in the pulldown assay against MDA-MB-231 cells (a triple negative breast cancer cell line), HCT116 cells (a colon cancer cell line), and H1299 cells (a non-small cell lung carcinoma cell line).

## 2.6 Conclusion

It is impossible to definitively prove the mechanism of interaction of the 4E-BP1 and eIF4G peptides, but our data shown here does indicate that they interact with eIF4E differently. Based on this evidence, we believe that 4E-BP1 goes through a conformational selection mechanism, whereas eIF4G binds through an induced fit mechanism, although we acknowledge that the actual method of interaction could be more complicated. In order to further dissect the peptide–protein interactions, the next logical study would be a stopped flow experiment in which one could measure the kinetics of interaction under pseudo first order conditions.

Interestingly, the mutant eIF4G peptide (eIF4G K<sup>608</sup>–F<sup>620</sup>, D<sup>613</sup>S, F<sup>616</sup>Q, F<sup>620</sup>L) seems to also go through an induced fit mechanism and has very similar properties compared to eIF4G (K<sup>608</sup>–F<sup>622</sup>). However, the stapled version of this mutant, sTIP-04 is significantly more helical than HCS eIF4G. This indicates that the mutations within this peptide do not promote ordering of the linear peptide, but allow the stapled peptide to achieve a stable and helical structure. This indicates that the secondary structure of a linear disordered peptide does not predict helical stabilization through stapling. We hypothesize that the linear eIF4G peptide is only capable of binding through an induced fit mechanism, but the mutations introduced by Lama et. al.<sup>1</sup> enable the sequence to

bind through either an induced fit or a conformational selection mechanism. This would indicate that only peptides which can bind through either mechanism are suitable for helical constraint. For peptides which cannot bind through a conformational selection mechanism, mutations to alter the folding landscape (as with sTIP-04) or receptor-templated stapling are potential alternatives for the design of constrained peptides.<sup>159</sup>

## 2.7 Materials and Methods

### Development of the SPR Assay

#### *pET19b-PP-eIF4E*

A pET19B vector containing a His10 tag and a precision protease cut site was gifted to me by Dr. Max Stefan in Dr. George Garcia's lab. The human eIF4E gene was amplified using PCR with the following primers:

Forward Primer	5'	GGTACATATGGCGACTGTCTGAACCGGA	3'
Reverse Primer	5'	CATCGGATCCTTAAACAACAAACCTAT	3'

The PCR reaction components were:

Component	Concentration	Volume
PFU Ultra Buffer	10X	5.0 $\mu$ L
dNTPs	25 mM (each base)	0.5 $\mu$ L
eIF4E Template	450 ng/ $\mu$ L	0.5 $\mu$ L
Forward Primer	100 ng/ $\mu$ L	2.0 $\mu$ L
Reverse Primer	100 ng/ $\mu$ L	2.0 $\mu$ L
PFU Ultra	2.5 U/ $\mu$ L	1.0 $\mu$ L
Water		39 $\mu$ L



The PCR reaction conditions were:

Initialization	95°C	2 min	
Denaturation	95°C	30 s	} 35 Cycles
Annealing	56°C	30 s	
Elongation	72°C	1 min	
Final Elongation	72°C	10 min	

The amplified eIF4E was purified with a Qiagen PCR Purification Kit. The pET19B vector and the amplified eIF4E were digested (in separate vessels) with NdeI and BamHI at 37°C for 1 hour. The reaction components were:

Component	Concentration	Volume
eIF4E	43.5 ng/μL	23.5 μL
OR		
pET19B PP	30 ng/μL	33.0 μL
Buffer B	10X	5.0 μL
NdeI	10 U/μL	1.0 μL
BamHI	10 U/μL	1.0 μL
Water		19.5 μL (eIF4E); 10 μL (pET19B PP)

The digested pET19B PP vector was further treated with calf-intestinal phosphatase for 30 minutes at 37°C and then purified with a Qiagen Gel Purification Kit. The eIF4E PCR digest was purified using a Qiagen PCR Purification Kit.

The purified pET19B PP vector and eIF4E insert were ligated over night at 16°C using the following reaction components:

Component	Concentration	Volume
eIF4E insert	14 ng/μL	1.14 μL
pET19B PP vector	7 ng/μL	7.0 μL
Ligase Buffer	10X	2.0 μL
DNA Ligase	6 U/μL	1.0 μL
Water		8.9 μL

DH5 $\alpha$  cells were transformed using 4  $\mu$ L of the ligation mixture. The competent cells were thawed on ice and incubated with the ligation mixture for 20 minutes. The cells were then heat-shocked at 42°C for 30 seconds, and then returned to ice for 2 minutes. 350  $\mu$ L of LB-media were added to the cells, and the mixture was shaken at 225 rpm at 37°C for 1 hour. 20  $\mu$ L of this mixture was plated onto an LB agar plate spiked with 50  $\mu$ g/mL ampicillin. Colonies were picked and sequenced to determine if the cloning was successful. The final plasmid was isolated via a Qiagen Mini Prep Kit and used to transform BL(21)-DE3 cells with the same method described above.

#### *m<sup>7</sup>GTP Cap-Affinity Resin*

The cap-affinity resin was synthesized as previously described.<sup>160</sup> 0.5 mL of 10 mM m<sup>7</sup>GTP, 0.1 mL of Sodium Acetate Buffer pH 6, and 5  $\mu$ moles of Sodium Periodate were mixed in a glass vial wrapped in foil. The vial was incubated at 4°C for 1.5 hours without shaking. 1 mL of packed adipic dihydrazide resin was washed with 20 mL of water followed by 20 mL of the Sodium Acetate Buffer. The m<sup>7</sup>GTP mixture was transferred to the resin along with 2 mL of the Sodium Acetate Buffer. This mixture was turned end over end at 4°C for 1.5 hours. 5 mg of Sodium Cyanoborohydride was added to the mixture, and it was turned end over end overnight at 4°C. The resin was washed at least 5 times with 10 mL of 1 M Sodium Chloride. It was then rinsed with Phosphate Buffer pH 7, suspended in about 2 mL of the Phosphate Buffer, and stored at 4°C.

### *His10 eIF4E Expression and Purification*

1 L of LB media was spiked with 50 µg/mL ampicillin and inoculated with 10 mL of starter culture. The culture was grown until the  $OD_{600} = 0.8$ , at which point it was cooled to 16°C, induced with 1 mM IPTG, and shaken over night at 180 rpm. The next morning, the cells were pelleted at 3095xg for 20 minutes. The pellets were frozen between protein expression and purification.

The cell pellets were thawed and resuspended in Lysis Buffer (50 mM Sodium Phosphate pH 7.4, 100 mM Sodium Chloride, 0.5 mM PMSF, 0.5 mM EDTA, 5 mM β-mercaptoethanol, 0.5% Tween 20, 1 mM DTT). The suspension was sonicated at 60% with 5 second pulses followed by 15 seconds of rest for a total of 2 minutes of sonication. The lysate was clarified by centrifugation at 38,000xg for 2 hours. The clarified lysate was incubated with  $m^7$ GTP cap-affinity resin for 45 minutes and the protein bound resin was collected via gravity filtration. The resin was washed with 8 mL of Lysis Buffer followed by two 8 mL washes with Wash Buffer (50 mM Sodium Phosphate pH 7.4, 100 mM Sodium Chloride). The resin was incubated with 5 mL Elution Buffer (50 mM Sodium Phosphate pH 7.4, 100 mM Sodium Chloride, 100 µM  $m^7$ GTP, 5% Glycerol) for 15 minutes, after which the eluate was collected by filtering off the resin. The eluted protein was typically about 0.5 mg/mL for a total yield of 2.5 mg. The protein was stored without concentrating in 50 µL aliquots at -80°C. A representative protein gel is shown in **Figure 2.11**. A large amount of the protein was not soluble, however enough was isolated from the soluble fraction for the SPR assay.

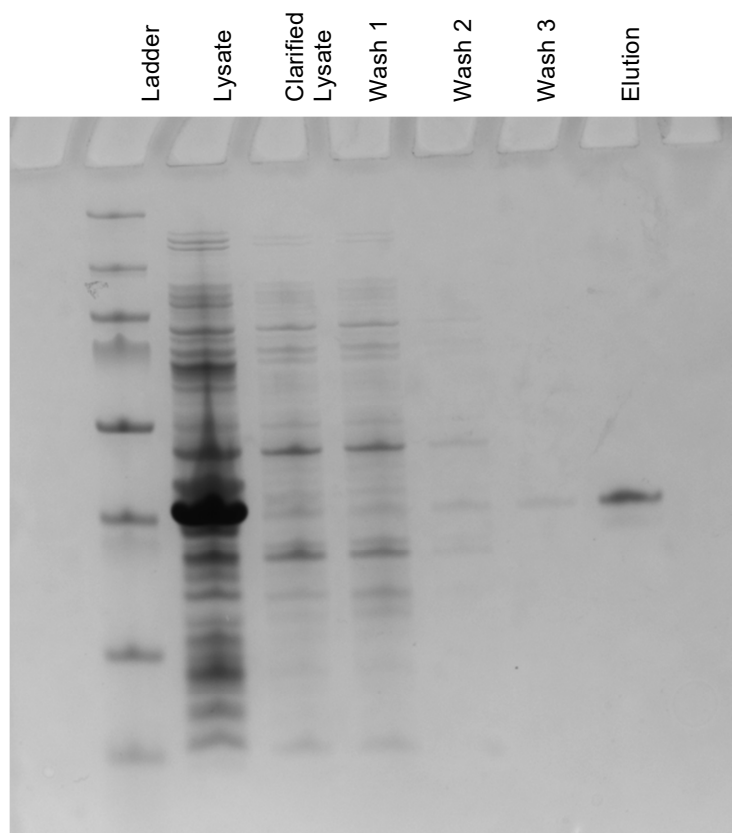


**Figure 2.11 – Typical coomassie gel of His10 eIF4E purification.**

*Optimization of the SPR Assay*

SPR assays were performed on a SensiQ Pioneer instrument using His Cap chips. The chip was conditioned with the following sequence of injections over all three channels:

Component	Injection Volume	Flow Rate
10 mM HCl	20 $\mu$ L	10 $\mu$ L/min
50 mM NaOH	20 $\mu$ L	10 $\mu$ L/min
0.1% SDS	20 $\mu$ L	10 $\mu$ L/min
10 mM HCl	20 $\mu$ L	10 $\mu$ L/min
50 mM NaOH	20 $\mu$ L	10 $\mu$ L/min
0.1% SDS	20 $\mu$ L	10 $\mu$ L/min
500 mM EDTA, pH 8	100 $\mu$ L	20 $\mu$ L/min

Due to the instability of eIF4E and the slow off-rates of our peptides, the chip was completely regenerated for each analyte injection. The following indicates the typical injection sequence for each cycle:

Component	Injection Volume	Flow Rate	Post Time
500 mM EDTA, pH 8	100 $\mu$ L	20 $\mu$ L/min	100 s
50 $\mu$ M NiCl <sub>2</sub>	20 $\mu$ L	10 $\mu$ L/min	30 s
18 $\mu$ g/mL His10 eIF4E	100 $\mu$ L	10 $\mu$ L/min	30 s
0.5 mg/mL BSA	10 $\mu$ L	10 $\mu$ L/min	
Analyte	50 $\mu$ L	50 $\mu$ L/min	120 s
10 mM HCl	5 $\mu$ L	10 $\mu$ L/min	
50 mM NaOH	5 $\mu$ L	10 $\mu$ L/min	
0.1% SDS	5 $\mu$ L	10 $\mu$ L/min	

The His10 eIF4E and BSA were diluted using SPR Running Buffer (10 mM Hepes pH 7.5, 225 mM Sodium Chloride, 10 mM Imidazole, 0.1% Tween 20, 5% Glycerol). The analyte was lyophilized from water and then dissolved in the SPR Running Buffer. Peptides were typically tested at 5 concentrations between 25 nM and 1  $\mu$ M.

Curves were analyzed with QDAT software using a 1:1 ratio to determine on-rates, off-rates, and binding constants.

For kinetic analysis, peptide binding kinetics were analyzed at 10, 15, 20, 25, and 30°C, and at 225, 500, and 1000 mM Sodium Chloride.

### **Cat-ELCCA**

IC<sub>50</sub>'s were calculated using a catalytic Enzyme Linked Click Chemistry Assay (cat-ELCCA), which was developed by my colleague and co-author Dr. James Song. In brief, biotinylated eIF4E was immobilized in a streptavidin coated 384 well plate. The peptide (at 18 different concentrations in duplicate) was added to the well first, followed by 4E-BP1 protein with an m-tetrazine tag. This mixture was allowed to incubate for 1 hour, at which point the wells were washed thoroughly prior to

incubation with HRP tagged with trans-cyclooctene for one hour. After the click reaction, the wells were washed and then incubated with HRP substrate. Chemiluminescence was read with a plate reader. Except where noted otherwise, this assay was performed in triplicate (on three separate days) to obtain final IC<sub>50</sub> curves. Data was analyzed using a nonlinear regression dose response analysis with variable slope in Graphpad Prism.

### **Peptide Synthesis**

Linear peptides were purchased from New England Peptide. Stapled peptides were synthesized by Dr. James Song, except for HCS-eIF4G, which was synthesized by Alyah Chmiel. The peptides were synthesized and purified using methods similar to those described in Chapter 3.

### **Circular Dichroism**

Peptides were dissolved to 100  $\mu$ M in 5 mM sodium phosphate buffer, pH 7.4. Data was recorded using a Jasco I-1500 CD-Spectropolarimeter. Measurements were taken between 180 and 260 nm with a step resolution of 0.1nm and a speed of 100 nm/sec. For the CD spectra of eIF4E, measurements were taken between 200 and 300 nm, and for the peptides dissolved in 1M NaCl, measurements were taken between 200 and 260 nm. 5 accumulations were taken with the response time set to 1 s, bandwidth to 5 nm, and pathlength of 0.1 cm. The  $\alpha$ -helical content of each peptide was calculated by dividing the mean residue ellipticity  $[\varphi]_{222_{\text{obs}}}$  by the theoretical  $[\varphi]_{222}$  for a helical acetylated peptide of equivalent length. For determination of temperature dependence, 100  $\mu$ M samples were equilibrated to 10

°C, 15 °C, 20 °C, 25 °C and 30°C, and measurements were taken as above at each temperature.

## Chapter 3

### Designing a Stapled Peptide to Probe the eIF4E–eIF4G PPI

#### 3.1 Stapled peptides

Peptides have several advantages over small molecule inhibitors when considering protein–protein interactions. While small molecules typically require some kind of pocket to bind with any specificity, peptides have been designed by nature to specifically bind to large, flat protein surfaces. However, peptides often require cell penetrating sequences in order to access targets in the cytoplasm or nucleus, which can increase the cost and the potential for toxicity, and once inside the cell they are subject to cleavage by proteases. Stapling, or covalently linking two amino acid side chains to stabilize the  $\alpha$ -helix, has been proposed as a solution to some of these problems, since increased helicity reduces the exposure of the amide backbone, which can potentially shield from proteases and increase cell penetration.

Early efforts to constrain peptides into a helix involved the use of hydrophobic residues, salt bridges, and the introduction of different helix capping groups to non-covalently stabilize the helix.<sup>161–166</sup> Stabilization with lactam staples<sup>167</sup> and disulfide bridges<sup>168</sup> have also been explored to covalently increase helicity. In 1998, the Grubbs group published the first use of olefin metathesis for peptide stapling, in which they used allyl serine derivatives for the metathesis and observed a small increase in



helicity.<sup>169</sup> This work was followed by the Verdine lab, which developed an all hydrocarbon staple which significantly increased peptide helicity.<sup>170</sup> This led to the development of several hydrocarbon stapled peptides,<sup>171,172</sup> some of which are in clinical trials. In addition to increased helicity, hydrocarbon stapled peptides have been shown in some cases to have increased cell permeability<sup>173,174</sup> and proteolytic stability.<sup>175</sup>

While the hydrocarbon staple has been used to successfully improve the drug-like characteristics of peptides, hydrocarbon stapled peptides do not necessarily have enhanced binding or cell penetration.<sup>176</sup> Additionally, hydrocarbon stapled peptides are sometimes not inherently more penetrant without other optimizations, such as adding positive charge.<sup>177</sup> There are many other staple options which have been discussed in the literature. Felix et al. reported the first lactam stapled peptides, which were analogues of growth hormone releasing factor 2 and demonstrated increased helicity and activity in cell culture,<sup>178</sup> and the Fairlie lab optimized short lactam stapled peptides which were very helical in water and stable to trypsin proteolysis when compared to the linear peptides.<sup>179</sup> Other staple options include cycloadditions, such as copper-catalyzed click reactions, formation of disulfides and thioethers, and a variety of two-component staples.<sup>180</sup> It is likely that the ideal staple type is both system and sequence dependent.

Most of the examples of stapled peptides are mimicking highly ordered binding sites. The goal of stapling is to achieve maximum helicity, sometimes over 95% helical even in the absence of the helix inducer trifluoroethanol. Our stapled peptides will be mimicking disordered proteins, and even when they order upon binding the

bound peptide is about 50% helical. One other stapled peptide, sTIP-04, has been reported for our system, and was compared to our other hydrocarbon stapled peptides in Chapter 2. sTIP-04 was designed using molecular dynamics simulations to determine the favored conformational states of bound and free eIF4G based peptides. The peptides were then mutated to alter their conformational distribution to favor the bound state. sTIP-04 introduced serine, glutamine, and leucine residues in place of aspartic acid and two phenylalanines. It had a  $K_D$  of 5 nM and was 63% helical. sTIP-04 uses a hydrocarbon staple which is 8 carbons long and has methyl groups in the  $\alpha$  position of the stapling amino acids.<sup>1</sup> Based on the success of this peptide, and the success of the hydrocarbon staple in the literature, our first 4E-BP1 stapled peptides were constructed using a hydrocarbon staple.

A few unstapled 4E-BP1 and eIF4G peptides have had some success in the literature. A Tat-fused eIF4G1 peptide which was optimized for helicity showed activity in cell culture at 400  $\mu$ M,<sup>109</sup> and a gonadotropin releasing hormone (GnRH) conjugated 4E-BP1 peptide inhibited cap-dependent translation in GnRH receptor expressing cells and reduced tumor size in mice.<sup>181</sup> These results are encouraging, although there is room for improvement since conjugated peptides are not ideal for probes or therapeutics. The same group which developed sTIP-04 also found that, when making their phage display optimized sequence, the binding position of the peptide changed slightly with each modification.<sup>110</sup> In this chapter, we use the information already known about the eIF4E-interacting peptides to design new peptides with different mutations and staple types with the goal of making a highly potent probe.

### 3.2 Structure activity relationships of linear 4E-BP1 and eIF4G peptides

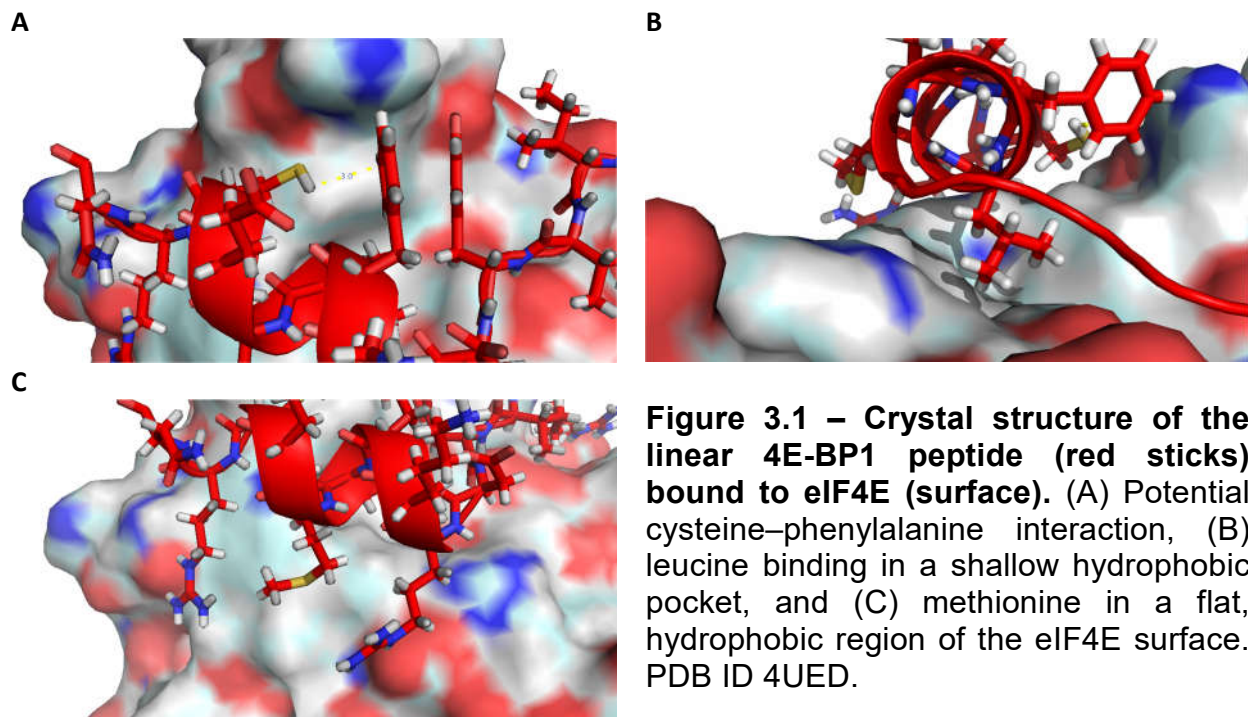
We purchased a series of linear peptides to determine the effects of certain amino acid changes on peptide affinity and helicity. Most of the peptides were based around the 4E-BP1 sequence, but some were based off of the eIF4G sequence. The 4E-BP1 peptides are shown in **Table 3.1**. Our parent sequence, denoted as 4E-BP1 (G<sup>49</sup>-N<sup>64</sup>) in Chapter 2, is called 4E-BP1-1 here. We also made a peptide based off the sequence of the 4E-BP2 protein, which is called 4E-BP1-2. This peptide had a 3-fold improvement in activity over the 4E-BP1 sequence. Removing the C-terminal asparagine and the N-terminal glycine and threonine (4E-BP1-3) resulted in equal activity as 4E-BP1-1, but re-instating that asparagine actually resulted in improved activity (4E-BP1-4). Extending the sequence towards the C-terminus (4E-BP1-5) did not provide an increase in activity.

**Table 3.1 – Series of linear 4E-BP1 based peptides and their IC<sub>50</sub>s obtained with cat-ELCCA and their helicities determined with circular dichroism.**

4E-BP1 (G <sup>49</sup> -P <sup>66</sup> )	G T R I I Y D R K F L M E C R N S P	IC <sub>50</sub> (nM)	%Helicity	% Helicity (40% TFE)
1	G T R I I Y D R K F L M E C R N	70 ± 20	16	37
2	R I I Y D R K F L L D R R N	13 ± 3	13	35
3	R I I Y D R K F L M E C R	70 ± 10	20	58
4	R I I Y D R K F L M E C R N	41 ± 9	12	41
5	R I I Y D R K F L M E C R N S P	40 ± 7	14	44
6	R I I Y S R K Q L M E C R N	12 ± 2	12	41
7	R I I Y D R K F L M E A R	160 ± 40	7	35
8	K K R Y D R K F L M E C R N	400 ± 100	8	28
9	Y D R K F L M E C R N S P	8000 ± 4000	10	38
10	G T R I I Y D R K F L L E C K N	500 ± 100	13	38
11	G T R I I Y D R K F A A E C R N	dnb	10	32

4E-BP1-6 attempts to make the same mutations to the 4E-BP1 sequence that are made in the sTIP-04 peptide. These mutations led to a 3-fold increase in activity.

Mutation of the cysteine residue to an alanine resulted in only a 2-fold loss in activity (4E-BP1-7), which is interesting since the cysteine does not appear to participate in any hydrogen bonding with the surface of eIF4E in the crystal structure (**Figure 3.1 A**). We suspect that the cysteine residue may be making a thiol- $\pi$  interaction with the phenylalanine, stabilizing the helix.



We wondered if adding the lysines and arginine to the N-terminus would give the 4E-BP1 peptide the kinetic advantage of the more disordered eIF4G peptide while maintaining the order of the 4E-BP1 peptides, but this hybrid (4E-BP1-8) had a 10-fold loss in activity. This could be because the N-terminal arginine and isoleucines were critical for activity in the 4E-BP1 sequence, because removing them (4E-BP1-9) resulted in the loss of nearly all activity, even though the canonical binding site (YXXXXL $\phi$ ) was still present. 4E-BP1-10 is based off the 4E-BP3 protein sequence and is 7-fold worse than the corresponding 4E-BP1 sequence. Finally, in

4E-BP1–11 we mutated the leucine and methionine residues to alanines. These residues are in the canonical binding site and, as expected, their mutation completely removes all activity (**Figure 3.1 B and C**).

Interestingly, there is no correlation between helicity and IC<sub>50</sub>, with or without the helix inducer TFE. However, some mutations did lead to interesting changes in conformation. Since the helicity listed is the percent of the sequence that is helical, these numbers are dependent on the length of the peptide. Therefore, the increased helicity of 4E-BP1–3 is likely in part simply because it is shorter. However, 4E-BP1–9 is of equivalent length and still contains the entire binding helix seen in the crystal structure, but is only half as helical as 4E-BP1–3. 4E-BP1–7 is also nearly 3–fold less helical as compared to the 4E-BP1 peptide of equivalent length, indicating that the cysteine contributes significantly to the helical nature of the peptide. We also know that the serine and glutamine residues introduced in 4E-BP1–6 increase the activity of the peptide, but not the helicity, but the lysine and arginine residues in 4E-BP1–8 reduce both the activity and the helicity. Finally the 4E-BP1–10 sequence has similar helicity to 4E-BP1–1, but significantly reduced activity, and while 4E-BP1–11 does not inhibit, it still is somewhat helical.

**Table 3.2 – eIF4G based peptides with IC<sub>50</sub>s determined using cat-ELCCA and helicities from circular dichroism.**

eIF4G (K <sup>608</sup> – L <sup>622</sup> )	K K R Y D R E F L L G F Q F	IC <sub>50</sub> (nM)	%Helicity	% Helicity (40% TFE)
1	K K R Y D R E F L L G F Q F	160 ± 30	3	24
2	K K Q Y D R E F L L D F Q F	900 ± 200	4	19
3	K K R Y S R E F L L G F	450 ± 70	2	21
4	K K R Y S R E Q L L G L	500 ± 100	4	13

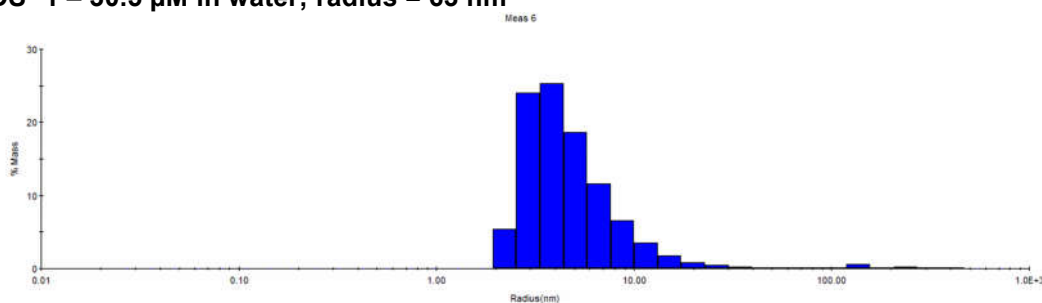
We next investigated the properties of a series of eIF4G peptides, shown in **Table 3.2**. As seen in Chapter 2, the peptides were universally weaker inhibitors and less helical than the 4E-BP1 peptides. eIF4G-2, which is based off of the sequence of the eIF4GII protein,<sup>182</sup> has 5-fold reduced activity compared to eIF4G-1. eIF4G-3 was designed to further discern the importance of the mutations made in sTIP-04, but our linear version of sTIP-04 (eIF4G-4) had such poor activity that we couldn't draw many conclusions. All of the eIF4G peptides were much less helical than the 4E-BP1 peptides, and they also had a decreased propensity for helicity with the addition of TFE. Curves for IC<sub>50</sub> and helicity are shown in Appendix B, Chapter 3 – Supplemental Information – IC<sub>50</sub>s and – CD.

### 3.3 Structure activity relationships of stapled 4E-BP1 peptides

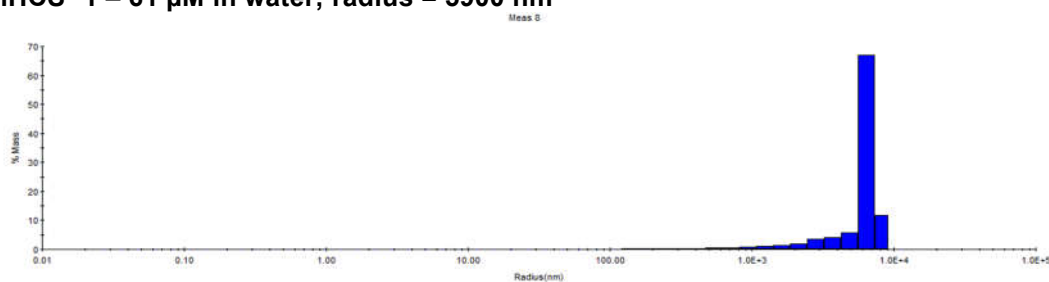
We hoped to use the information from our linear peptides to design potent stapled peptides. Our first stapled peptides were hydrocarbon staples based off of Verdine's work. Dr. Lauren Mishra initiated the project with the synthesis of mHCS-1 (shown in **Table 3.3**), and most of our early studies both in cells and *in vitro* were done with that peptide. As such, most of our early SAR focused on that staple type. Unfortunately, the mHCS staple along with the HCS staple discussed in Chapter 2 had significant problems with their physical properties that hindered progress. For instance, they were poorly soluble, and on several occasions formed a gel which was impossible to completely dissolve in any solvent. Additionally, the methionine and cysteine residues, which we still have not managed to get rid of, made the peptides unstable in DMSO because they would quickly oxidize or dimerize. The peptides also

aggregated in water, even at very low concentrations (**Figure 3.2**), and we think this aggregation was irreversible (or at least difficult to reverse) above a certain concentration, which caused our peptides to be sometimes active in cells, and sometimes not, potentially based on the concentration of the stock solution.

**mHCS-1 – 30.5  $\mu$ M in water; radius = 63 nm**



**mHCS-1 – 61  $\mu$ M in water; radius = 5900 nm**



**mHCS-1 – 122  $\mu$ M in water; radius = 1300 nm**

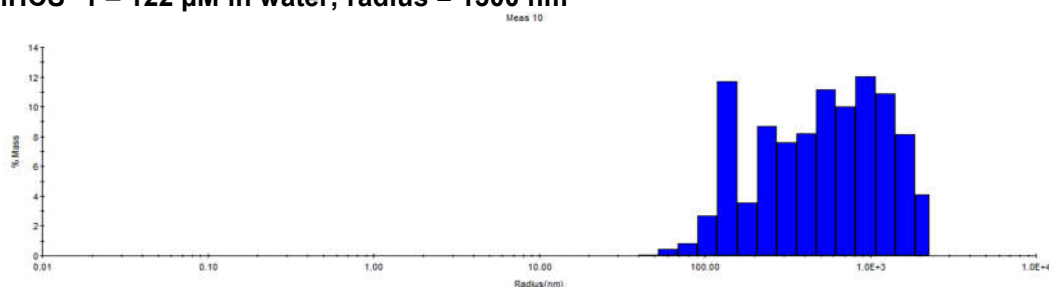


**Figure 3.2 – Aggregation of mHCS-1 visualized by dynamic light scattering.**

Despite these issues, we were able to make a series of hydrocarbon stapled peptides, which are shown in **Table 3.3**. Fortunately, the addition of the staple did improve the activity of the 4E-BP1-1 sequence by 2-fold (mHCS-1). Unfortunately, very few of the trends observed with the linear peptides held true for the stapled peptides. For instance, mHCS-2 is the stapled version of 4E-BP1-2, which is based

on the 4E-BP2 protein sequence. While 4E-BP1-2 showed significant improvement over 4E-BP1-1, mHCS-2 is significantly worse than mHCS-1 (**Figure 3.3 A**). Furthermore, the truncation of the 4E-BP1 sequence in 4E-BP1-3 appeared to be tolerated, but its stapled version, mHCS-3, is 7-fold worse than mHCS-1 (**Figure 3.3 B**). Finally, introducing the serine and glutamine mutations in the linear sequence (4E-BP1-6) improved activity, but the stapled equivalent was 5-fold less active (**Figure 3.3 C**).

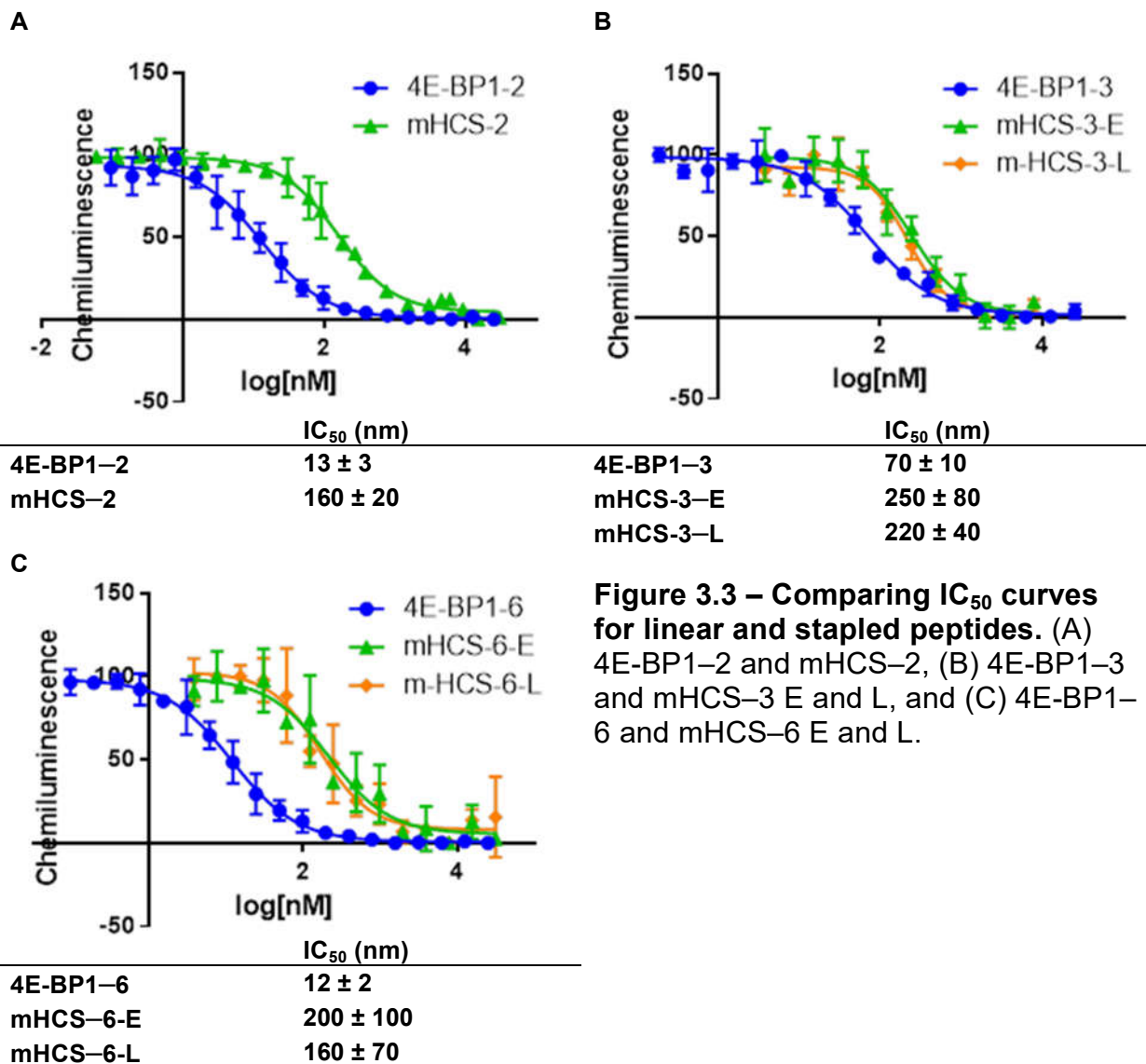




**Table 3.3 – Series of mHCS peptides.** IC<sub>50</sub>s were determined with cat-ELCCA and helicities with circular dichroism. \* indicates that two isomers were isolated, but only data for the most active isomer is shown. N<sub>L</sub> = Norleucine

mHCS		IC <sub>50</sub> (nM)	%Helicity	% Helicity (40% TFE)
1	G T R I I Y D R X F L M X C R N	30 ± 10	12	38
2	G T R I I Y D R X F L L X R R N	160 ± 20	27	
3*	R I I Y D R X F L M X C R	220 ± 40	8	37
4	G T R I I Y D R X F L N <sub>L</sub> X V R N	310 ± 70	11	
5	G T R I I Y D R X F L N <sub>L</sub> X S R N	130 ± 50	5	
6*	R I I Y S R X Q L M X C R N	160 ± 70	9	45
7*	R I I Y D R X F * M X C R	430 ± 90	8	
8	R I I Y D R X F * M X C R	1000 ± 100	3	1
9*	R I I Y D R X F L * X C R	300 ± 90	16	56
10	R I I * D R X F L M X C R	2500 ± 800	16	44

Our efforts to mutate the methionine and cysteine in order to improve peptide stability were unsuccessful. mHCS-4, which mutated the cysteine to a valine and methionine to norleucine, had a 10-fold higher IC<sub>50</sub> than mHCS-1. Interestingly, this peptide's K<sub>D</sub> was similar to mHCS-1 (**Table 3.7**), but it showed no activity in cells. For mHCS-5, in which we mutated the cysteine to a serine and methionine to norleucine, had an improved IC<sub>50</sub> but worse K<sub>D</sub> when compared to mHCS-4. In the crystal structure, it appears that the cysteine is not hydrogen bonding with eIF4E, but is in fact interacting with the phenylalanine residue in the helix (**Figure 3.1 A**). Perhaps mHCS-4 and 5 are unable to interact in the same manner. These mutations need to

be made separately to further determine the effects of each amino acid. Attempts to mutate the leucine residue failed (mHCS–7 and 8), and exchanging the methionine residue for O-methylhomoserine (mHCS–9) or the tyrosine for homotyrosine (mHCS–10) also resulted in decreased activity.

Introducing the hydrocarbon staple did not generally have the expected effect on helicity. mHCS–1 and 3 are less helical than their linear counterparts, although mHCS1 has improved activity and mHCS–3 has decreased activity. In fact, nearly every peptide we made with the mHCS staple is less helical than the linear 4E-BP1 peptides examined. Many of the peptides with the most dramatic losses in helicity (mHCS 3, 5, and 8) did also have drastic losses in activity, but many of the less active peptides were also relatively quite helical (i.e. mHCS–2, 9, and 10).

**Table 3.4 – Comparison between early (E) and late (L) isomers for certain mHCS peptides.**

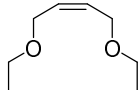
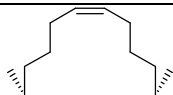
mHCS	IC <sub>50</sub> (nM)	%Helicity	% Helicity (40% TFE)
3 E	250 ± 80	7	31
3 L	220 ± 40	8	37
6 E	200 ± 100	6	32
6 L	160 ± 70	9	45
7 E	1500 ± 300	28	
7 L	430 ± 90	8	
9 E	300 ± 90	16	56
9 L	700 ± 80	9	25

Work on this staple was further complicated by the fact that with every one of these mHCS stapled peptides, we observed two peptides of the same mass with slightly different retention times in our crude peptide cleavage. We suppose these two different peptides are two different isomers, and we suspect they are cis and trans isomers of the staple. However, my colleague Dr. James Song found that the

peptides are too flexible in solution to prove this theory by NMR. Regardless, the presence of the two peptides made purification extremely difficult, because we needed to separate the isomers from each other, as well as from all of the other impurities from synthesis. The fact that the peptides smeared on the HPLC column under all conditions didn't help. Even so, we did manage to at least isolate one pure isomer from each synthesis, and in some cases we were able to isolate both. **Table 3.3** shows the most active isomer that we isolated in the case where we got both, but **Table 3.4** compares the two isomers side-by-side.

Since we were unable to determine difference between the two isomers, we simply referred to them as “early” or E and “late” or L based on their retention time. In some cases, the isomers were nearly identical both in terms of activity and helicity (for instance, mHCS 3 and 6). In other cases, the peptides were quite different. mHCS–7-E and mHCS–10-L are both more helical and less active than their counterparts, but mHCS–9-E was more helical more active than mHCS–9-L.

**Table 3.5 – Series of OAISer and HCS peptides.**

OAISer		IC <sub>50</sub> (nM)	%Helicity	% Helicity (40% TFE)
1	G T R I I Y D R X F L M X C R N	28 ± 7		
HCS				
1	G T R I I Y D R X F L M X C R N	5 ± 2	44	83
2	G T R I I Y D R X F A A X C R N	8000 ± 7000	35	64
3	K K R Y D R X F L L X F	6000 ± 1000	3	20
4	K K R Y S R X Q L L X L	23 ± 7	38	58

While the mHCS peptides were initially very promising, we elected to explore other staple types in order to mitigate the problems with solubility and purification. We made an O-Allyl Serine stapled peptide, OAISer–1, shown in **Table 3.5**. This peptide

was even less soluble than mHCS-1, and it seemed to degrade very quickly, so we instead proceeded with an HCS staple, discussed in Chapter 2 and shown in **Table 3.5**. The HCS staple resulted in a significant increase in helicity for the 4E-BP1 peptides and for sTIP-04. Also, HCS-1 had significantly better activity than 4E-BP1-1 and mHCS-1 (**Figure 3.4**), had the best *in vitro* activity of any peptide we had tested so far, it was active in our cell assays, it got into cells, and it did not form two isomers, so it was (relatively) easy to purify.

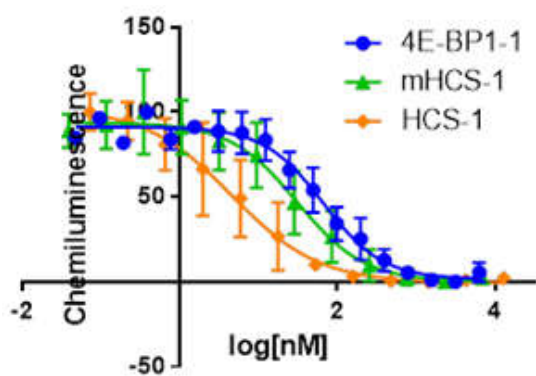


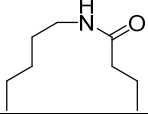
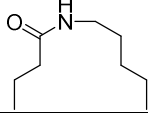
**Figure 3.4 – Comparison of IC<sub>50</sub> curves between 4E-BP1-1, mHCS-1, and HCS-1.**

	IC <sub>50</sub> (nM)
4E-BP1-1	70 ± 20
mHCS-1	30 ± 10
HCS-1	5 ± 2

The HCS peptides solved a lot of our problems, but they still were poorly soluble, they aggregated in solution, and sometimes suffered from poor reproducibility. Additionally, the amino acid used to make them was very difficult to make and very expensive to buy. We therefore tried lactam staples to see if we could maintain the excellent activity of HCS-1 while improving upon the physical properties of the peptides. We made two orientations of the lactam staple, LacA and LacB, shown in **Table 3.6**. At this point, we also elected to focus on the shorter 4E-BP1 sequence in hopes that we could decrease the cost and labor associated with making these

peptides. LacA-1 had similar activity as mHCS-1, but worse activity than HCS-1. However, it did have better solubility (by about 4-fold), so this result was encouraging. We also tried adding an N-methylated aspartic acid, shown in LacA-2, with the hopes of improving its proteolytic stability. However, this mutation significantly reduced activity.

**Table 3.6 – Series of lactam stapled peptides, LacA and LacB.**

LacA		IC <sub>50</sub> (nM)	%Helicity	% Helicity (40% TFE)
1	R I I Y D R X F L M X C R	27 ± 5	19	55
2	R I I Y * R X F L M X C R	300 ± 200	14	34
LacB				
1	R I I Y D R X F L M X C R	8 ± 3	40	80
2	R I I Y S R X Q L M X C R N	7 ± 4	20	47

LacB-1, on the other hand, had similar activity as HCS-1 despite its shortened sequence. It also had a 3-fold improvement in *in vitro* activity over LacA-1. While we wondered if the significant increase in activity was due to the significantly increased helicity, we found that the serine and glutamine mutant, LacB-2, had equal potency as LacB-1 but similar helicity to LacA-1. We therefore used SPR to collect kinetic data for all of the stapled peptides to help determine the reasons for the differences in activity that we saw.

### 3.4 Kinetic analysis of 4E-BP1 stapled peptides

When examining the stapled peptide kinetics, we found some surprising trends (Table 3.7). For instance, the  $K_D$  does not correlate very well with the  $IC_{50}$ . There is also no strong correlation between  $k_a$  or  $k_d$  and  $IC_{50}$ . However, in the case of the mHCS isomers, the isomer with the faster off-rate has a worse  $IC_{50}$ . In general, it seems that the kinetics of interaction and their effect on inhibition is peptide specific. In some cases, the off-rate appears to drive inhibition, but in others the on-rate seems to be the bigger contributor. Sensorgrams for all peptides are found in Chapter 3 – Supplemental Information – SPR.

**Table 3.7 – Binding kinetics of the mHCS and OAISer peptides determined by SPR.**

mHCS	$K_a$ ( $M^{-1}s^{-1}$ )	$K_d$ ( $s^{-1}$ )	$K_D$ (nM)	$IC_{50}$ (nM)
1	$4.69 \pm 0.02 \times 10^5$	$11.27 \pm 0.02 \times 10^{-3}$	$24.0 \pm 0.1$	$30 \pm 10$
2	$2.7 \pm 0.4 \times 10^5$	$9 \pm 1 \times 10^{-3}$	$36 \pm 4$	$160 \pm 20$
3-E	$0.773 \pm 0.002 \times 10^5$	$6.66 \pm 0.01 \times 10^{-3}$	$86.2 \pm 0.3$	$250 \pm 80$
3-L	$0.732 \pm 0.001 \times 10^5$	$5.276 \pm 0.008 \times 10^{-3}$	$72.0 \pm 0.2$	$220 \pm 40$
4	$7.22 \pm 0.03 \times 10^5$	$21.26 \pm 0.02 \times 10^{-3}$	$24.9 \pm 0.1$	$310 \pm 70$
5	$0.2 \pm 0.1 \times 10^5$	$28 \pm 3 \times 10^{-3}$	$2000 \pm 120$	$130 \pm 50$
6-E	$1.34 \pm 0.01 \times 10^5$	$4.62 \pm 0.2 \times 10^{-3}$	$35 \pm 5$	$200 \pm 100$
6-L	$1.05 \pm 0.09 \times 10^5$	$3.6 \pm 0.2 \times 10^{-3}$	$35 \pm 6$	$160 \pm 70$
7-E	$3.0 \pm 0.8 \times 10^5$	$18 \pm 3 \times 10^{-3}$	$65 \pm 7$	$1500 \pm 300$
7-L	$0.1947 \pm 0.0006 \times 10^5$	$8.41 \pm 0.02 \times 10^{-3}$	$432 \pm 1$	$430 \pm 90$
9-E	$1.80 \pm 0.02 \times 10^5$	$5.17 \pm 0.02 \times 10^{-3}$	$28.8 \pm 0.5$	$300 \pm 90$
9-L	$5.43 \pm 0.07 \times 10^5$	$12.5 \pm 0.4 \times 10^{-3}$	$23 \pm 1$	$700 \pm 80$
10	$0.32 \pm 0.04 \times 10^5$	$5 \pm 1 \times 10^{-3}$	$180 \pm 60$	$2500 \pm 800$
<b>OAISer</b>				
1	$0.8 \pm 0.2 \times 10^5$	$5.1 \pm 0.7 \times 10^{-3}$	$80 \pm 20$	$28 \pm 7$

For the remaining peptides in Table 3.8, the trend is more consistent. HCS-1 has a very fast on rate and a rather slow off-rate, which explains why that compound is such a strong inhibitor *in vitro*. sTIP-04 (HCS-4) has a similar  $K_D$  to HCS-1, but a weaker  $IC_{50}$ . This could potentially be explained by its slower on-rate. LacA-1 has

similar kinetic trends as compared to HCS–1, and LacB–1 has an on-rate that is twice as fast as HCS–1’s, which results in a  $K_D$  of 2 nM. This data confirms that we have effectively designed a stapled peptide with equivalent potency as HCS–1 but with superior solubility. As a bonus, LacB–1 is also much easier to purify because it does not smear on the column. With this data in hand, we proceeded to test our best peptides in cell assays to determine how to proceed.

**Table 3.8 – Binding kinetics for the HCS and lactam stapled peptides.**

HCS	$K_a$ ( $M^{-1}s^{-1}$ )	$K_d$ ( $s^{-1}$ )	$K_D$ (nM)	$IC_{50}$ (nM)
1	$15 \pm 2 \times 10^5$	$5 \pm 4 \times 10^{-3}$	$4 \pm 3$	$5 \pm 2$
3	$3.3 \pm 0.1 \times 10^5$	$30 \pm 4 \times 10^{-3}$	$90.0 \pm 0.3$	$6000 \pm 1000$
4	$8.3 \pm 0.5 \times 10^5$	$5.2 \pm 0.1 \times 10^{-3}$	$6.3 \pm 0.4$	$23 \pm 7$
<b>LacA</b>				
1	$5.82 \pm 0.06 \times 10^5$	$4.18 \pm 0.03 \times 10^{-3}$	$7.2 \pm 0.1$	$27 \pm 5$
2	$1.5 \pm 0.2 \times 10^5$	$10.9 \pm 0.8 \times 10^{-3}$	$74 \pm 3$	$300 \pm 200$
<b>LacB</b>				
1	$30.9 \pm 0.2 \times 10^5$	$6.87 \pm 0.01 \times 10^{-3}$	$2.23 \pm 0.01$	$8 \pm 3$

### 3.5 Cell activity of 4E-BP1 stapled peptides

The cell data for the HCS peptides is shown in Chapter 2. All cell data (excluding the CAPA assay in section 3.6) was collected by Arya Menon. Cells were treated with the peptide for 6 hours and then lysed. Resin-bound  $m^7GDP$  was added to bind to the eIF4E. The resin was boiled and a Western blot was used to visualize the levels of 4E-BP1 and eIF4G pulled down. **Figure 3.5** shows that LacA–1 was not active in cells, despite the fact that its  $IC_{50}$  is equivalent to mHCS–1, which is active in cells. LacB–1 did inhibit the pull-down of 4E-BP1 and eIF4G in Tamoxifen resistant MCF7 cells and in MDA-MB-231 cells. We also confirmed that the effect was dose dependent in MDA-MB-231 cells, which is shown in **Figure 3.6**. Interestingly, the

effect on eIF4G appears to be less pronounced than the effect on 4E-BP1. This could be due to the levels of the eIF4G and 4E-BP1 proteins in the cell.

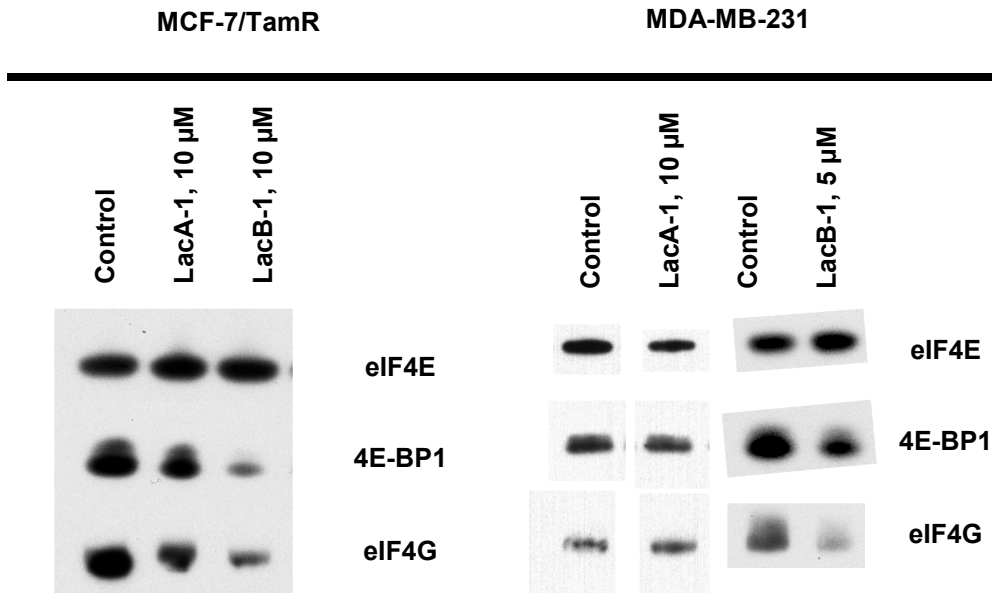


Figure 3.5 – Pulldown data for LacA-1 and LacB-1 in Tamoxifen resistant MCF-7 and MDA-MB-231 cells.

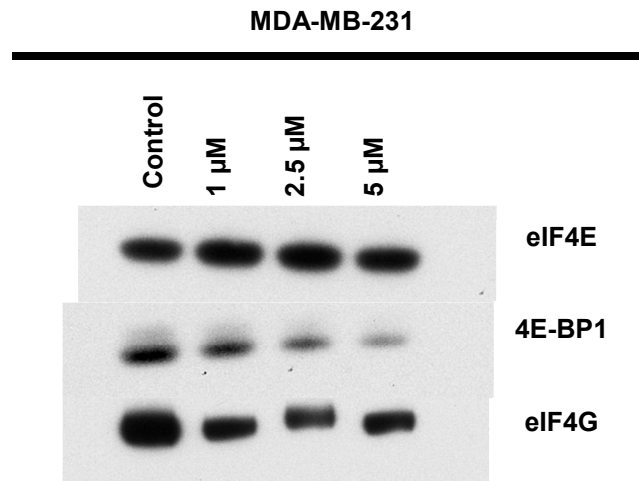


Figure 3.6 – Concentration dependence in pulldown assay for LacB-1 in MDA-MB-231 cells.



### 3.6 Cell penetration of lactam stapled peptides

The cell penetration of the HCS peptides was measured by imaging of FITC-labeled peptides as shown in Chapter 2. However, the FITC tag decreased the solubility of these peptides significantly, so we decided to pursue other options for measuring cell penetration. LacA-1, LacB-1, and LacB-2 were all tested in a Chloroalkane Penetration Assay (CAPA) developed by the Kritzer lab and run by Kirsten Deprey.<sup>183</sup> In brief, Hela cells expressing the Halotag protein in the cytoplasm were treated with peptide with a chloroalkane linker on the N-terminus for 4 hours. The cells were then treated with a fluorophore with the same chloroalkane linker. The assay measured the decrease in signal from the fluorophore to obtain a CP<sub>50</sub>, or the concentration at which 50% of the fluorescent signal is present. LacA-1, LacB-1, and LacB-2 were tested, as well as a LacB-1 peptide with the addition of three arginine residues on the amino terminus. The results of this assay are shown in **Figures 3.7 and 3.8**.

The cell penetration of our peptides is within the range of other well-known peptides. When tested in the same assay, the hydrocarbon stapled peptide Bim-SAHB<sup>172</sup> had a CP<sub>50</sub> of 0.65  $\mu$ M, Arg9 had a CP<sub>50</sub> of 0.3  $\mu$ M, and TAT had a CP<sub>50</sub> value of 3.1  $\mu$ M. This data indicates that our peptides successfully penetrate the cell without the use of a tag. Interestingly, LacB-1 is 6 times more cell penetrant than LacA-1, which likely explains why LacB-1 shows activity in our eIF4E pulldown assay while LacA-1 does not. The addition of three arginines to the amino terminus of LacB-1 did not increase cell penetration, which is likely because LacB-1 is already

equally penetrant as Arg9. Finally, while LacB-2 has an encouraging IC<sub>50</sub> value, it is 3-fold less penetrant than LacB-1.

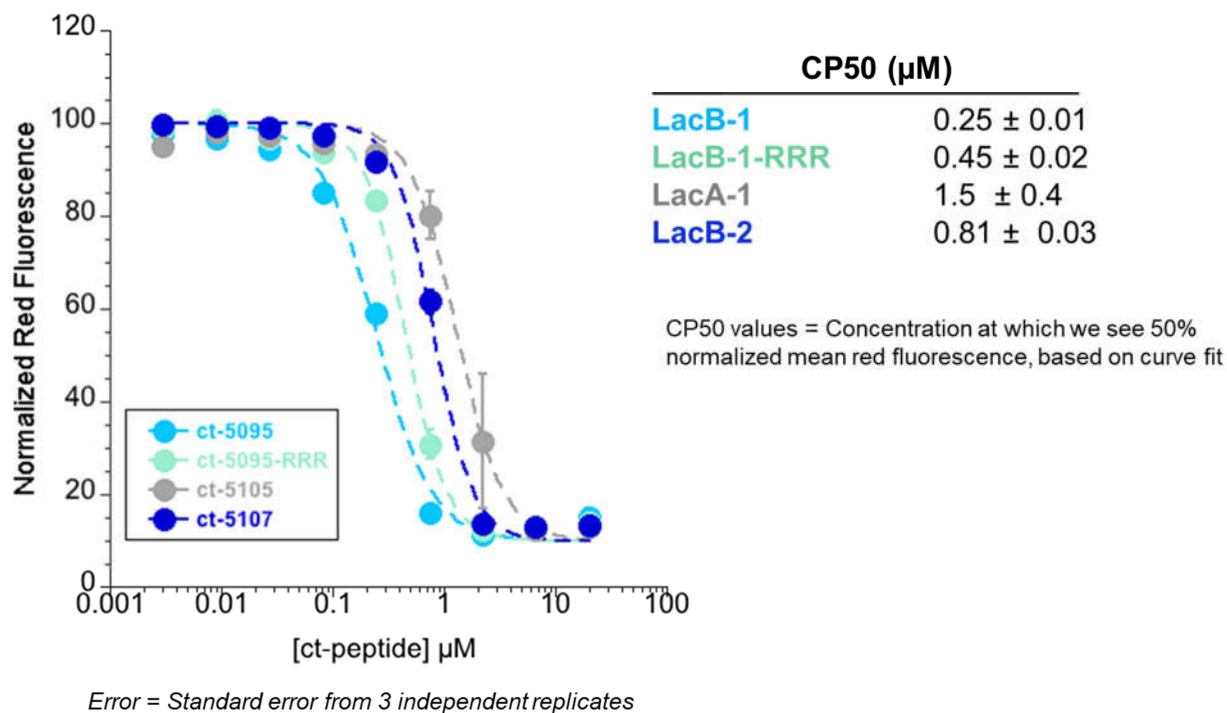


**Figure 3.7 – Cell-penetration of lactam stapled peptides, as determined using the CAPA assay.**

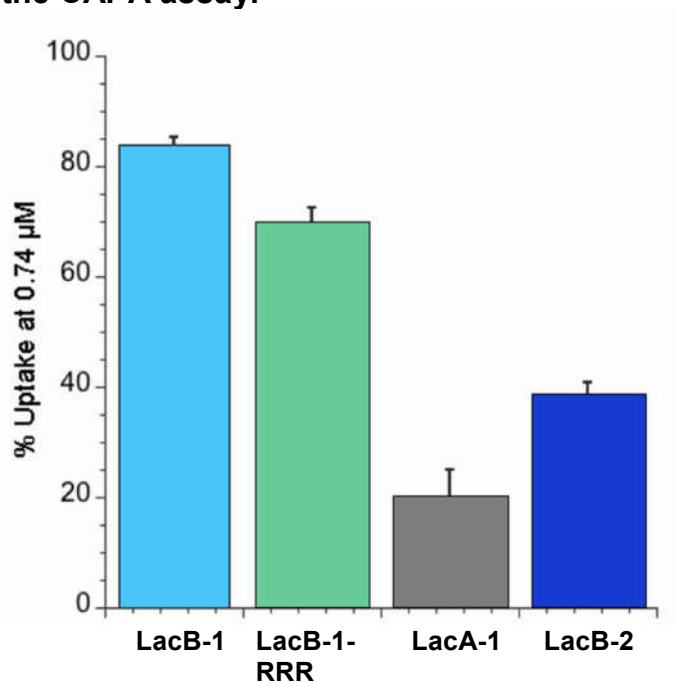


**Figure 3.8 – Percent uptake of peptide at 0.74 μM, as determined by CAPA.**

**Figure 3.8** shows that the peptide is entering the cell, at least somewhat, at the concentrations tested in our cap pulldown assay. However, the difference in penetration between the peptides is quite surprising. We cannot at this time explain the difference in penetration between LacB-1 and LacA-1. LacB-1 is twice as helical as LacA-1, however, so we hypothesize that LacB-1 is more efficient at shielding its amide backbone to travel through the membrane. This process could also be involved in release from the endosomes once inside the cell. We are currently solving the solution NMR structure of LacB-1 and LacA-1 to help explain the difference in cell uptake.

### **3.7 Conclusions**

We found that the mHCS staple is very difficult to work with, at least with the 4E-BP1 sequence, due to its tendency to form two different isomers. While the more constrained HCS staple did not form multiple isomers, it was still very hydrophobic and the peptides were poorly soluble and tended to aggregate in solution. Even the synthesis of the hydrocarbon stapled 4E-BP1 peptides was difficult, and it was necessary to use low loading resin to avoid aggregation, even in organic solvent when most of the amino acids were protected. This is in contrast to the sTIP-04 peptide, which is relatively very soluble in water, has a high-yielding synthesis, and does not appear to aggregate. This could potentially be because the sTIP-04 peptide is shorter (12 amino acids), but we found that the mHCS truncated 4E-BP1 peptide (mHCS-3), which is 13 amino acids long, was not active. Based on this data, we can say that the

ideal staple type depends on sequence, and while the hydrocarbon staple can pose problems due to hydrophobicity, it does not always cause problems.

With regards to the 4E-BP1 peptides, we found that the lactam staple dramatically improved the physical properties of the peptides while maintaining the strong binding affinity and inhibition. This is not surprising, because the lactam stapled peptide is much less hydrophobic than the hydrocarbon staples. However, we were not expecting to see such a large difference between the LacA and LacB staples. While their affinities were similar (7 nM vs. 2 nM, respectively), the difference in helicity (19% vs. 40%), cell activity, and cell penetration were dramatic.

With regards to cell penetration, a balance of helicity, hydrophobicity and PI are required for optimal cell uptake. Bird et al report that for a hydrocarbon stapled peptide, an ideal isoelectric point (PI) is between 8.8 and 9.34, and the ideal helicity is between 61 and 86%. Finally, excessive hydrophobicity and positive charge can lead to nonspecific membrane disruption rather than membrane penetration.<sup>173</sup> Both of these peptides have the same PI and hydrophobicity; the PI is 9.08, well within the ideal range, and the Log P (consensus Log P, calculated using SwissADME) is -2.05, which is not excessively hydrophobic. The only physical difference between the two peptides is their helicity; while neither peptide is within the ideal range, LacB-1 is much more helical than LacA-1. While maximizing alpha helicity does not guarantee optimal biochemical or biological activity,<sup>175</sup> it seems that for these peptides the difference in cell uptake is related to the helicity or conformation of the peptides.

Still, it is surprising that changing the orientation of the lactam staple led to a 2–fold increase in helicity. However, this has been observed before in the literature.

There are many examples in which only one orientation was tested (usually the LacA orientation),<sup>184–186</sup> but Houston et al directly compared E to K staples (as in LacB) with K to E staples (as in LacA). They found that an  $i, i + 4$  LacA stapled peptide was actually less helical (29%) than its linear counterpart (61%). Furthermore, the equivalent LacB stapled peptide was more helical than the linear, at 71%.<sup>187</sup> While the linear sequence in this case was more helical than our peptides (due to stabilization by salt bridges), this trend is consistent with what we have seen. They hypothesize that the orientation of the lactam bridge in the LacA staple may have a destabilizing interaction between the lactam carbonyl and the backbone. We have taken NMRs of our peptides and are currently solving the structure to see if that is the case.

### **3.8 Materials and Methods**

#### **Peptide Synthesis**

##### *Solid Phase Peptide Synthesis*

##### Coupling and Fmoc Deprotection

Peptides were synthesized using Solid Phase Peptide Synthesis (SPPS) on Rink-Amide Resin. Reactions were done in a fritted syringe which was placed on a shaker during incubations. The resin was washed thoroughly between each step with four washes of 10 mL of DMF, followed by one wash of 10 mL DCM, and one final wash of 10 mL of DMF.

The loading of the resin was artificially lowered by using excess resin (1g for 0.2 mmol scale) and coupling only 1.5 equivalents of the first amino acid. The remaining un-

reacted amines were acetylated, and then the synthesis was completed as usual. Each amino acid (excluding amino acids used in stapling, which were coupled only once using 3 equivalents) was double coupled using 5 equivalents of amino acid for 2 hours for the first coupling and 1 equivalent for 1 hour for the second. HBTU was used as a coupling reagent in a 1:1 ratio with amino acid and 10 equivalents of DIPEA in NMP. Fmoc deprotection was performed with two 10 minute washes with 20% piperidine and 90 mM HOBt in NMP.

#### Acetylation

All peptides were acetylated at their amino terminus and amidinated at their carboxy terminus. Acetylation was performed by mixing 1.6 mL of DIPEA with 0.9 mL of Acetic Anhydride and 4 mL of NMP. The solution was incubated with the resin for 5 minutes.

#### Olefin Metathesis

Olefin metathesis was performed after all amino acids had been added to the resin, but before the final Fmoc deprotection by adding 20 mg of Grubbs I catalyst to 10 mL of dichloroethane and the resin. The mixture was bubbled with Nitrogen for at least 2 hours. This process was repeated for a total of two times. Stapling was confirmed with mass spec.

#### Lactamization

The lactam stapled peptides were synthesized using Fmoc-Lys(Mtt)-OH and Fmoc-Glu(O-2-PhiPr)-OH to construct the staple. After the addition of the second stapling amino acid (lysine for LacA and glutamate for LacB), the resin was equilibrated with DCM. The resin was then washed with four 2 minute washes with 2.25% TFA and 5% TIPS in DCM. The resin was then washed four times with DCM, once with DCM with

2% DIPEA to neutralize the resin, and then washed with DMF and DCM as usual. The amino acid side chains were stapled with 6 equivalents of Pybop and 10 equivalents of DIPEA in NMP for at least 2 hours.

### Cleavage

Cleavage was performed with TFA/Phenol/Thioanisole/Water/Triisopropylsilane in a ratio of 83/6.25/4.2/4.2/2 for 3 hours. The peptide was precipitated from the cleavage with ice cold ether, collected by filtration, and washed with 40 mL of cold ether.

### Purification

The crude peptide was purified using reverse phase HPLC with 0.1% Formic Acid in Acetonitrile or water. In cases where this was insufficient, purification was repeated using 0.1% Formic Acid in Methanol or water. Pure fractions were lyophilized, dissolved in 50% acetic acid and water, and lyophilized again. The final peptide was dissolved in water or a combination of water and DMF, filtered, and the concentration was determined by amino acid analysis. The dissolved peptide was aliquoted and stored at -80°C.

### **Circular Dichroism**

Circular Dichroism was completed using the same method described in Chapter 2.

### **Cat-ELCCA**

Cat-ELCCA was completed using the same method described in Chapter 2.

### **SPR**

SPR was performed as described in Chapter 2.

## Chapter 4

### Future Directions

#### 4.1 Additional structural modifications for lactam stapled peptides

##### *Modifications for Chemical Stability*

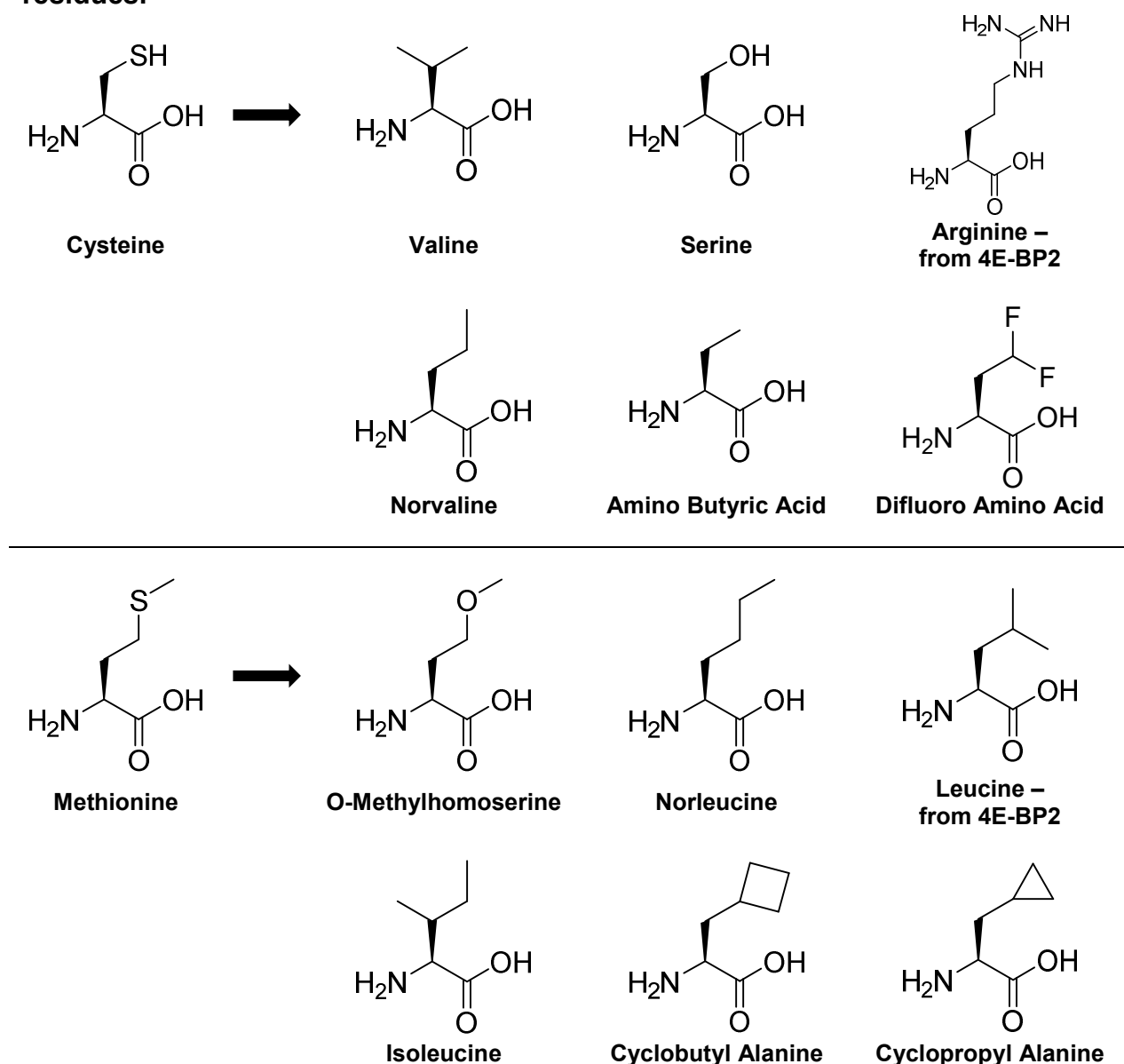
The 4E-BP1 sequence contains both a cysteine and a methionine. These residues are difficult to work with due to their tendency to dimerize and oxidize. We have optimized peptide storage conditions to minimize this occurrence. For instance, the peptide is kept under acidic conditions until the final pure peptide is dissolved in water. At that point, the peptide is aliquoted and frozen at  $-80^{\circ}\text{C}$ . Even still, peptides stored at  $-80^{\circ}\text{C}$  have been observed to dimerize over the course of a year. Therefore, it is important to continue our efforts to mutate the cysteine and methionine residues away to improve the chemical stability of the peptides.

Since we have observed a significant difference in peptide sequence activity with different staple types, some modifications which we tried before would be worth trying again with the lactam stapled peptide. These include the valine and serine as substitutes for cysteine, and O-methylhomoserine and norleucine as substitutes for methionine, which have all been tried with the mHCS staple. Additionally, the 4E-BP2 protein sequence does not have a cysteine or methionine residue, and while the mHCS version of this peptide is not active, it is possible that the lactam staple will be active.



Additionally, our lab has made considerable efforts towards the synthesis of a difluoro amino acid to act as a mimetic of cysteine. While our attempts so far have failed, this goal may still be worth pursuing, because a difluoro amino acid would have similar size and hydrophobicity as cysteine. Finally, a variety of other hydrophobic amino acids could be tried at both positions. Some of the potential cysteine and methionine replacing amino acids are shown in **Table 4.1**.

**Table 4.1 – Potential replacements for the unstable cysteine and methionine residues.**



### Modifications for Proteolytic Stability

We hope that the staple will provide some stability to protease activity, which is the primary method of metabolism for peptides. However, once we determine the half-life and sites of metabolism of the peptide, it is likely that further modification will be necessary to increase its stability. Several different methods could be used, including introducing methyl groups at the sites of cleavage, the use of D-amino acids, or the use of other unnatural amino acids.

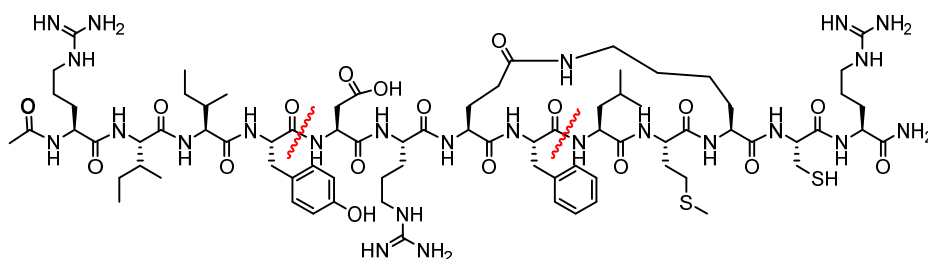


**Figure 4.1 – Chymotrypsin cleavage sites in LacB-1.**

Chymotrypsin, which is a digestive protease produced in the pancreas and found in the duodenum, has two known cleavage sites on our lead peptide, LacB-1, which are shown in **Figure 4.1**. Chymotrypsin cleaves on the C-terminal side of aromatic residues, including phenylalanine and tyrosine, which are both present in our sequence.<sup>188</sup> While we hope the staple will shield the phenylalanine site, tyrosine is still exposed. We already made an N-methyl aspartic acid substituted peptide (LacA-2), but found that this peptide was less active than the un-methylated peptide. We also made the homotyrosine substituted peptide (mHCS-10), which also significantly lost activity, although this peptide was not made with the lactam staple. If this site is shown to be metabolically unstable, we will try D-tyrosine and D-aspartic acid to see if those substitutions are tolerated. Unfortunately, the tyrosine residue is part of the consensus

sequence and is conserved across both the 4E-BP and eIF4G isoforms, so it will likely be difficult to remove. At this stage, it is most important to first identify the sites of metabolism, and then use these strategies to mask them.

## 4.2 Pharmacokinetic studies of lactam stapled peptides

While small molecules are typically metabolized in the liver, peptides are primarily metabolized in the kidneys.<sup>189</sup> Additionally, serum and tissue proteases and nonspecific protease activity are the primary methods of degradation, as opposed to CYPs for small molecules. Peptides are typically rapidly cleared and poorly bioavailable (less than 2%), which is why we introduce unnatural modifications (such as the staple) to improve their stability.<sup>190</sup> Considering this information, it is unlikely that a microsomal stability assay, which uses liver enzymes to predict *in vivo* clearance, would be particularly helpful in our case.

Measuring the serum and plasma stability of our peptides is a better *in vitro* model for metabolism. However, a recent study indicated that peptides are actually more stable in whole blood than in serum or plasma, and that serum stability assays can mislead a researcher into modifying a site of instability *in vitro* that is not relevant *in vivo*.<sup>191</sup> On the other hand, the use of anticoagulants, such as EDTA, can deactivate some proteases present in the whole blood. The most ideal method for measuring stability *in vitro* would therefore be to use whole blood stability without the use of anticoagulants.<sup>191</sup> However, we will be working with the PK core at the University of Michigan to collect this data and will consult with them to determine the best method according to their expertise and available resources. This *in vitro* data will be used to

determine the most likely sites of hydrolysis or other modification, and the methods discussed in section 4.1 will be used to address the sites of instability. At that point, the use of *in vivo* models for metabolic stability will be more appropriate.

### 4.3 Pulldown experiments with stapled peptides

The stapled peptides bind to eIF4E with high affinity, but they still may potentially have other targets in the cell. For instance, several years ago Arya Menon did a Western blot to observe the effects of mHCS-1 treatment on 4E-BP1 phosphorylation. We observed what appeared to be inhibition of 4E-BP1 phosphorylation, which is not consistent with a peptide that is only inhibiting the eIF4E–eIF4G (or eIF4E–4E-BP1) PPI (**Figure 4.2**). Furthermore, we did not observe inhibition of S6K phosphorylation, which would be expected if the peptide was inhibiting mTORC1. Unfortunately, we have not had the chance to repeat this study using any of the other peptides, and prior to making a pulldown probe we would confirm that this effect repeats with the appropriate peptides. However, if there is a difference between different peptides, we would make pulldown probes of both to compare. These probes would consist of the peptide conjugated to a biotin, which would allow the live cells to be treated and lysed, at which point streptavidin beads would be added to the lysate to pulldown the probe.

Synthetically, it would be easiest to introduce a biotin on the amino terminus of the peptide. However, we could also introduce it on the carboxy terminus using Mtt(lysine), which is protected with a very acid sensitive protecting group, as the first residue in the sequence. The resin bound peptide would be treated with dilute TFA and then the biotin linker would be added using normal coupling conditions. In the case of

the lactam stapled peptides, the biotin and any linker would have to be added early in the synthesis, because the same acid sensitive protecting group is used to make the staple on resin. Even for hydrocarbon stapled peptides, it would be ideal to add a C-terminal biotin early in the synthesis to avoid accessibility problems.

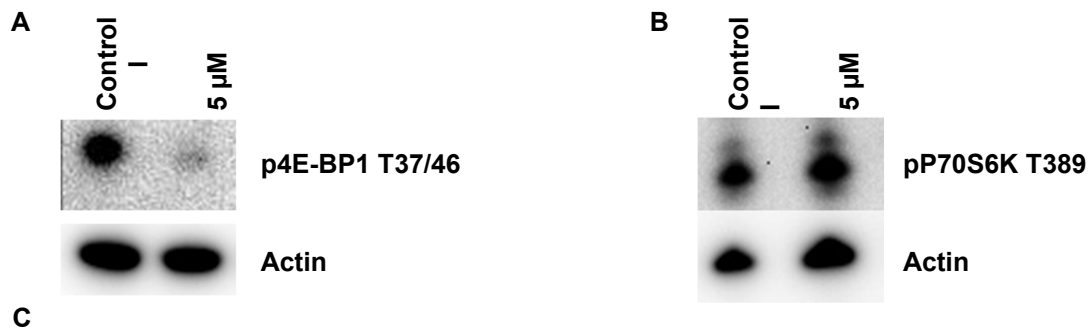


**Figure 4.2 – The effect of peptide treatment on (A) 4E-BP1 phosphorylation and (B) S6K phosphorylation.** MDA-MB-231 cells were treated with mHCS-1 for 6 hours. Section (C) shows the mTORC1 mediated phosphorylation of both proteins.

The biotin could be added directly, or a short linker could be included. The addition of a PEG linker would improve the solubility of the peptide, but early data indicates that PEG reduces the activity of our 4E-BP1 peptides, so a  $\beta$ -alanine linker should also be considered. The linker and placement would first be optimized for

peptide activity before attempting any pulldown assay. We would also have to consider the effect of a biotin on the cell penetration of our peptides. Finally, it would be ideal to have completed *in vitro* PK studies prior to this experiment and optimized the peptide sequence to minimize metabolism, because the study will be ineffective if the biotin is cleaved off of the active portion of the peptide.

Initial pulldown results would be analyzed by Western blot. Confirming that the peptide pulls down eIF4E is critical to confirm that the peptide is still active in cells. Additionally, the biotin conjugated peptide should still perform similarly in our eIF4E pulldown assay. If the probe passes these tests, we can blot for mTOR and other potential 4E-BP1 phosphorylating kinases. Finally, we can use proteomics to assist in the identification of unexpected targets of the peptides.

An additional use of the pulldown probe could be to identify off-target mechanisms of toxicity. When Arya Menon tested HCS-1 and sTIP-04 in a cell titer glo assay, which measure cell viability, she found that sTIP-04 is much more toxic than HCS 4E-BP1. As expected, the negative control HCS 4E-BP1 LM->AA did not kill cells. These results are shown in **Figure 4.3 A-C**. **Figure 4.3 D** also shows that the sTIP-04 toxicity is not due to nonspecific membrane disruption. Based on the fact that sTIP-04 and HCS-1 have similar behavior in our eIF4E pulldown assays, we hypothesize that either sTIP-04 has an off-target effect which is mediating its toxicity, or HCS 4E-BP1 has an off-target effect which is rescuing cells. In either case, pulldown probes for each peptide could be used to identify additional targets using proteomics to analyze the pulldown results. This information could be used to explain the observed toxicity and to design a better eIF4E–eIF4G PPI inhibitor.

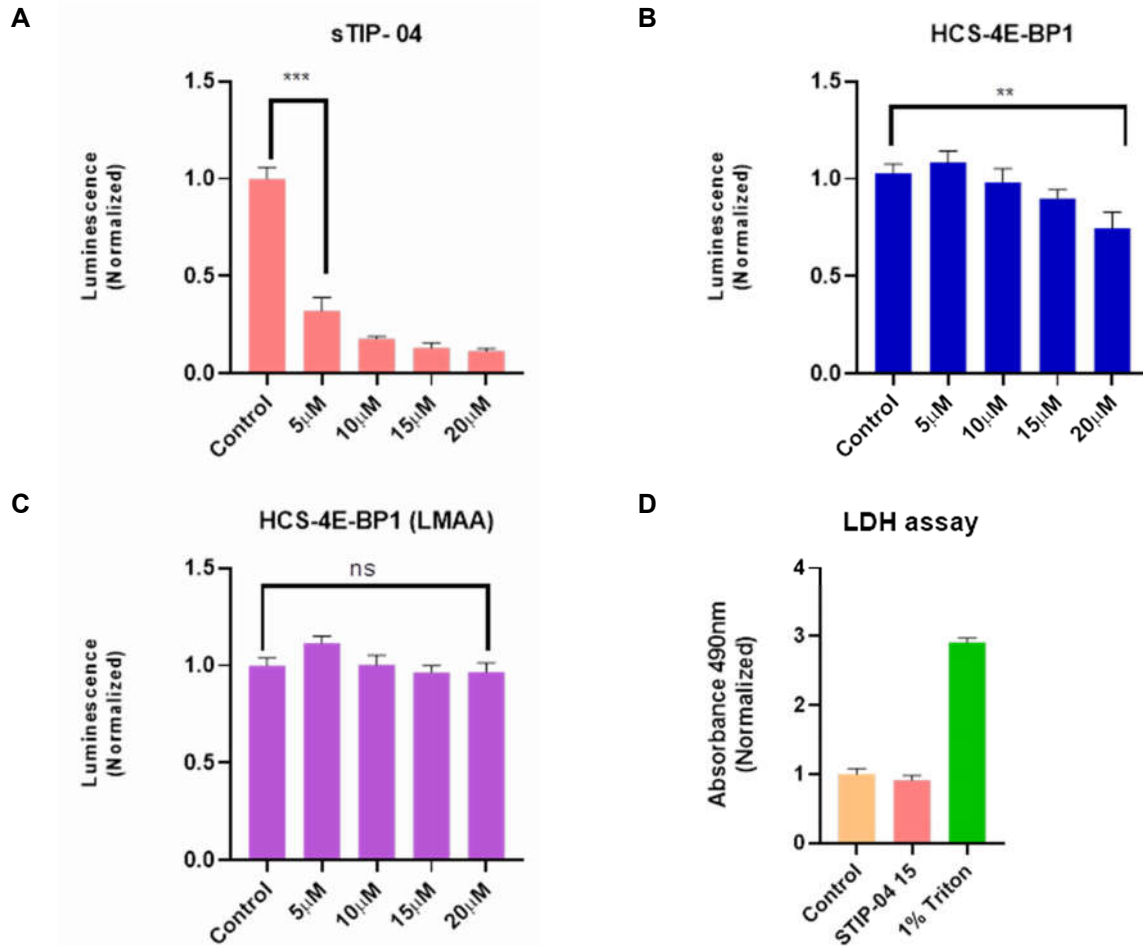


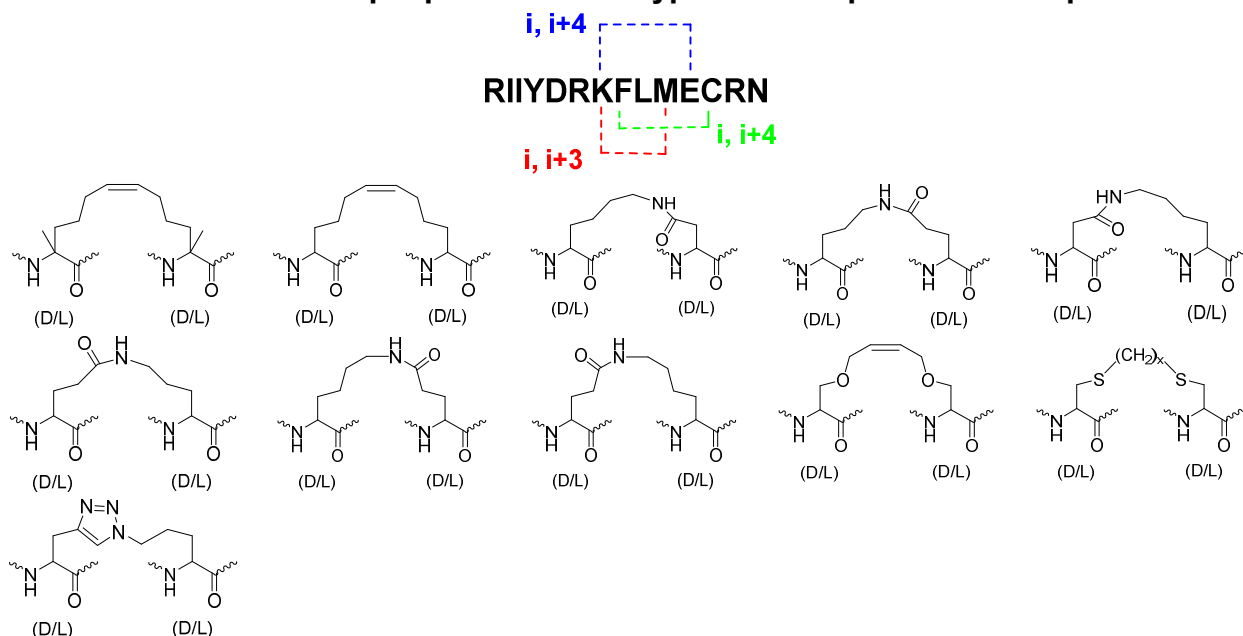
**Figure 4.3 – Cell viability measured by a Cell Titer Glo assay after treatment with (A) sTIP-04, (B) HCS 4E-BP1, and (C) HCS 4E-BP1 LM→AA. (D) An LDH assay indicates that sTIP-04 does not cause membrane leakage.**

#### 4.4 Relationship between staple type and cell penetration

We found that the cell penetration of the 4E-BP1 peptides was significantly affected by the orientation of the lactam staple. It would therefore be interesting to compare multiple staple types with one 4E-BP1 sequence to determine the effect on cell penetration. The FITC labeled peptides described in Chapter 2 were not very soluble, but the modifications required for the CAPA assay developed by the Kritzer lab<sup>183</sup> are better tolerated. This assay would therefore be ideal for measuring the cell penetration of these peptides.

Modifications to the length of the staple and the position of the amide bond would be made first. Additionally, different staple stereochemistries could be used for any of the staples types. Hydrocarbon, O-allyl serine, triazole, and thioether staples would all be relatively simple to introduce. Two component stapling could be used as well, although it may be best to see the effect of the basic staples first. The staple position is not very flexible due to the length of the 4E-BP1 helix, but some modifications could be made. For instance, making an  $i, i+3$  staple between the lysine and methionine residues may be tolerated. Even if the peptides lose affinity for eIF4E, they can still be used to make observations about the effect of a modification on cell penetration. All peptides would be analyzed for helicity with and without TFE and would be tested in the CAPA assay for cell penetration. **Table 4.2** outlines a list of initial stapling ideas to try for this experiment.

**Table 4.2 – Potential staple positions and types for cell penetration experiments.**





## 4.5 Development of a functionalized staple

We had tried to shift the position of the hydrocarbon staple one step towards the amino terminus, replacing arginine and methionine residues. This would cause the staple to rest against the surface of the protein. However, this stapled peptide showed no activity in cells (data not shown), which we presumed was due to the disruption of an arginine-aspartic acid salt bridge between the peptide and the surface of eIF4E. However, a staple which maintains the arginine functional group may be more successful. We made some attempts to synthesize such a staple using olefin metathesis and lactamization, which were both chemistries that we were already familiar with. However, these attempts were unsuccessful, and are shown in **Figure 4.4**.

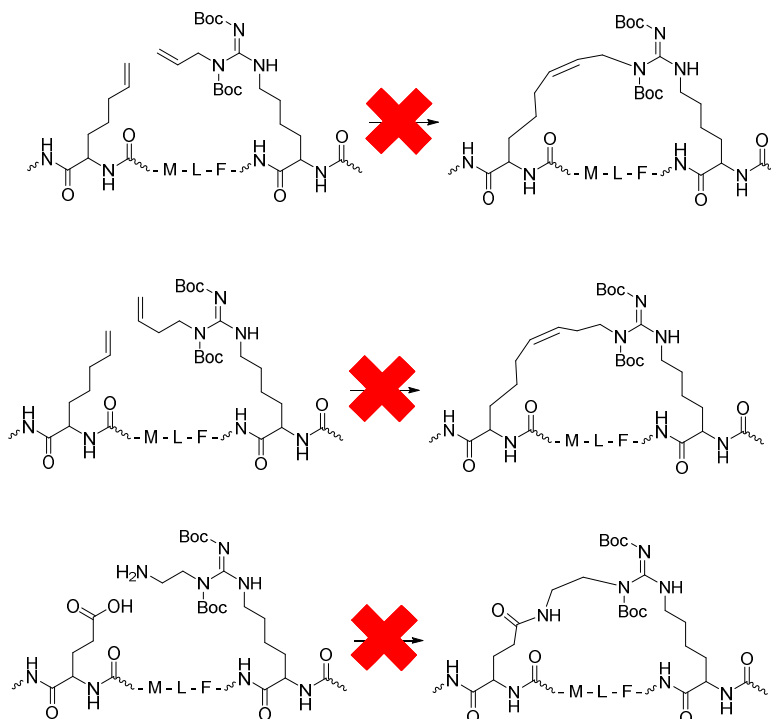


**Figure 4.4 – Unsuccessful attempts towards designing an arginine functionalized stapled peptide.**

An alternative strategy to making a functionalized staple could involve synthesizing the entire staple in solution and then adding it to the peptide on resin. This would involve the use of many protecting groups so that the staple could be added in the right order. A proposed synthesis is shown in **Figure 4.5**, and the method for incorporating the staple into the resin-bound peptide is shown in **Figure 4.6**.

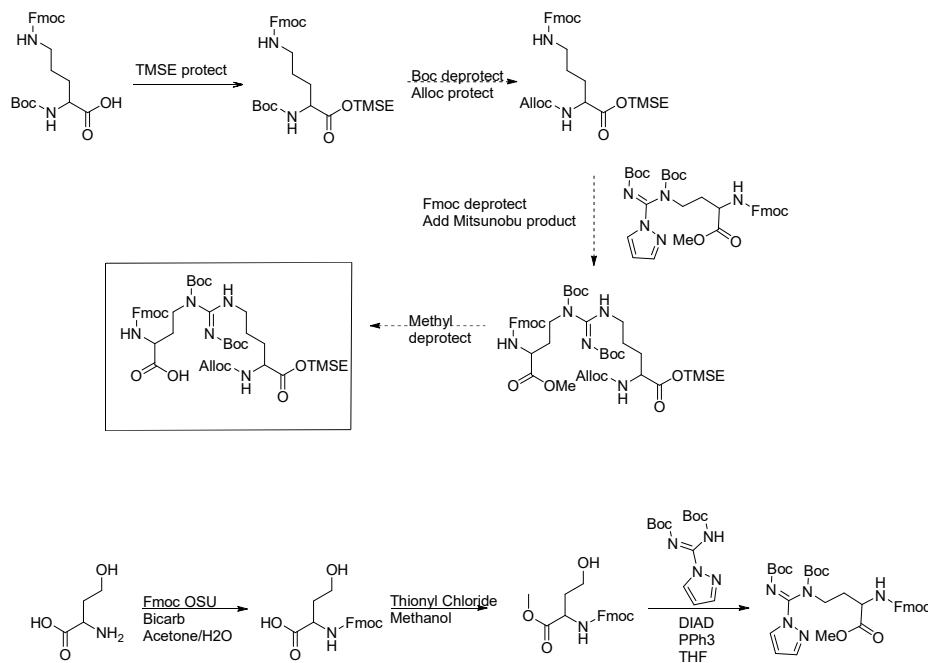


**Figure 4.5 – Proposed scheme for the synthesis of a functionalized staple in solution.**

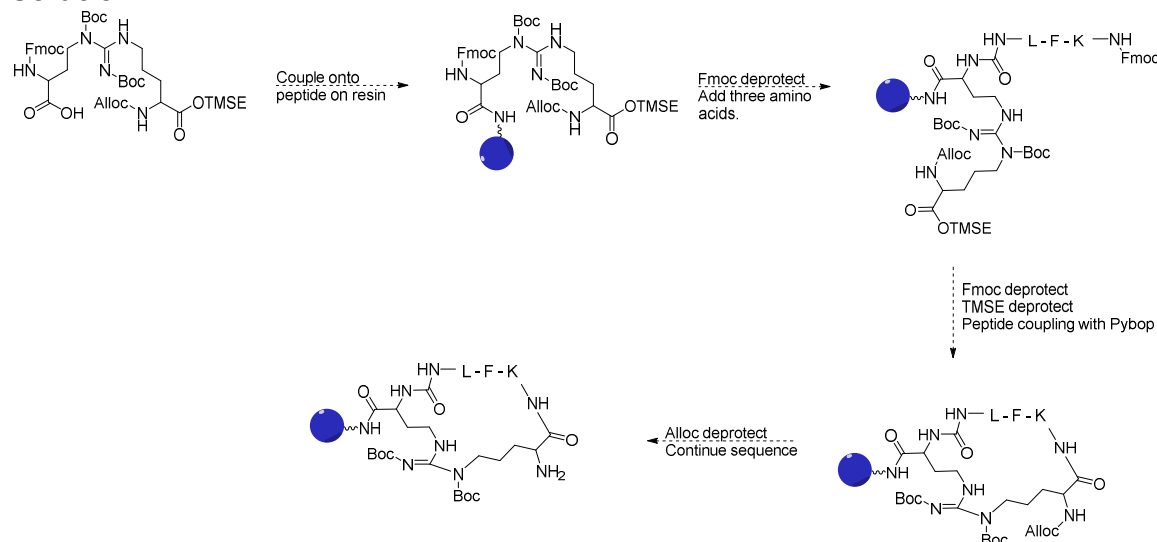


**Figure 4.6 – Proposed scheme for the incorporation of the solution synthesized functionalized staple into the resin-bound peptide.**

## 4.6 Conclusions

The work presented in this chapter will hopefully take a promising lead and turn it into a useful probe. Optimization for chemical and metabolic stability will minimize the controllable problems associated with peptide therapeutics. Ideally, we will be able to find tolerated substitutions for the oxidizing residues, which will improve the shelf life of this peptide and make it much easier to work with. Additionally, identifying the most likely sites of metabolism will enable us to modify those sites for stability. If basic modifications (such as N-methylation, homo-amino acids, or D-amino acids) are not tolerated, we can try more drastic measures, such as synthesizing the entire peptide using D-amino acids. In this case, we would likely need to re-optimize the staple length, type, and position.

With regards to off-target effects, our peptide could still be effective if it inhibits 4E-BP1 phosphorylation as well as the eIF4E–eIF4G PPI. However, it would be useful to know what, if any, other protein is being affected. This would allow us to learn more about the mechanisms of 4E-BP1 phosphorylation, and to potentially target that pathway deliberately. Separately, finding the mechanism of toxicity of the sTIP-04 peptide would be useful in the validation of the eIF4E–eIF4G PPI as a cancer target; if either peptide has significant off-target effects, it will not be a good candidate for validation.

The stapled peptide field has advanced significantly over the last 20 years, but there is still more room for advancement, particularly with intrinsically disordered parent sequences. Optimization of the staple and cell penetration will be useful in our work towards developing a stable and highly active probe, but it can also provide interesting

information regarding the benefits of certain staple types over others. Of particular interest will be if the cell penetration continues to correlate with helicity, or if hydrophobicity or some other property seems to be more important. This will be particularly interesting to see with the non-hydrocarbon staples, because while the hydrocarbon staple type has been well studied and often successful, it is clearly not a universal approach.

Lastly, most of the available staple types to date rely on chemistries which can be performed on resin. The synthesis of the staple in solution would allow for more complicated functionalization, such as the arginine functional group presented here. However, this chemistry could likely be tuned to introduce many different kinds of functional groups in peptide staples, which would allow for the development of more complex peptide mimics.

## **Appendices**

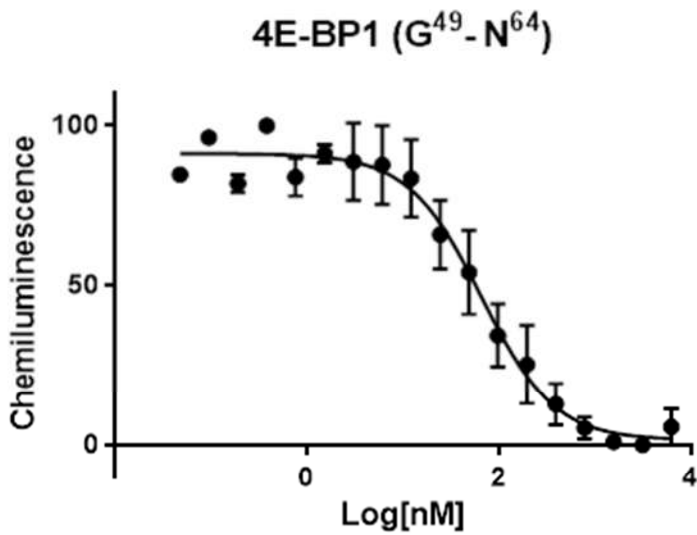
## Appendix A

### Chapter 2 – Supplemental Information

#### IC50 Curves for Peptides

##### *4E-BP1 Peptides*

##### 4E-BP1 Linear Peptides



Best-fit values

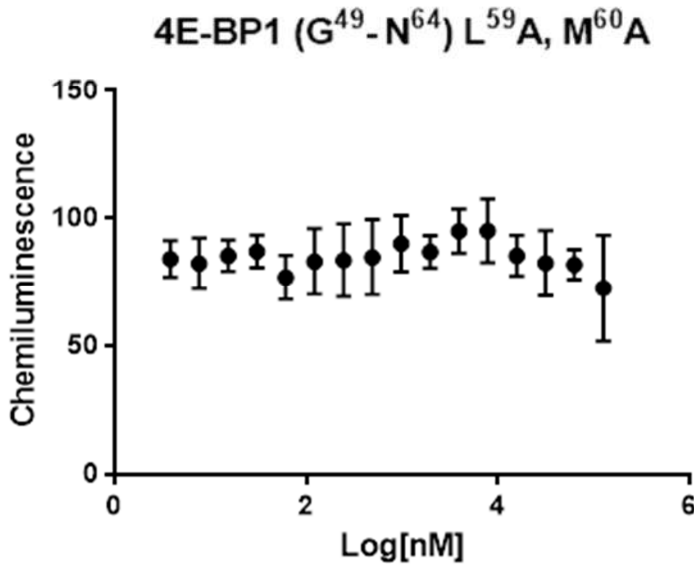
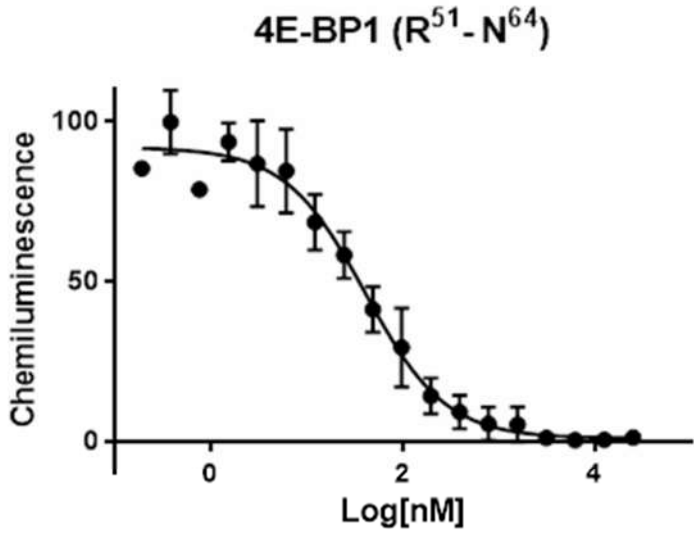
HillSlope	-1.146
IC50	65.79

95% Confidence Intervals

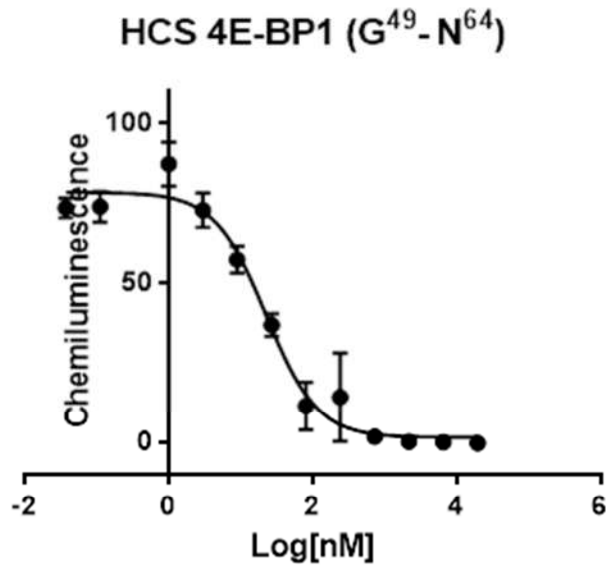
HillSlope	-1.415 to -0.8759
IC50	52.45 to 82.52

Goodness of Fit

R square	0.9434
----------	--------



## 4E-BP1 Stapled Peptides



Best-fit values

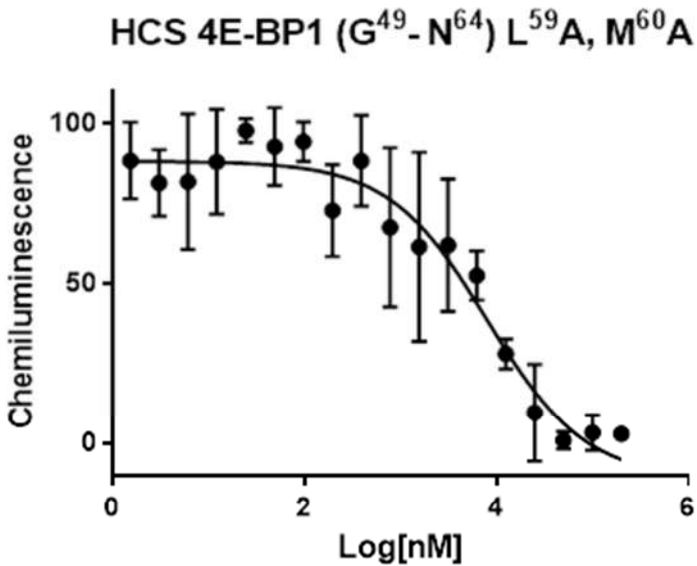
HillSlope	-1.218
IC50	22.68

95% Confidence Intervals

HillSlope	-1.625 to -0.8115
IC50	16.57 to 31.04

Goodness of Fit

R square	0.9620
----------	--------



Best-fit values

HillSlope	-0.8512
IC50	7998

95% Confidence Intervals

HillSlope	-1.263 to -0.4399
IC50	3533 to 18106

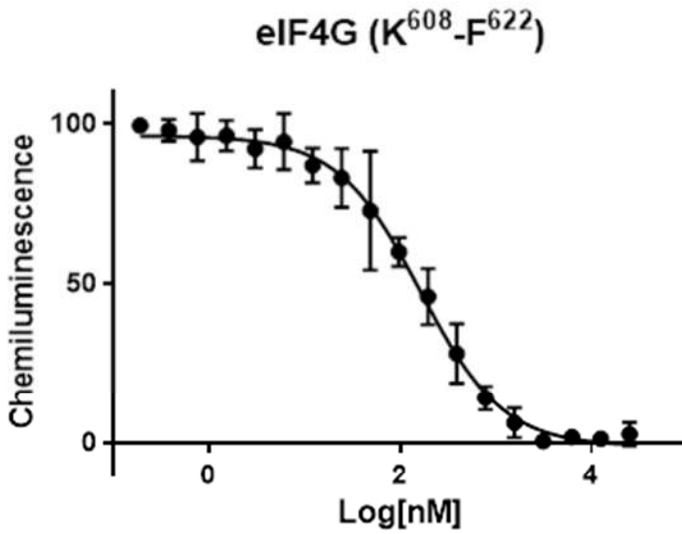
Goodness of Fit

R square	0.7715
----------	--------



eIF4G Peptides

eIF4G Linear Peptides



Best-fit values

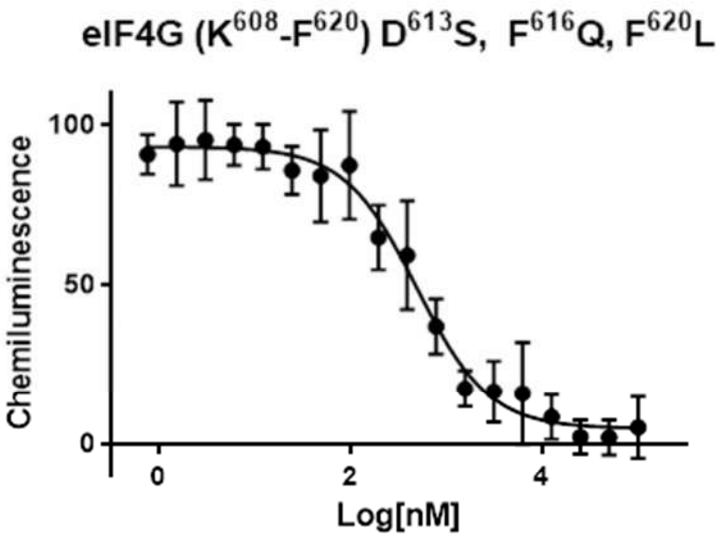
HillSlope	-1.005
IC50	163.5

95% Confidence Intervals

HillSlope	-1.168 to -0.8413
IC50	137.2 to 194.9

Goodness of Fit

R square	0.9711
----------	--------



Best-fit values

HillSlope	-1.153
IC50	492.9

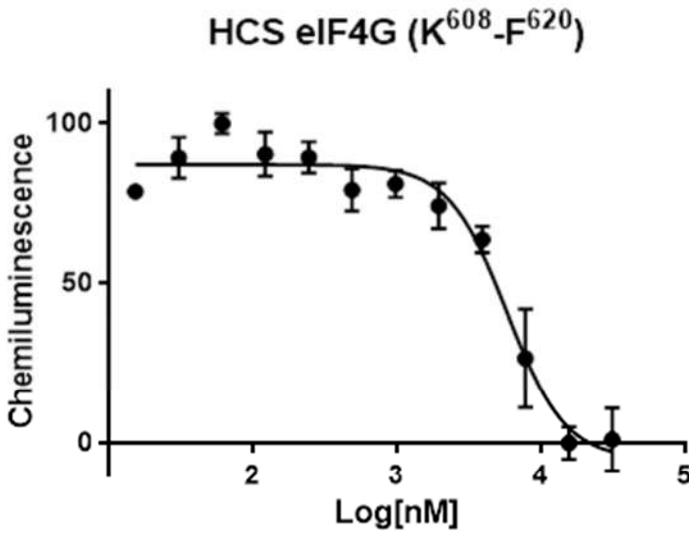
95% Confidence Intervals

HillSlope	-1.452 to -0.8532
IC50	384.0 to 632.6

Goodness of Fit

R square	0.9271
----------	--------

eIF4G Stapled Peptides



Best-fit values

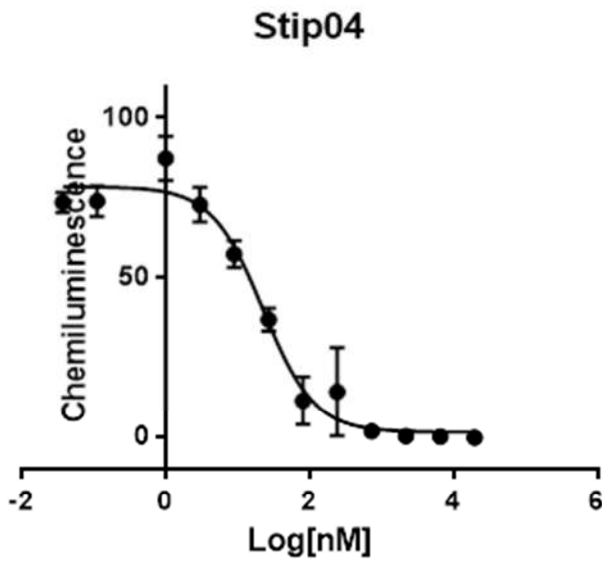
HillSlope	-2.150
IC50	5778

95% Confidence Intervals

HillSlope	-3.055 to -1.246
IC50	4566 to 7314

Goodness of Fit

R square	0.9472
----------	--------



Best-fit values

HillSlope	-1.218
IC50	22.68

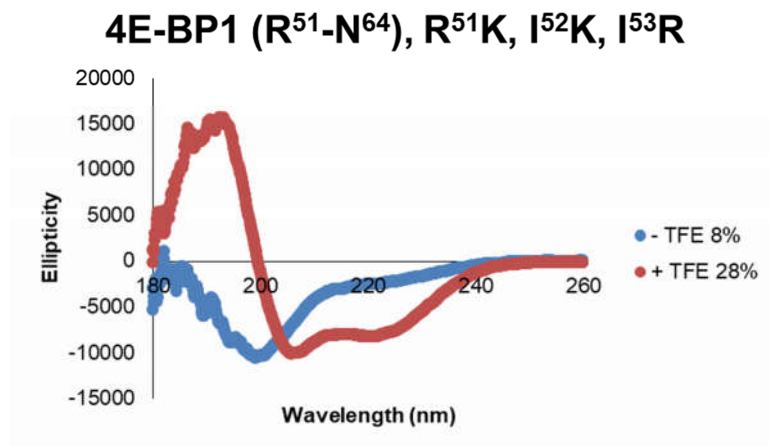
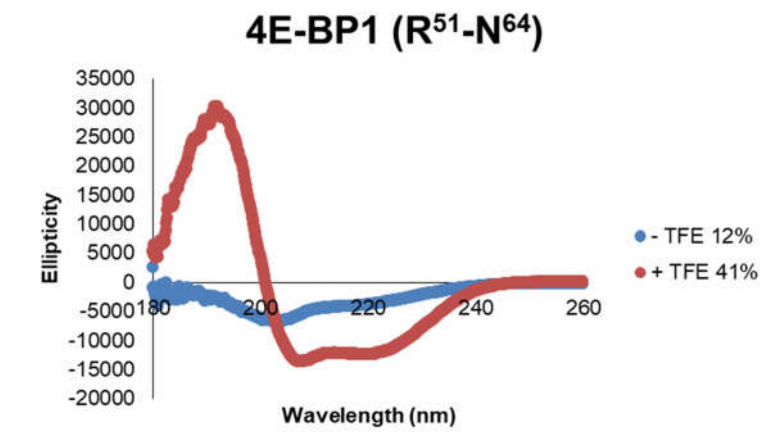
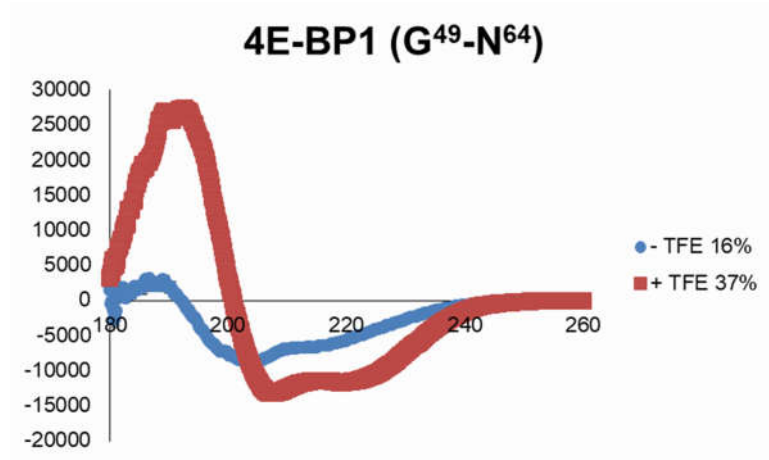
95% Confidence Intervals

HillSlope	-1.625 to -0.8115
IC50	16.57 to 31.04

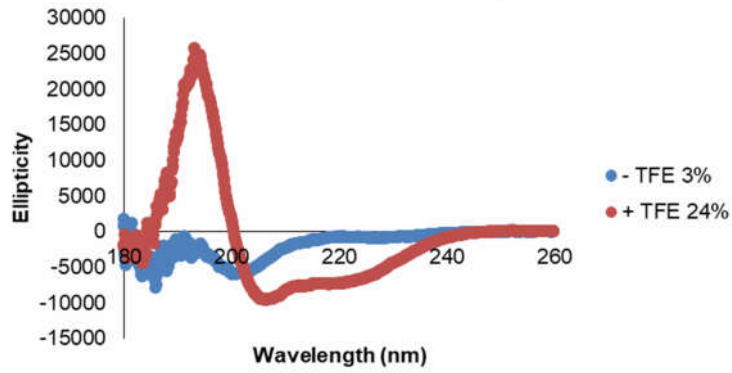
Goodness of Fit

R square	0.9620
----------	--------

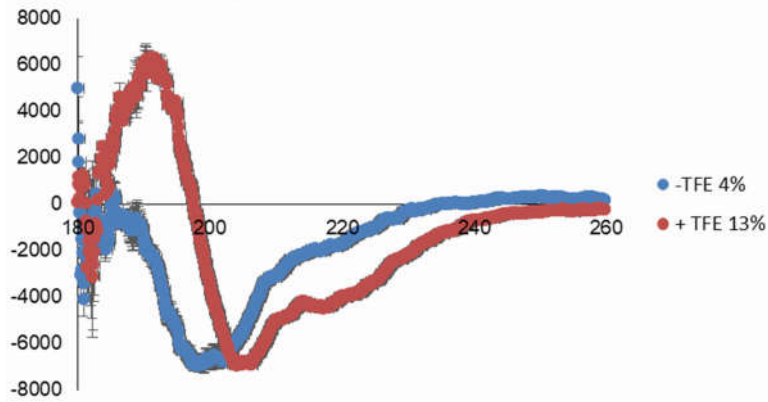
## CD Curves for Peptides



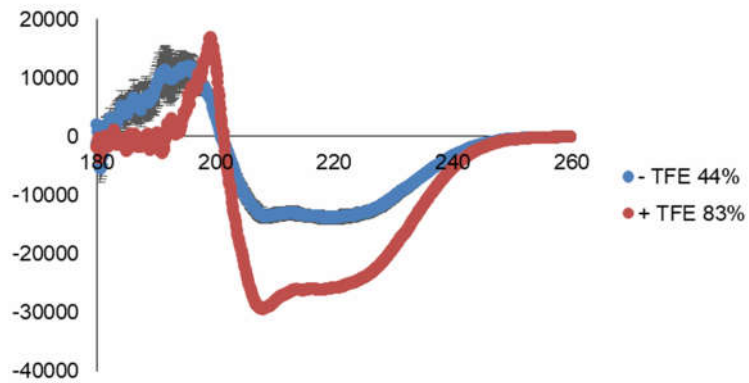
### eIF4G (K<sup>608</sup>-F<sup>622</sup>)



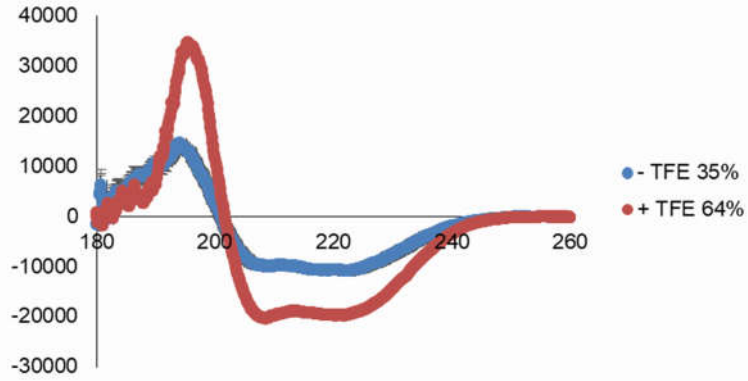
### eIF4G (K<sup>602</sup>-F<sup>220</sup>), D<sup>613</sup>S, F<sup>616</sup>Q, F<sup>620</sup>L



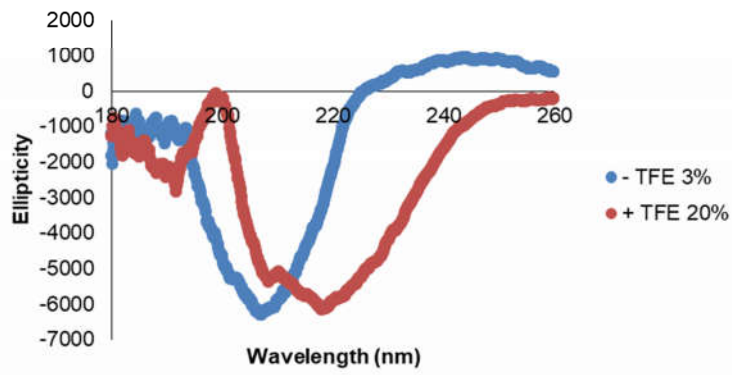
### HCS 4E-BP1



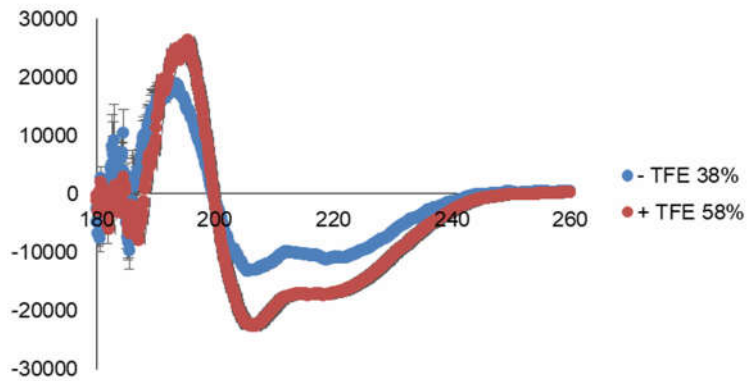
### HCS 4E-BP1 LM->AA



### HCS eIF4G



### Staple 04



## SPR Curves for Peptides

### Data for Kinetic Analysis

**Table A2.1 – Kinetic binding data at a variety of temperatures for linear peptides determined by SPR.**

	Temperature (°C)	$K_a$ ( $M^{-1}s^{-1}$ )	$K_d$ ( $s^{-1}$ )	$K_D$ (nM)
4E-BP1 (G <sup>49</sup> -N <sup>64</sup> )	10	$0.4 \pm 0.2 \times 10^6$	$8.2 \pm 0.8 \times 10^{-3}$	$17 \pm 4$
	15	$0.5 \pm 0.2 \times 10^6$	$9.6 \pm 0.9 \times 10^{-3}$	$17 \pm 2$
	20	$0.6 \pm 0.3 \times 10^6$	$13 \pm 2 \times 10^{-3}$	$21 \pm 7$
	25	$0.8 \pm 0.3 \times 10^6$	$21 \pm 4 \times 10^{-3}$	$26 \pm 6$
	30	$1.3 \pm 0.4 \times 10^6$	$32 \pm 5 \times 10^{-3}$	$24 \pm 5$
4E-BP1 (R <sup>51</sup> -N <sup>64</sup> )	10	$1.47 \pm 0.03 \times 10^6$	$6.9 \pm 0.5 \times 10^{-3}$	$4.7 \pm 0.5$
	15	$1.0 \pm 0.1 \times 10^6$	$9.3 \pm 0.7 \times 10^{-3}$	$9 \pm 1$
	20	$1.2 \pm 0.1 \times 10^6$	$13 \pm 0.1 \times 10^{-3}$	$11 \pm 1$
	25	$1.10 \pm 0.06 \times 10^6$	$19.2 \pm 0.5 \times 10^{-3}$	$17.5 \pm 0.4$
	30	$1.1 \pm 0.1 \times 10^6$	$31 \pm 2 \times 10^{-3}$	$28 \pm 2$
eIF4G (K <sup>602</sup> -F <sup>622</sup> )	10	$1.8 \pm 0.3 \times 10^6$	$18 \pm 7 \times 10^{-3}$	$9.8 \pm 0.7$
	15	$1.7 \pm 0.5 \times 10^6$	$22 \pm 4 \times 10^{-3}$	$12 \pm 2$
	20	$1.7 \pm 0.3 \times 10^6$	$35 \pm 7 \times 10^{-3}$	$24 \pm 4$
	25	$1.7 \pm 0.3 \times 10^6$	$48 \pm 9 \times 10^{-3}$	$29 \pm 6$
	30	$2.00 \pm 0.09 \times 10^6$	$100 \pm 20 \times 10^{-3}$	$54 \pm 11$
eIF4G (K <sup>602</sup> -F <sup>620</sup> ), D <sup>613</sup> S, F <sup>616</sup> Q, F <sup>620</sup> L	10	$1.46 \pm 0.04 \times 10^6$	$34 \pm 4 \times 10^{-3}$	$23 \pm 2$
	15	$2.3 \pm 0.1 \times 10^6$	$70 \pm 20 \times 10^{-3}$	$32 \pm 7$
	20	$2.6 \pm 0.2 \times 10^6$	$147 \pm 9 \times 10^{-3}$	$57 \pm 1$
	25	$2.0 \pm 0.1 \times 10^6$	$120 \pm 10 \times 10^{-3}$	$62 \pm 6$
	30	$2.0 \pm 0.1 \times 10^6$	$177 \pm 7 \times 10^{-3}$	$92 \pm 6$

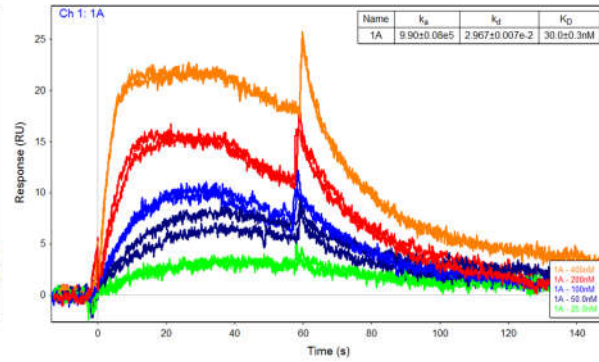
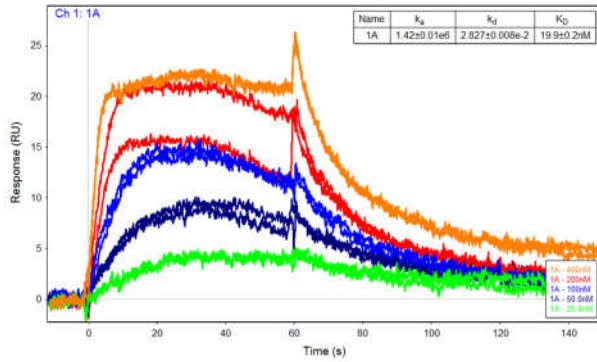
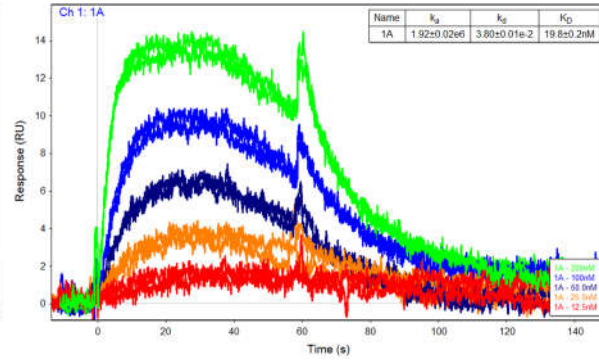
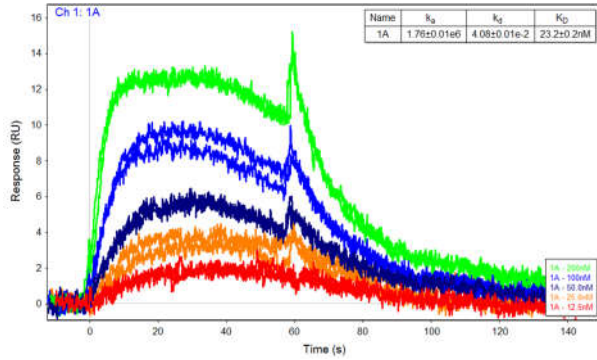
**Table A2.2 – Kinetic binding data at a variety of salt concentrations for linear peptides determined by SPR.**

	[NaCl] (mM)	$K_a$ ( $M^{-1}s^{-1}$ )	$K_d$ ( $s^{-1}$ )	$K_D$ (nM)
4E-BP1 (G <sup>49</sup> -N <sup>64</sup> )	225	$0.9 \pm 0.3 \times 10^6$	$23 \pm 5 \times 10^{-3}$	$25 \pm 6$
	500	$0.8 \pm 0.3 \times 10^6$	$55 \pm 2 \times 10^{-3}$	$29 \pm 1$
	1000	$2.0 \pm 0.4 \times 10^6$	$16 \pm 7 \times 10^{-3}$	$8 \pm 1$
4E-BP1 (R <sup>51</sup> -N <sup>64</sup> )	225	$1.10 \pm 0.06 \times 10^6$	$19.2 \pm 0.5 \times 10^{-3}$	$17.5 \pm 0.4$
	500	$1.3 \pm 0.3 \times 10^6$	$37 \pm 6 \times 10^{-3}$	$34 \pm 9$
	1000	$1.2 \pm 0.1 \times 10^6$	$86 \pm 20 \times 10^{-3}$	$67 \pm 9$
eIF4G (K <sup>602</sup> -F <sup>622</sup> )	225	$1.7 \pm 0.3 \times 10^6$	$46 \pm 6 \times 10^{-3}$	$27 \pm 5$
	500	$2.7 \pm 0.8 \times 10^6$	$150 \pm 60 \times 10^{-3}$	$65 \pm 4$
	1000	$5.3 \pm 0.1 \times 10^6$	$270 \pm 70 \times 10^{-3}$	$51 \pm 14$
eIF4G (K <sup>602</sup> -F <sup>620</sup> ), D <sup>613</sup> S, F <sup>616</sup> Q, F <sup>620</sup> L	225	$2.0 \pm 0.1 \times 10^6$	$123 \pm 14 \times 10^{-3}$	$62 \pm 6$
	1000	$0.15 \pm 0.05 \times 10^6$	$2 \pm 1 \times 10^{-3}$	$14 \pm 3$

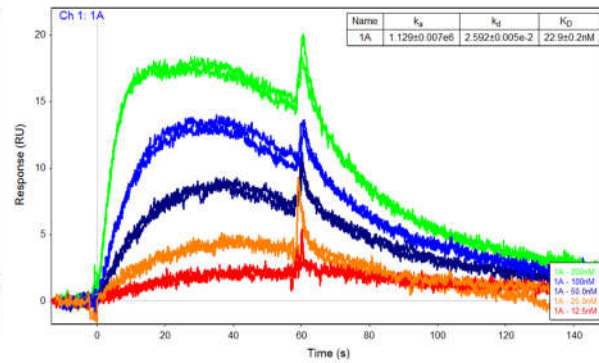
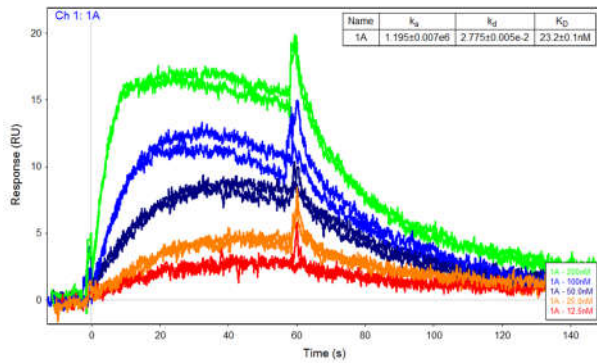
## 4E-BP1 Linear Peptides

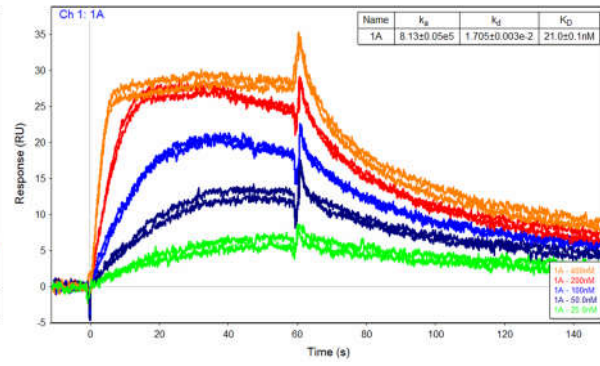
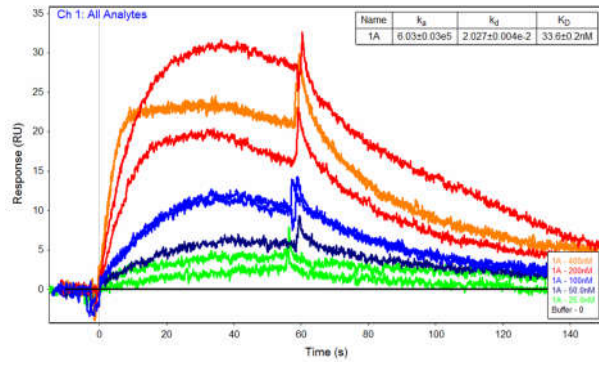
4E-BP1 (G<sup>49</sup>-N<sup>64</sup>)

30°C - 4E-BP1 (G<sup>49</sup>-N<sup>64</sup>)

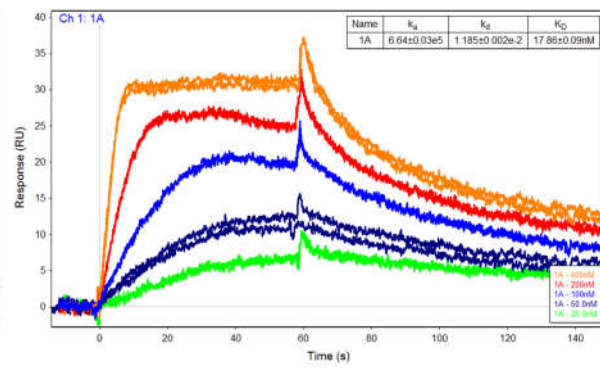
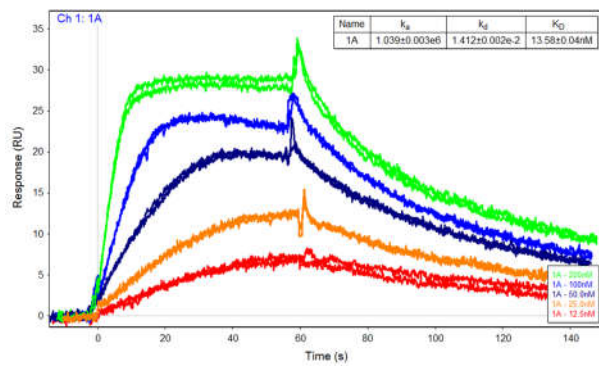


25°C - 4E-BP1 (G<sup>49</sup>-N<sup>64</sup>)

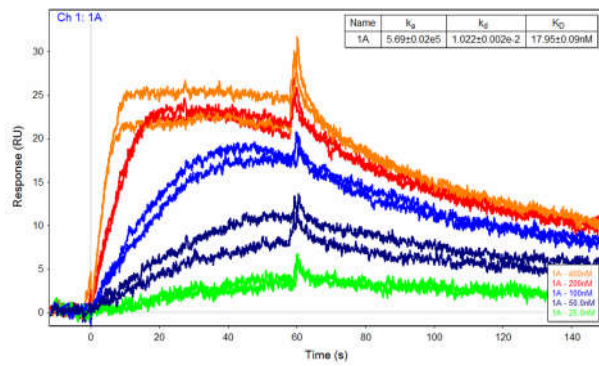
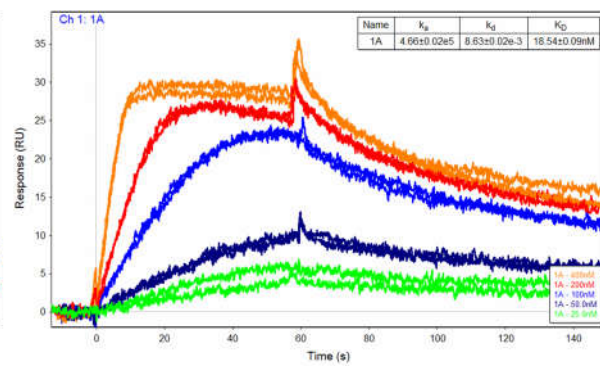
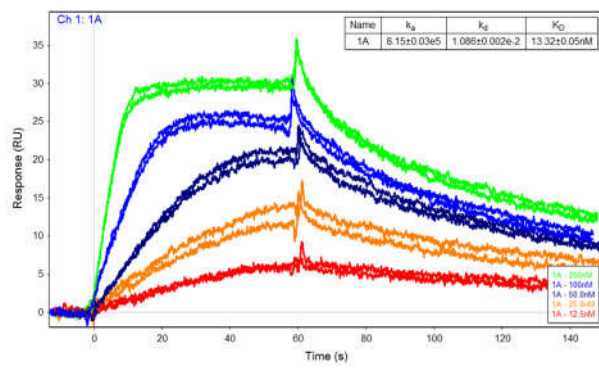




20°C - 4E-BP1 (G<sup>49</sup>-N<sup>64</sup>)

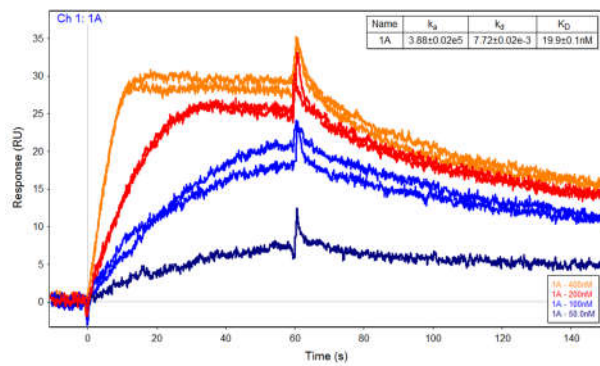
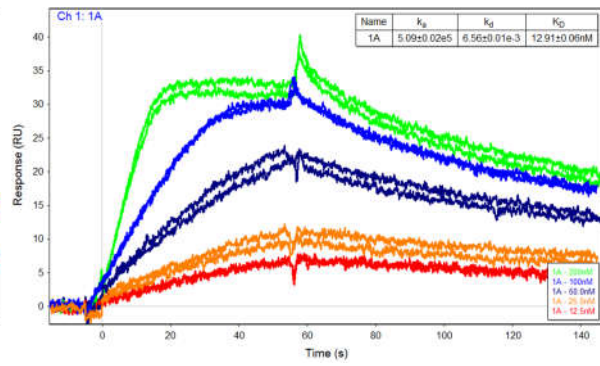
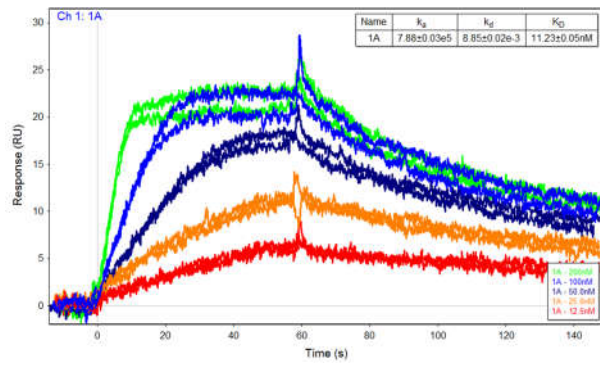


15°C - 4E-BP1 (G<sup>49</sup>-N<sup>64</sup>)

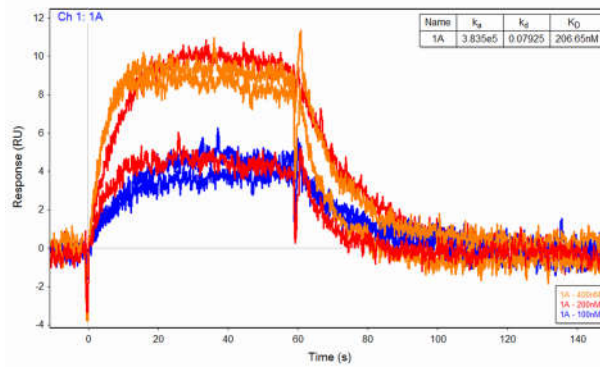
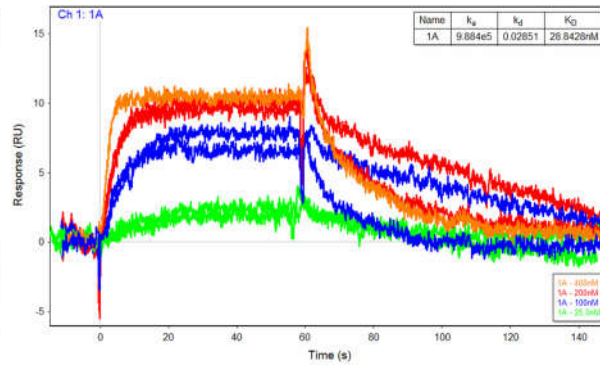
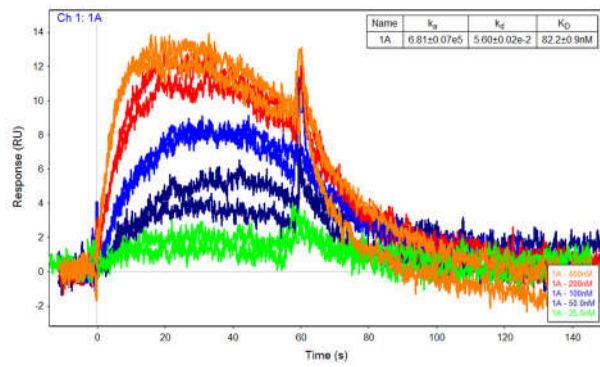




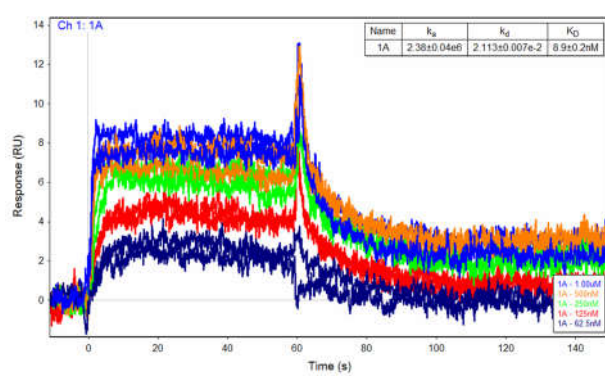
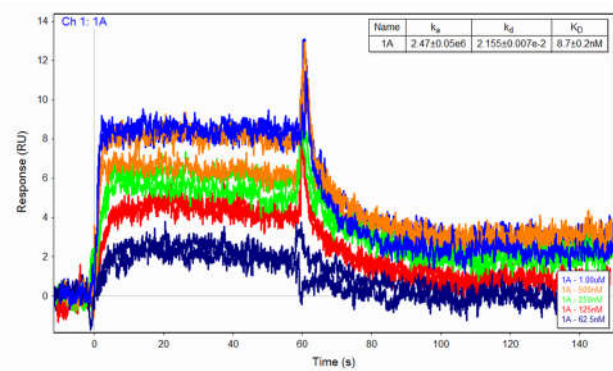
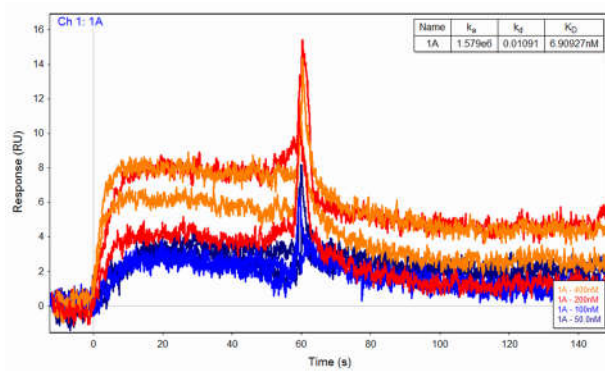
10°C - 4E-BP1 (G<sup>49</sup>-N<sup>64</sup>)



500 mM Sodium Chloride - 4E-BP1 (G<sup>49</sup>-N<sup>64</sup>)

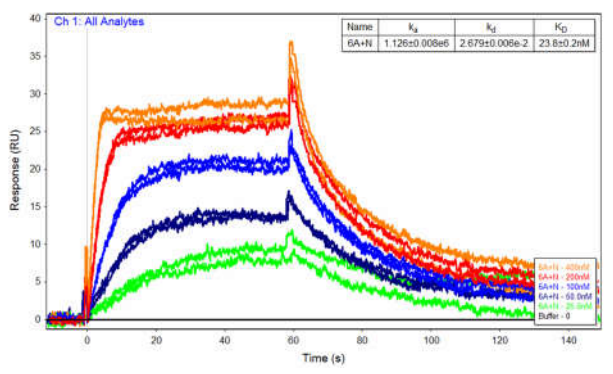
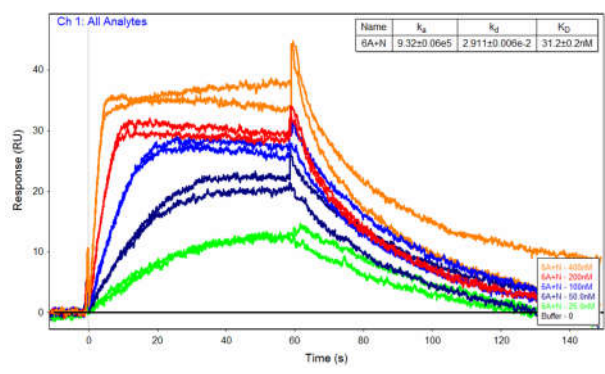


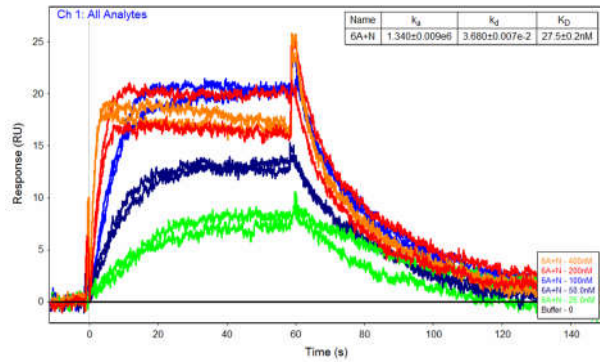
### 1000 mM Sodium Chloride – 4EBP1 (G<sup>49</sup>-N<sup>64</sup>)



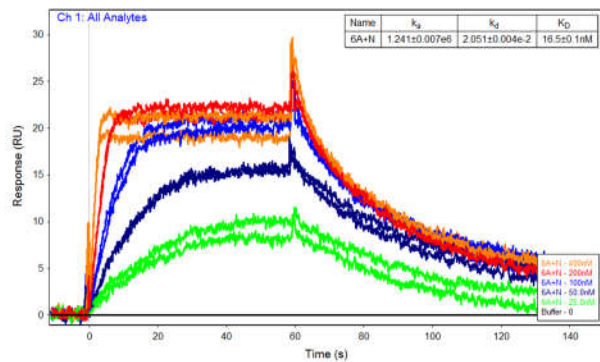
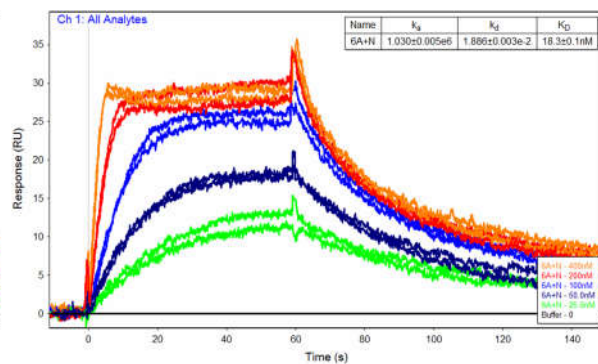
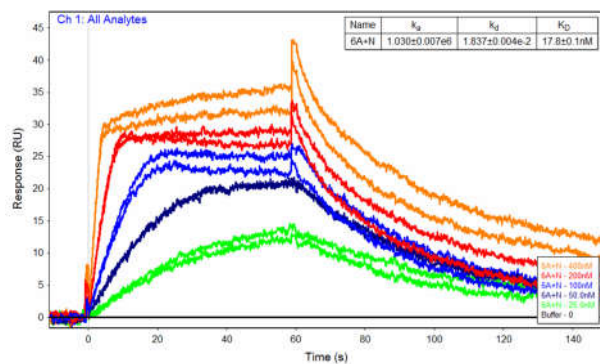
### 4E-BP1 (R<sup>51</sup>-N<sup>64</sup>)

### 30°C - 4E-BP1 (R<sup>51</sup>-N<sup>64</sup>)

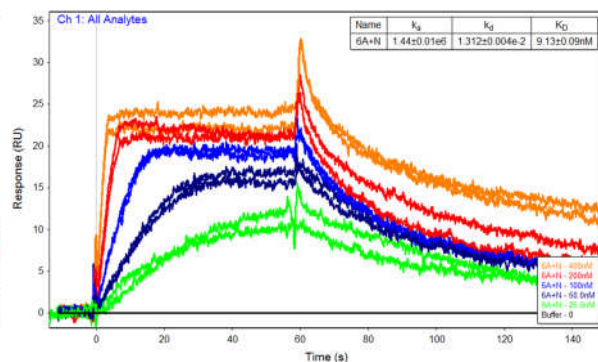
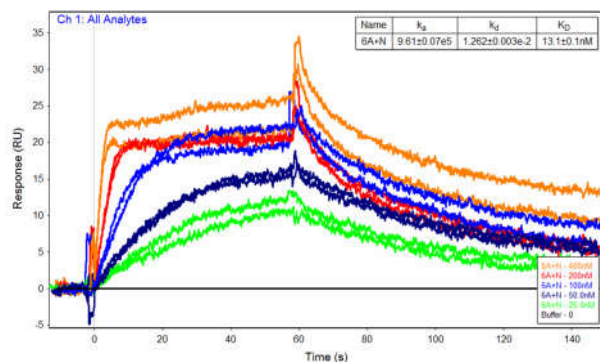


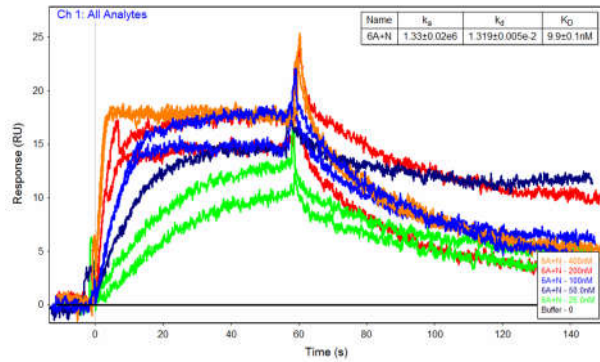


25°C - 4E-BP1 (R<sup>51</sup>-N<sup>64</sup>)

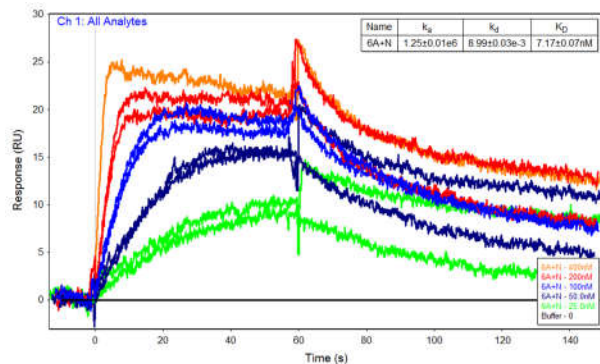
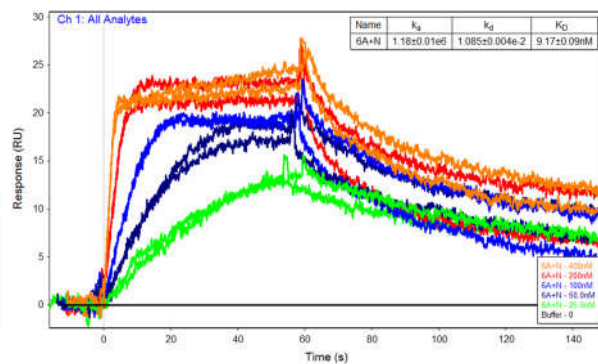
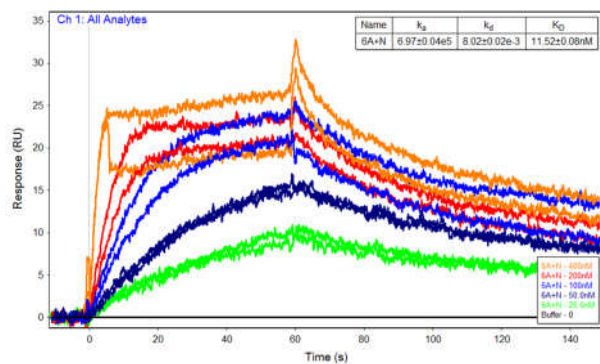


20°C - 4E-BP1 (R<sup>51</sup>-N<sup>64</sup>)

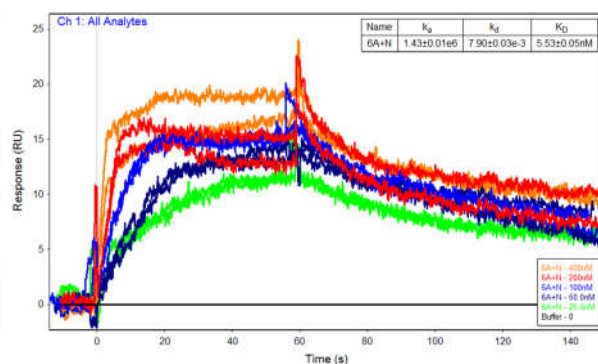
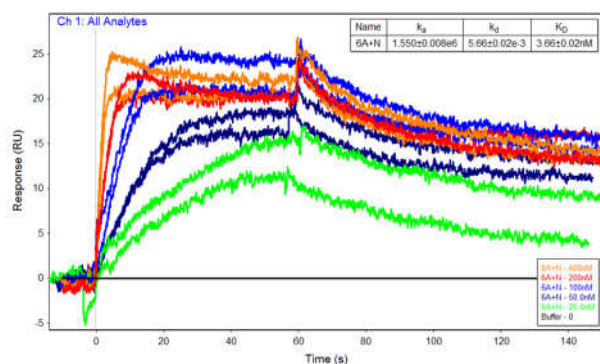


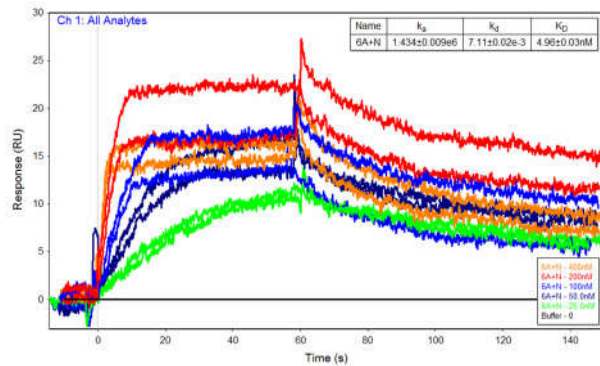


15°C - 4E-BP1 (R<sup>51</sup>-N<sup>64</sup>)

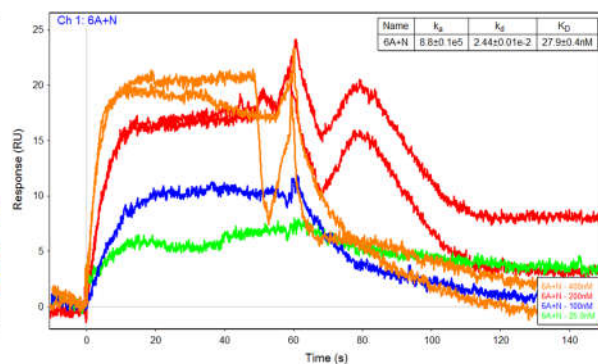
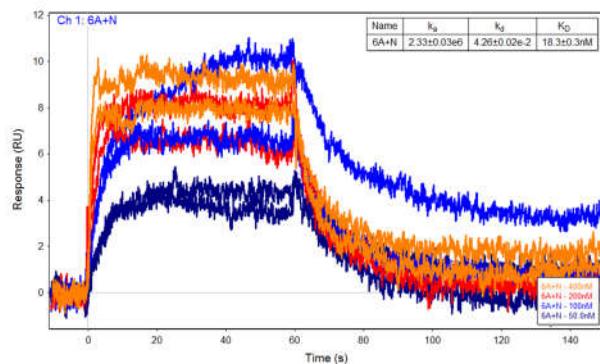
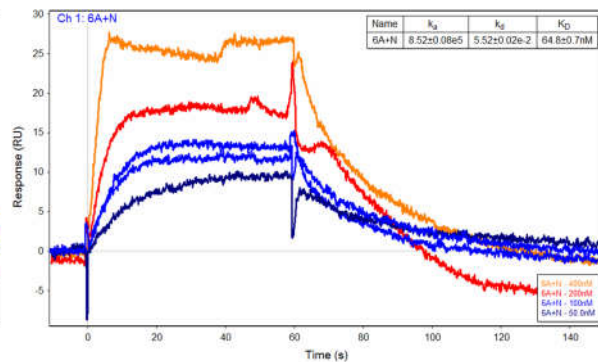
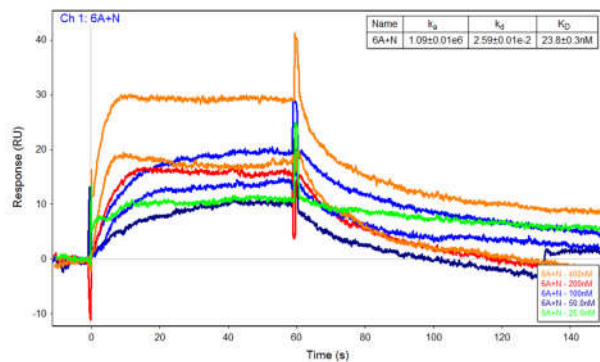


10°C - 4E-BP1 (R<sup>51</sup>-N<sup>64</sup>)

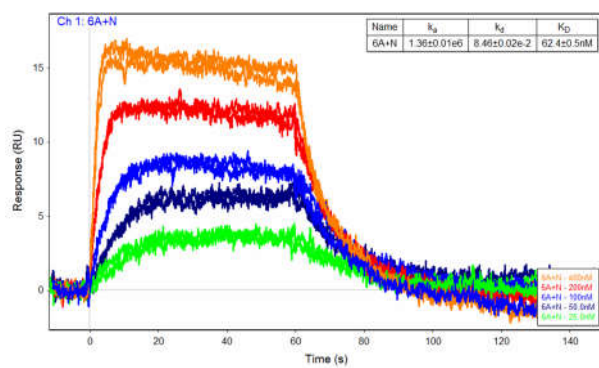
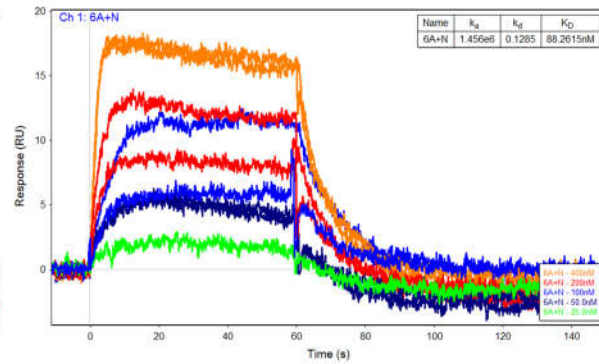
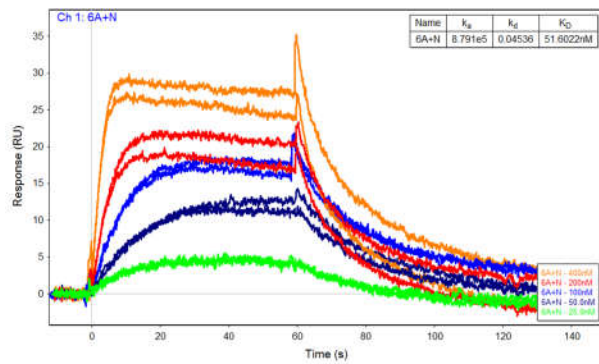




500 mM Sodium Chloride - 4E-BP1 ( $R^{51}$ - $N^{64}$ ) – the instrument was experiencing a partial clog during these experiments. Many curves needed to be removed due to spikes in the spectra, and the remaining curves are still quite ugly. Therefore, the following sets of data need to be taken with a grain of salt (ha ha). This data is not shown in the figure in the main text.



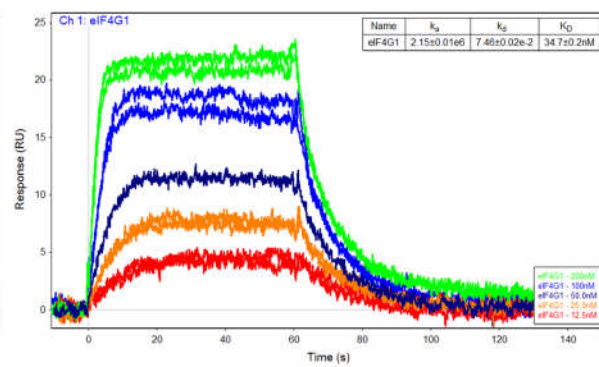
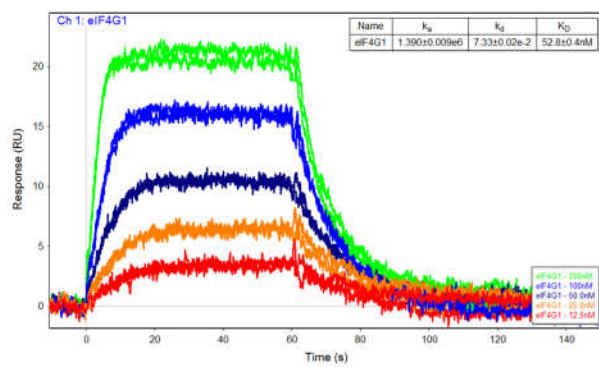
## 1000 mM Sodium Chloride - 4E-BP1 (R<sup>51</sup>-N<sup>64</sup>)

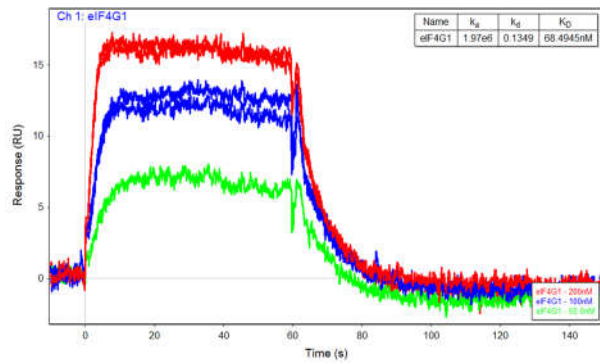
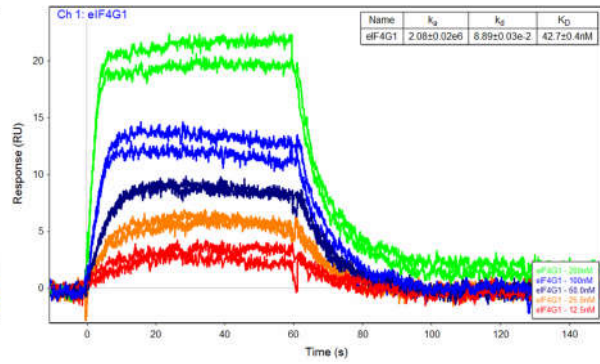
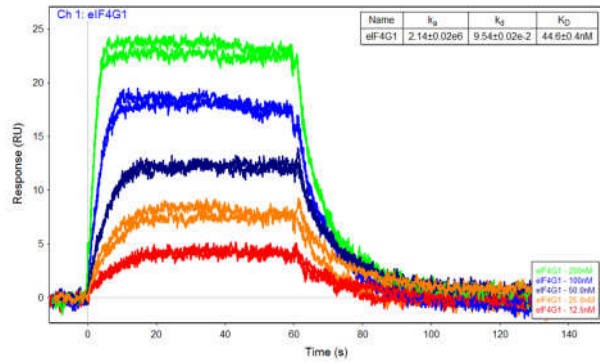


## eIF4G Linear Peptides

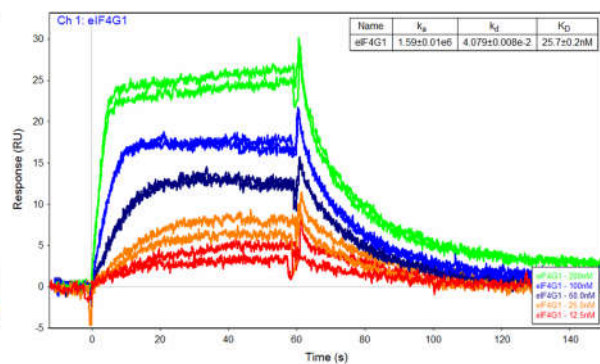
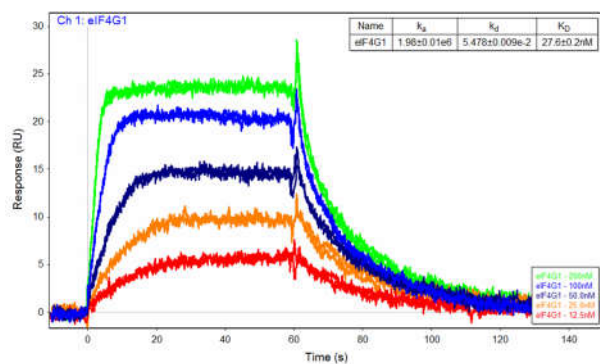
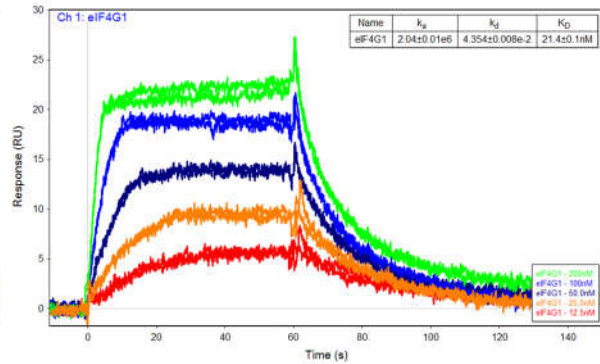
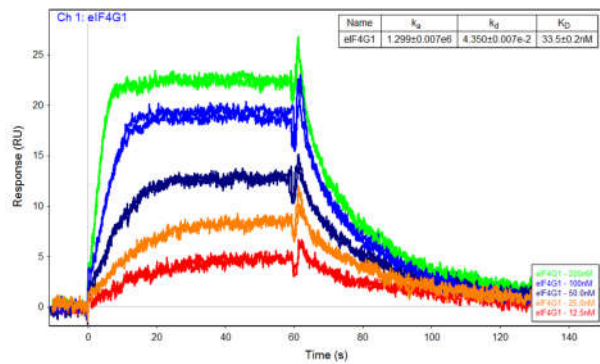
eIF4G (K<sup>608</sup>-F<sup>622</sup>)

30°C - eIF4G (K<sup>608</sup>-F<sup>622</sup>)

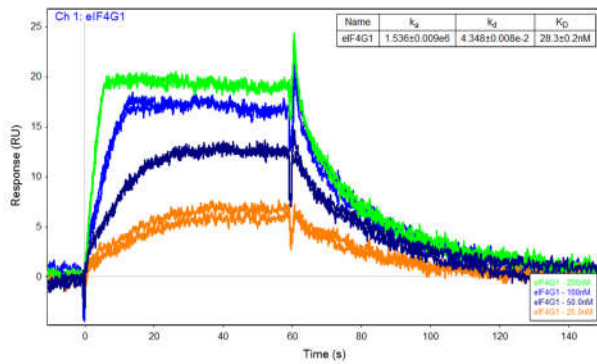
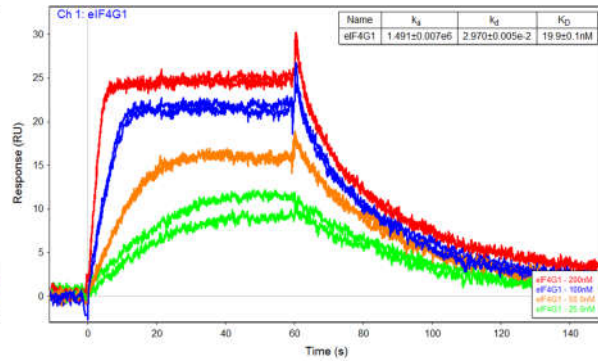
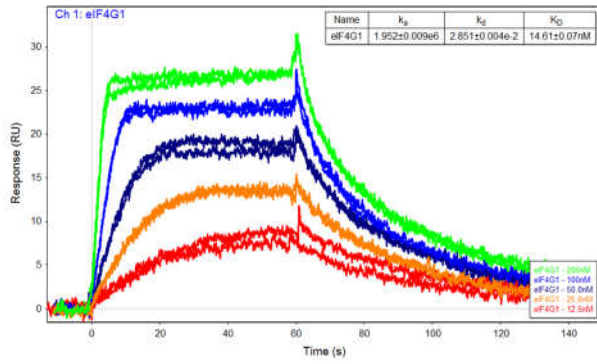




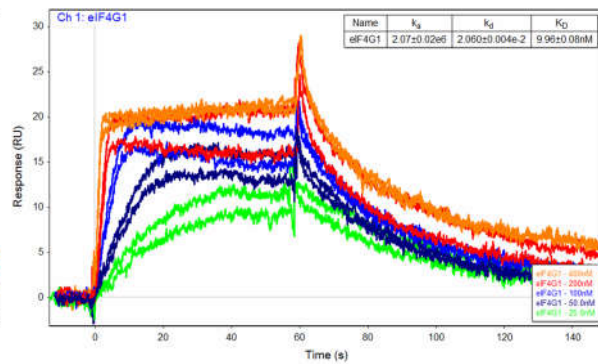
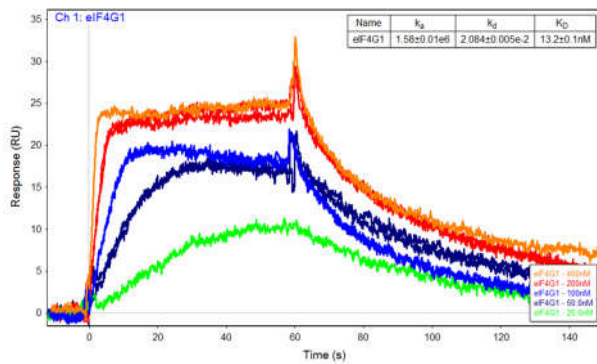
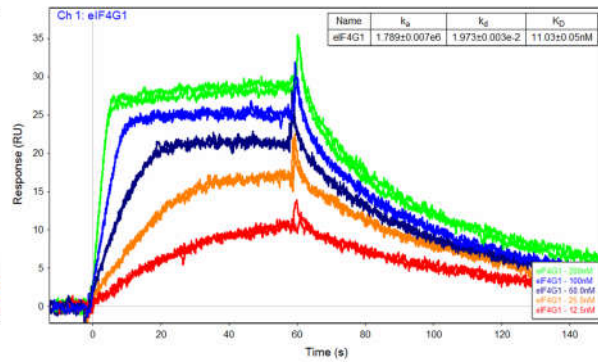
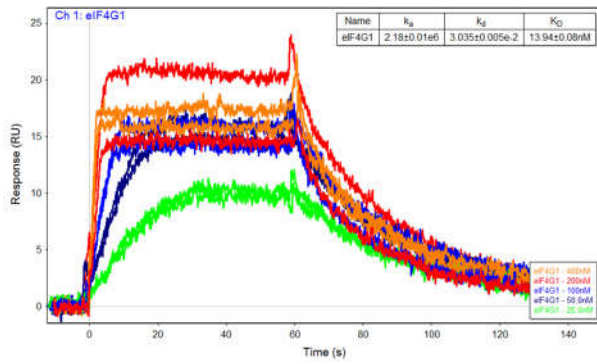
25°C - eIF4G (K<sup>608</sup>-F<sup>622</sup>)



20°C - eIF4G (K<sup>608</sup>-F<sup>622</sup>)

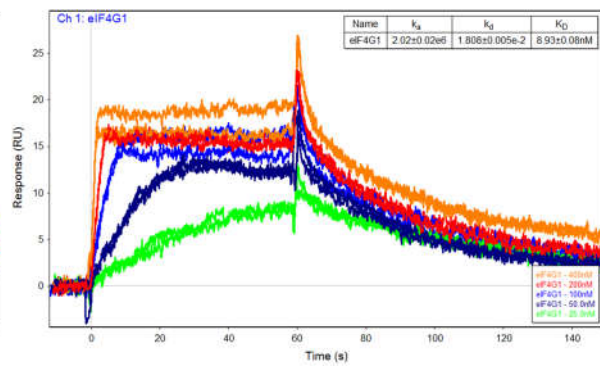
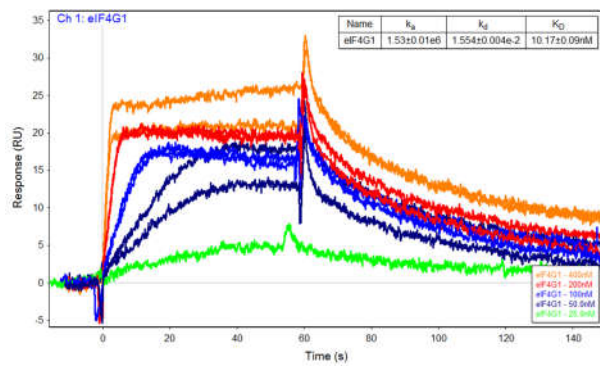
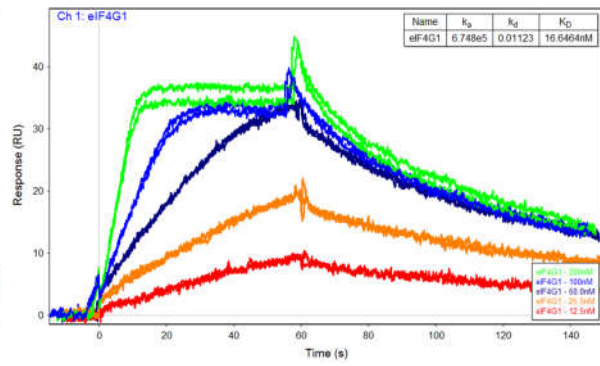
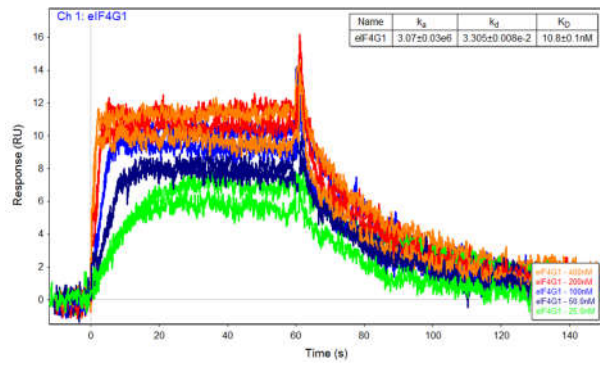


15°C - eIF4G (K<sup>608</sup>-F<sup>622</sup>)

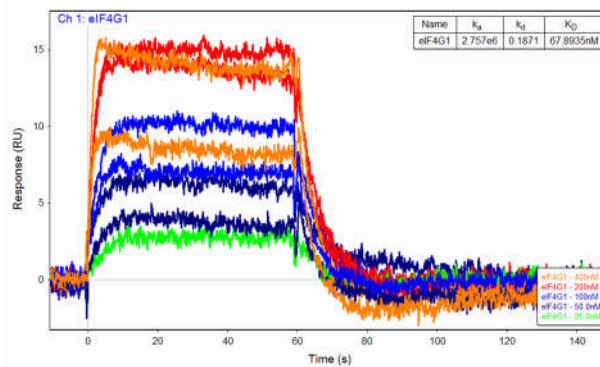
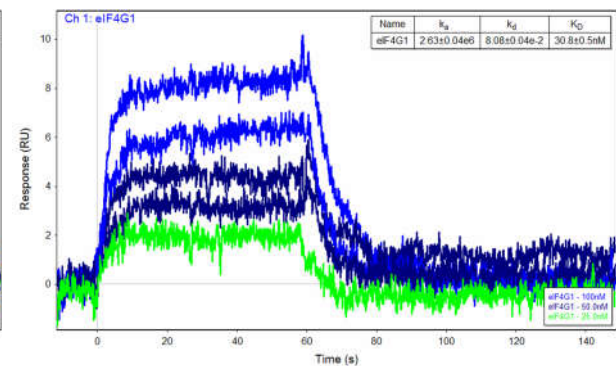
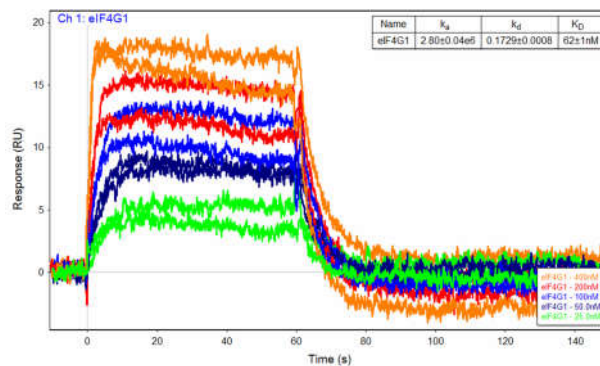




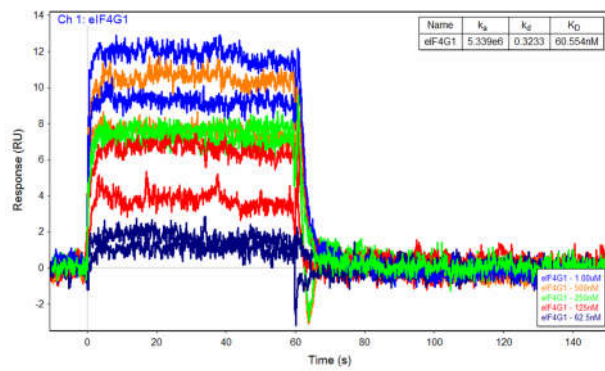
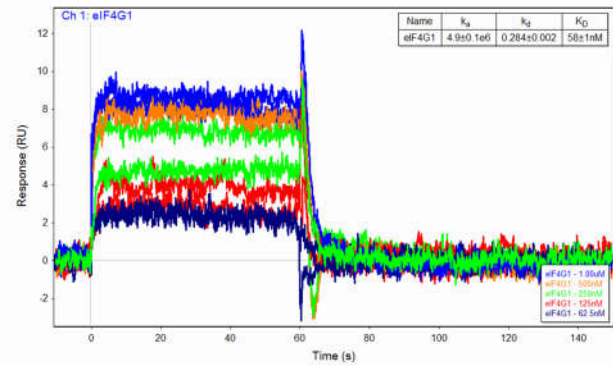
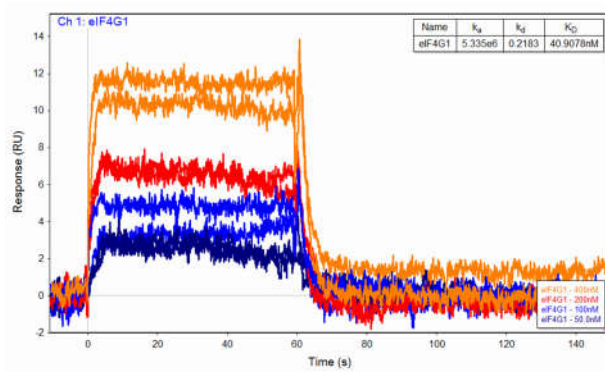
10°C - eIF4G (K<sup>608</sup>-F<sup>622</sup>)



500 mM Sodium Chloride - eIF4G (K<sup>608</sup>-F<sup>622</sup>)

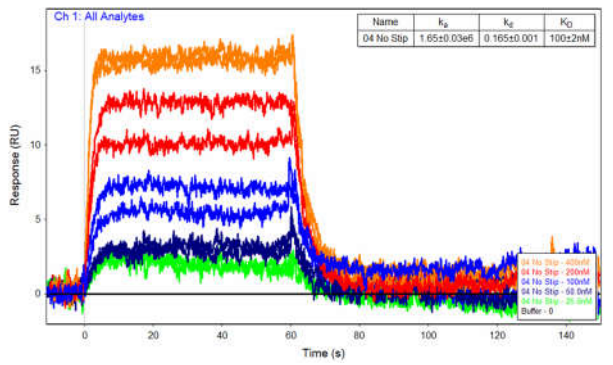
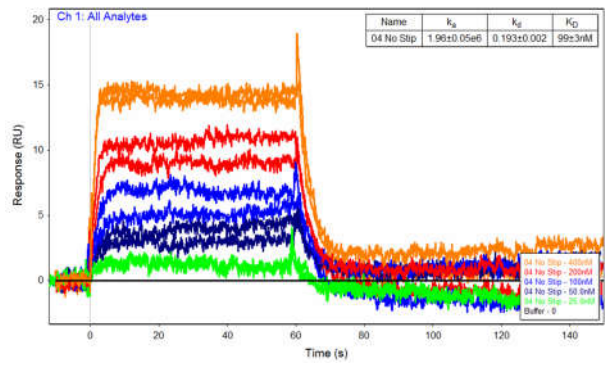


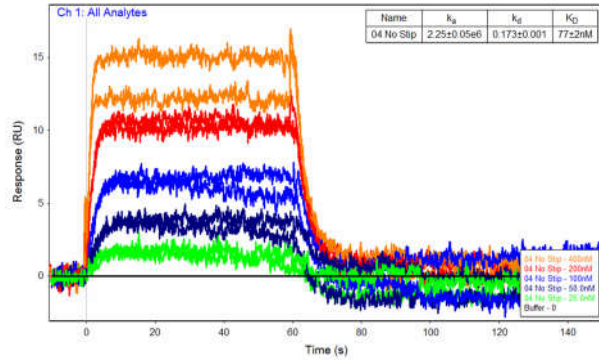
1000 mM Sodium Chloride - eIF4G (K<sup>608</sup>-F<sup>622</sup>)



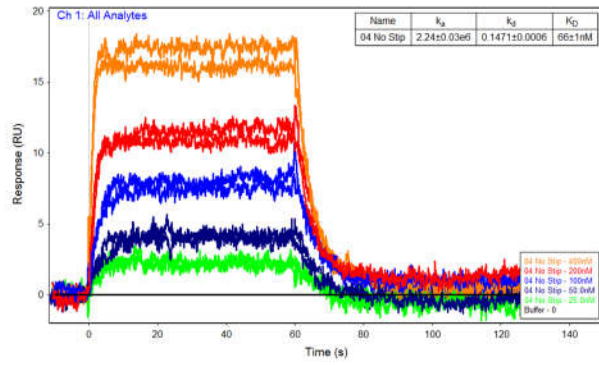
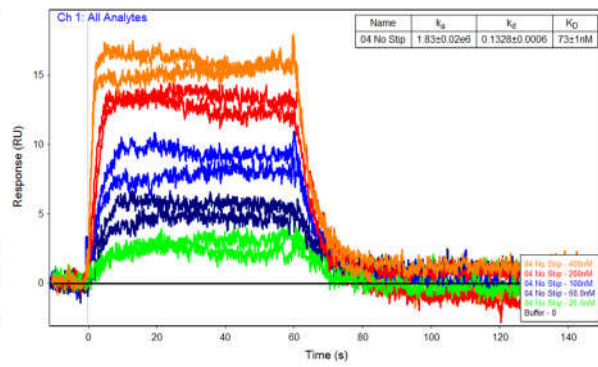
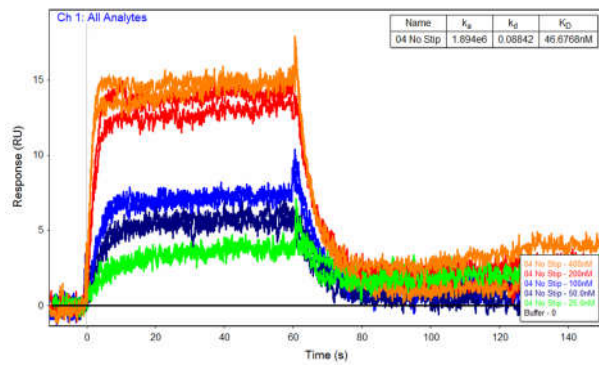
eIF4G (K<sup>608</sup>-F<sup>620</sup>) D<sup>613</sup>S, F<sup>616</sup>Q

30°C - eIF4G (K<sup>608</sup>-F<sup>620</sup>) D<sup>613</sup>S, F<sup>616</sup>Q

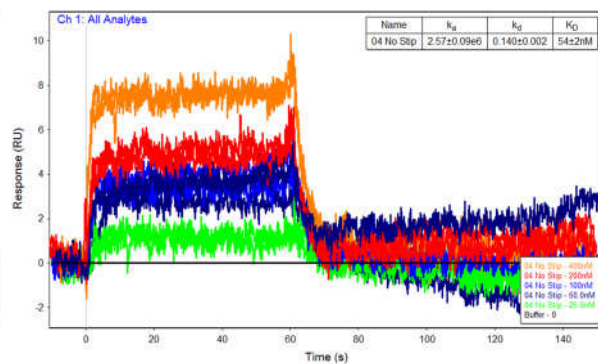
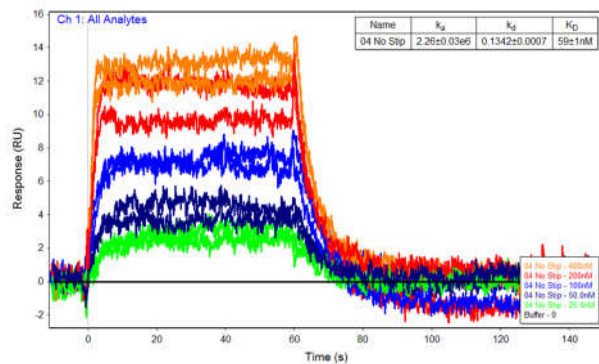


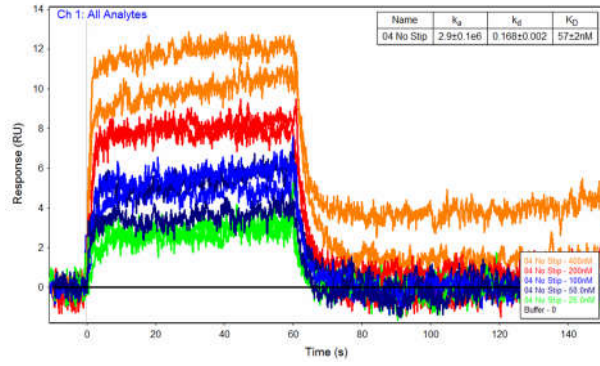


25°C - eIF4G (K<sup>608</sup>-F<sup>620</sup>) D<sup>613</sup>S, F<sup>616</sup>Q

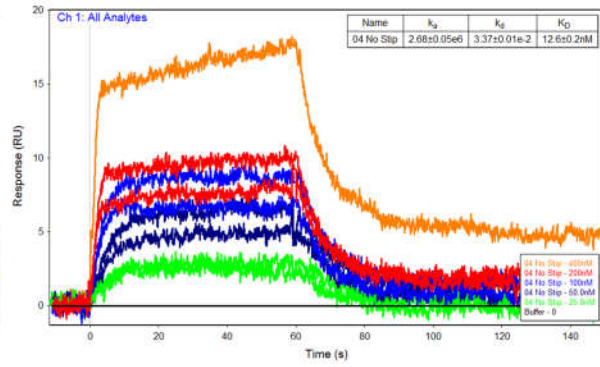
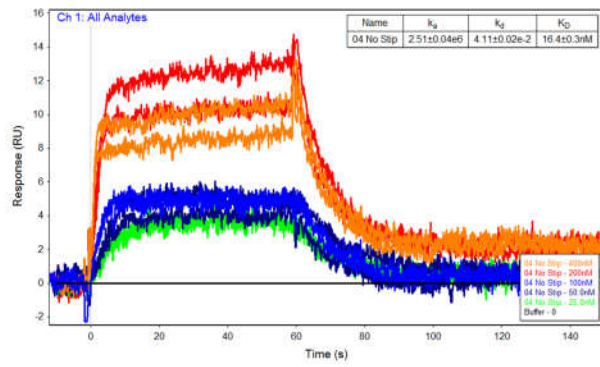
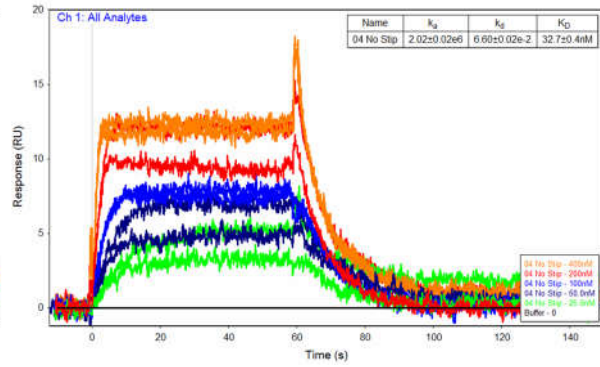
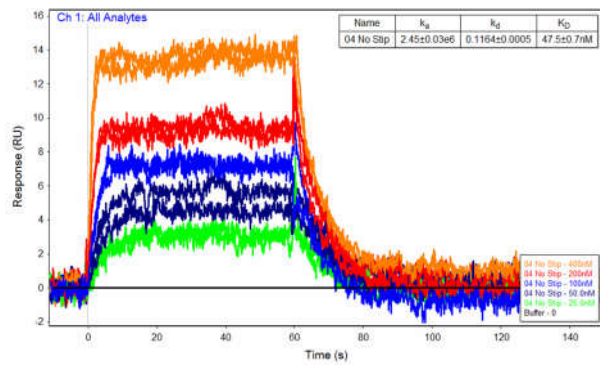


20°C - eIF4G (K<sup>608</sup>-F<sup>620</sup>) D<sup>613</sup>S, F<sup>616</sup>Q

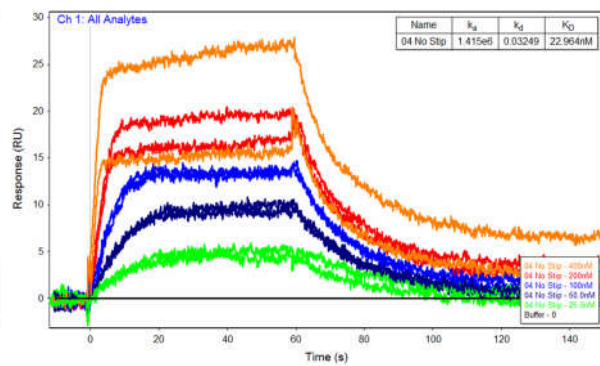
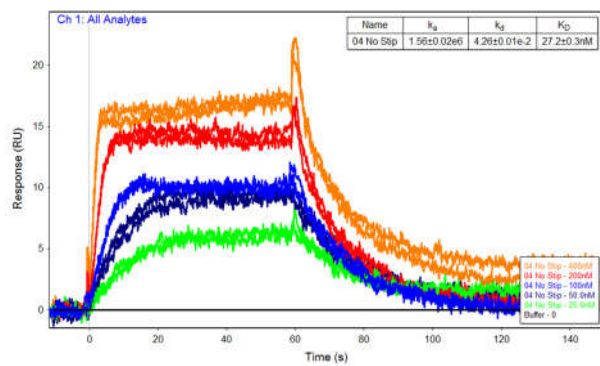


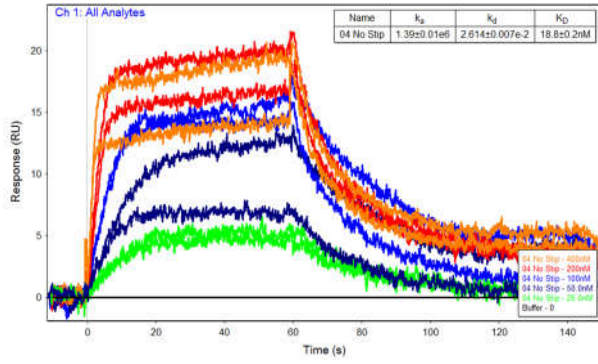


15°C - eIF4G (K<sup>608</sup>-F<sup>620</sup>) D<sup>613</sup>S, F<sup>616</sup>Q

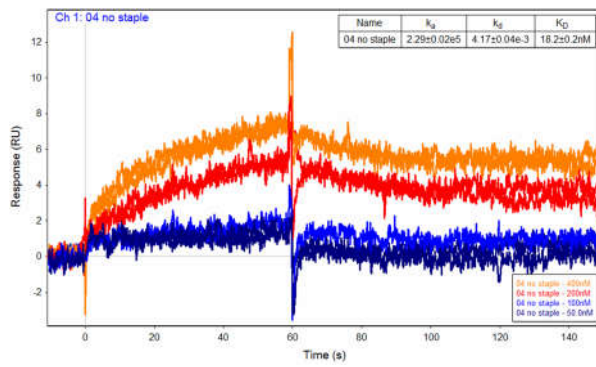
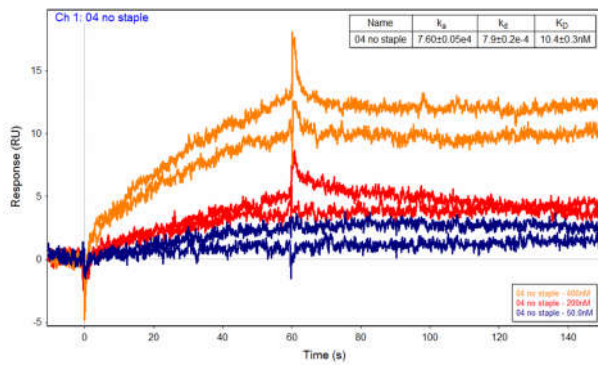


10°C - eIF4G (K<sup>608</sup>-F<sup>620</sup>) D<sup>613</sup>S, F<sup>616</sup>Q



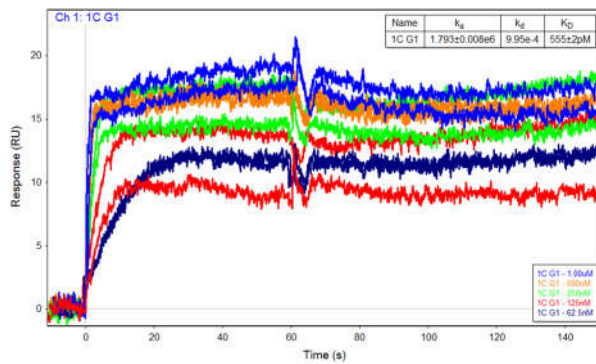
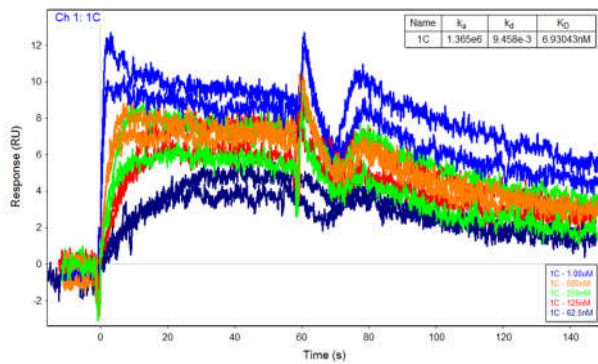


1000 mM Sodium Chloride - eIF4G (K<sup>608</sup>-F<sup>620</sup>) D<sup>613</sup>S, F<sup>616</sup>Q

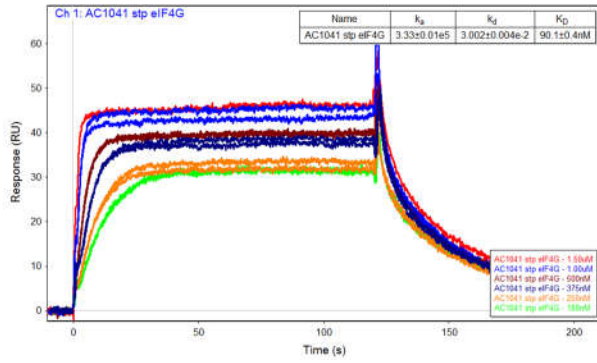


Data for Other Peptides

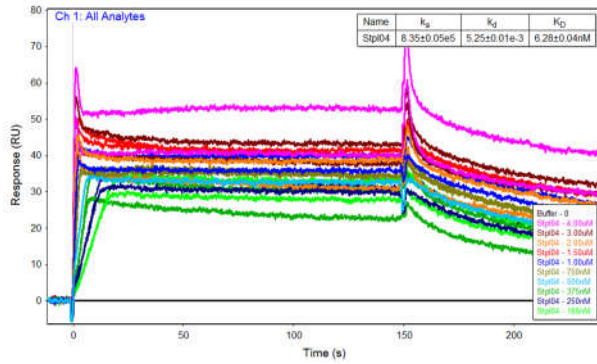
HCS-4E-BP1



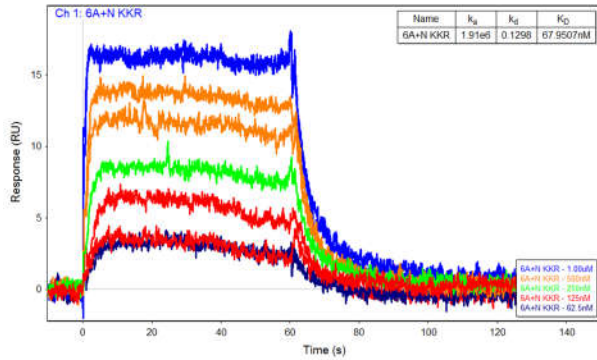
## HCS-eIF4G



## sTIP-04



## 4E-BP1 (R<sup>51</sup>-N<sup>64</sup>) R<sup>51</sup>K, I<sup>52</sup>K, I<sup>53</sup>R



## Appendix B

### Chapter 3 - Supplemental Information

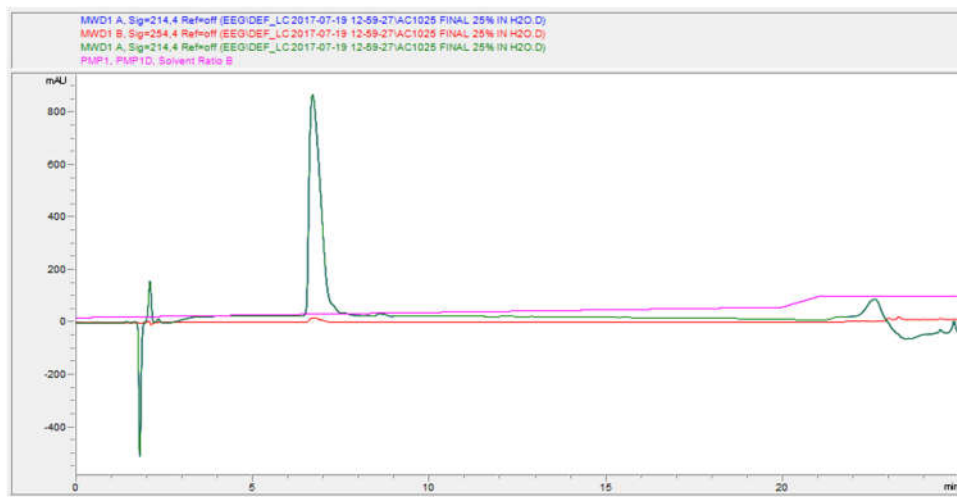
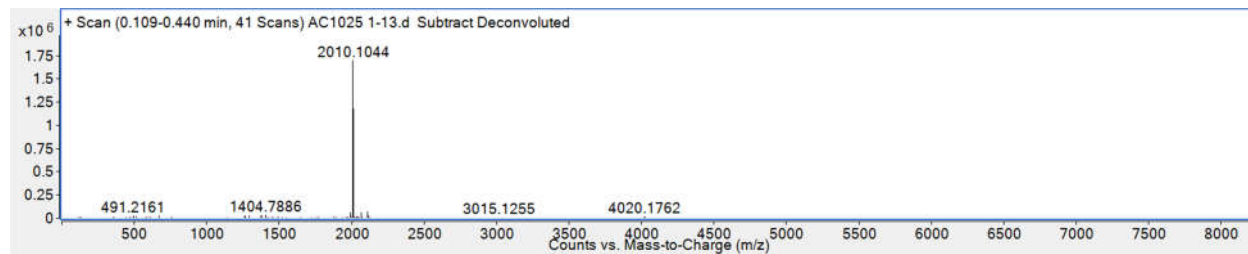
#### Compound Characterization

All of the linear peptides were purchased through New England Peptide with the exception of 4E-BP1-10. All peptides are acetylated on the amino terminus and amides on the carboxy terminus.

**4E-BP1-10** – Synthesized by Alyah Chmiel

Sequence: GTRIIYDRKFLLECKN

Mass Expected: 2009.09

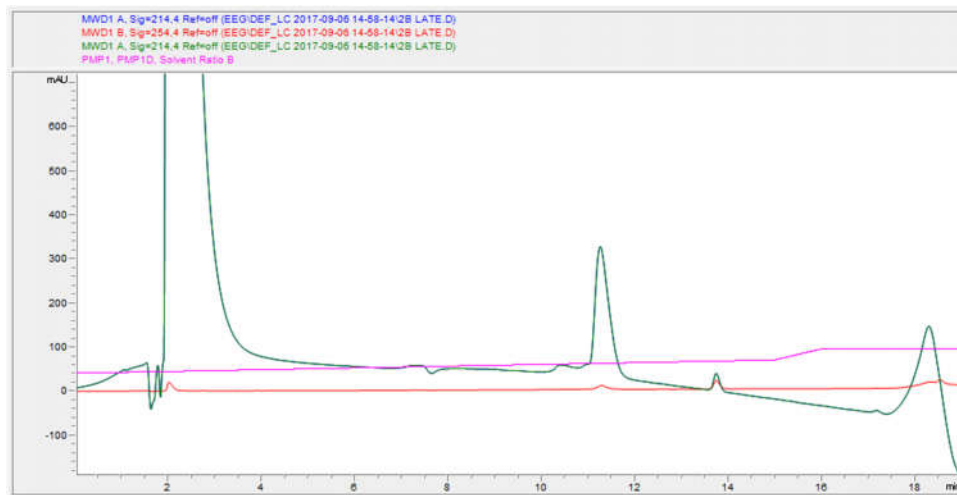
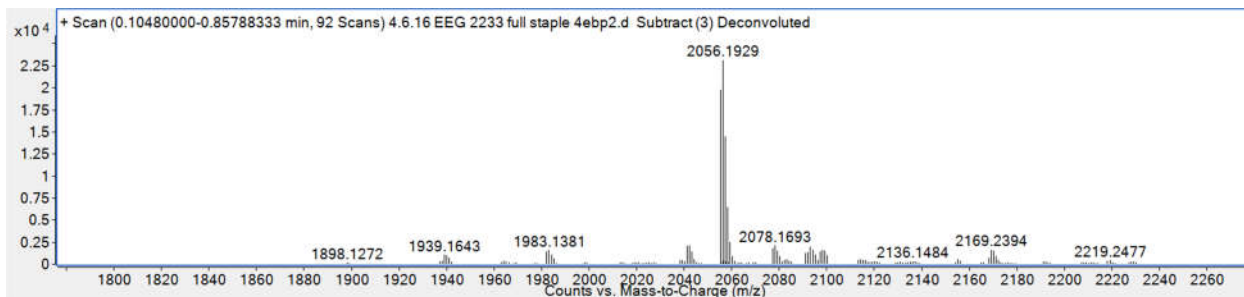


mHCS-1 – Synthesized by Dr. James Song; characterization is in his thesis

## mHCS-2

Sequence: GTRIIYDRXFLLXRRN; X = pentenyl glycine

Mass Expected: 2055.99

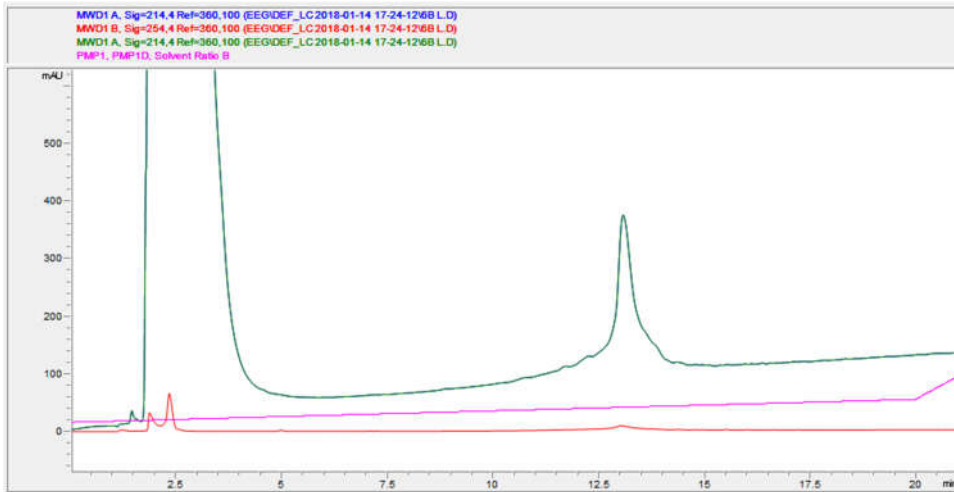
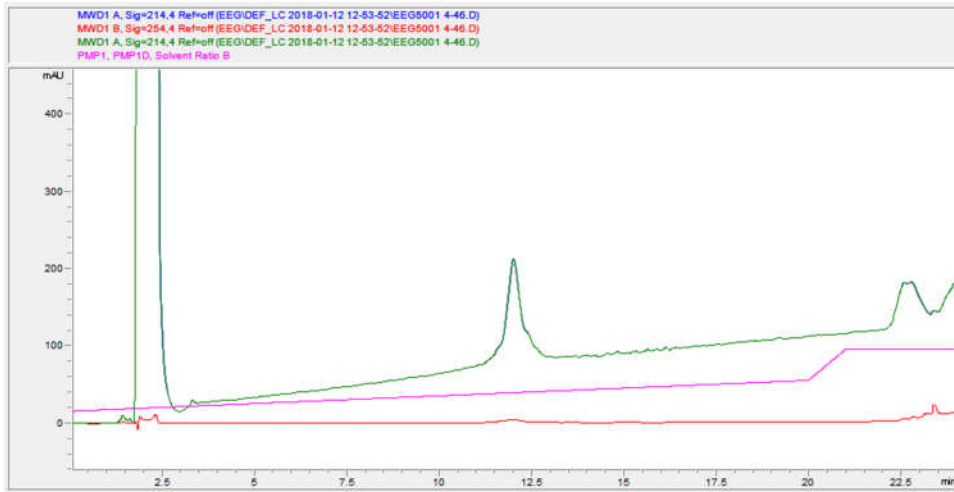
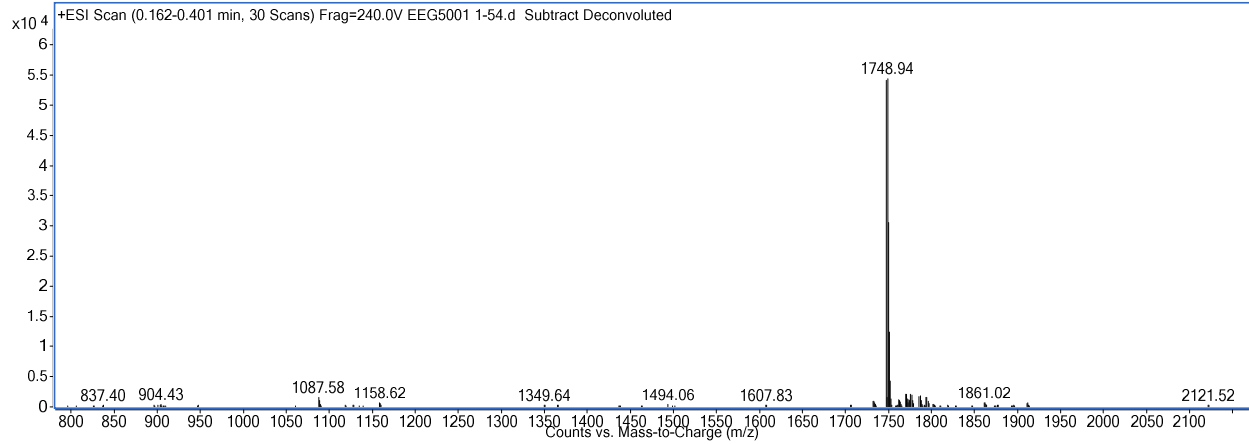


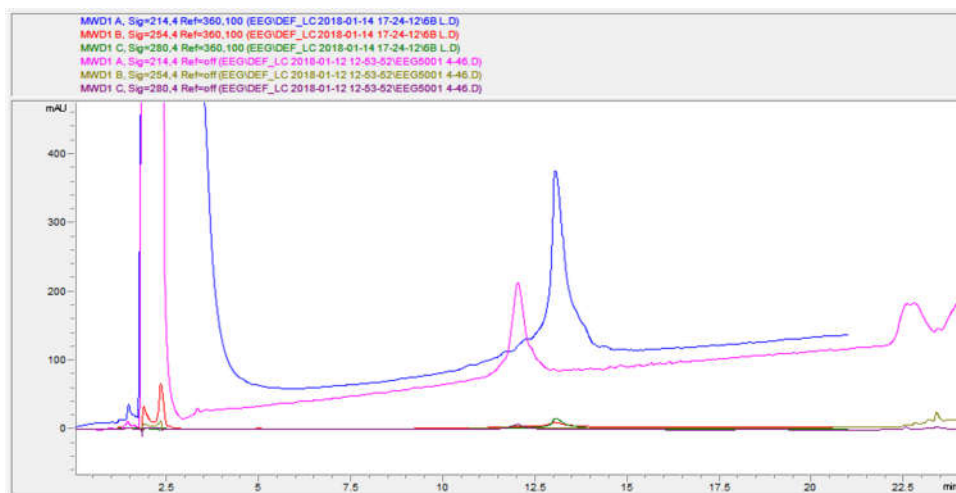


### mHCS-3

Sequence: RIIYDRXFLMXCR; X = pentenyl glycine

Mass Expected: 1747.94

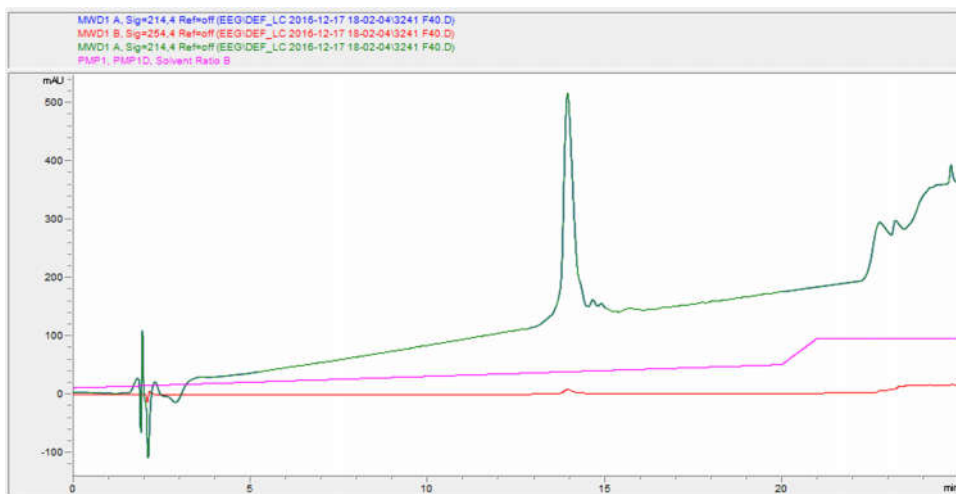
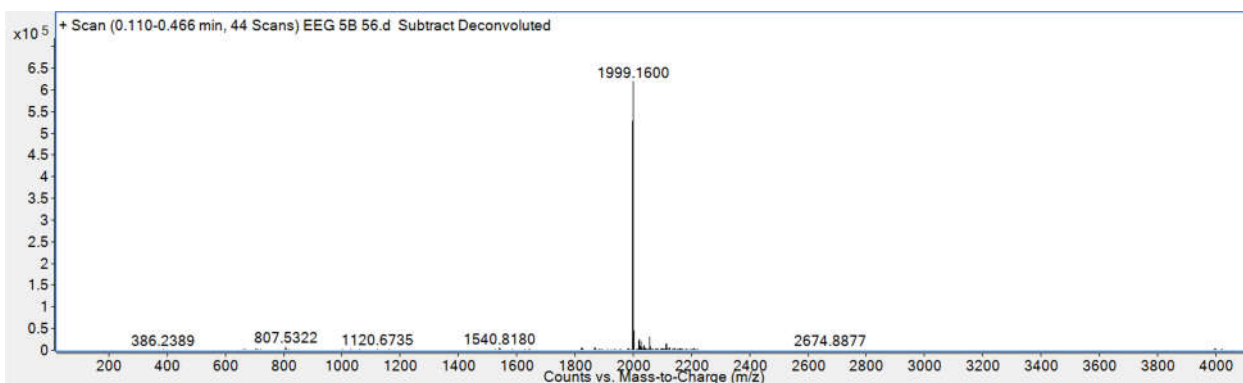




### mHCS-4

Sequence: GTRIIYDRXFLN<sub>L</sub>XVRN; X = pentenyl glycine, N<sub>L</sub> = norleucine

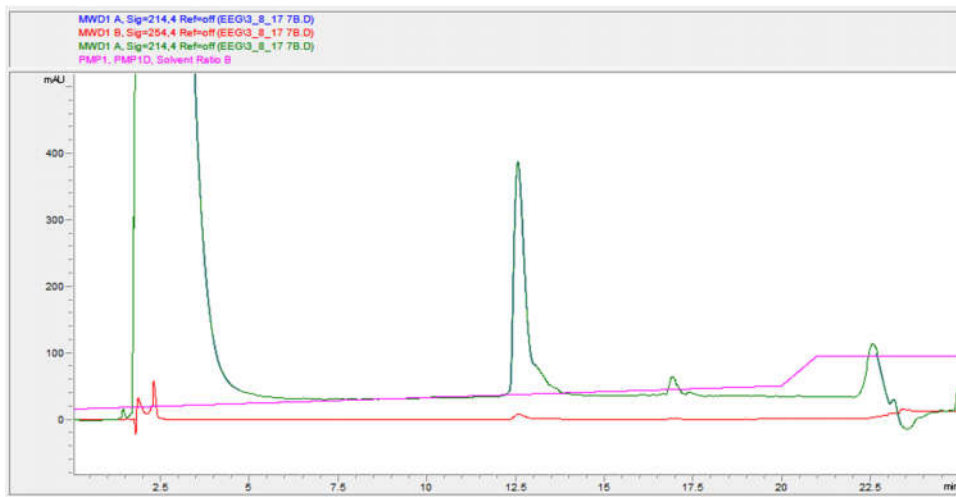
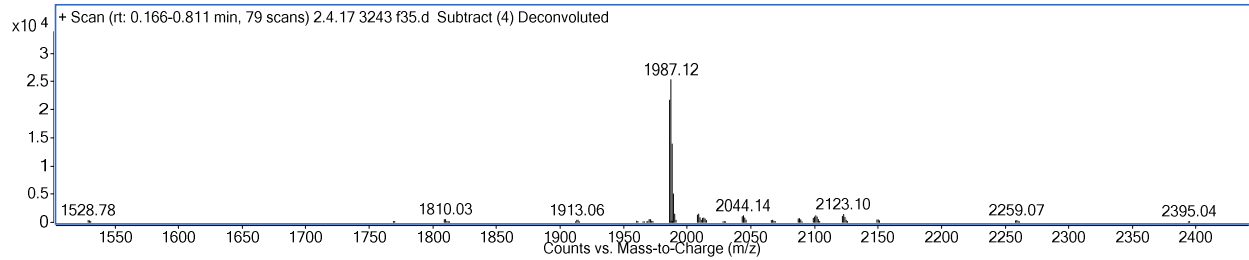
Mass Expected: 1998.15



## mHCS-5

Sequence: GTRIIYDRXFLN<sub>L</sub>XSRN; X = pentenyl glycine, N<sub>L</sub> = norleucine

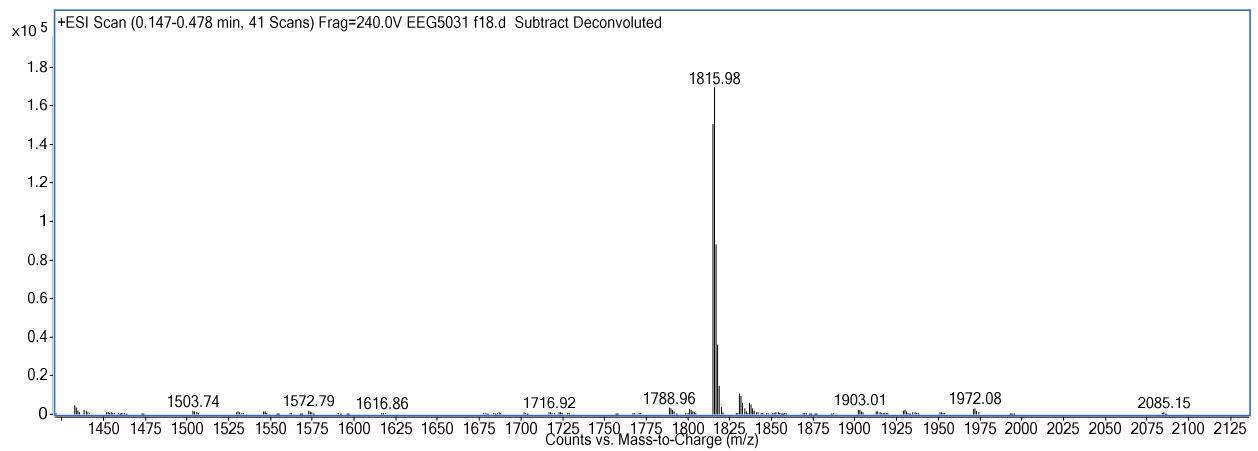
Mass Expected: 1986.12

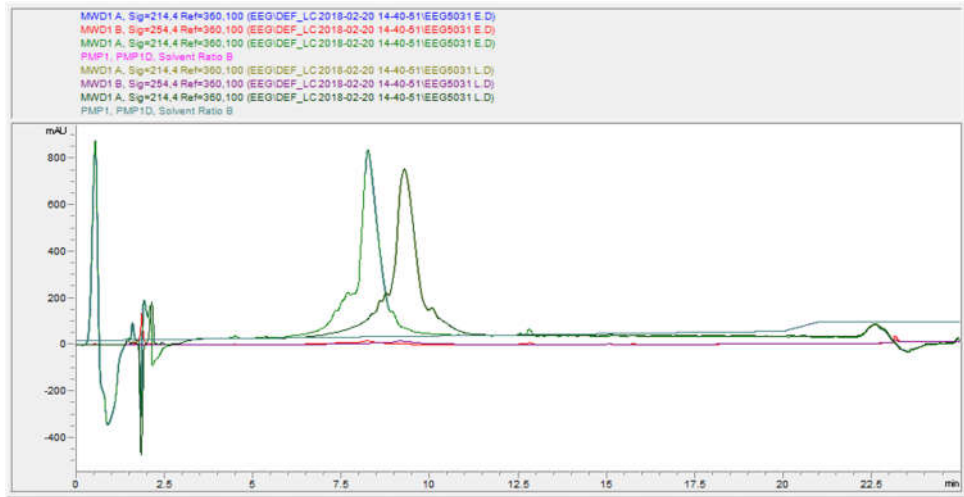
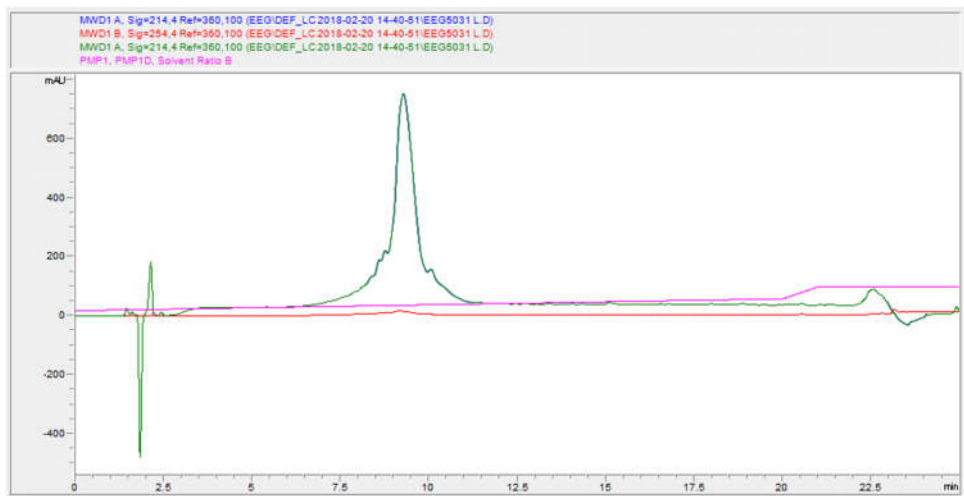
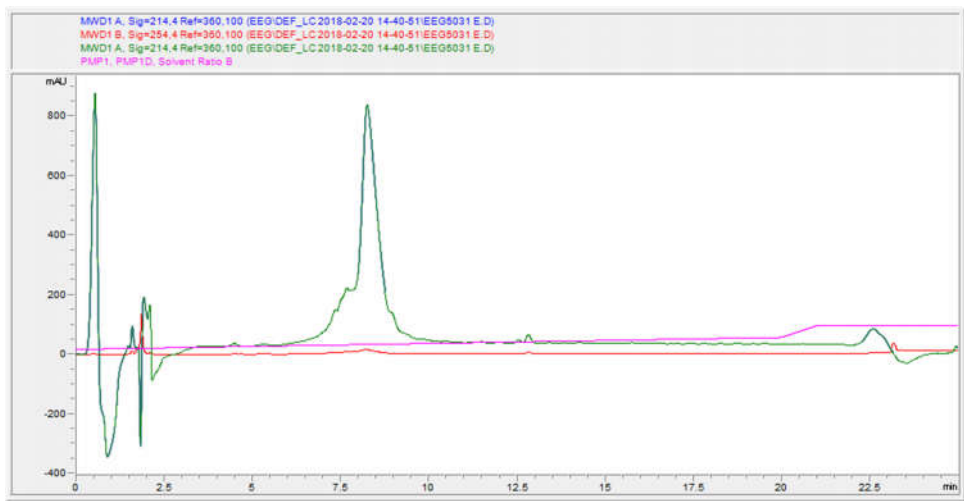


## mHCS-6

Sequence: RIIYSRXQLMXCRN; X = pentenyl glycine

Mass Expected: 1814.98

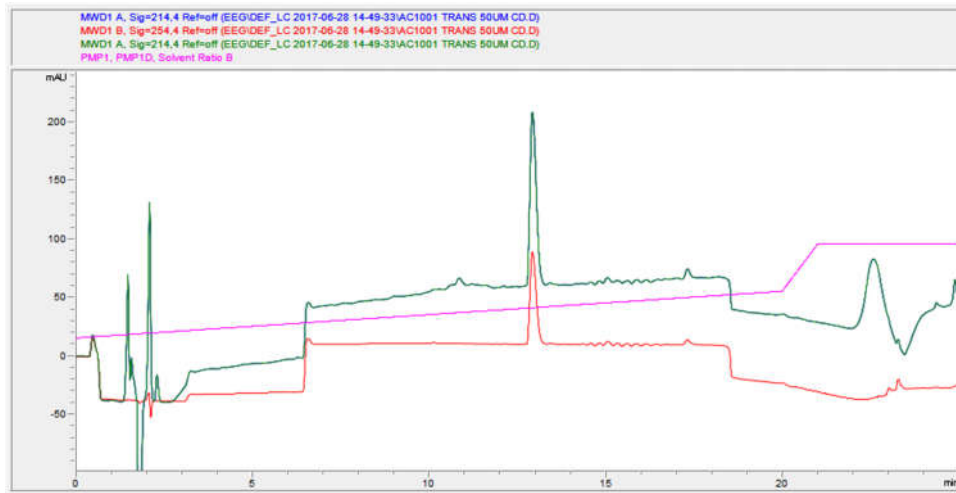
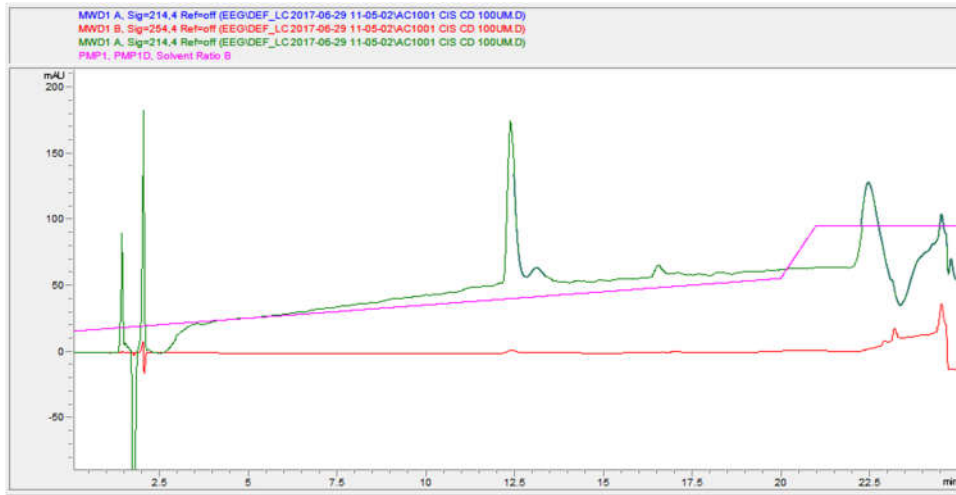
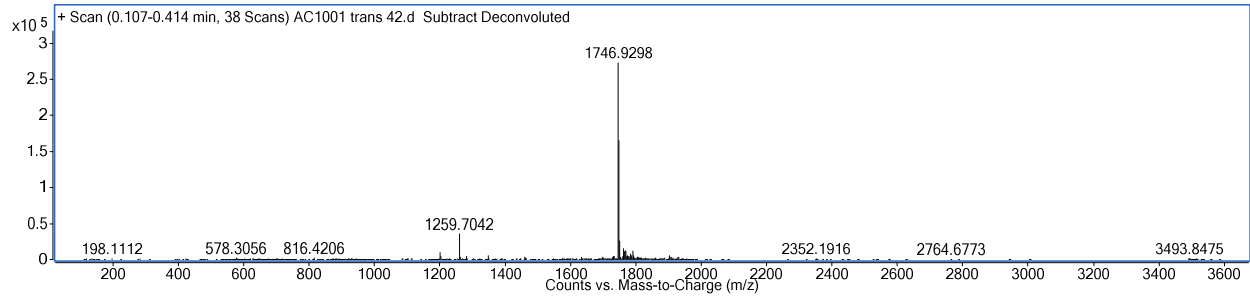


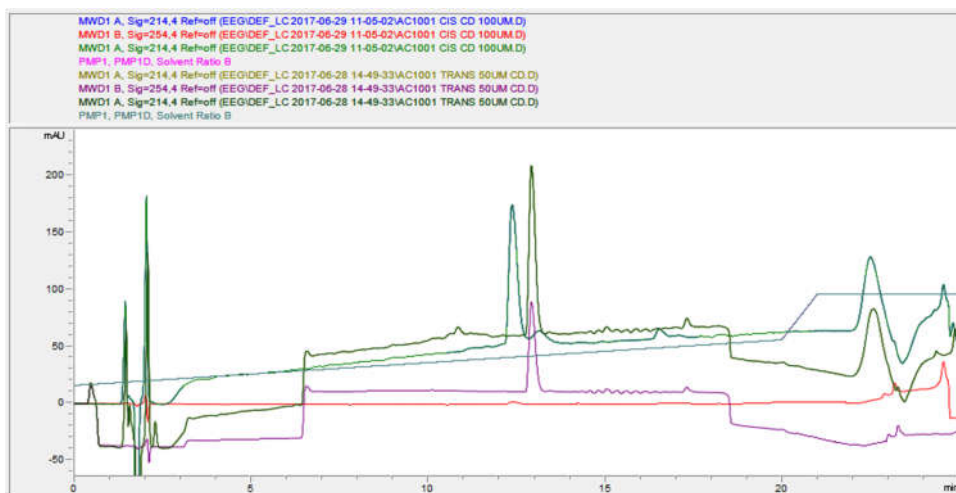


# mHCS-7 – Synthesized by Alyah Chmiel

Sequence: RIIYDRXF\*MXCRN; X = pentenyl glycine; \* = cyclopropyl alanine

Mass Expected: 1745.92

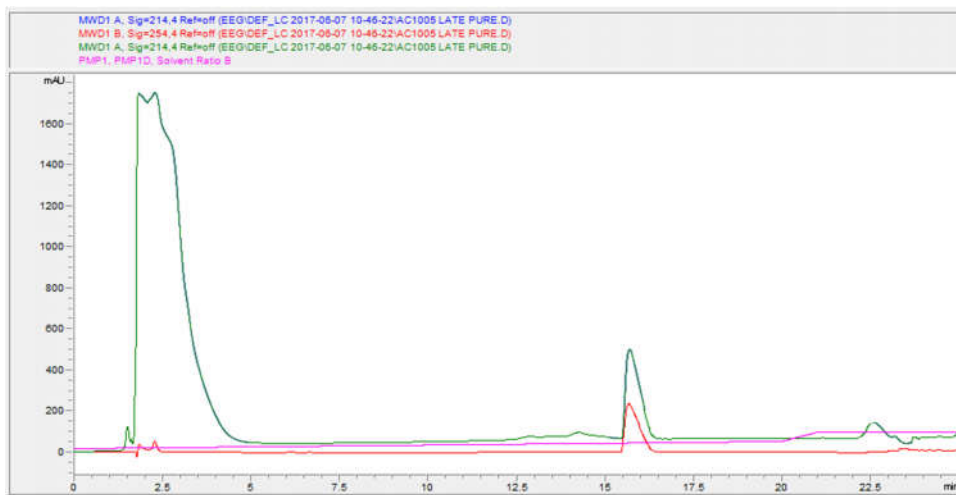
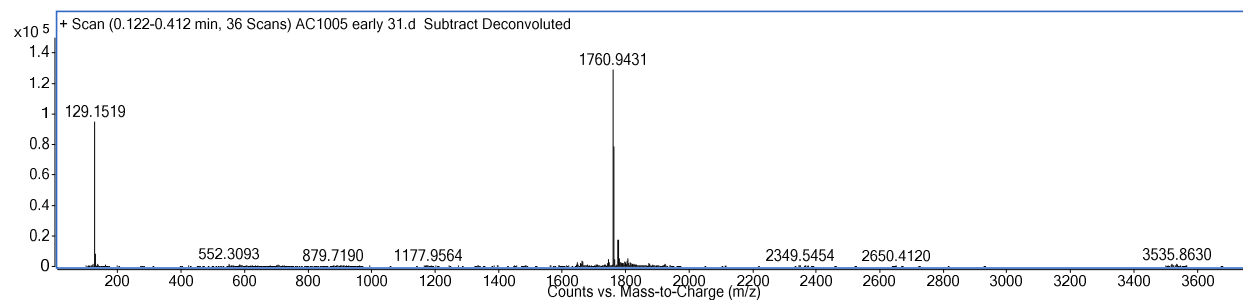




### mHCS-8 – Synthesized by Alyah Chmiel

Sequence: RIYDRXF\*MXCRN; X = pentenyl glycine; \* = cyclobutyl alanine

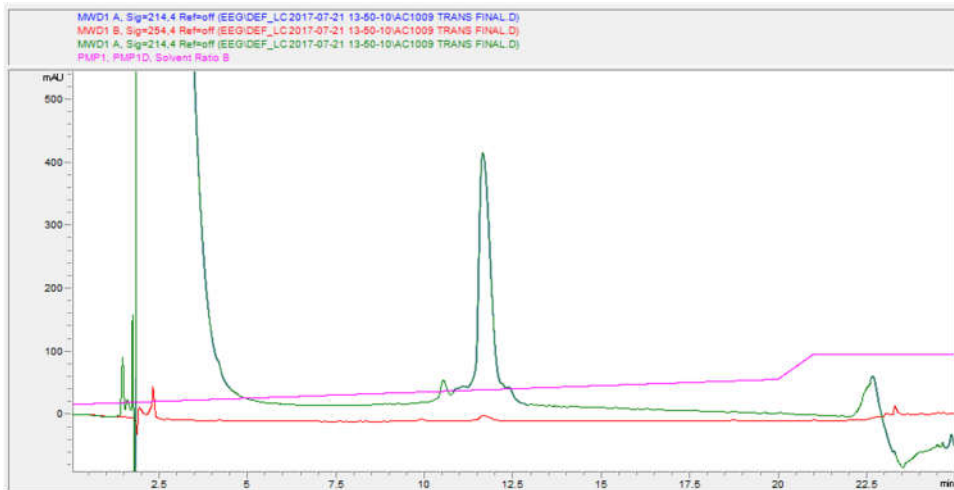
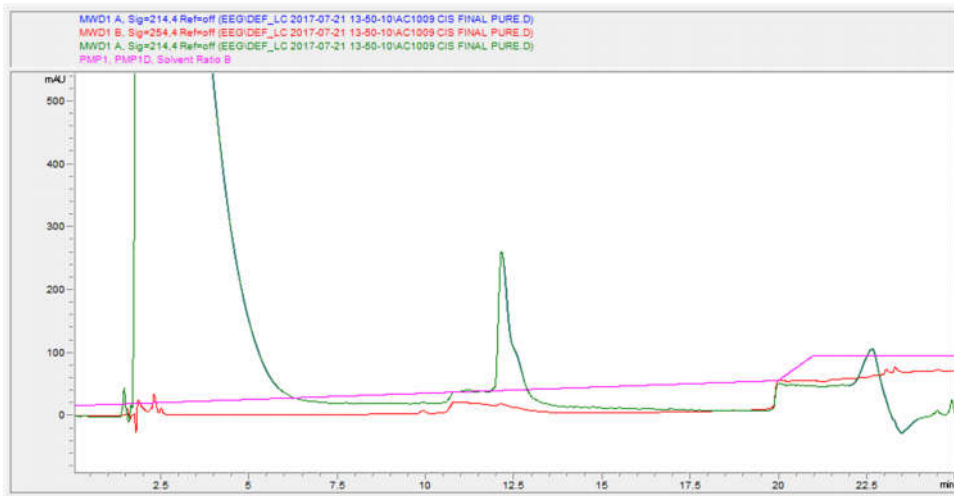
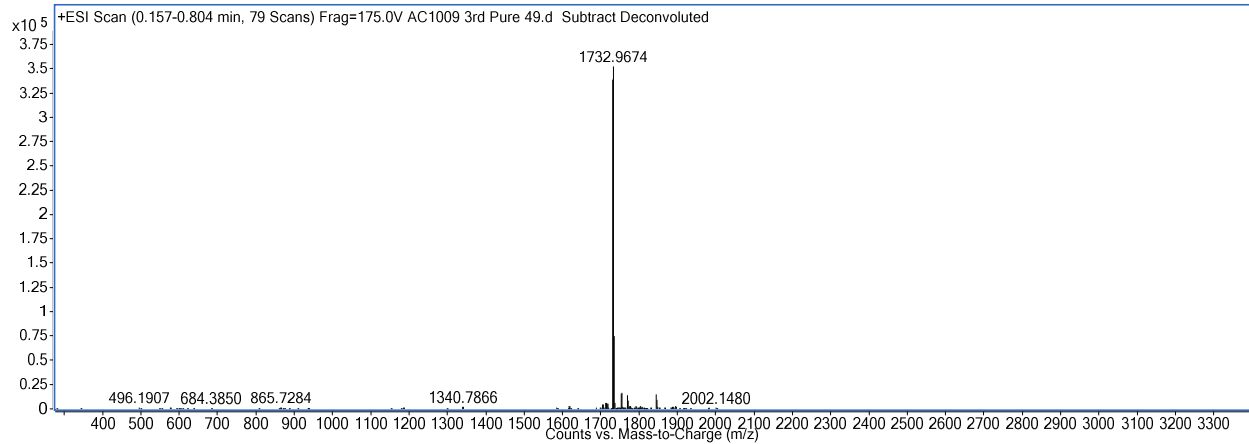
Mass Expected: 1759.94

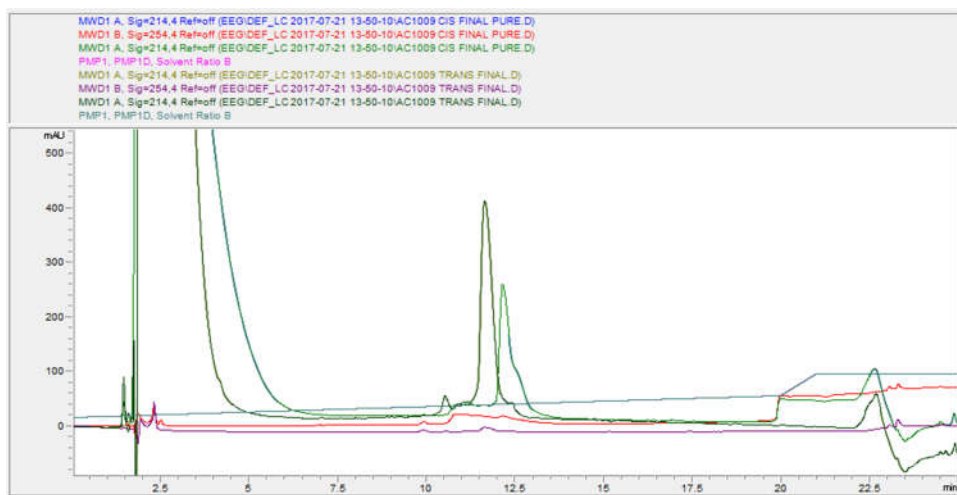


# mHCS-9 – Synthesized by Alyah Chmiel

Sequence: RIIYDRXFL\*XCRN; X = pentenyl glycine; \* = O-methyl homoserine

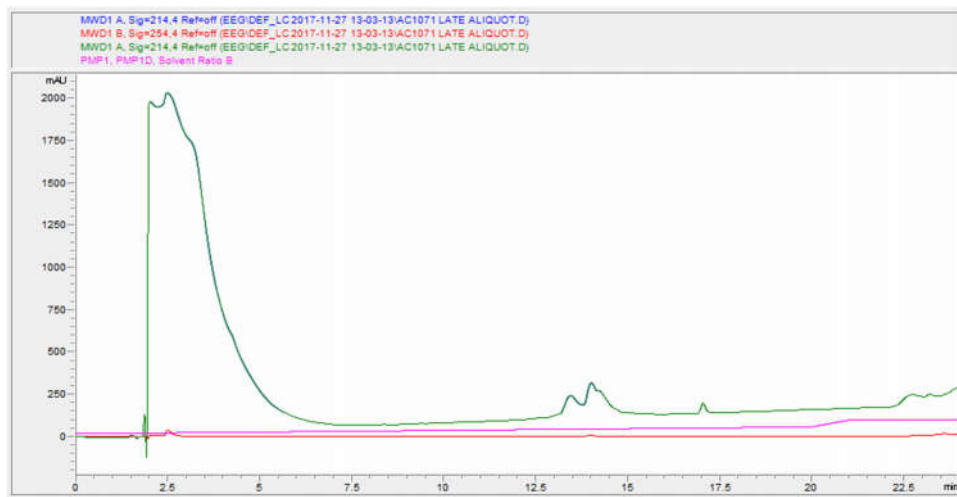
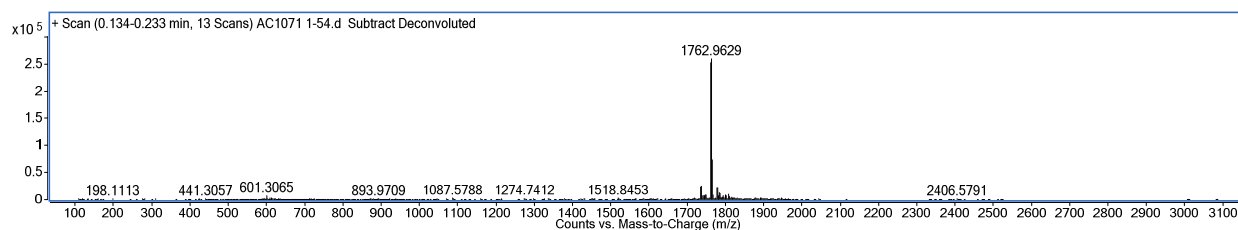
Mass Expected: 1731.96





**mHCS-10** – Synthesized by Alyah Chmiel

Mass Expected: 1761.95

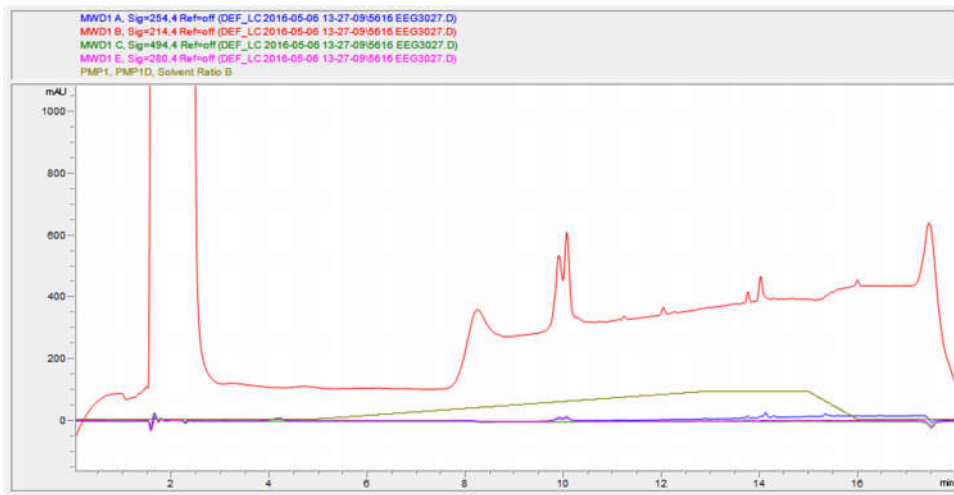
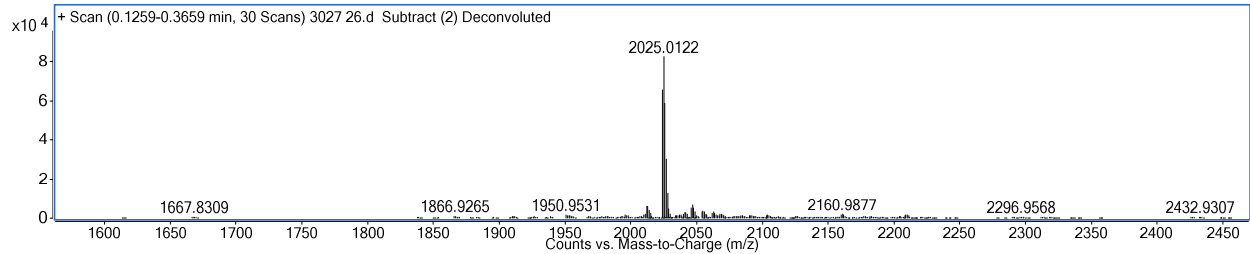




## OASer-1

Sequence: GTRIIYDRXFLMXCRN; X = O-allyl serine

Mass Expected: 2024.01

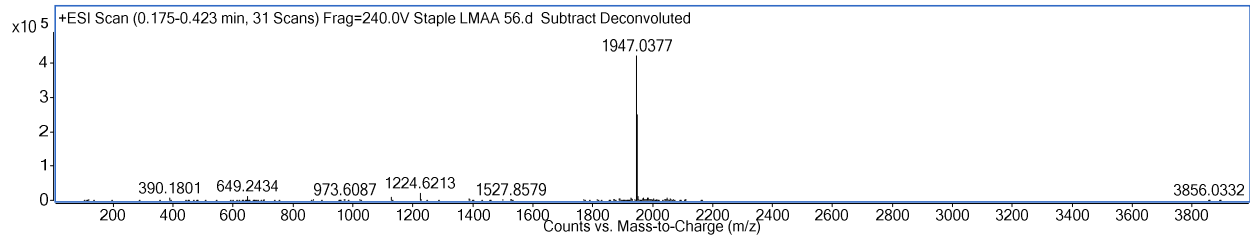


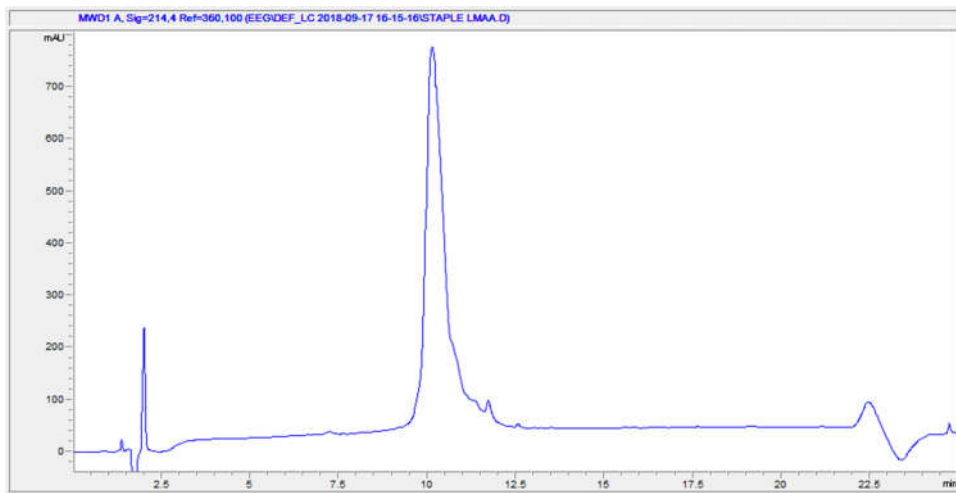
HCS-1 – Synthesized by Dr. James Song; characterization is in his thesis

HCS-2 – Synthesized by Dr. James Song, but purified by me

Sequence: GTRIIYDRXFAAXCRN; X = pentenyl alanine

Mass Expected: 1946.03

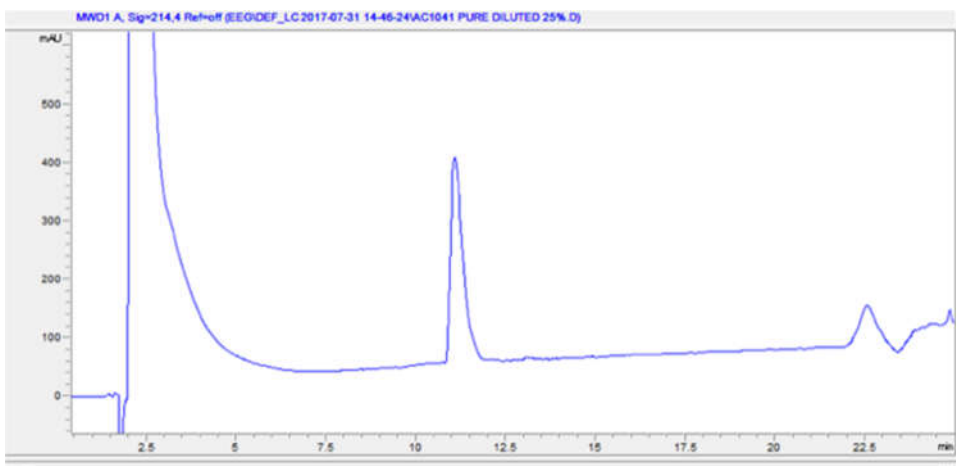
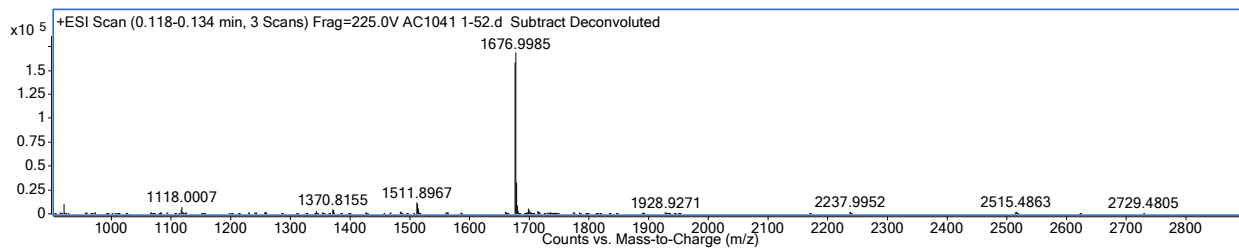




**HCS-3** – Synthesized by Alyah Chmiel

Sequence: KKRYDRXFLFXF; X = pentenyl alanine

Mass Expected: 1675.99

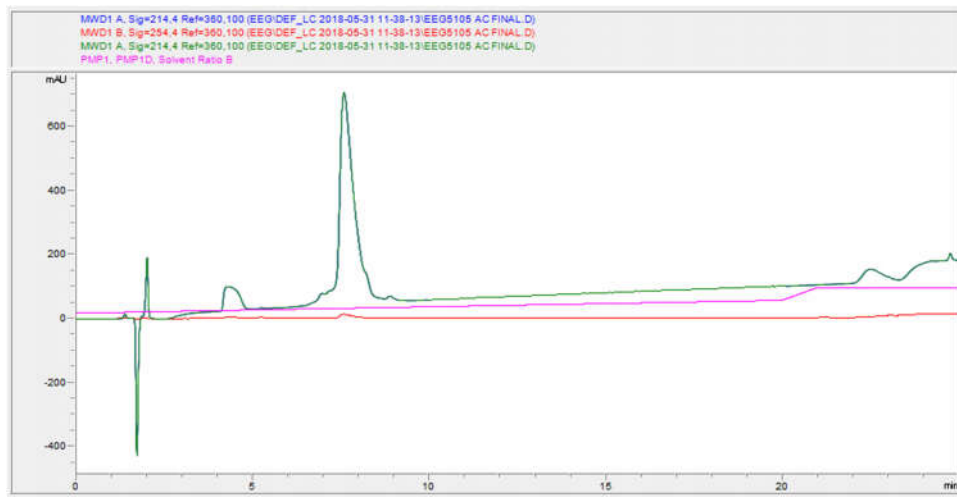
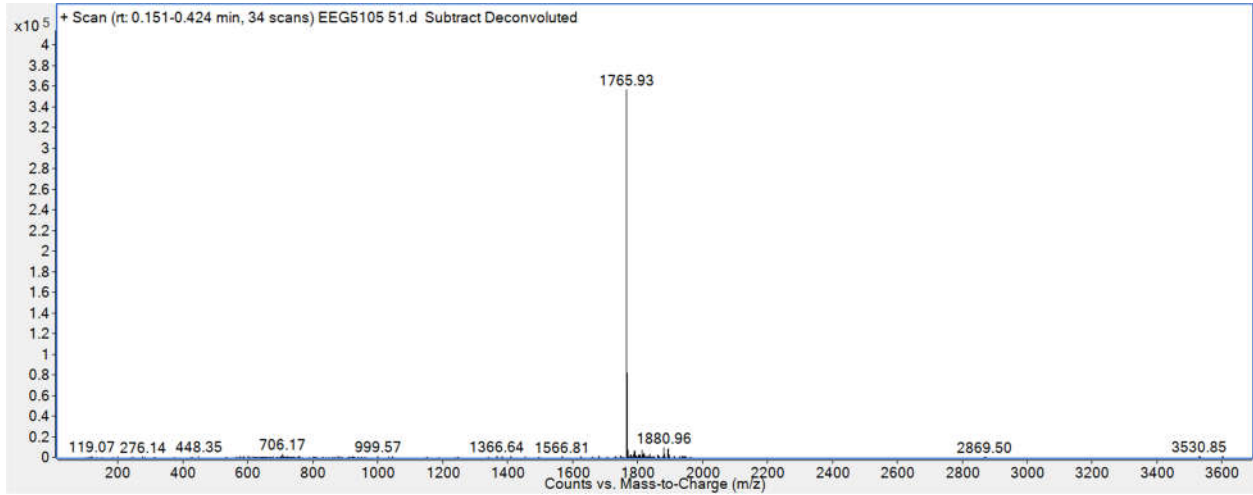


**HCS-4** – Synthesized by Dr. James Song; characterization is in his thesis

**LacA-1** – Synthesized separately by both Alyah Chmiel and me

Sequence: RIIYDR(K)FLM(E)CR; (K) and (E) are cyclized

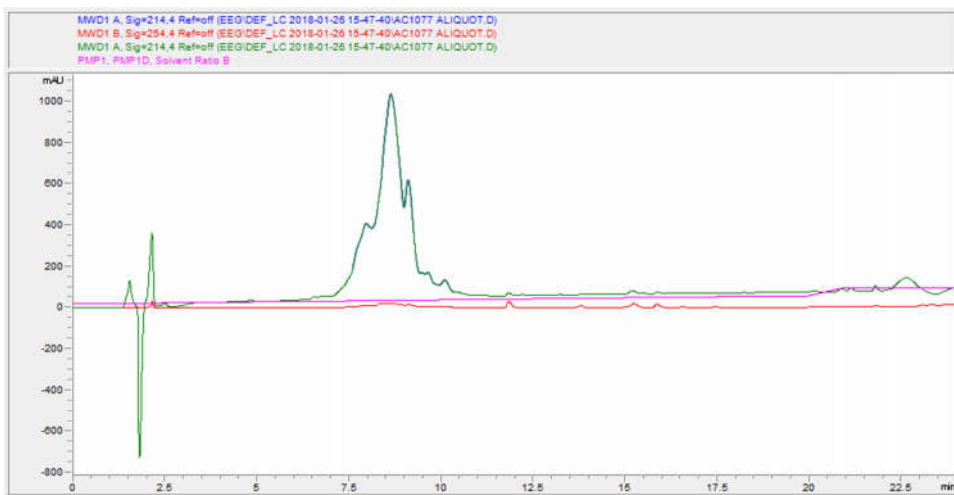
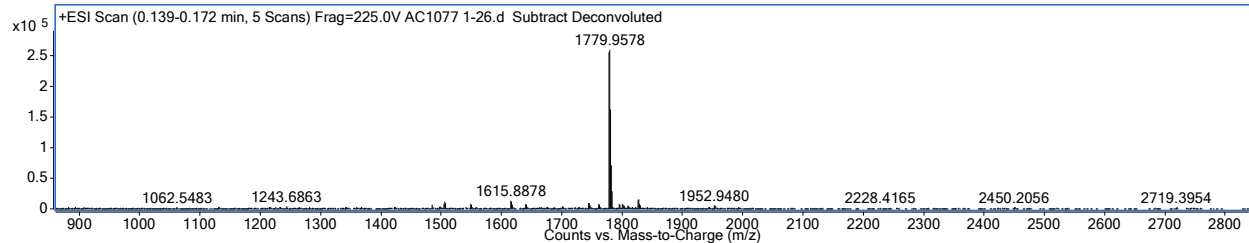
Mass Expected: 1764.93



## LacA-2 – Synthesized by Alyah Chmiel

Sequence: RIIY\*R(K)FLM(E)CR; (K) and (E) are cyclized; \* = N-methyl aspartic acid

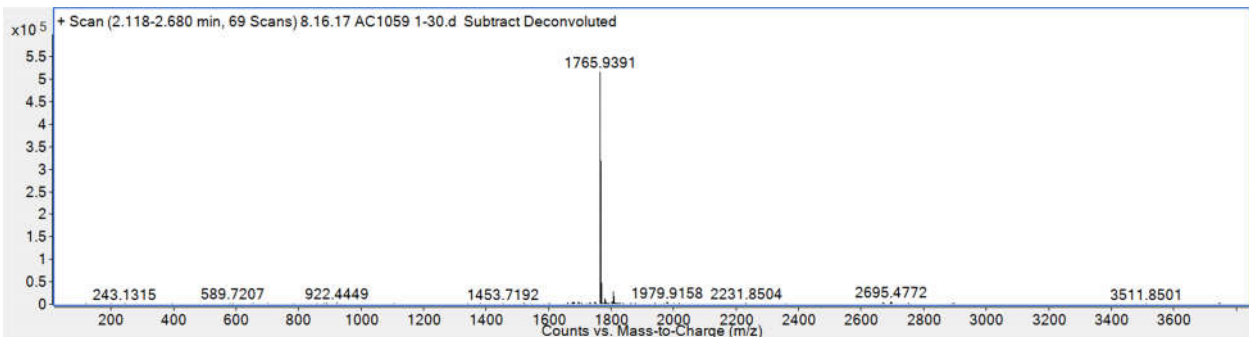
Mass Expected: 1778.94

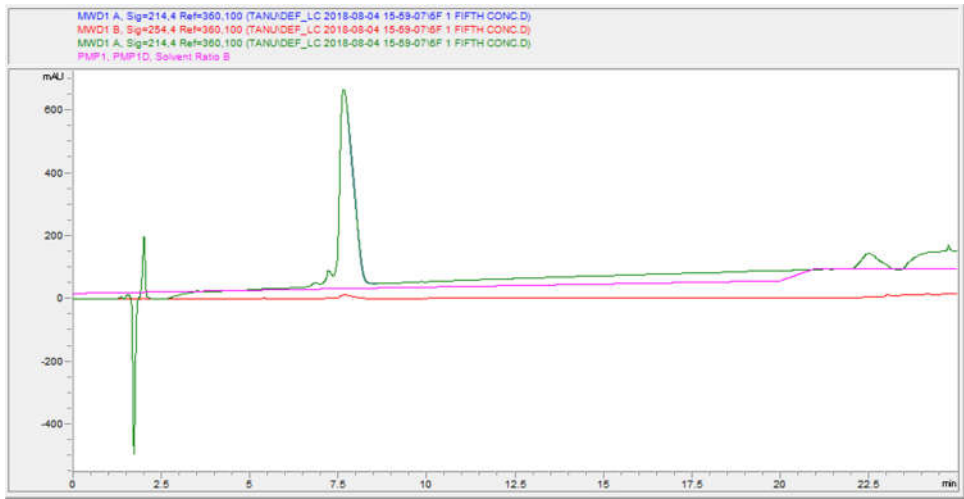


## LacB-1 – Synthesized separately by both Alyah Chmiel and me

Sequence: RIIYDR(E)FLM(K)CR; (E) and (K) are cyclized

Mass Expected: 1764.93

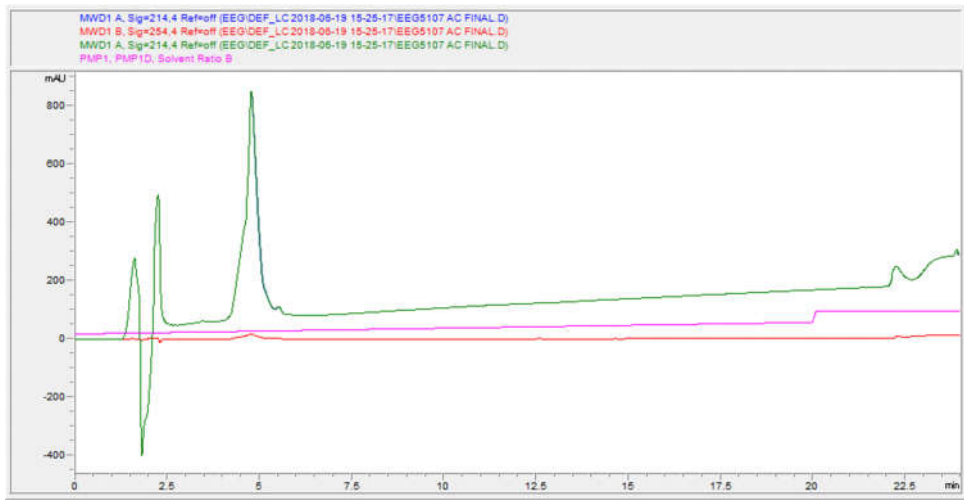
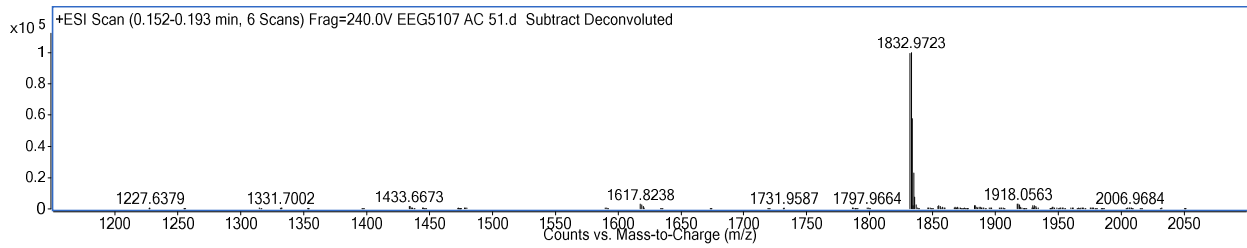




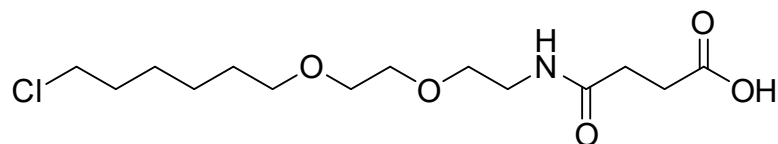
**LacB-2**

Sequence: RIIYSR(E)QLM(K)CRN; (E) and (K) are cyclized

Mass Expected: 1831.97



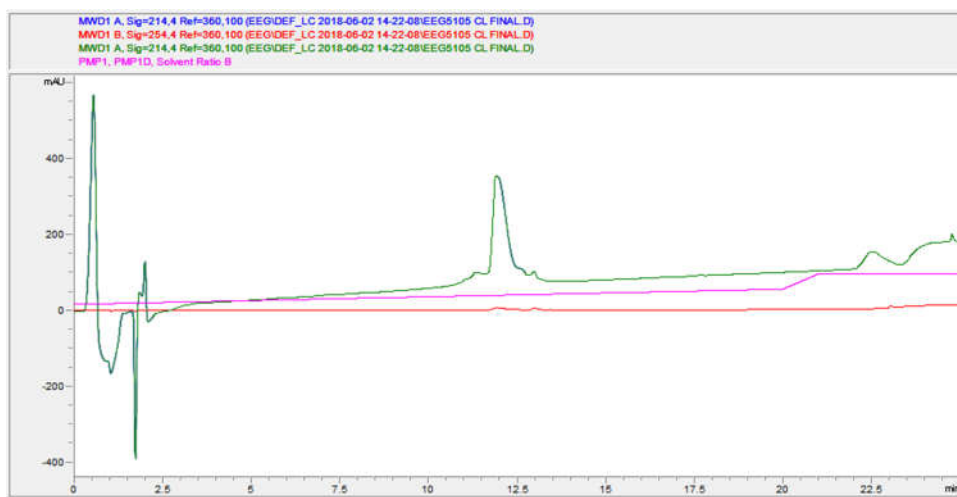
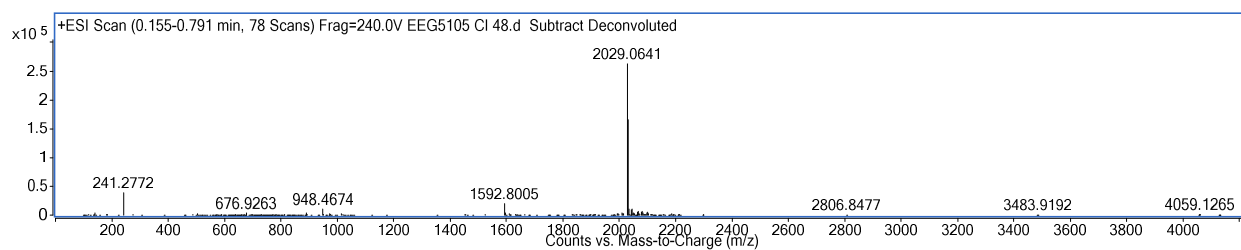
The chloroalkane peptides had the following compound (abbreviated ct for chloroalkane tag) conjugated to their amino terminus.



### LacA-1 Cl

Sequence: ct-RIIYDR(K)FLM(E)CR; (K) and (E) are cyclized

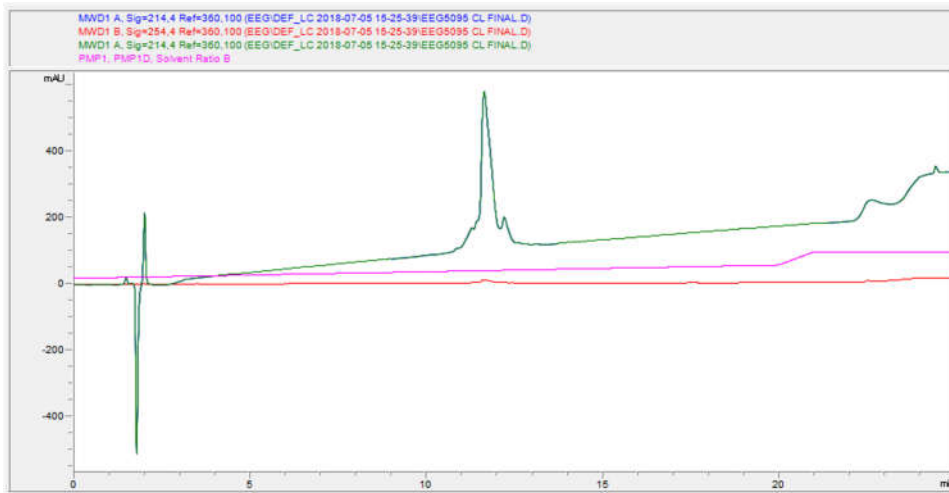
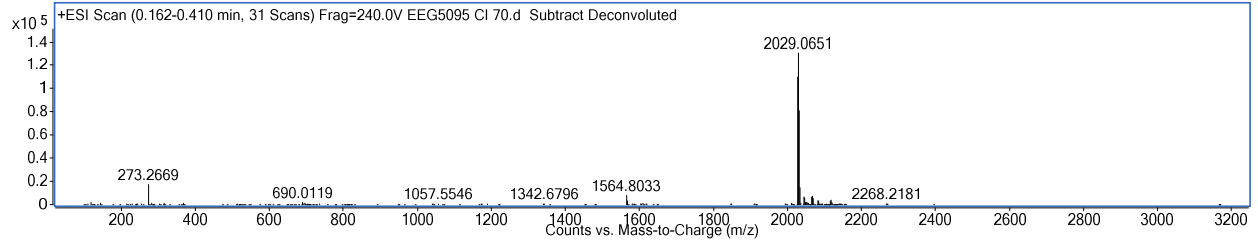
Mass Expected: 2028.06



## LacB-1 CI

Sequence: ct-RIIYDR(E)FLM(K)CR; (E) and (K) are cyclized

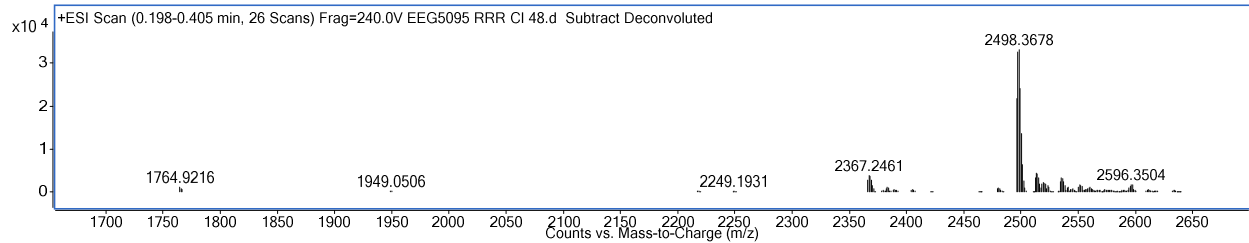
Mass Expected: 2028.06

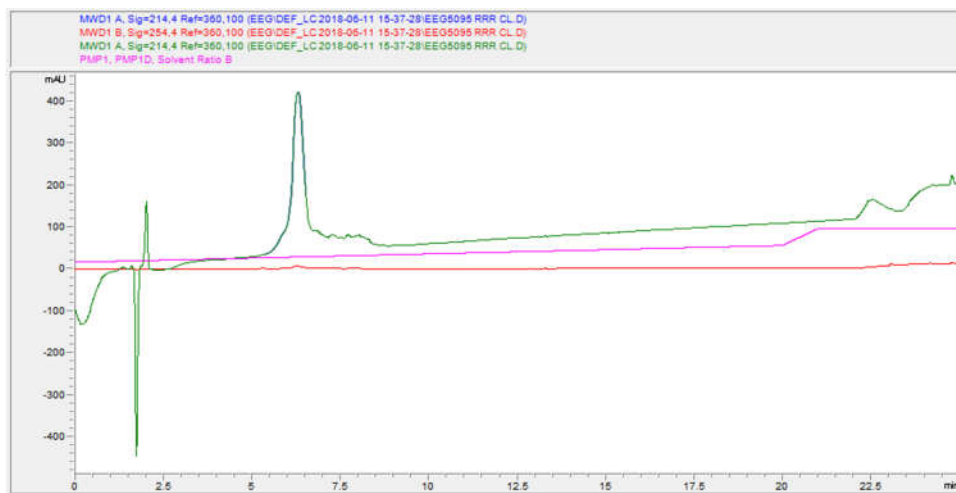


## RRR-LacB-1 CI

Sequence: ct-RRRRIIYDR(E)FLM(K)CR; (E) and (K) are cyclized

Mass Expected: 2496.36

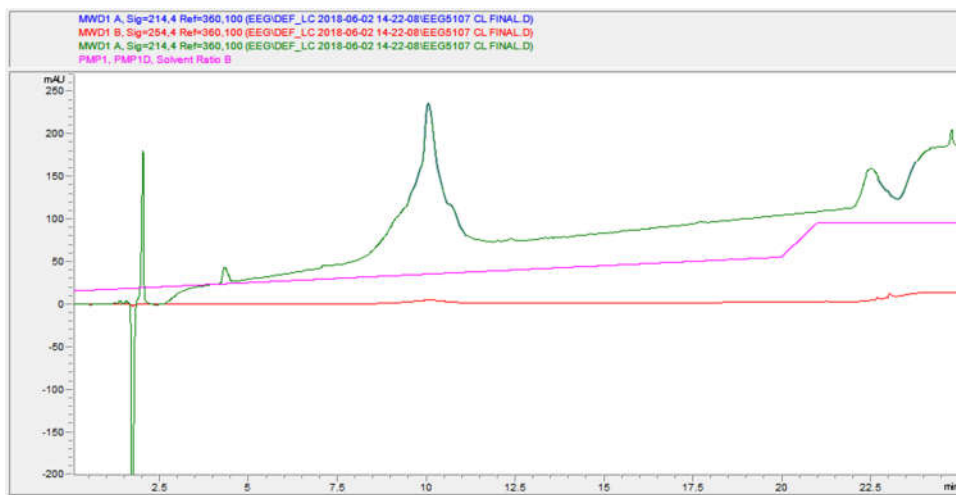
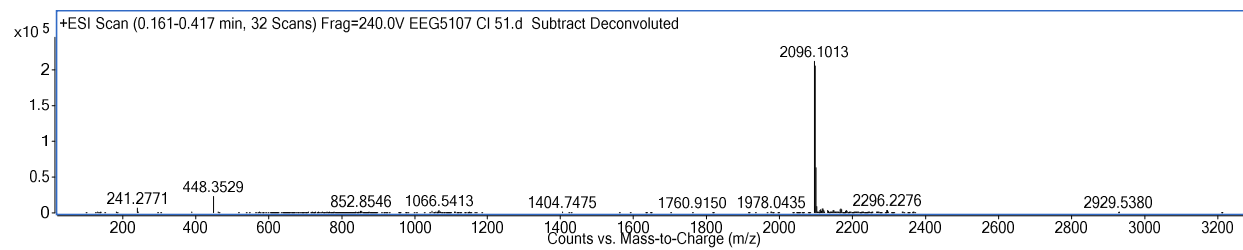




## LacB-2 CI

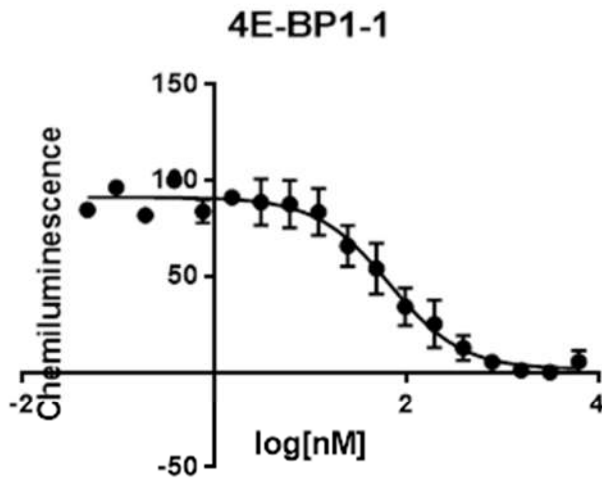
Sequence: ct-RIIYSR(E)QLM(K)CRN; (E) and (K) are cyclized

Mass Expected: 2095.10





## IC<sub>50</sub> Curves for Peptides



Best-fit values

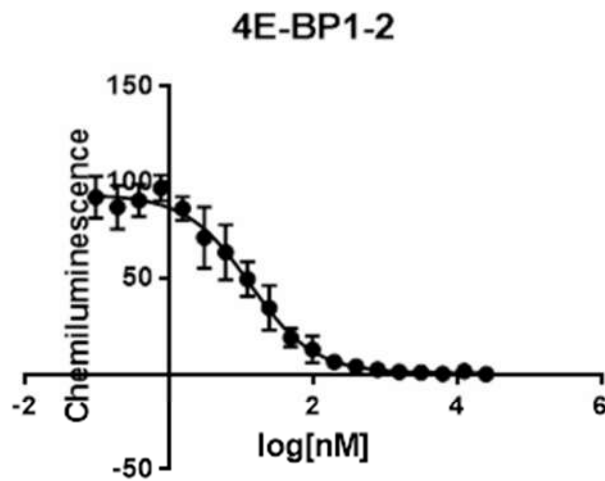
HillSlope	-1.146
IC50	65.79

95% Confidence Intervals

HillSlope	-1.415 to -0.8759
IC50	52.45 to 82.52

Goodness of Fit

R square	0.9434
----------	--------



Best-fit values

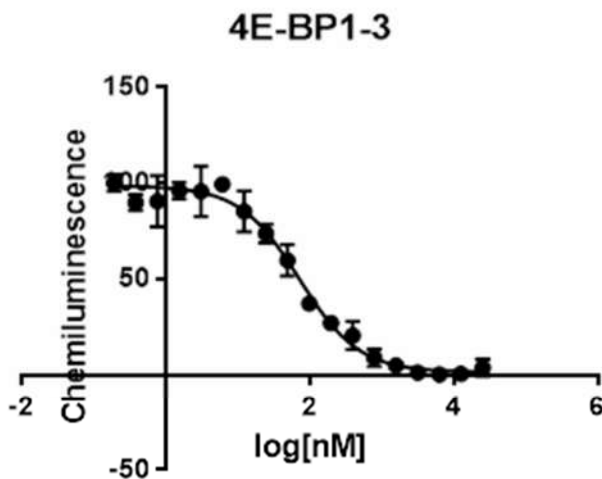
HillSlope	-0.9803
IC50	13.12

95% Confidence Intervals

HillSlope	-1.166 to -0.7950
IC50	10.59 to 16.24

Goodness of Fit

R square	0.9576
----------	--------



Best-fit values

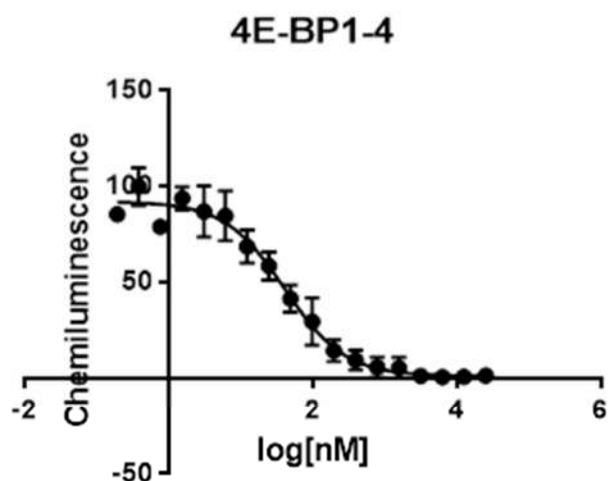
HillSlope	-1.050
IC50	71.17

95% Confidence Intervals

HillSlope	-1.213 to -0.8869
IC50	60.27 to 84.04

Goodness of Fit

R square	0.9730
----------	--------



Best-fit values

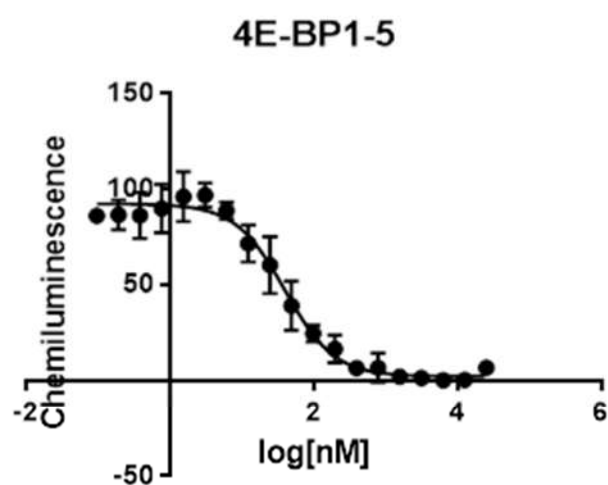
HillSlope	-1.041
IC50	40.61

95% Confidence Intervals

HillSlope	-1.244 to -0.8378
IC50	32.84 to 50.21

Goodness of Fit

R square	0.9576
----------	--------



Best-fit values

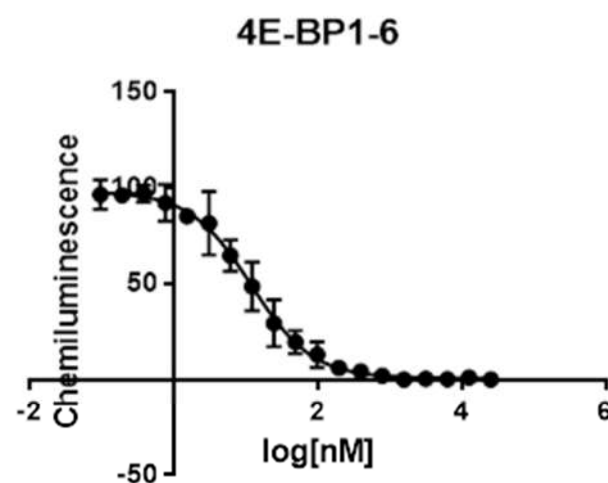
HillSlope	-1.264
IC50	39.46

95% Confidence Intervals

HillSlope	-1.533 to -0.9956
IC50	32.72 to 47.58

Goodness of Fit

R square	0.9551
----------	--------



Best-fit values

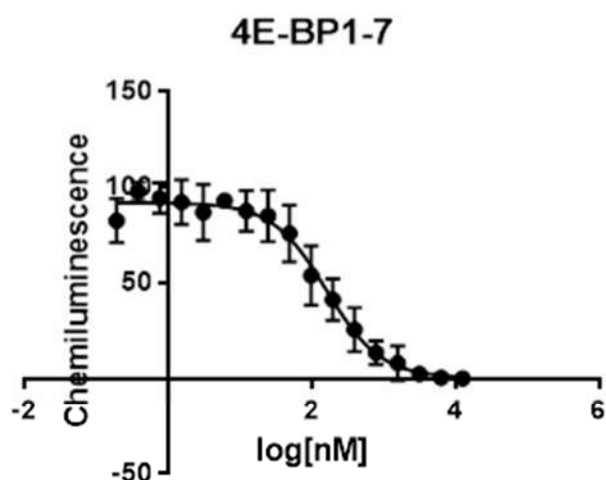
HillSlope	-1.025
IC50	11.79

95% Confidence Intervals

HillSlope	-1.185 to -0.8651
IC50	9.931 to 14.00

Goodness of Fit

R square	0.9698
----------	--------



Best-fit values

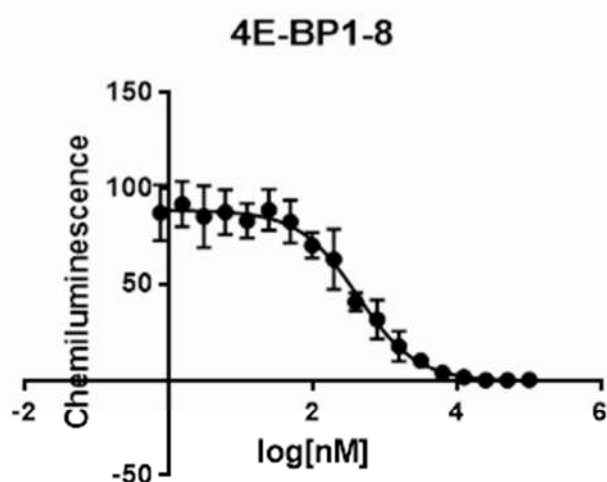
HillSlope	-1.155
IC50	159.5

95% Confidence Intervals

HillSlope	-1.467 to -0.8429
IC50	122.7 to 207.3

Goodness of Fit

R square	0.9270
----------	--------



Best-fit values

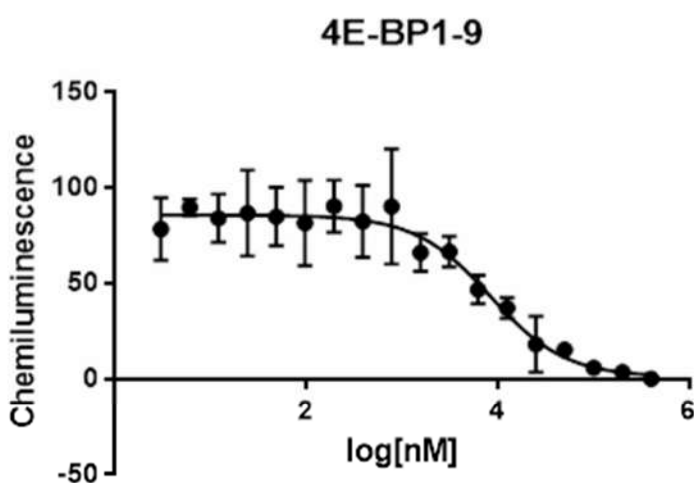
HillSlope	-1.063
IC50	416.0

95% Confidence Intervals

HillSlope	-1.304 to -0.8215
IC50	329.1 to 525.8

Goodness of Fit

R square	0.9446
----------	--------



Best-fit values

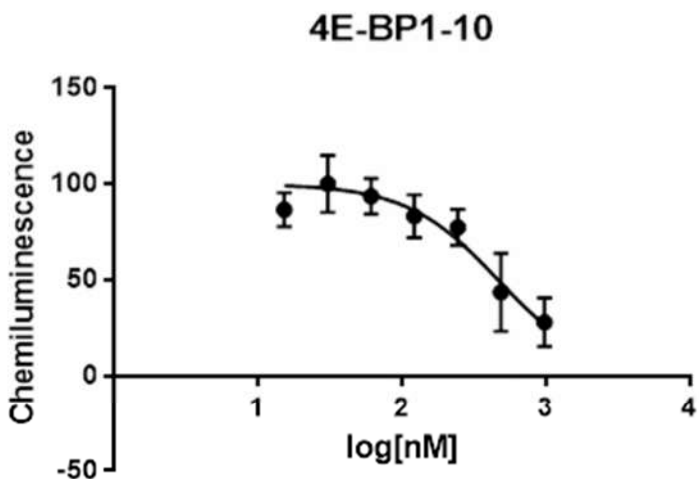
HillSlope	-1.108
IC50	8328

95% Confidence Intervals

HillSlope	-1.557 to -0.6594
IC50	5422 to 12792

Goodness of Fit

R square	0.8242
----------	--------



Best-fit values

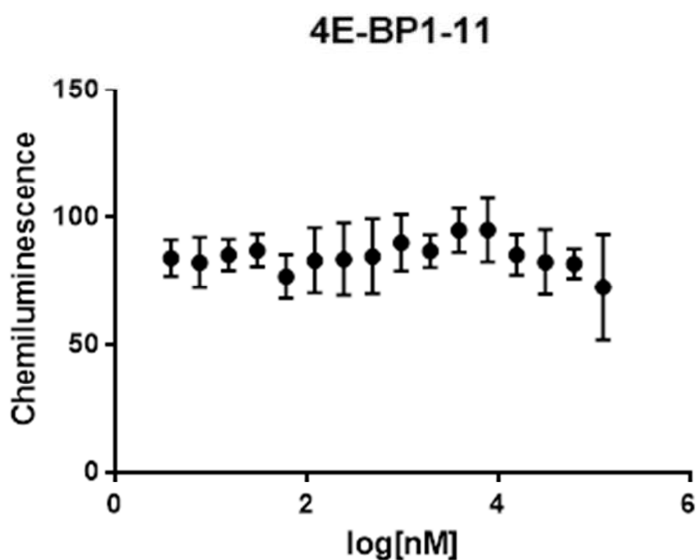
HillSlope	-1.366
IC50	465.6

95% Confidence Intervals

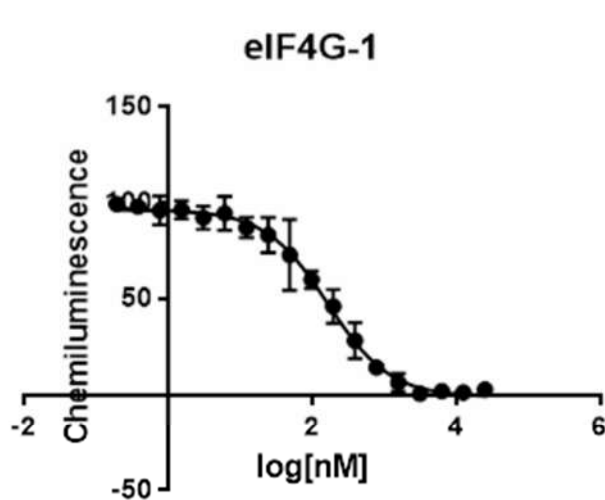
HillSlope	-1.912 to -0.8186
IC50	349.9 to 619.5

Goodness of Fit

R square	0.8016
----------	--------



Not converged



Best-fit values

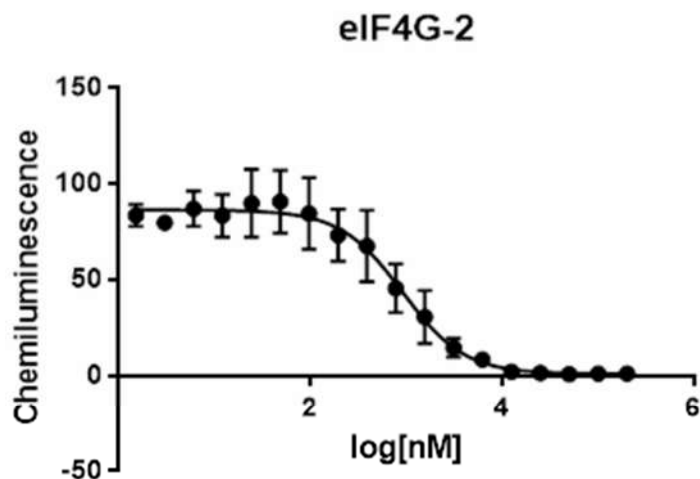
HillSlope	-1.005
IC50	163.5

95% Confidence Intervals

HillSlope	-1.168 to -0.8413
IC50	137.2 to 194.9

Goodness of Fit

R square	0.9711
----------	--------



Best-fit values

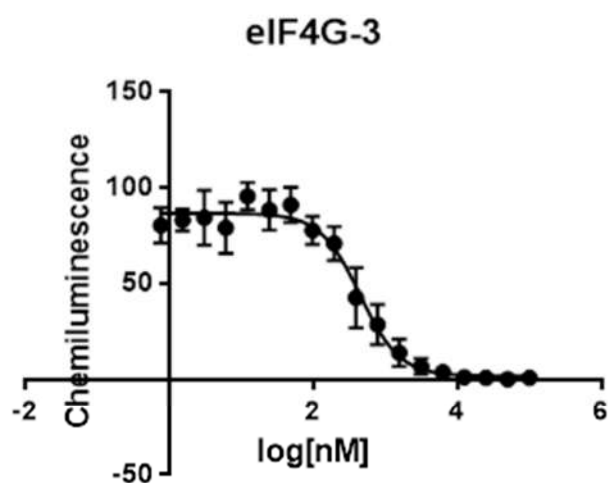
HillSlope	-1.343
IC50	916.2

95% Confidence Intervals

HillSlope	-1.689 to -0.9972
IC50	737.6 to 1138

Goodness of Fit

R square	0.9201
----------	--------



Best-fit values

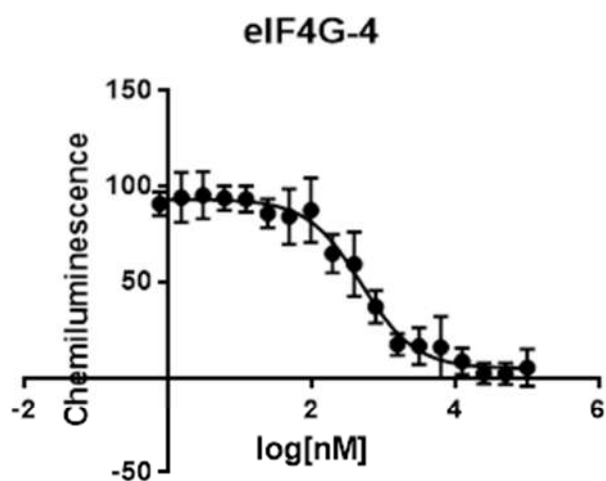
HillSlope	-1.571
IC50	445.2

95% Confidence Intervals

HillSlope	-1.931 to -1.212
IC50	376.5 to 526.4

Goodness of Fit

R square	0.9450
----------	--------



Best-fit values

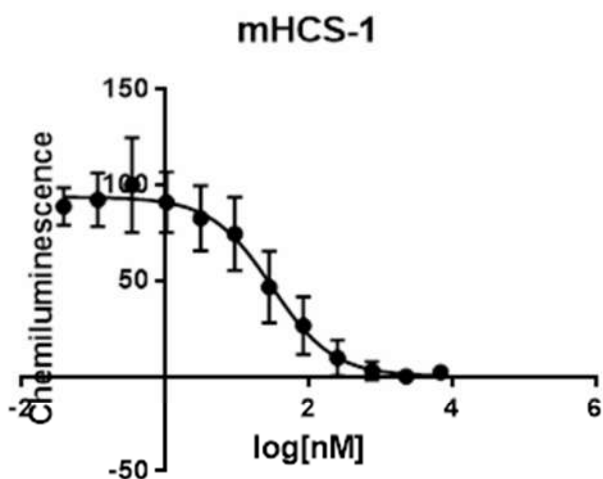
HillSlope	-1.153
IC50	492.9

95% Confidence Intervals

HillSlope	-1.452 to -0.8532
IC50	384.0 to 632.6

Goodness of Fit

R square	0.9271
----------	--------



Best-fit values

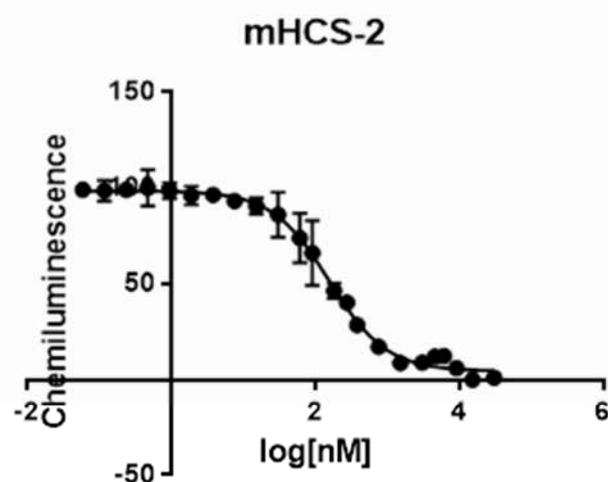
HillSlope	-1.018
IC50	30.72

95% Confidence Intervals

HillSlope	-1.333 to -0.7031
IC50	21.96 to 42.99

Goodness of Fit

R square	0.8819
----------	--------



Best-fit values

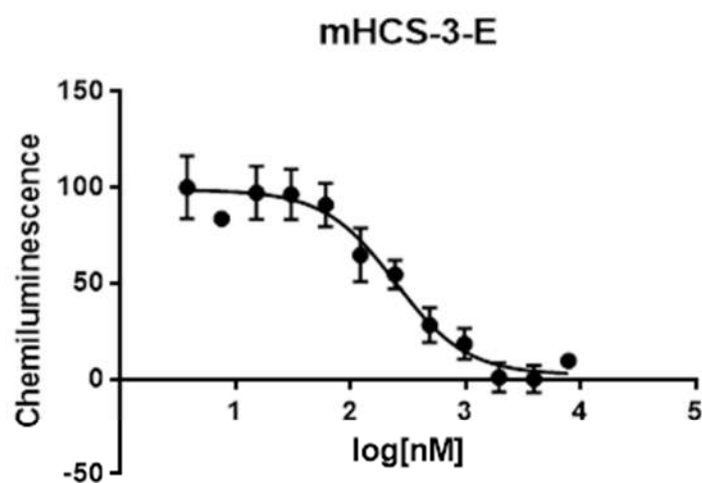
HillSlope	-1.093
IC50	156.3

95% Confidence Intervals

HillSlope	-1.254 to -0.9317
IC50	135.7 to 180.1

Goodness of Fit

R square	0.9786
----------	--------



Best-fit values

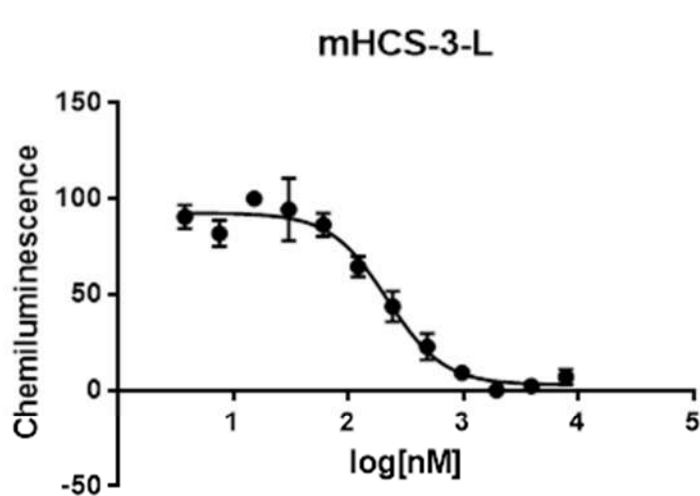
HillSlope	-1.396
IC50	245.9

95% Confidence Intervals

HillSlope	-1.997 to -0.7943
IC50	176.5 to 342.6

Goodness of Fit

R square	0.9365
----------	--------



Best-fit values

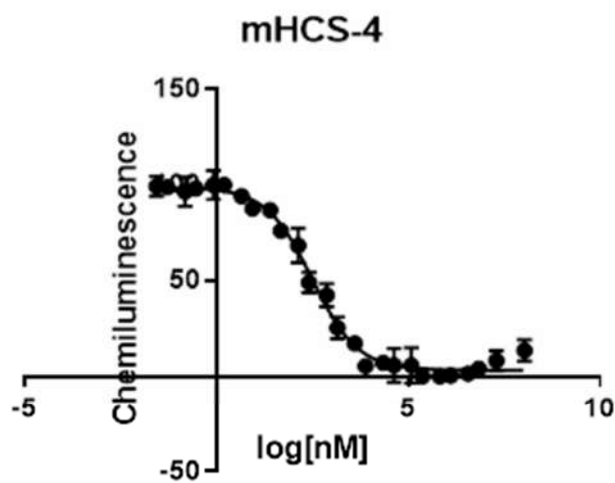
HillSlope	-1.762
IC50	217.9

95% Confidence Intervals

HillSlope	-2.326 to -1.197
IC50	177.8 to 267.1

Goodness of Fit

R square	0.9647
----------	--------



Best-fit values

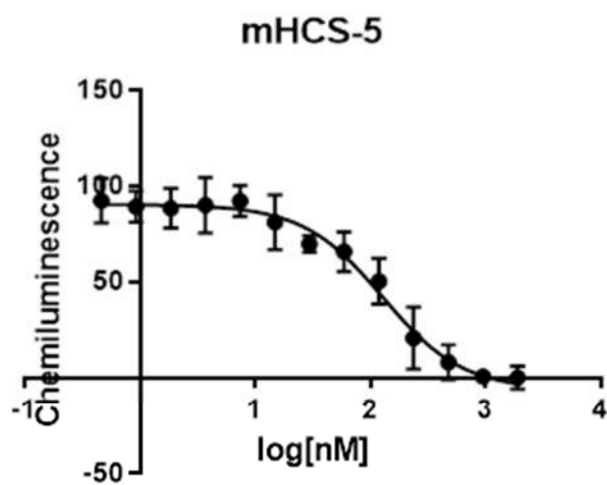
HillSlope	-0.7278
IC50	309.0

95% Confidence Intervals

HillSlope	-0.8337 to -0.6219
IC50	244.8 to 390.1

Goodness of Fit

R square	0.9836
----------	--------



Best-fit values

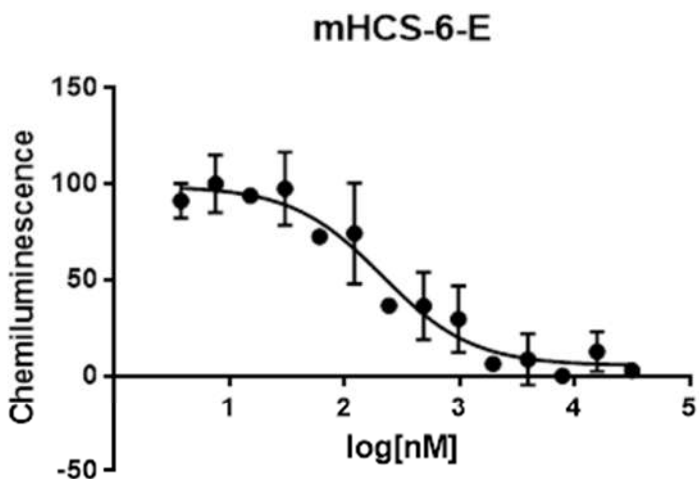
HillSlope	-1.255
IC50	127.9

95% Confidence Intervals

HillSlope	-1.703 to -0.8067
IC50	89.78 to 182.2

Goodness of Fit

R square	0.9147
----------	--------



Best-fit values

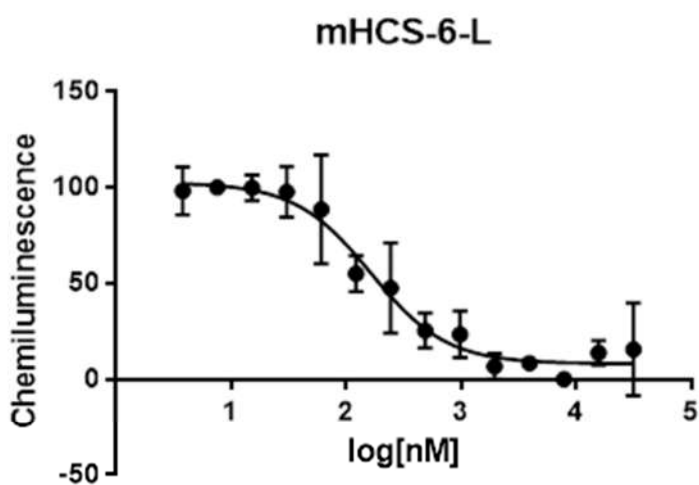
HillSlope	-1.106
IC50	213.3

95% Confidence Intervals

HillSlope	-1.688 to -0.5241
IC50	129.2 to 352.1

Goodness of Fit

R square	0.8916
----------	--------



Best-fit values

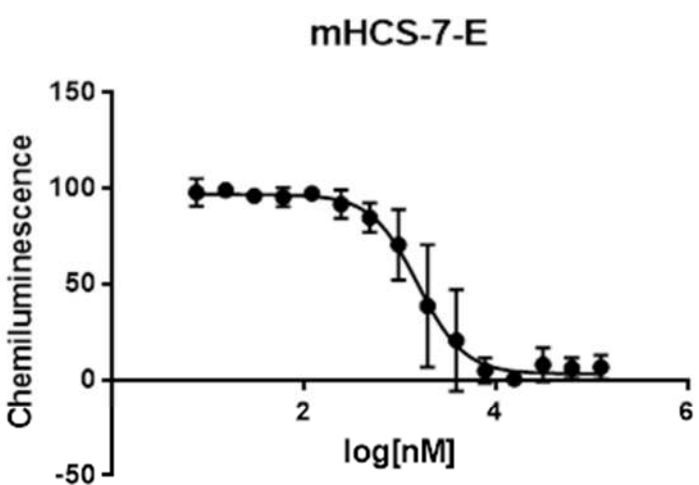
HillSlope	-1.320
IC50	164.8

95% Confidence Intervals

HillSlope	-1.950 to -0.6902
IC50	111.9 to 242.7

Goodness of Fit

R square	0.9178
----------	--------



Best-fit values

HillSlope	-1.793
IC50	1548

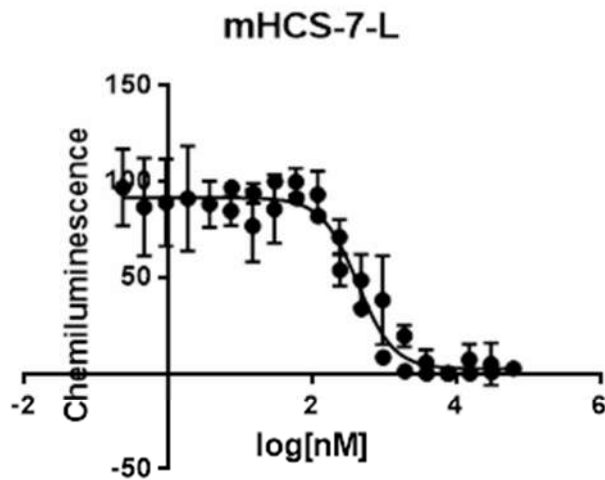
95% Confidence Intervals

HillSlope	-2.375 to -1.210
IC50	1256 to 1908

Goodness of Fit

R square	0.8913
----------	--------





Best-fit values

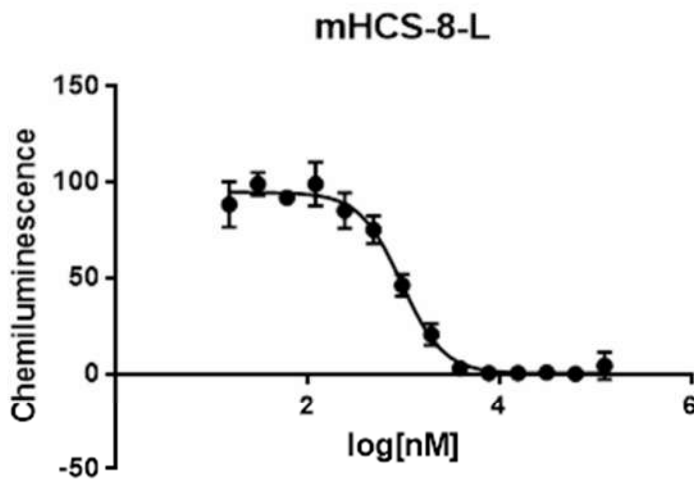
HillSlope	-1.727
IC50	429.0

95% Confidence Intervals

HillSlope	-2.288 to -1.167
IC50	346.1 to 531.9

Goodness of Fit

R square	0.9114
----------	--------



Best-fit values

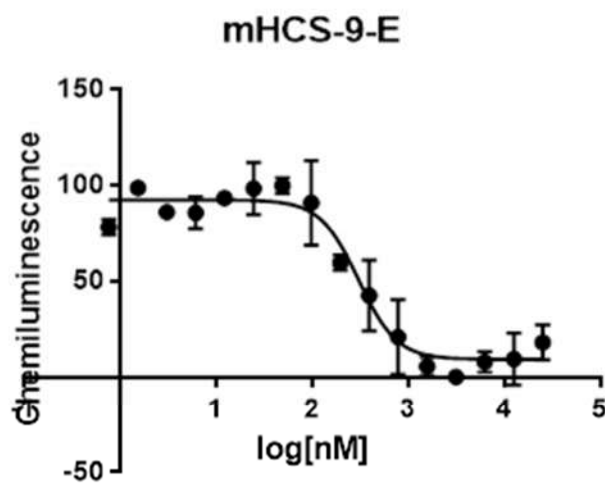
HillSlope	-1.971
IC50	956.0

95% Confidence Intervals

HillSlope	-2.330 to -1.612
IC50	860.7 to 1062

Goodness of Fit

R square	0.9751
----------	--------



Best-fit values

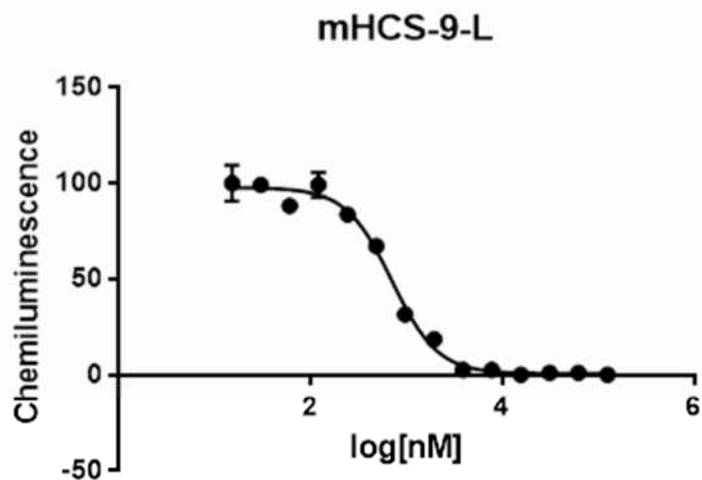
HillSlope	-2.173
IC50	302.1

95% Confidence Intervals

HillSlope	-3.370 to -0.9748
IC50	224.9 to 405.9

Goodness of Fit

R square	0.9141
----------	--------



Best-fit values

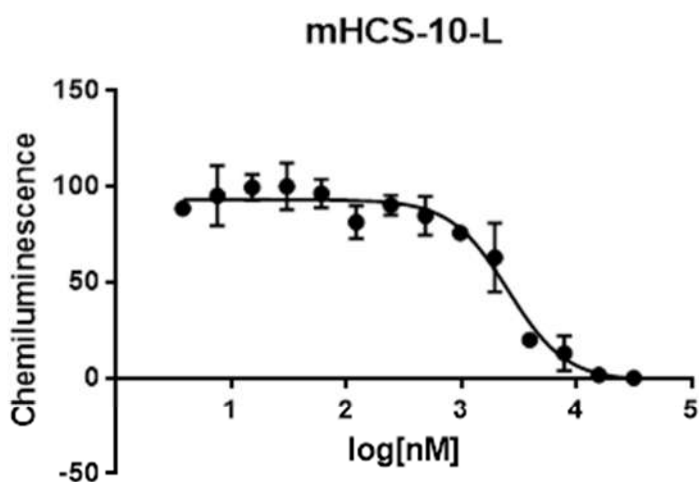
HillSlope	-1.818
IC50	707.8

95% Confidence Intervals

HillSlope	-2.163 to -1.472
IC50	628.7 to 796.9

Goodness of Fit

R square	0.9871
----------	--------



Best-fit values

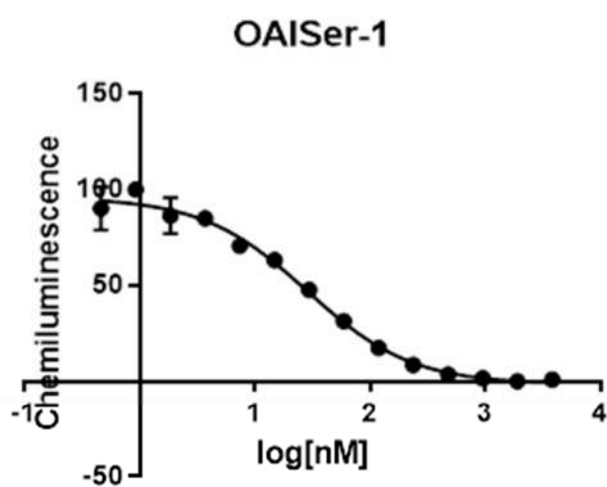
HillSlope	-1.736
IC50	2542

95% Confidence Intervals

HillSlope	-2.495 to -0.9763
IC50	1871 to 3453

Goodness of Fit

R square	0.9330
----------	--------



Best-fit values

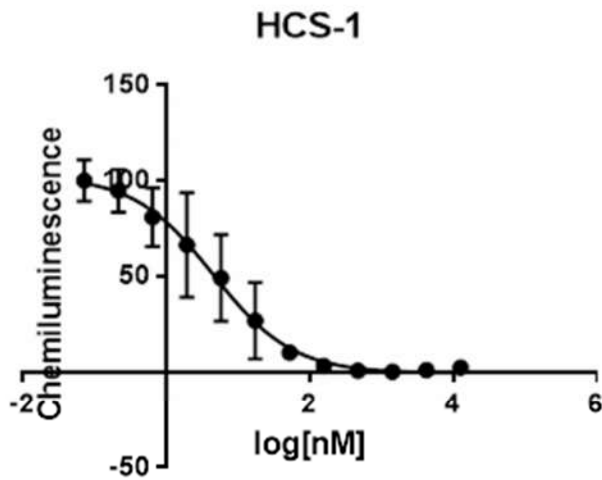
HillSlope	-0.9564
IC50	28.34

95% Confidence Intervals

HillSlope	-1.168 to -0.7452
IC50	22.43 to 35.80

Goodness of Fit

R square	0.9872
----------	--------



Best-fit values

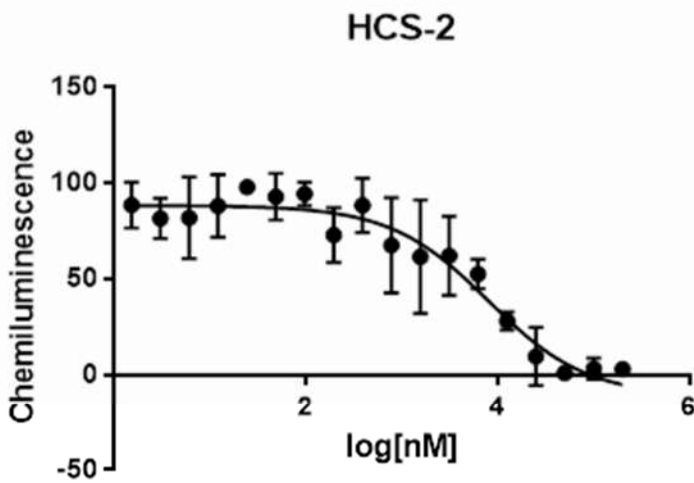
HillSlope	-0.7846
IC50	4.546

95% Confidence Intervals

HillSlope	-0.9934 to -0.5759
IC50	3.102 to 6.660

Goodness of Fit

R square	0.8939
----------	--------



Best-fit values

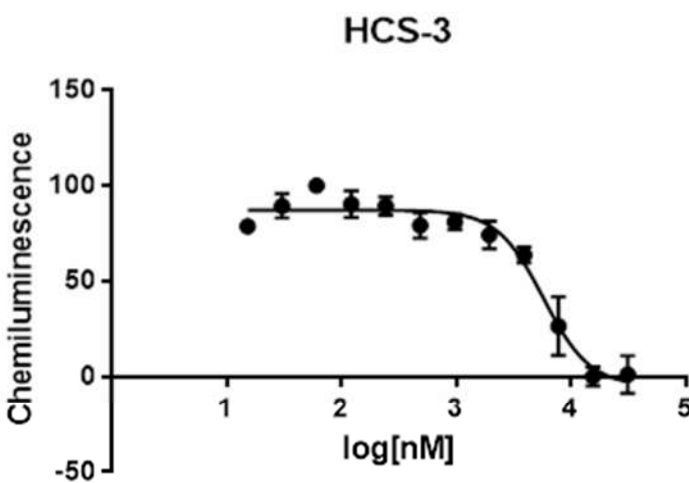
HillSlope	-0.8512
IC50	7998

95% Confidence Intervals

HillSlope	-1.263 to -0.4399
IC50	3533 to 18106

Goodness of Fit

R square	0.7715
----------	--------



Best-fit values

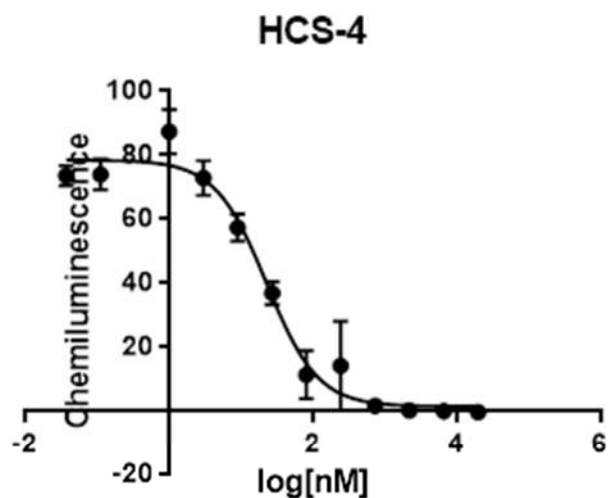
HillSlope	-2.150
IC50	5778

95% Confidence Intervals

HillSlope	-3.055 to -1.246
IC50	4566 to 7314

Goodness of Fit

R square	0.9472
----------	--------



Best-fit values

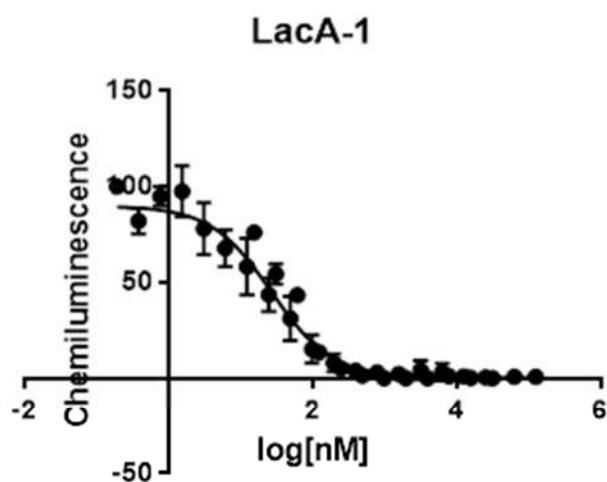
HillSlope	-1.218
IC50	22.68

95% Confidence Intervals

HillSlope	-1.625 to -0.8115
IC50	16.57 to 31.04

Goodness of Fit

R square	0.9620
----------	--------



Best-fit values

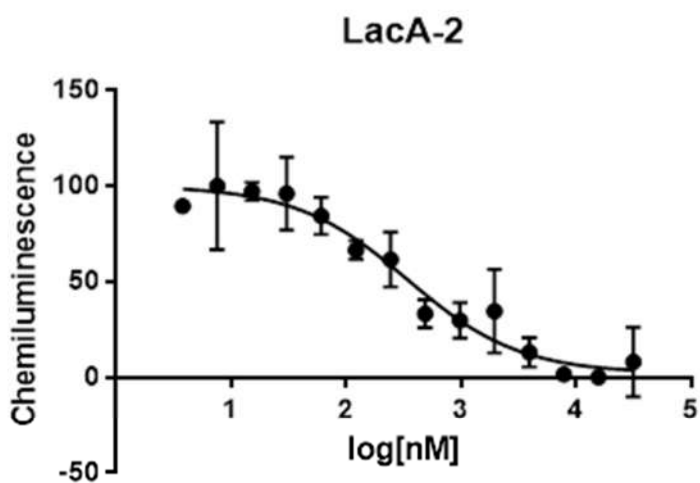
HillSlope	-1.037
IC50	26.59

95% Confidence Intervals

HillSlope	-1.218 to -0.8547
IC50	21.69 to 32.59

Goodness of Fit

R square	0.9393
----------	--------



Best-fit values

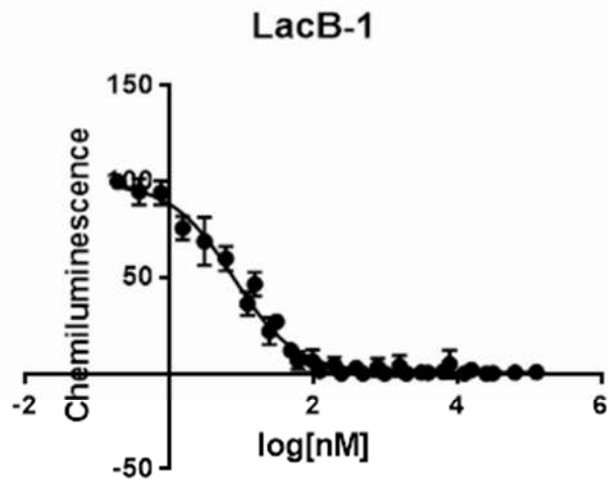
HillSlope	-0.8939
IC50	343.5

95% Confidence Intervals

HillSlope	-1.397 to -0.3909
IC50	184.7 to 638.9

Goodness of Fit

R square	0.8913
----------	--------



Best-fit values

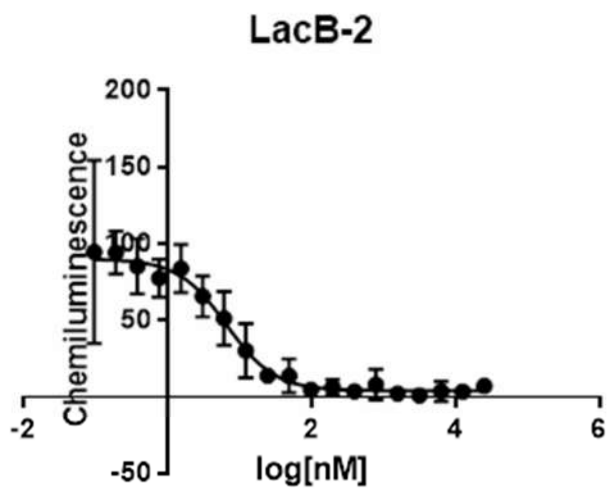
HillSlope	-1.005
IC50	7.754

95% Confidence Intervals

HillSlope	-1.137 to -0.8736
IC50	6.528 to 9.211

Goodness of Fit

R square	0.9672
----------	--------



Best-fit values

HillSlope	-1.296
IC50	6.584

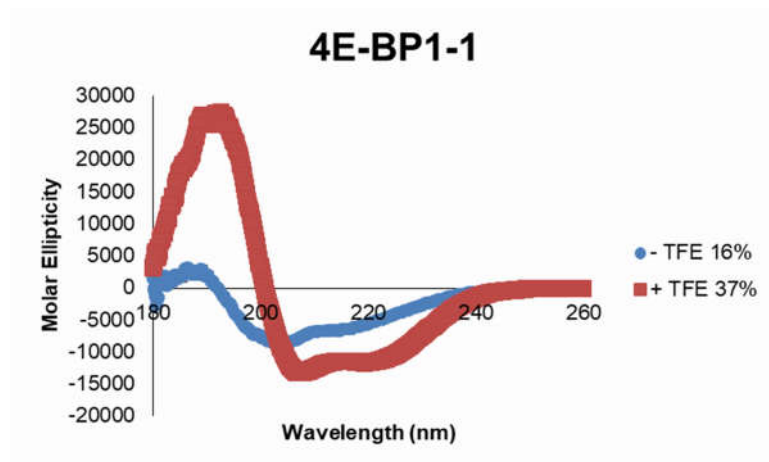
95% Confidence Intervals

HillSlope	-1.709 to -0.8832
IC50	4.921 to 8.809

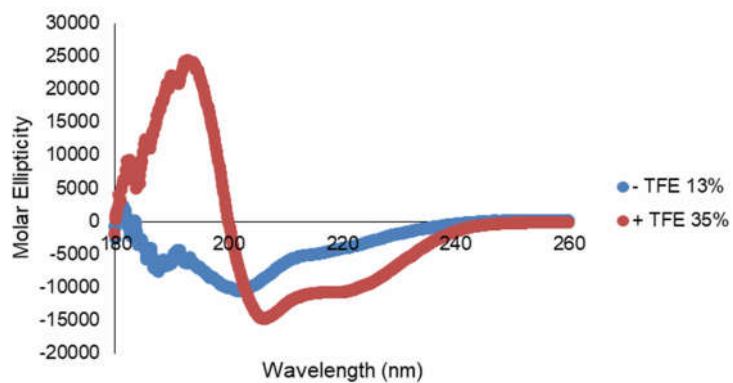
Goodness of Fit

R square	0.8933
----------	--------

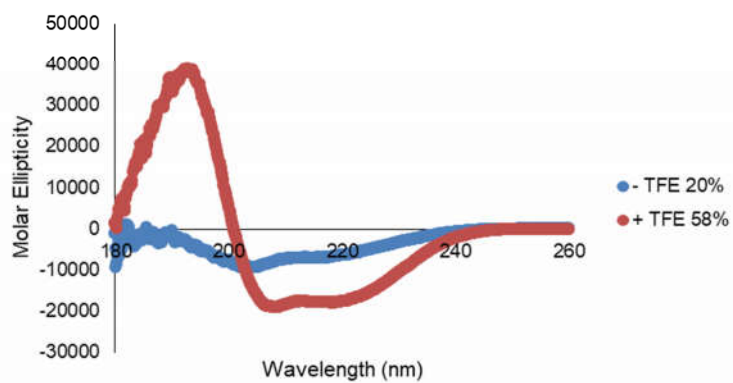
## CD Curves for Peptides



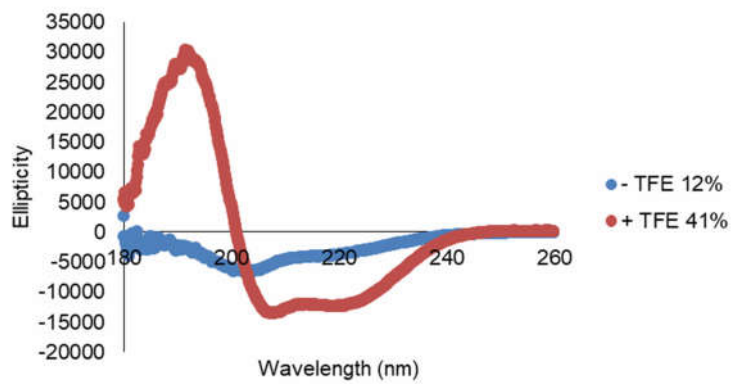
### 4E-BP1-2

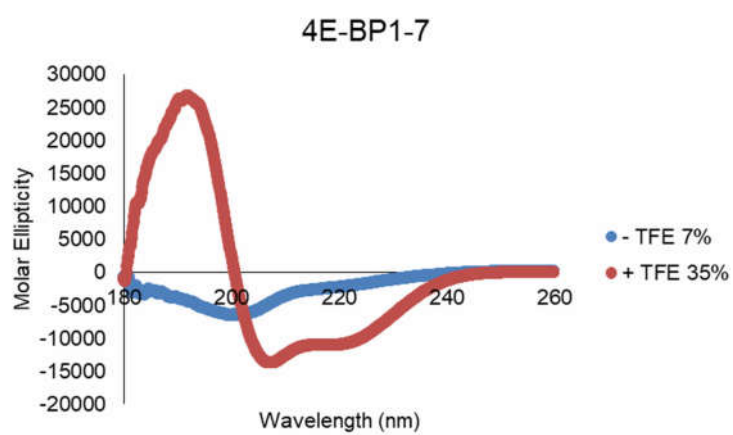
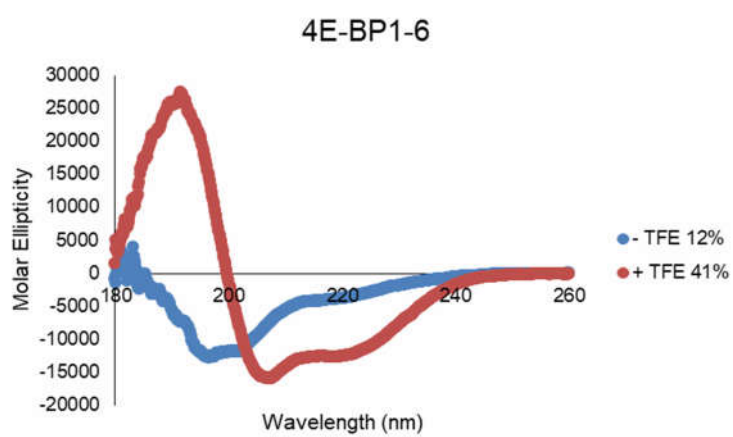
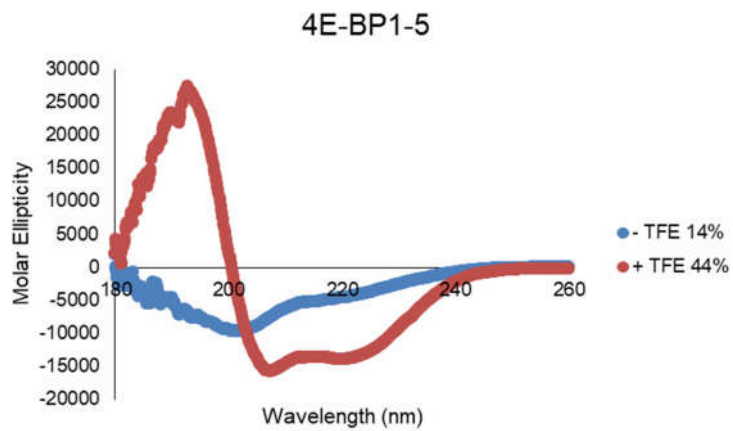


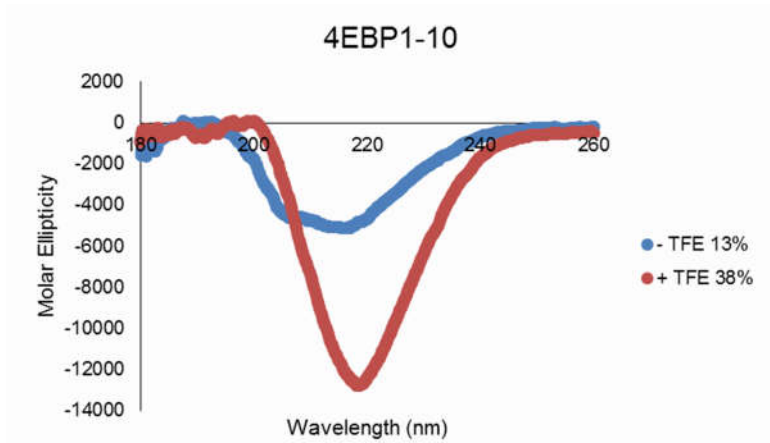
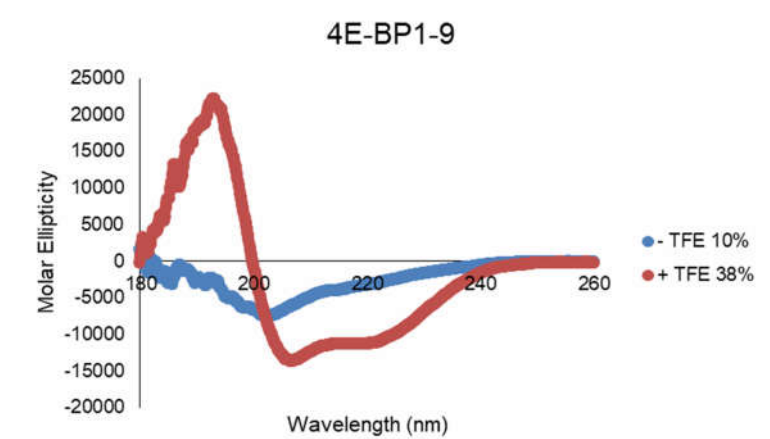
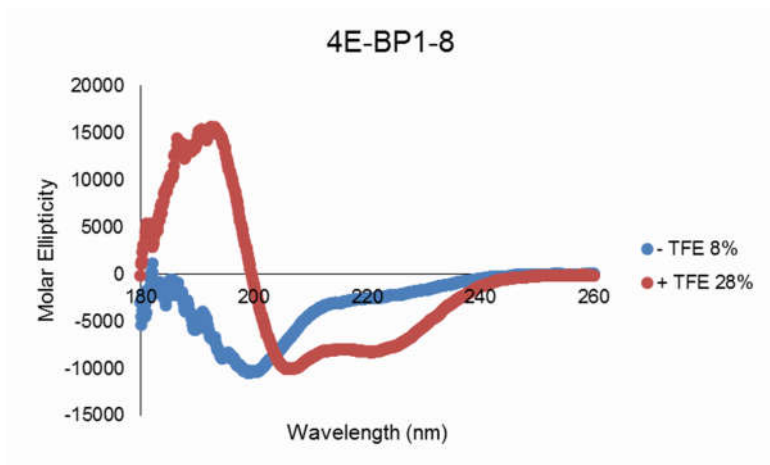
### 4E-BP1-3



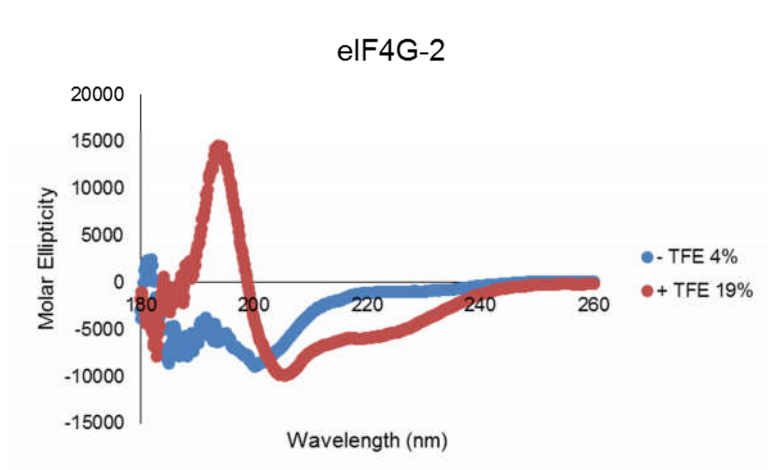
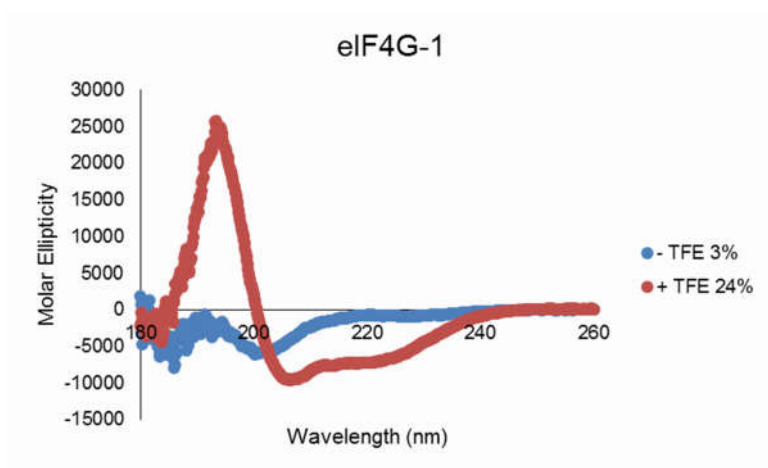
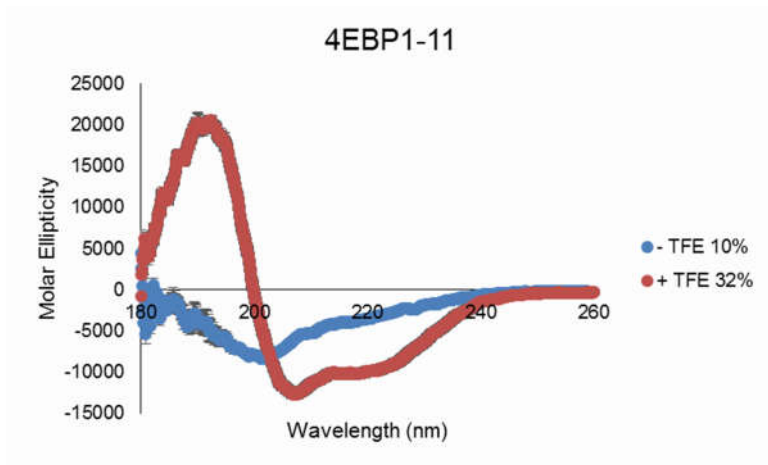
### 4E-BP1-4



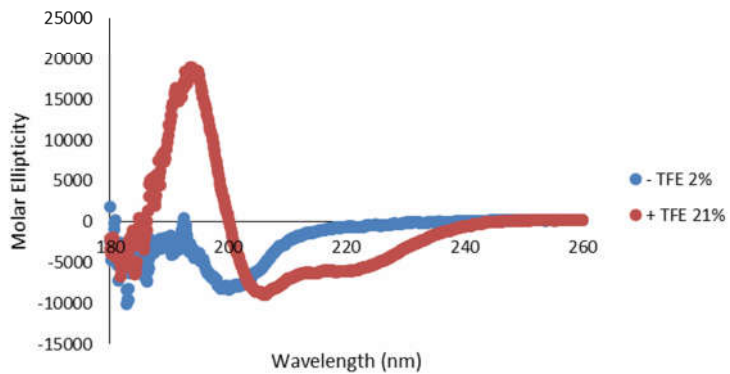




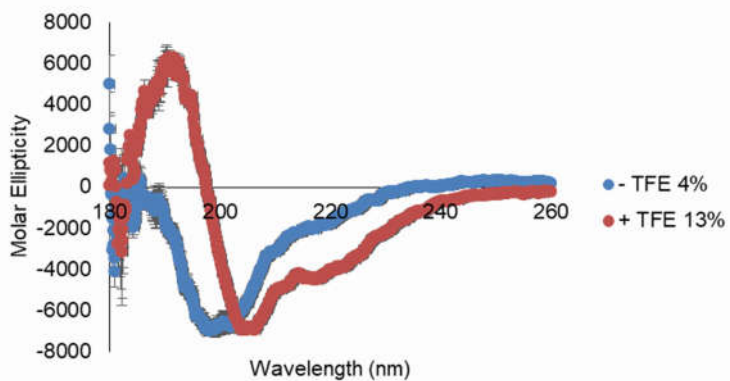




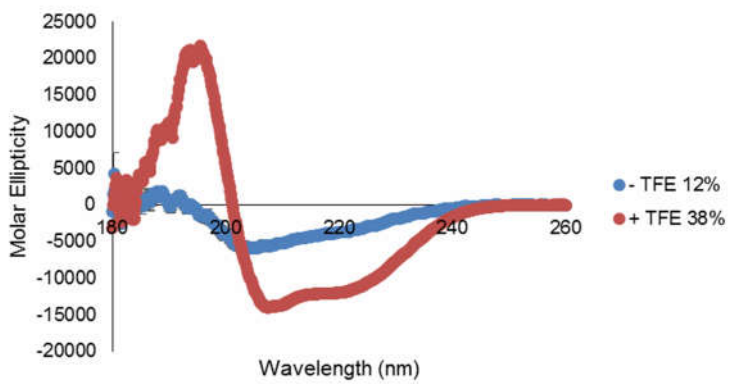
eIF4G-3

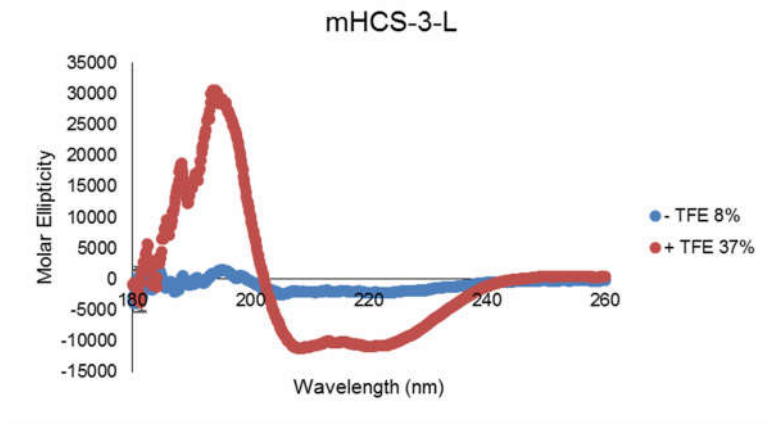
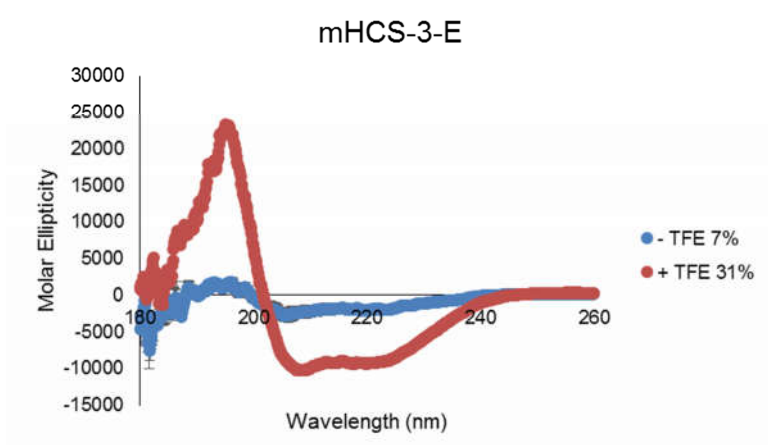
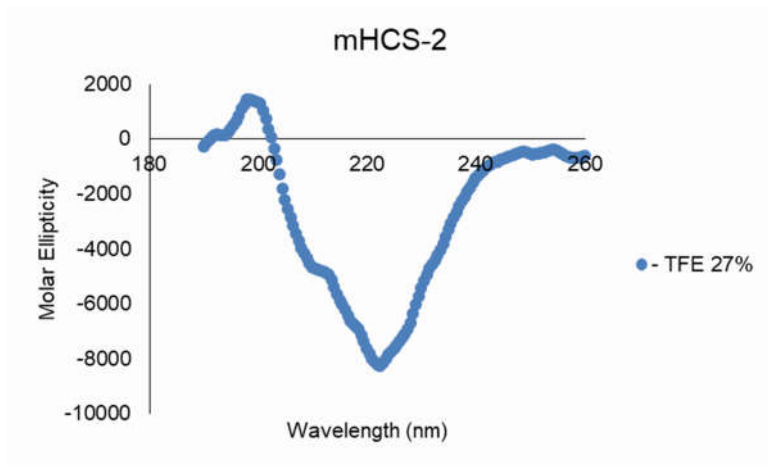


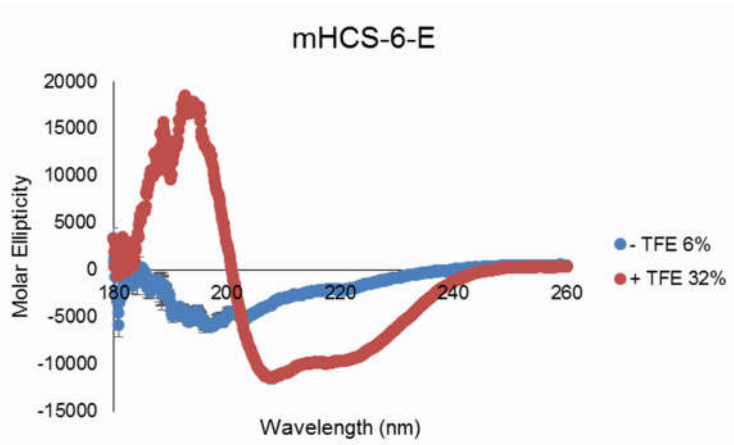
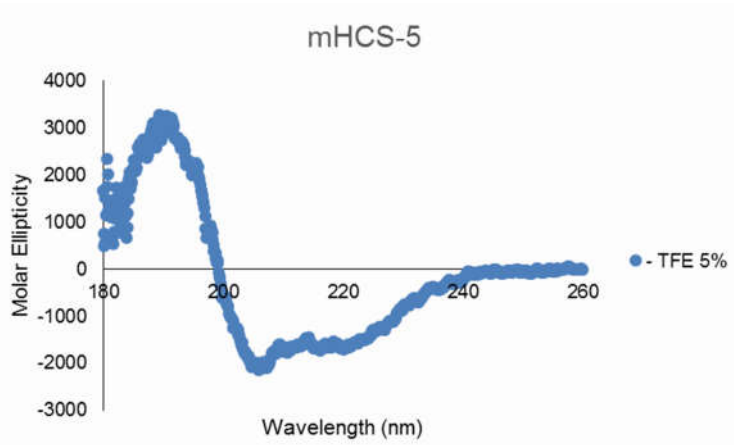
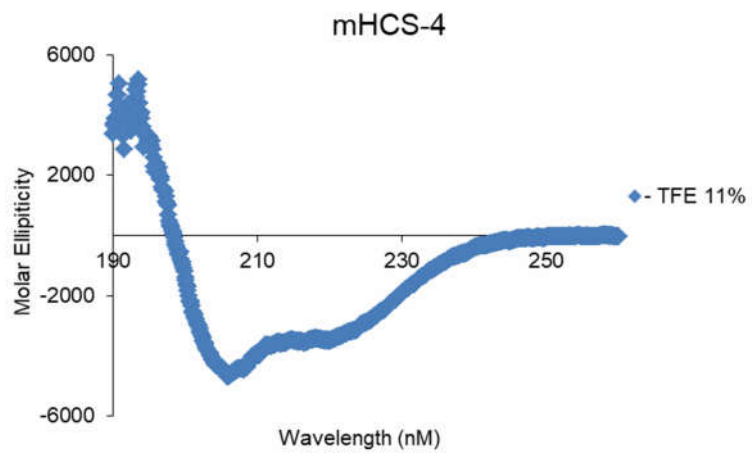
eIF4G-4

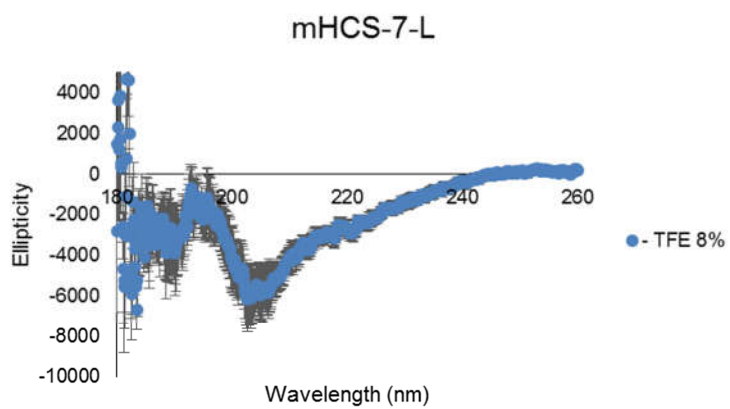
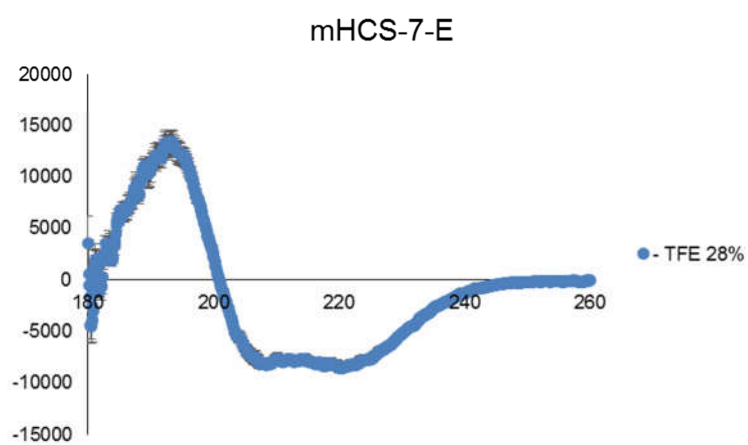
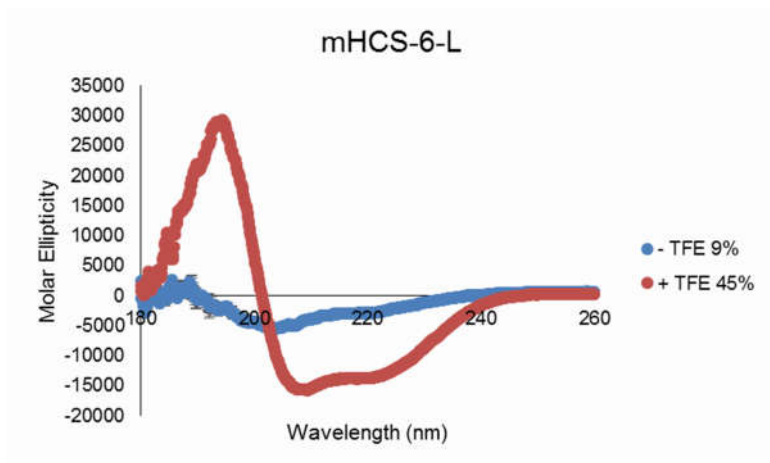


mHCS-1

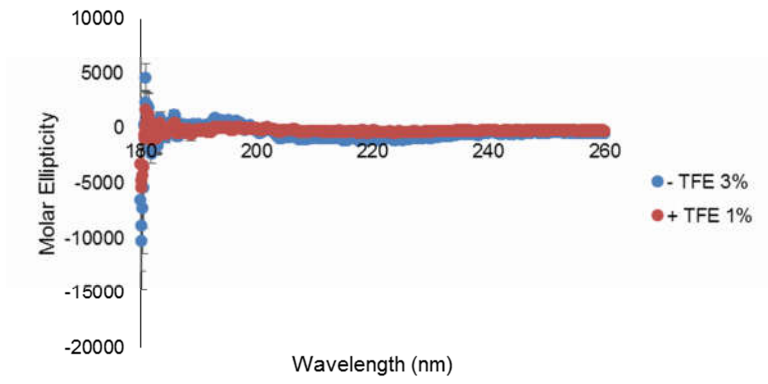




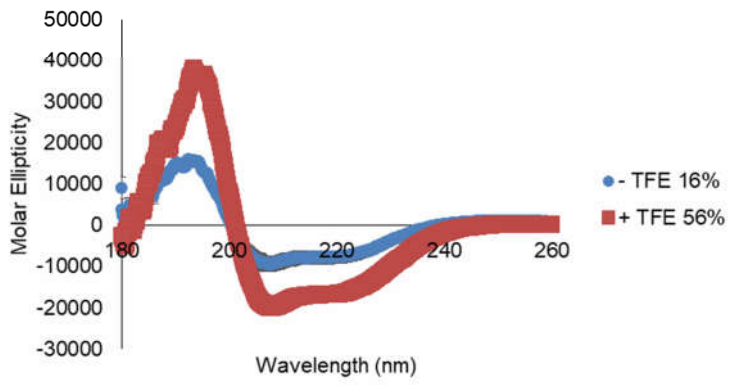




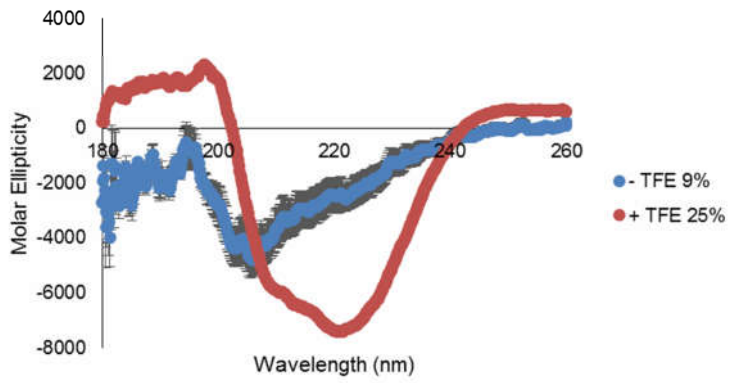
mHCS-8-L

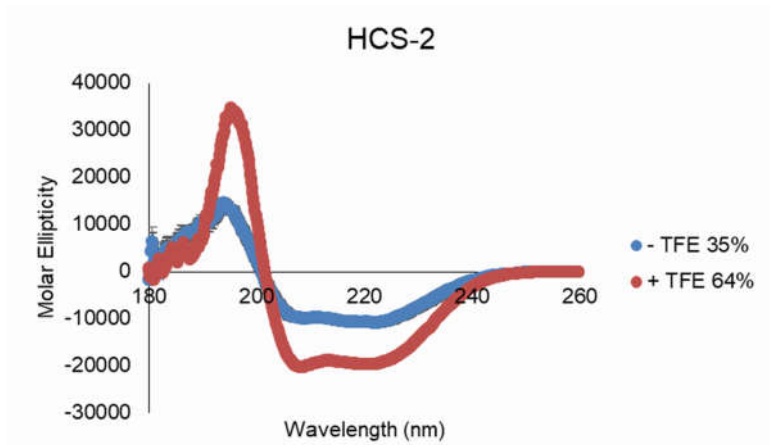
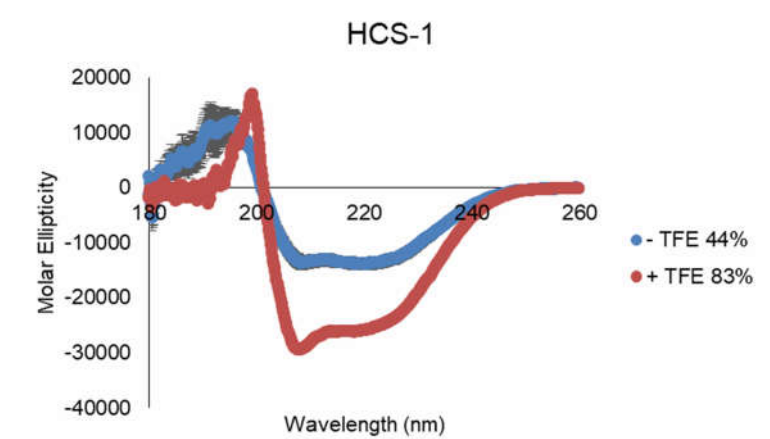
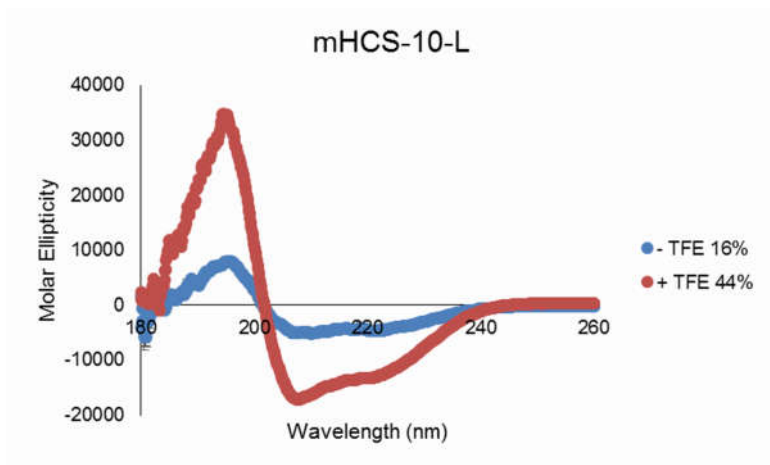


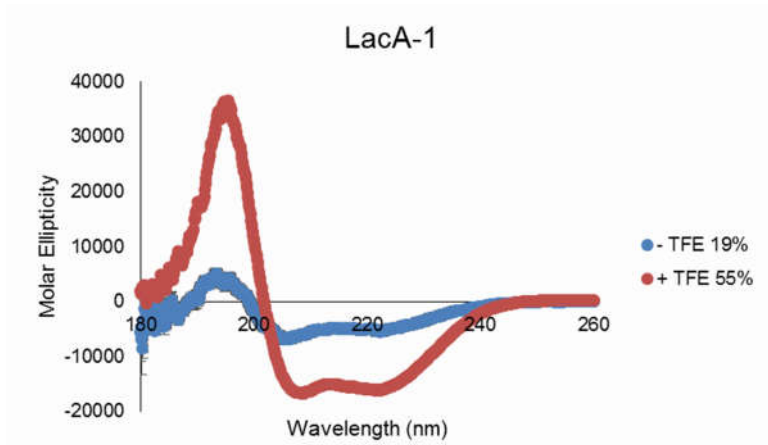
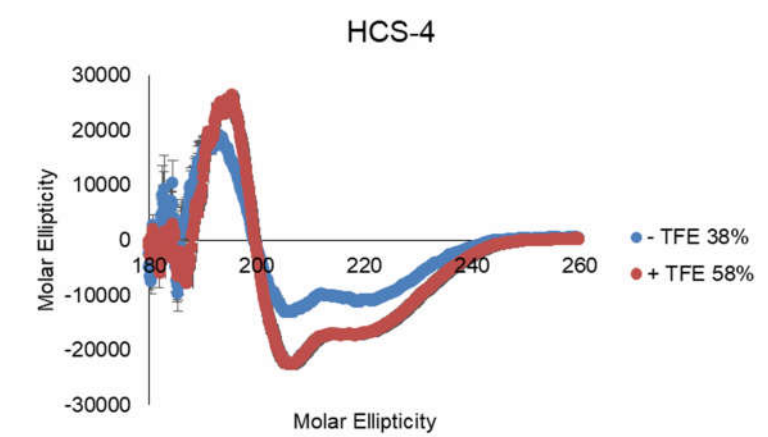
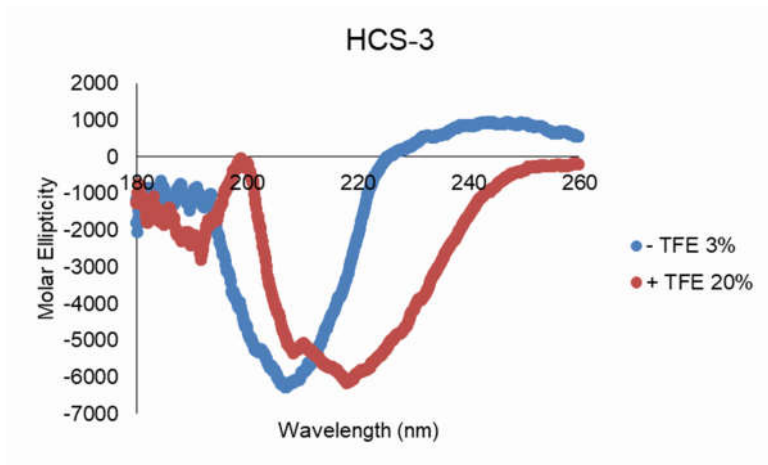
mHCS-9-E



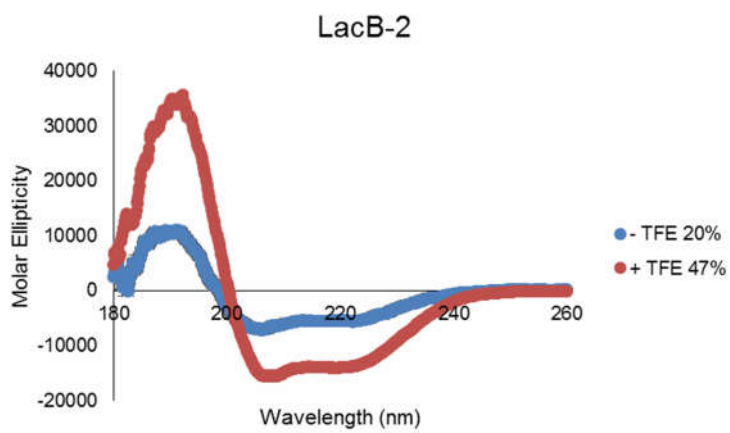
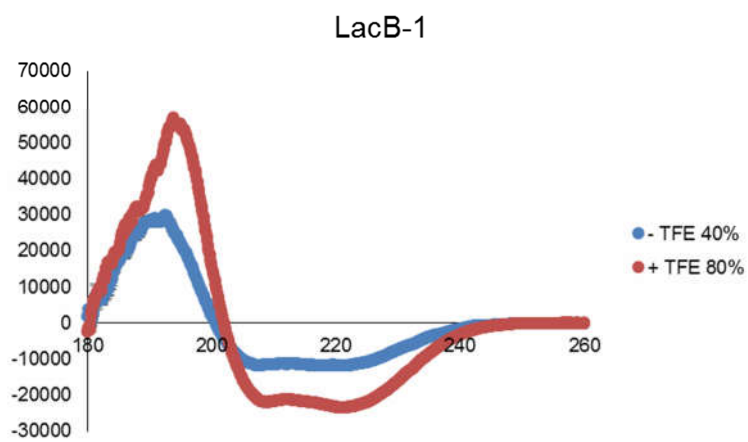
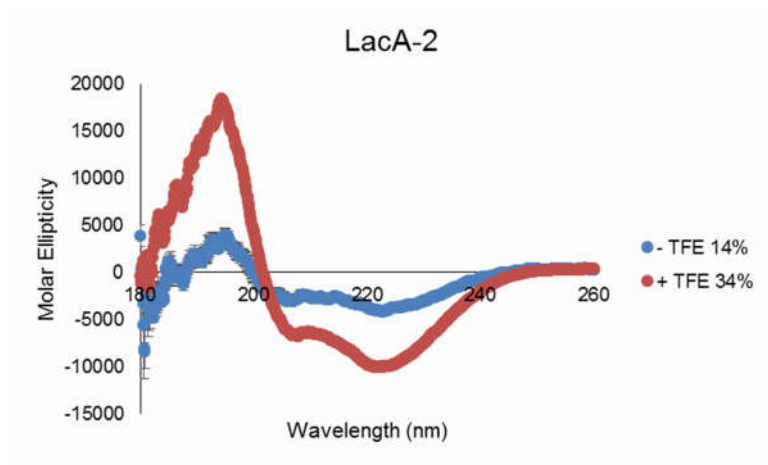
mHCS-9-L





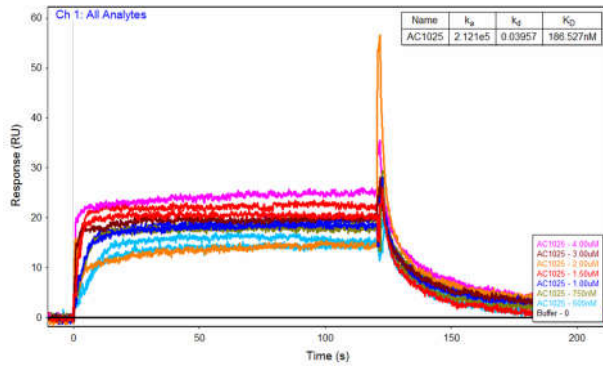




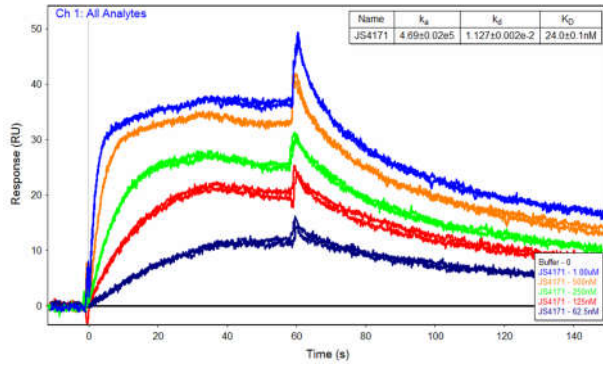


# SPR Curves for Peptides

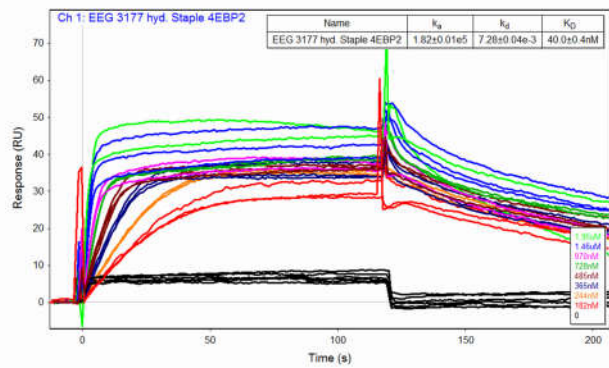
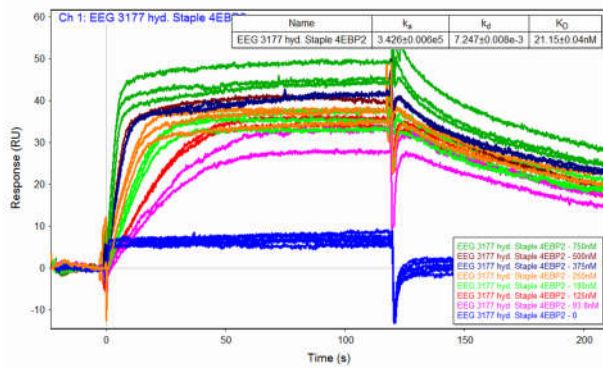
## 4E-BP1-10

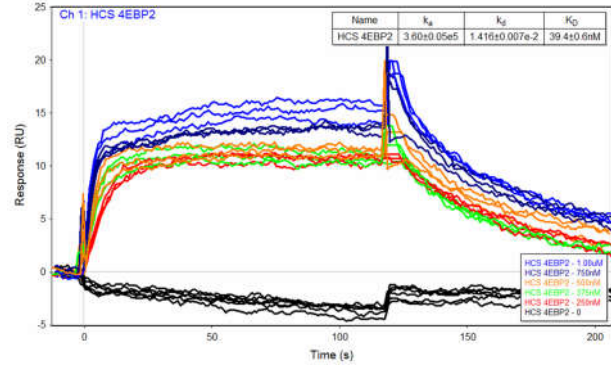
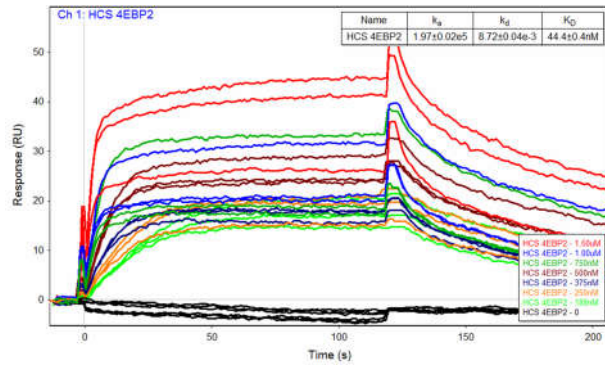


## mHCS-1

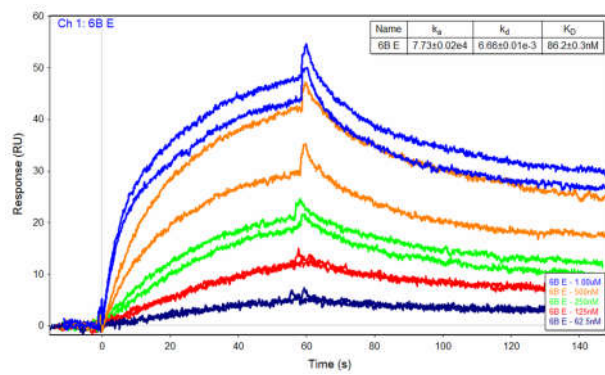


## mHCS-2

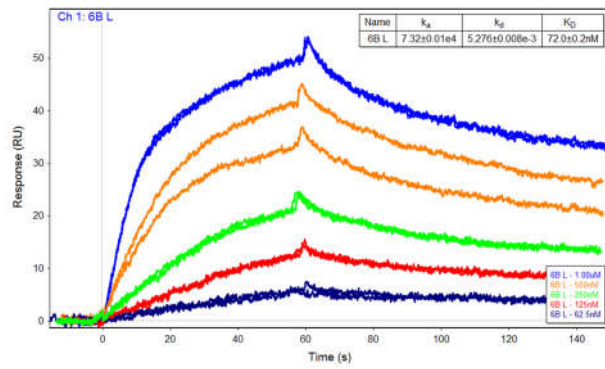




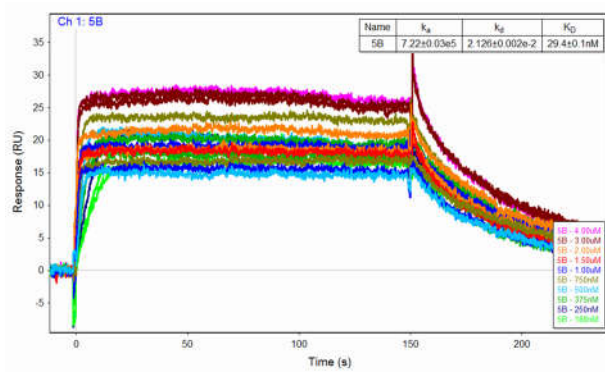
### mHCS-3-E



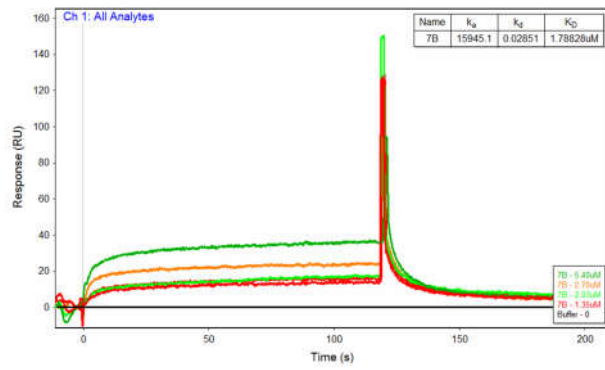
### mHCS-3-L



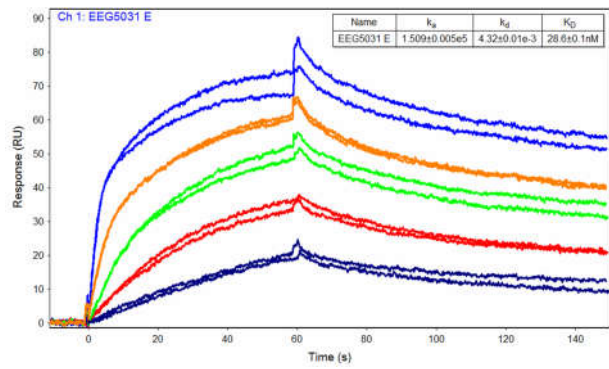
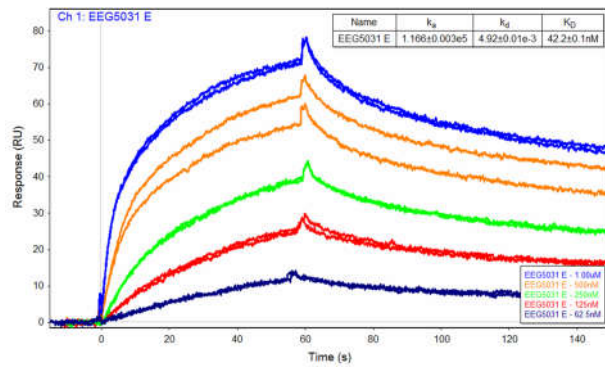
### mHCS-4



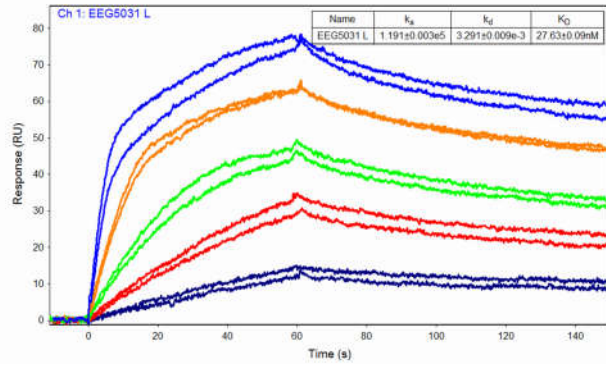
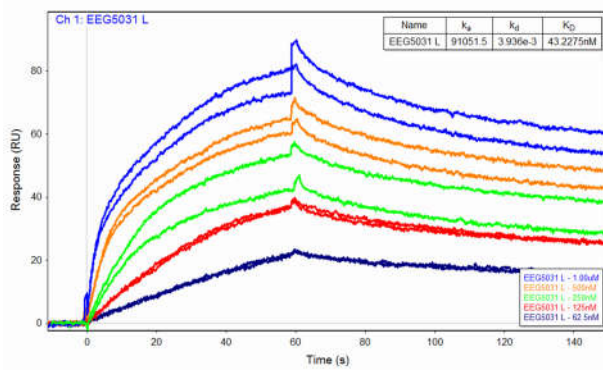
### mHCS-5



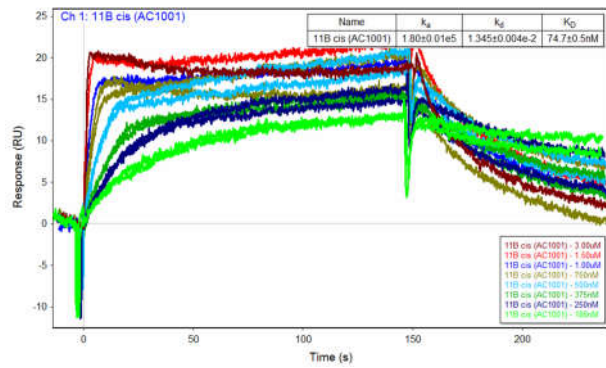
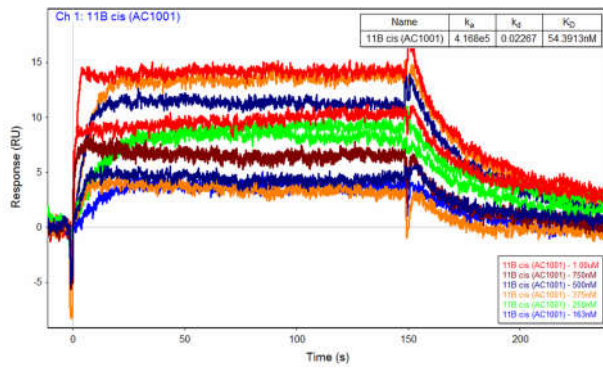
### mHCS-6-E



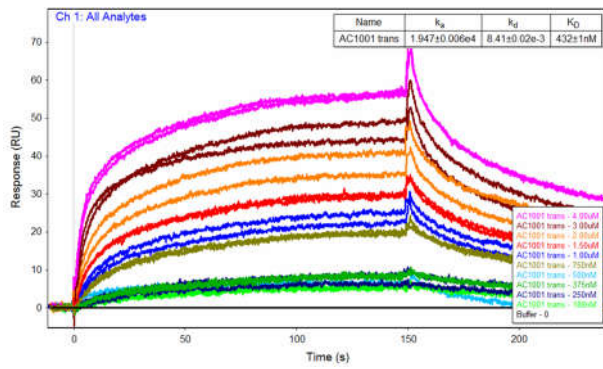
### mHCS-6-L



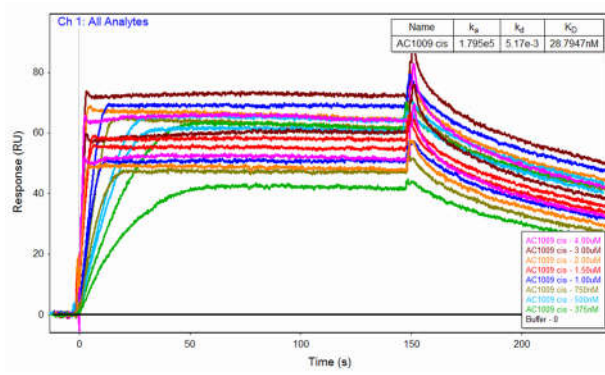
### mHCS-7-E



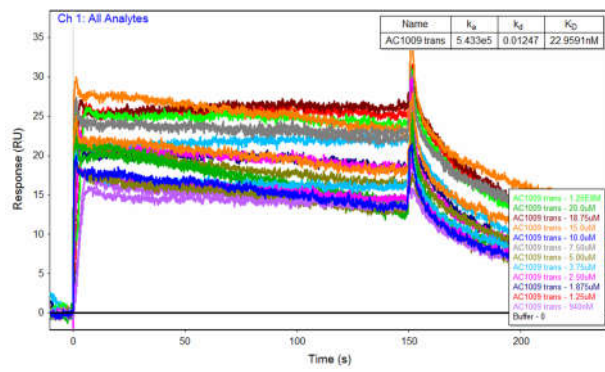
### mHCS-7-L



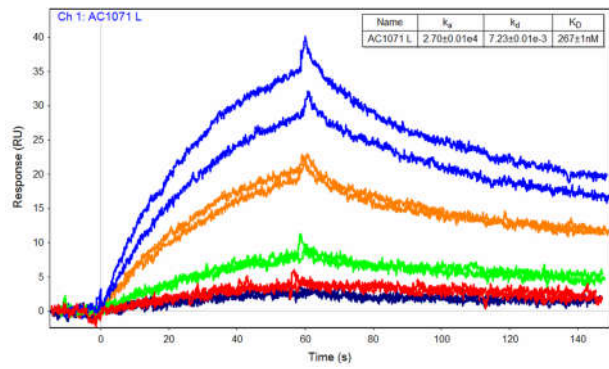
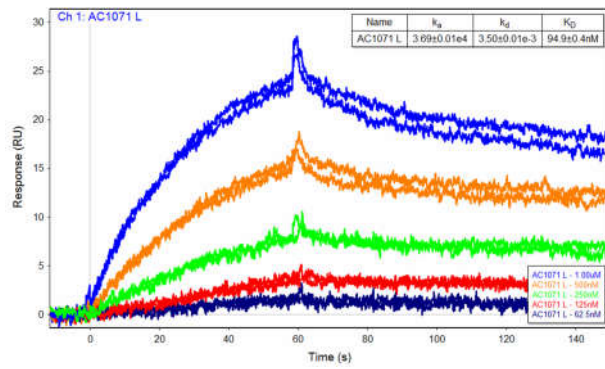
### mHCS-9-E



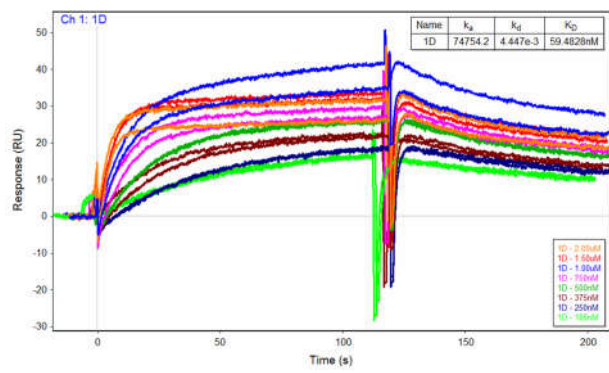
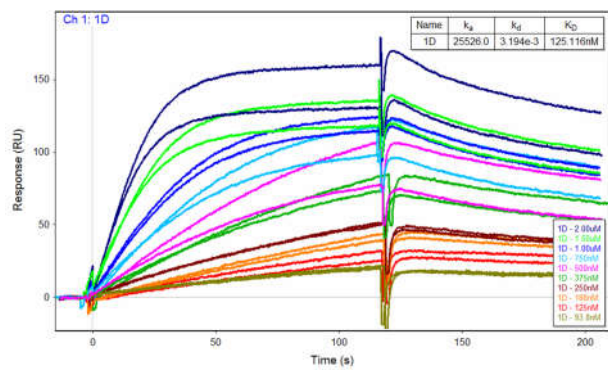
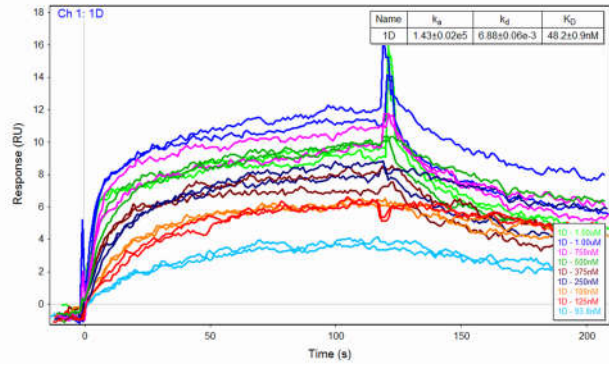
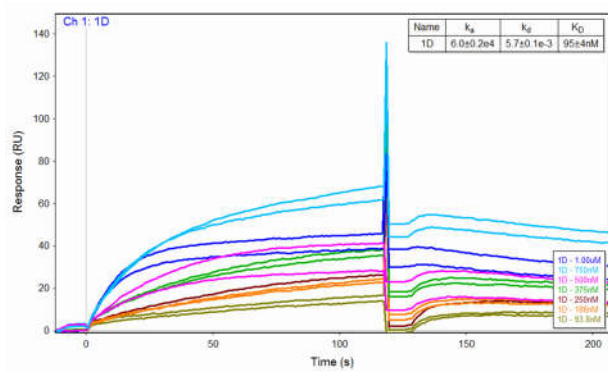
### mHCS-9-L



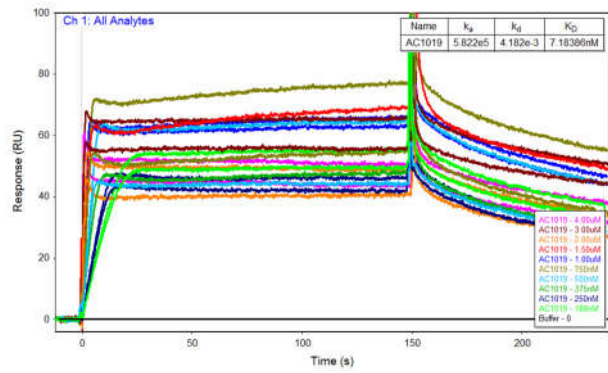
### mHCS-10-L



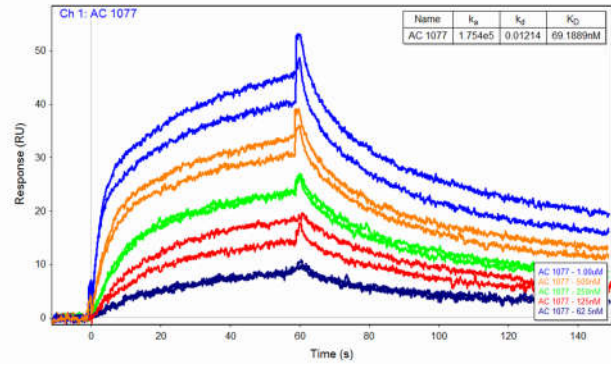
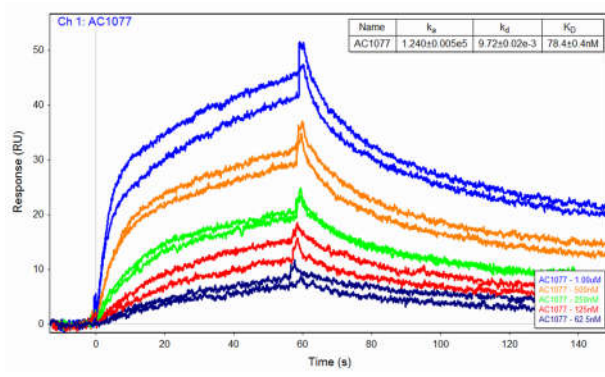
# OASer-1



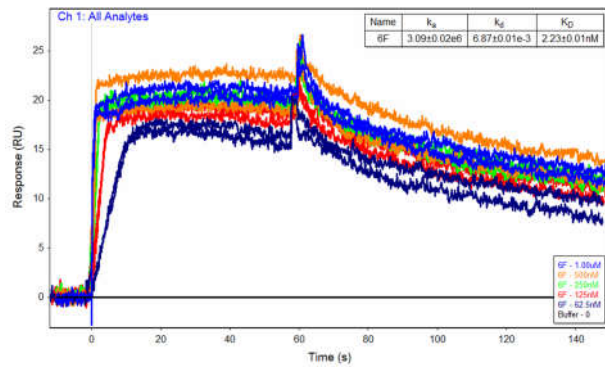
# LacA-1



## LacA-2



## LacB-1





## References

- (1) Lama, D.; Quah, S. T.; Verma, C. S.; Lakshminarayanan, R.; Beuerman, R. W.; Lane, D. P.; Brown, C. J. Rational Optimization of Conformational Effects Induced by Hydrocarbon Staples in Peptides and Their Binding Interfaces. *Sci. Rep.* **2013**, *3*, 3451.
- (2) Yuan, T. L.; Cantley, L. C. PI3K Pathway Alterations in Cancer : Variations on a Theme. *Oncogene* **2008**, *27*, 5497–5510.
- (3) Gorgisen, G.; Pehlivanoglu, S.; Ozes, D.; Ozes, O. N. Personalized Treatment Options in Non-Small Cell Lung Cancer. *Recept. Clin. Investig.* **2014**, *1* (Figure 1), 1–10.
- (4) Singla, H.; Ludhiadch, A.; Preet, R.; Chander, H. European Journal of Medicinal Chemistry Recent Advances in HER2 Positive Breast Cancer Epigenetics : Susceptibility and Therapeutic Strategies. *Eur. J. Med. Chem.* **2017**, *142*, 316–327.
- (5) Fruman, D. A.; Chiu, H.; Hopkins, B. D.; Bagrodia, S.; Cantley, L. C.; Abraham, R. T. The PI3K Pathway in Human Disease. *Cell* **2017**, *170* (4), 605–635.
- (6) Janku, F.; Yap, T. A.; Meric-bernstam, F. Targeting the PI3K Pathway in Cancer: Are We Making Headway? *Nat. Publ. Gr.* **2018**, *15* (5), 273–291.
- (7) Saxton, R. A.; Sabatini, D. M. MTOR Signaling in Growth, Metabolism, and Disease. *Cell* **2017**, *168* (6), 960–976.
- (8) Zoncu, R.; Efeyan, A.; Sabatini, D. M. MTOR: From Growth Signal Integration to Cancer, Diabetes and Ageing. *Nat. Rev. Mol. Cell Biol.* **2011**, *12* (1), 21–35.
- (9) Menon, S.; Manning, B. D. Common Corruption of the MTOR Signaling Network in Human Tumors. *Oncogene* **2008**, *27 Suppl 2* (S2), S43-51.
- (10) Fruman, D. a; Rommel, C. PI3K and Cancer: Lessons, Challenges and Opportunities. *Nat. Rev. Drug Discov.* **2014**, *13* (2), 140–156.
- (11) Thoreen, C. C.; Chantranupong, L.; Keys, H. R.; Wang, T.; Gray, N. S.; Sabatini, D. M. A Unifying Model for MTORC1-Mediated Regulation of mRNA Translation. *Nature* **2105**, *486* (7396), 109–113.
- (12) Silvera, D.; Formenti, S. C.; Schneider, R. J. Translational Control in Cancer. *Nat. Rev. Cancer* **2010**, *10* (4), 254–266.
- (13) Blagden, S. P.; Willis, A. E. The Biological and Therapeutic Relevance of mRNA Translation in Cancer. *Nat. Rev. Clin. Oncol.* **2011**, *8* (5), 280–291.
- (14) Dowling, R. J. O.; Topisirovic, I.; Alain, T.; Bidinosti, M.; Fonseca, B. D.; Petroulakis, E.; Wang, X.; Larsson, O.; Selvaraj, A.; Liu, Y.; Kozma, S. C.; Thomas, G.; Sonenberg, N. MTORC1-Mediated Cell Proliferation, but Not Cell Growth, Controlled by the 4E-BPs. *Science* **2010**, *328* (5982), 1172–1176.
- (15) Li, J.; Kim, S. G.; Blenis, J. Rapamycin: One Drug, Many Effects. *Cell Metab.* **2014**, *19* (3), 373–379.

- (16) Wander, S. A.; Hennessy, B. T.; Slingerland, J. M. Next-Generation MTOR Inhibitors in Clinical Oncology : How Pathway Complexity Informs Therapeutic Strategy. *J. Clin. Invest.* **2011**, *121* (4), 1231–1241.
- (17) Hsieh, A. C.; Costa, M.; Zollo, O.; Davis, C.; Feldman, M. E.; Testa, J. R.; Meyuhas, O.; Shokat, K. M.; Ruggero, D. Genetic Dissection of the Oncogenic MTOR Pathway Reveals Druggable Addiction to Translational Control via 4EBP-EIF4E. *Cancer Cell* **2010**, *17* (3), 249–261.
- (18) Thoreen, C. C.; Kang, S. a; Chang, J. W.; Liu, Q.; Zhang, J.; Gao, Y.; Reichling, L. J.; Sim, T.; Sabatini, D. M.; Gray, N. S. An ATP-Competitive Mammalian Target of Rapamycin Inhibitor Reveals Rapamycin-Resistant Functions of MTORC1. *J. Biol. Chem.* **2009**, *284* (12), 8023–8032.
- (19) Feldman, M. E.; Apsel, B.; Uotila, A.; Loewith, R.; Knight, Z. a; Ruggero, D.; Shokat, K. M. Active-Site Inhibitors of MTOR Target Rapamycin-Resistant Outputs of MTORC1 and MTORC2. *PLoS Biol.* **2009**, *7* (2), e38.
- (20) Choo, A. Y.; Blenis, J. Not All Substrates Are Treated Equally; Implications for MTOR, Rapamycin-Resistance, and Cancer Therapy. *Cell Cycle* **2009**, *8* (4), 567–572.
- (21) Choo, A. Y.; Yoon, S.; Gyun, S.; Roux, P. P.; Blenis, J. Rapamycin Differentially Inhibits S6Ks and 4E-BP1 to Mediate Cell-Type-Specific Repression of mRNA Translation. *PNAS* **2008**, *105* (45), 17414–17419.
- (22) She, Q.-B.; Halilovic, E.; Ye, Q.; Zhen, W.; Shirasawa, S.; Sasazuki, T.; Solit, D. B.; Rosen, N. 4E-BP1 Is a Key Effector of the Oncogenic Activation of the AKT and ERK Signaling Pathways That Integrates Their Function in Tumors. *Cancer Cell* **2010**, *18* (1), 39–51.
- (23) Hsieh, A. C.; Liu, Y.; Edlind, M. P.; Ingolia, N. T.; Janes, M. R.; Sher, A.; Shi, E. Y.; Stumpf, C. R.; Christensen, C.; Bonham, M. J.; Wang, S.; Ren, P.; Martin, M.; Jessen, K.; Feldman, M. E.; Weissman, J. S.; Shokat, K. M.; Rommel, C.; Ruggero, D. The Translational Landscape of MTOR Signalling Steers Cancer Initiation and Metastasis. *Nature* **2012**, *485*, 55–61.
- (24) Guertin, D. a; Sabatini, D. M. The Pharmacology of MTOR Inhibition. *Sci. Signal.* **2009**, *2* (67), pe24.
- (25) Sun, S.-Y.; Rosenberg, L. M.; Wang, X.; Zhou, Z.; Yue, P.; Fu, H.; Khuri, F. R. Activation of Akt and EIF4E Survival Pathways by Rapamycin-Mediated Mammalian Target of Rapamycin Inhibition. *Cancer Res.* **2005**, *65* (16), 7052–7058.
- (26) O'Reilly, K. E.; Rojo, F.; She, Q.-B.; Solit, D.; Mills, G. B.; Smith, D.; Lane, H.; Hofmann, F.; Hicklin, D. J.; Ludwig, D. L.; Baselga, J.; Rosen, N. MTOR Inhibition Induces Upstream Receptor Tyrosine Kinase Signaling and Activates Akt. *Cancer Res.* **2006**, *66* (3), 1500–1508.
- (27) Carracedo, A.; Ma, L.; Teruya-Feldstein, J.; Rojo, F.; Salmena, L.; Alimonti, A.; Egia, A.; Sasaki, A. T.; Thomas, G.; Kozma, S. C.; Papa, A.; Nardella, C.; Cantley, L. C.; Baselga, J.; Pandolfi, P. P. Inhibition of MTORC1 Leads to MAPK Pathway Activation through a PI3K-Dependent Feedback Loop in Human Cancer. *J. Clin. Invest.* **2008**, *118* (9), 3065–3074.
- (28) Cope, C. L.; Gilley, R.; Balmanno, K.; Sale, M. J.; Howarth, K. D.; Hampson, M.; Smith, P. D.; Guichard, S. M.; Cook, S. J. Adaptation to MTOR Kinase Inhibitors

- by Amplification of EIF4E to Maintain Cap-Dependent Translation. *J. Cell Sci.* **2014**, *127*, 788–800.
- (29) Ilic, N.; Utermark, T.; Widlund, H. R.; Roberts, T. M. PI3K-Targeted Therapy Can Be Evaded by Gene Amplification along the MYC-Eukaryotic Translation Initiation Factor 4E (EIF4E) Axis. *Proc. Natl. Acad. Sci. U. S. A.* **2011**, *108* (37), E699-708.
- (30) Martineau, Y.; Azar, R.; Müller, D.; Lasfargues, C.; El Khawand, S.; Anesia, R.; Pelletier, J.; Bousquet, C.; Pyronnet, S. Pancreatic Tumours Escape from Translational Control through 4E-BP1 Loss. *Oncogene* **2014**, *33*, 1367–1374.
- (31) Mallya, S.; Fitch, B. a.; Lee, J. S.; So, L.; Janes, M. R.; Fruman, D. a. Resistance to MTOR Kinase Inhibitors in Lymphoma Cells Lacking 4EBP1. *PLoS One* **2014**, *9* (2), 1–10.
- (32) Alain, T.; Morita, M.; Fonseca, B. D.; Yanagiya, A.; Siddiqui, N.; Bhat, M.; Zammit, D.; Marcus, V.; Metrakos, P.; Voyer, L.-A.; Gandin, V.; Liu, Y.; Topisirovic, I.; Sonenberg, N. EIF4E/4E-BP Ratio Predicts the Efficacy of MTOR Targeted Therapies. *Cancer Res.* **2012**, *72* (24), 6468–6476.
- (33) Dienstmann, R.; Rodon, J.; Serra, V.; Tabernero, J. Picking the Point of Inhibition : A Comparative Review of PI3K / AKT / MTOR Pathway Inhibitors. *Mol. Cancer Ther.* **2014**, *13* (5), 1021–1032.
- (34) Zhang, Y.; Zheng, X. F. S. MTOR-Independent 4E-BP1 Phosphorylation Is Associated with Cancer Resistance to MTOR Kinase Inhibitors. *Cell Cycle* **2012**, *11* (3), 594–603.
- (35) Ducker, G. S.; Atreya, C. E.; Simko, J. P.; Hom, Y. K.; Matli, M. R.; Benes, C. H.; Hann, B.; Nakakura, E. K.; Bergsland, E. K.; Donner, D. B.; Settleman, J.; Shokat, K. M.; Warren, R. S. Incomplete Inhibition of Phosphorylation of 4E-BP1 as a Mechanism of Primary Resistance to ATP-Competitive MTOR Inhibitors. *Oncogene* **2014**, *33* (12), 1590–1600.
- (36) Willis, A. E. Translational Control of Growth Factor and Proto-Oncogene Expression. *Int. J. Biochem. Cell Biol.* **1999**, *31* (1), 73–86.
- (37) Mamane, Y.; Petroulakis, E.; Rong, L.; Yoshida, K.; Ler, L. W.; Sonenberg, N. EIF4E--from Translation to Transformation. *Oncogene* **2004**, *23* (18), 3172–3179.
- (38) Hsieh, A. C.; Ruggero, D. Targeting Eukaryotic Translation Initiation Factor 4E (EIF4E) in Cancer. *Clin. Cancer Res.* **2010**, *16* (20), 4914–4920.
- (39) Pelletier, J.; Graff, J.; Ruggero, D.; Sonenberg, N. Targeting the EIF4F Translation Initiation Complex: A Critical Nexus for Cancer Development. *Cancer Res.* **2015**, *75* (2), 250–263.
- (40) De Benedetti, A.; Graff, J. R. EIF-4E Expression and Its Role in Malignancies and Metastases. *Oncogene* **2004**, *23* (18), 3189–3199.
- (41) Richter, J. D.; Sonenberg, N. Regulation of Cap-Dependent Translation by EIF4E Inhibitory Proteins. *Nature* **2005**, *433* (7025), 477–480.
- (42) Graff, J. R.; Zimmer, S. G. Translational Control and Metastatic Progression : Enhanced Activity of the MRNA Cap-Binding Protein EIF-4E Selectively Enhances Translation of Metastasis-Related MRNAs. *Clin. Exp. Metastasis* **2003**, *20*, 265–273.
- (43) Graff, J. R.; Konicek, B. W.; Carter, J. H.; Marcusson, E. G. Targeting the Eukaryotic Translation Initiation Factor 4E for Cancer Therapy. *Cancer Res.* **2008**, *68* (3), 631–634.

- (44) Lazaris-Karatzas, A.; Montine, K.; Sonenberg, N. Malignant Transformation by a Eukaryotic Initiation Factor Subunit That Binds to mRNA 5'cap. *Nature* **1990**, *345*, 544–547.
- (45) Wendel, H.; Stanchina, E. De; Fridman, J. S.; Malina, A.; Sagarika, R.; Kogan, S.; Cordon-Cardo, C.; Pelletier, J.; Low, S. W. Survival Signalling by Akt and EIF4E in Oncogenesis and Cancer Therapy. *Nature* **2004**, *428* (March), 332–337.
- (46) Hariri, F.; Arguello, M.; Volpon, L.; Culjkovic-Kraljacic, B.; Nielsen, T. H.; Hiscott, J.; Mann, K. K.; Borden, K. L. B. The Eukaryotic Translation Initiation Factor EIF4E Is a Direct Transcriptional Target of NF-KB and Is Aberrantly Regulated in Acute Myeloid Leukemia. *Leukemia* **2013**, *27* (10), 2047–2055.
- (47) Soni, A.; Akcakanat, A.; Singh, G.; Luyimbazi, D.; Zheng, Y.; Kim, D.; Gonzalez-Angulo, A.; Meric-Bernstam, F. EIF4E Knockdown Decreases Breast Cancer Cell Growth without Activating Akt Signaling. *Mol. Cancer Ther.* **2008**, *7* (7), 1782–1788.
- (48) Moerke, N. J.; Aktas, H.; Chen, H.; Cantel, S.; Reibarkh, M. Y.; Fahmy, A.; Gross, J. D.; Degterev, A.; Yuan, J.; Chorev, M.; Halperin, J. a; Wagner, G. Small-Molecule Inhibition of the Interaction between the Translation Initiation Factors EIF4E and EIF4G. *Cell* **2007**, *128* (2), 257–267.
- (49) Mokas, S.; Mills, J. R.; Garreau, C.; Fournier, M.-J.; Robert, F.; Arya, P.; Kaufman, R. J.; Pelletier, J.; Mazroui, R. Uncoupling Stress Granule Assembly and Translation Initiation Inhibition. *Mol. Biol. Cell* **2009**, *20* (11), 2673–2683.
- (50) Fan, S.; Li, Y.; Yue, P.; Khuri, F. R.; Sun, S.-Y. The EIF4E/EIF4G Interaction Inhibitor 4EGI-1 Augments TRAIL-Mediated Apoptosis through c-FLIP Down-Regulation and DR5 Induction Independent of Inhibition of Cap-Dependent Protein Translation. *Neoplasia* **2010**, *12* (4), 346–356.
- (51) McMahon, R.; Zaborowska, I.; Walsh, D. Noncytotoxic Inhibition of Viral Infection through EIF4F-Independent Suppression of Translation by 4EGi-1. *J. Virol.* **2011**, *85* (2), 853–864.
- (52) Redondo, N.; García-Moreno, M.; Sanz, M. A.; Carrasco, L. Translation of Viral MRNAs That Do Not Require EIF4E Is Blocked by the Inhibitor 4EGI-1. *Virology* **2013**, *444* (1–2), 171–180.
- (53) Descamps, G.; Gomez-Bougie, P.; Tamburini, J.; Green, a; Bouscary, D.; Maïga, S.; Moreau, P.; Le Gouill, S.; Pellat-Deceunynck, C.; Amiot, M. The Cap-Translation Inhibitor 4EGI-1 Induces Apoptosis in Multiple Myeloma through Noxa Induction. *Br. J. Cancer* **2012**, *106* (10), 1660–1667.
- (54) Willimott, S.; Beck, D.; Ahearne, M. J.; Adams, V. C.; Wagner, S. D. Cap-Translation Inhibitor, 4EGI-1, Restores Sensitivity to ABT-737 Apoptosis through Cap-Dependent and -Independent Mechanisms in Chronic Lymphocytic Leukemia. *Clin. Cancer Res.* **2013**, *19* (12), 3212–3223.
- (55) Schwarzer, a; Holtmann, H.; Brugman, M.; Meyer, J.; Schauerte, C.; Zuber, J.; Steinemann, D.; Schlegelberger, B.; Li, Z.; Baum, C. Hyperactivation of MTORC1 and MTORC2 by Multiple Oncogenic Events Causes Addiction to EIF4E-Dependent mRNA Translation in T-Cell Leukemia. *Oncogene* **2014**, No. August, 1–12.
- (56) Attar-Schneider, O.; Drucker, L.; Zismanov, V.; Tartakover-Matalon, S.; Lishner, M. Targeting EIF4GI Translation Initiation Factor Affords an Attractive Therapeutic

- Strategy in Multiple Myeloma. *Cell. Signal.* **2014**, *26* (9), 1878–1887.
- (57) Chen, L.; Aktas, B. H.; Wang, Y.; He, X.; Sahoo, R.; Denoyelle, S.; Kabha, E.; Yang, H.; Yefidoff, R. Tumor Suppression by Small Molecule Inhibitors of Translation Initiation ABSTRACT : *Oncotarget* **2012**, *3* (8), 869–881.
- (58) Yefidoff-Freedman, R.; Chen, T.; Sahoo, R.; Chen, L.; Wagner, G.; Halperin, J. a; Aktas, B. H.; Chorev, M. 3-Substituted Indazoles as Configurationally Locked 4EGI-1 Mimetics and Inhibitors of the EIF4E/EIF4G Interaction. *Chembiochem* **2014**, *15* (4), 595–611.
- (59) Jones, R. M.; Branda, J.; Johnston, K. A.; Polymenis, M.; Gadd, M.; Rustgi, A.; Callanan, L.; Schmidt, E. V. An Essential E Box in the Promoter of the Gene Encoding the mRNA Cap-Binding Protein ( Eukaryotic Initiation Factor 4E ) Is a Target for Activation by c-Myc. **1996**, *16* (9), 4754–4764.
- (60) Rosenwald, I. B.; Rhoads, D. B.; Callanan, L. D.; Isselbacher, K. J.; Schmidt, E. V. Increased Expression of Eukaryotic Translation Initiation Factors EIF-4E and EIF-2a in Response to Growth Induction by c-Myc. *Proc. Natl. Acad. Sci. USA* **1993**, *90*, 6175–6178.
- (61) Bonneau, A.; Sonenberg, N. Involvement of the 24-KDa Cap-Binding Protein in Regulation of Protein Synthesis in Mitosis. *J. Biol. Chem.* **1987**, *262* (23), 11134–11139.
- (62) Morley, S. J.; Traugh, J. A. Differential Stimulation of Phosphorylation of Initiation Factors EIF-4F, EIF-4B, EIF-3, and Ribosomal Protein S6 by Insulin and Phorbol Esters. *J. Biol. Chem.* **1990**, *265* (18), 10611–10616.
- (63) Pause, A.; Belsham, G. J.; Gingras, A.-C.; Donze, O.; Lin, T.; Lawrence, J. C.; Sonenberg, N. Insulin-Dependent Stimulation of Protein Synthesis by Phosphorylation of a Regulator of 5'-Cap Function. *Nature* **1994**, *371*, 762–767.
- (64) Lin, T.; Kong, X.; Haystead, T. A. J.; Pause, A.; Belsham, G.; Sonenberg, N.; Jr, J. C. L. PHAS-I as a Link Between Mitogen-Activated Protein Kinase and Translation Initiation. *Science (80- )*. **1994**, *266*, 653–656.
- (65) Haghghat, A.; Mader, S.; Pause, A.; Sonenberg, N. Repression of Cap-Dependent Translation by 4E-Binding Protein 1: Competition with P220 for Binding to Eukaryotic Initiation Factor-4E. *EMBO J.* **1995**, *14* (22), 5701–5709.
- (66) Mader, S.; Lee, H. A. N.; Pause, A.; Sonenberg, N. The Translation Initiation Factor EIF-4E Binds to a Common Motif Shared by the Translation Factor EIF-4G and the Translational Repressors 4E-Binding Proteins. *Mol. Cell. Biol.* **1995**, *15* (9), 4990–4997.
- (67) Marcotrigiano, J.; Gingras, A.-C.; Sonenberg, N.; Burley, S. K. Cap-Dependent Translation Initiation in Eukaryotes Is Regulated by a Molecular Mimic of EIF4G. *Mol. Cell* **1999**, *3* (6), 707–716.
- (68) Ptushkina, M.; von der Haar, T.; Karim, M. M.; Hughes, J. M.; McCarthy, J. E. Repressor Binding to a Dorsal Regulatory Site Traps Human EIF4E in a High Cap-Affinity State. *EMBO J.* **1999**, *18* (14), 4068–4075.
- (69) Gingras, a C.; Raught, B.; Sonenberg, N. Regulation of Translation Initiation by FRAP/MTOR. *Genes Dev.* **2001**, *15* (7), 807–826.
- (70) Brunn, G. J.; Hudson, C. C.; Sekulić, A.; Williams, J. M.; Hosoi, H.; Houghton, P. J.; Jr, J. C. L.; Abraham, R. T. Phosphorylation of the Translational Repressor PHAS-I by the Mammalian Target of Rapamycin. *Science (80- )*. **1997**, *277*, 99–

- 101.
- (71) Gingras, a.-C.; Gygi, S. P.; Raught, B.; Polakiewicz, R. D.; Abraham, R. T.; Hoekstra, M. F.; Aebersold, R.; Sonenberg, N. Regulation of 4E-BP1 Phosphorylation: A Novel Two-Step Mechanism. *Genes Dev.* **1999**, *13* (11), 1422–1437.
- (72) Gingras, a C.; Raught, B.; Gygi, S. P.; Niedzwiecka, a; Miron, M.; Burley, S. K.; Polakiewicz, R. D.; Wyslouch-Cieszynska, a; Aebersold, R.; Sonenberg, N. Hierarchical Phosphorylation of the Translation Inhibitor 4E-BP1. *Genes Dev.* **2001**, *15* (21), 2852–2864.
- (73) Li, S.; Sonenberg, N.; Gingras, a.-C.; Peterson, M.; Avdulov, S.; Polunovsky, V. a.; Bitterman, P. B. Translational Control of Cell Fate: Availability of Phosphorylation Sites on Translational Repressor 4E-BP1 Governs Its Proapoptotic Potency. *Mol. Cell. Biol.* **2002**, *22* (8), 2853–2861.
- (74) Armengol, G.; Rojo, F.; Castellví, J.; Iglesias, C.; Cuatrecasas, M.; Pons, B.; Baselga, J.; Ramón Y Cajal, S. 4E-Binding Protein 1: A Key Molecular “Funnel Factor” in Human Cancer with Clinical Implications. *Cancer Res.* **2007**, *67* (16), 7551–7555.
- (75) Martineau, Y.; Azar, R.; Bousquet, C.; Pyronnet, S. Anti-Oncogenic Potential of the EIF4E-Binding Proteins. *Oncogene* **2013**, *32* (6), 671–677.
- (76) Rojo, F.; Najera, L.; Lirola, J.; Jiménez, J.; Guzmán, M.; Sabadell, M. D.; Baselga, J.; Ramon y Cajal, S. 4E-Binding Protein 1, a Cell Signaling Hallmark in Breast Cancer That Correlates with Pathologic Grade and Prognosis. *Clin. Cancer Res.* **2007**, *13* (1), 81–89.
- (77) Castellvi, J.; Garcia, A.; Rojo, F.; Ruiz-Marcellan, C.; Gil, A.; Baselga, J.; Ramon y Cajal, S. Phosphorylated 4E Binding Protein 1: A Hallmark of Cell Signaling That Correlates with Survival in Ovarian Cancer. *Cancer* **2006**, *107* (8), 1801–1811.
- (78) O'Reilly, K. E.; Warycha, M.; Davies, M. a; Rodrik, V.; Zhou, X. K.; Yee, H.; Polsky, D.; Pavlick, A. C.; Rosen, N.; Bhardwaj, N.; Mills, G.; Osman, I. Phosphorylated 4E-BP1 Is Associated with Poor Survival in Melanoma. *Clin. Cancer Res.* **2009**, *15* (8), 2872–2878.
- (79) Graff, J. R.; Konicek, B. W.; Lynch, R. L.; Dumstorf, C. a; Dowless, M. S.; McNulty, A. M.; Parsons, S. H.; Brail, L. H.; Colligan, B. M.; Koop, J. W.; Hurst, B. M.; Deddens, J. a; Neubauer, B. L.; Stancato, L. F.; Carter, H. W.; Douglass, L. E.; Carter, J. H. EIF4E Activation Is Commonly Elevated in Advanced Human Prostate Cancers and Significantly Related to Reduced Patient Survival. *Cancer Res.* **2009**, *69* (9), 3866–3873.
- (80) Rousseau, D.; Gingras, A. C.; Pause, A.; Sonenberg, N. The EIF4E-Binding Proteins 1 and 2 Are Negative Regulators of Cell Growth. *Oncogene* **1996**, *13*, 2415–2420.
- (81) Polunovsky, V. a; Gingras, a C.; Sonenberg, N.; Peterson, M.; Tan, a; Rubins, J. B.; Manivel, J. C.; Bitterman, P. B. Translational Control of the Antiapoptotic Function of Ras. *J. Biol. Chem.* **2000**, *275* (32), 24776–24780.
- (82) Jiang, H.; Coleman, J.; Miskimins, R.; Miskimins, W. K. Expression of Constitutively Active 4EBP-1 Enhances P27Kip1 Expression and Inhibits Proliferation of MCF7 Breast Cancer Cells. *Cancer Cell Int.* **2003**, *3* (2).
- (83) Avdulov, S.; Li, S.; Michalek, V.; Burrichter, D.; Peterson, M.; Perlman, D. M.;

- Manivel, J. C.; Sonenberg, N.; Yee, D.; Bitterman, P. B.; Polunovsky, V. A. Activation of Translation Complex EIF4F Is Essential for the Genesis and Maintenance of the Malignant Phenotype in Human Mammary Epithelial Cells. **2004**, *5* (June), 553–563.
- (84) Jacobson, B. a; Alter, M. D.; Kratzke, M. G.; Frizelle, S. P.; Zhang, Y.; Peterson, M. S.; Avdulov, S.; Mohorn, R. P.; Whitson, B. a; Bitterman, P. B.; Polunovsky, V. a; Kratzke, R. a. Repression of Cap-Dependent Translation Attenuates the Transformed Phenotype in Non-Small Cell Lung Cancer Both in Vitro and in Vivo. *Cancer Res.* **2006**, *66* (8), 4256–4262.
- (85) Ye, Q.; Cai, W.; Zheng, Y.; Evers, B. M.; She, Q.-B. ERK and AKT Signaling Cooperate to Translationally Regulate Survivin Expression for Metastatic Progression of Colorectal Cancer. *Oncogene* **2014**, *33* (April 2013), 1828–1839.
- (86) Dilling, M. B.; Germain, G. S.; Dudkin, L.; Jayaraman, A. L.; Zhang, X.; Harwood, F. C.; Houghton, P. J. 4E-Binding Proteins, the Suppressors of Eukaryotic Initiation Factor 4E, Are down-Regulated in Cells with Acquired or Intrinsic Resistance to Rapamycin. *J. Biol. Chem.* **2002**, *277* (16), 13907–13917.
- (87) Cencic, R.; Hall, D. R.; Robert, F.; Du, Y.; Min, J.; Li, L.; Qui, M.; Lewis, I.; Kurtkaya, S.; Dingleline, R.; Fu, H.; Kozakov, D.; Vajda, S.; Pelletier, J. Reversing Chemoresistance by Small Molecule Inhibition of the Translation Initiation Complex EIF4F. *PNAS* **2010**, *108* (3), 1046–1051.
- (88) Boussemart, L.; Malka-Mahieu, H.; Girault, I.; Allard, D.; Hemmingsson, O.; Tomasic, G.; Thomas, M.; Basmadjian, C.; Ribeiro, N.; Thuaud, F.; Mateus, C.; Routier, E.; Kamsu-Kom, N.; Agoussi, S.; Eggermont, A. M.; Désaubry, L.; Robert, C.; Vagner, S. EIF4F Is a Nexus of Resistance to Anti-BRAF and Anti-MEK Cancer Therapies. *Nature* **2014**.
- (89) Baell, J. B.; Ferrins, L.; Falk, H.; Nikolakopoulos, G. PAINS: Relevance to Tool Compound Discovery and Fragment-Based Screening. *Aust. J. Chem.* **2013**, *66*, 1483–1494.
- (90) Mahalingam, P.; Takrouri, K.; Chen, T.; Sahoo, R.; Papadopoulos, E.; Chen, L.; Wagner, G.; Aktas, B. H.; Halperin, J. a.; Chorev, M. Synthesis of Rigidified EIF4E/EIF4G Inhibitor-1 (4EGI-1) Mimetic and Their in Vitro Characterization as Inhibitors of Protein-Protein Interaction. *J. Med. Chem.* **2014**, *57*, 5094–5111.
- (91) Yi, T.; Kabha, E.; Papadopoulos, E.; Wagner, G. 4EGI-1 Targets Breast Cancer Stem Cells by Selective Inhibition of Translation That Persists in CSC Maintenance , Proliferation and Metastasis. *Oncotarget* **2014**, *5* (15), 6028.
- (92) Papadopoulos, E.; Jenni, S.; Kabha, E.; Takrouri, K. J.; Yi, T.; Salvi, N.; Luna, R. E.; Gavathiotis, E.; Mahalingam, P.; Arthanari, H.; Rodriguez-Mias, R.; Yefidoff-Freedman, R.; Aktas, B. H.; Chorev, M.; Halperin, J. a; Wagner, G. Structure of the Eukaryotic Translation Initiation Factor EIF4E in Complex with 4EGI-1 Reveals an Allosteric Mechanism for Dissociating EIF4G. *Proc. Natl. Acad. Sci. U. S. A.* **2014**.
- (93) Baell, J. B.; Holloway, G. a. New Substructure Filters for Removal of Pan Assay Interference Compounds (PAINS) from Screening Libraries and for Their Exclusion in Bioassays. *J. Med. Chem.* **2010**, *53*, 2719–2740.
- (94) Baell, J.; Walters, M. a. Chemical Con Artists Foil Drug Discovery. *Nature* **2014**, *513*, 8–10.

- (95) Devine, S. M.; Mulcair, M. D.; Debono, C. O.; Leung, E. W. W.; Nissink, J. W. M.; Lim, S. S.; Chandrashekar, I. R.; Vazirani, M.; Mohanty, B.; Simpson, J. S.; Baell, J. B.; Scammells, P. J.; Norton, R. S.; Scanlon, M. J. Promiscuous 2-Aminothiazoles (PrATs): A Frequent Hitting Scaffold. *J. Med. Chem.* **2015**, *58*, 1205–1214.
- (96) Hoeffler, C. a; Cowansage, K. K.; Arnold, E. C.; Banko, J. L.; Moerke, N. J.; Rodriguez, R.; Schmidt, E. K.; Klosi, E.; Chorev, M.; Lloyd, R. E.; Pierre, P.; Wagner, G.; LeDoux, J. E.; Klann, E. Inhibition of the Interactions between Eukaryotic Initiation Factors 4E and 4G Impairs Long-Term Associative Memory Consolidation but Not Reconsolidation. *Proc. Natl. Acad. Sci. U. S. A.* **2011**, *108*, 3383–3388.
- (97) Gkogkas, C. G.; Khoutorsky, A.; Ran, I.; Rampakakis, E.; Nevarko, T.; Weatherill, D. B.; Vasuta, C.; Yee, S.; Truitt, M.; Dallaire, P.; Major, F.; Lasko, P.; Ruggero, D.; Nader, K.; Lacaille, J.-C.; Sonenberg, N. Autism-Related Deficits via Dysregulated EIF4E-Dependent Translational Control. *Nature* **2013**, *493* (7432), 371–377.
- (98) Santini, E.; Huynh, T. N.; MacAskill, A. F.; Carter, A. G.; Pierre, P.; Ruggero, D.; Kaphzan, H.; Klann, E. Exaggerated Translation Causes Synaptic and Behavioural Aberrations Associated with Autism. *Nature* **2013**, *493* (7432), 411–415.
- (99) Ziemniak, M.; Strenkowska, M.; Kowalska, J.; Jemielity, J. Potential Therapeutic Applications of RNA Cap Analogs. *Futur. Med. Chem.* **2013**, *5* (10), 1141–1172.
- (100) Chen, X.; Kopecky, D. J.; Mihalic, J.; Je, S.; Min, X.; Heath, J.; Deignan, J.; Lai, S.; Fu, Z.; Guimaraes, C.; Shen, S.; Li, S.; Johnstone, S.; Thibault, S.; Xu, H.; Cardozo, M.; Shen, W.; Walker, N.; Kayser, F.; Wang, Z. Structure-Guided Design, Synthesis, and Evaluation of Guanine- Derived Inhibitors of the EIF4E mRNA Cap Interaction †. **2012**.
- (101) Ghosh, B.; Benyumov, A. O.; Guosh, P.; Jia, Y.; Avdulov, S.; Dahlberg, P. S.; Peterson, M.; Smith, K.; Polunovsky, V. A.; Bitterman, P. B.; Wagner, C. R. Nontoxic Chemical Interdiction of the Epithelial-to-Mesenchymal Transition by Targeting Cap-Dependent Translation. *ACS Chem. Biol.* **2009**, *4* (5), 367–377.
- (102) Li, S.; Jia, Y.; Jacobson, B.; McCauley, J.; Kratzke, R.; Bitterman, P. B.; Wagner, C. R. Treatment of Breast and Lung Cancer Cells with a N-7 Benzyl Guanosine Monophosphate Tryptamine Phosphoramidate Pronucleotide (4Ei-1) Results in Chemosensitization to Gemcitabine and Induced EIF4E Proteasomal Degradation. *Mol. Pharm.* **2013**, *10* (2), 523–531.
- (103) Kentsis, A.; Topisirovic, I.; Culjkovic, B.; Shao, L.; Borden, K. L. B. Ribavirin Suppresses EIF4E-Mediated Oncogenic Transformation by Physical Mimicry of the 7-Methyl Guanosine mRNA Cap. *Proc. Natl. Acad. Sci. U. S. A.* **2004**, *101* (52), 18105–18110.
- (104) Yan, Y.; Svitkin, Y.; Lee, J. M.; Bisailon, M.; Pelletier, J. Ribavirin Is Not a Functional Mimic of the 7-Methyl Guanosine mRNA Cap. *RNA* **2005**, *11* (8), 1238–1244.
- (105) Chang, S.-H.; Kim, J.-E.; Lee, J.-H.; Minai-Tehrani, a; Han, K.; Chae, C.; Cho, Y.-H.; Yun, J.-H.; Park, K.; Kim, Y.-S.; Cho, M.-H. Aerosol Delivery of Eukaryotic Translation Initiation Factor 4E-Binding Protein 1 Effectively Suppresses Lung



- Tumorigenesis in K-Ras(LA1) Mice. *Cancer Gene Ther.* **2013**, *20* (6), 331–335.
- (106) Herbert, T. P.; Fåhraeus, R.; Prescott, A.; Lane, D. P.; Proud, C. G. Rapid Induction of Apoptosis Mediated by Peptides That Bind Initiation Factor EIF4E. *Curr. Biol.* **2000**, *10*, 793–796.
- (107) Ko, S. Y.; Guo, H.; Barengo, N.; Naora, H. Inhibition of Ovarian Cancer Growth by a Tumor-Targeting Peptide That Binds Eukaryotic Translation Initiation Factor 4E. *Clin. Cancer Res.* **2009**, *15* (13), 4336–4347.
- (108) Masse, M.; Glippa, V.; Saad, H.; Le Bloas, R.; Gauffeny, I.; Berthou, C.; Czjzek, M.; Cormier, P.; Cosson, B. An EIF4E-Interacting Peptide Induces Cell Death in Cancer Cell Lines. *Cell Death Dis.* **2014**, *5* (10), e1500.
- (109) Brown, C. J.; Lim, J. J.; Leonard, T.; Lim, H. C. a; Chia, C. S. B.; Verma, C. S.; Lane, D. P. Stabilizing the EIF4G1  $\alpha$ -Helix Increases Its Binding Affinity with EIF4E: Implications for Peptidomimetic Design Strategies. *J. Mol. Biol.* **2011**, *405* (3), 736–753.
- (110) Zhou, W.; Quah, S. T.; Verma, C. S.; Liu, Y.; Lane, D. P.; Brown, C. J. Improved EIF4E Binding Peptides by Phage Display Guided Design: Plasticity of Interacting Surfaces Yield Collective Effects. *PLoS One* **2012**, *7* (10), e47235.
- (111) Anfinsen, C. B. Principles That Govern the Folding of Protein Chains. *Science* (80-. ). **1973**, *181* (4096), 223–230.
- (112) Dishman, A. F.; Volkman, B. F. Unfolding the Mysteries of Protein Metamorphosis. *ACS Chem. Biol.* **2018**, *13*, 1438–1446.
- (113) Henzler-wildman, K.; Kern, D. Dynamic Personalities of Proteins. *Nature* **2007**, *450*, 7–9.
- (114) Csizmok, V.; Follis, A.; Kriwacki, R.; Forman-Kay, J. Dynamic Protein Interaction Networks and New Structural Paradigms in Signaling. *Chem. Rev.* **2016**, *116*, 6424–6462.
- (115) Wright, P.; Dyson, H. Intrinsically Disordered Proteins in Cellular Signaling and Regulation. *Nat Rev Mol Cell Biol* **2015**, *16*, 18–29.
- (116) Ward, J. J.; Sodhi, J. S.; MCGuffin, L. J.; Buxton, B. F.; Jones, D. T. Prediction and Functional Analysis of Native Disorder in Proteins from the Three Kingdoms of Life. **2004**, 635–645.
- (117) Dyson, H. J.; Wright, P. E.; Pines, N. T. INTRINSICALLY UNSTRUCTURED PROTEINS AND THEIR FUNCTIONS. *Nat. Rev. Mol. Cell Biol.* **2005**, *6*, 197–208.
- (118) Marsh, J. A.; Teichmann, S. A.; Forman-kay, J. D. Probing the Diverse Landscape of Protein Flexibility and Binding. *Curr. Opin. Struct. Biol.* **2012**, *22*, 643–650.
- (119) Mittag, T.; Forman-kay, J. D. Atomic-Level Characterization of Disordered Protein Ensembles. *Curr. Opin. Struct. Biol.* **2007**, *17*, 3–14.
- (120) Berlow, R. B.; Dyson, H. J.; Wright, P. E. Expanding the Paradigm: Intrinsically Disordered Proteins and Allosteric Regulation. *J. Mol. Biol.* **2018**, *Ahead of P.*
- (121) Berlow, R.; Dyson, H.; Wright, P. Functional Advantages of Dynamic Protein Disorder. *FEBS* **2015**, *589*, 2433–2440.
- (122) van der Lee, R.; Buljan, M.; Lang, B.; Weatheritt, R.; Daughdrill, G.; Dunker, A. Classification of Intrinsically Disordered Regions and Proteins. *Chem. Rev.* **2014**, *114*, 6589–6631.
- (123) Dunker, A. K.; Bondos, S. E.; Huang, F.; Oldfield, C. J. Intrinsically Disordered

- Proteins and Multicellular Organisms. *Semin. Cell Dev. Biol.* **2015**, *37*, 44–55.
- (124) Haynes, C.; Oldfield, C.; Ji, F.; Klitgord, N.; Cusick, M.; Radivojic, P. Intrinsic Disorder Is a Common Feature of Hub Proteins from Four Eukaryotic Interactomes. *PLoS Comput. Biol.* **2006**, *2*, 100.
- (125) Dosztanyi, Z.; Chen, J.; Dunker, A.; Simon, I.; Tompa, P. Disorder and Sequence Repeats in Hub Proteins and Their Implications for Network Evolution. *J Proteome Res.* **2006**, *5*, 2985–2995.
- (126) Saglam, A. S.; Wang, D. W.; Zwier, M. C.; Chong, L. T. Flexibility vs Preorganization: Direct Comparison of Binding Kinetics for a Disordered Peptide and Its Exact Preorganized Analogues. *J. Phys. Chem.* **2017**, *121*, 10046–10054.
- (127) Shoemaker, B. A.; Portman, J. J.; Wolynes, P. G. Speeding Molecular Recognition by Using the Folding Funnel: The Fly-Casting Mechanism. *Proc. Natl. Acad. Sci., U. S. A.* **2000**, *97*, 8868–8873.
- (128) Dyson, H.; Wright, P. Coupling of Folding and Binding for Unstructured Proteins. *Curr. Opin. Struct. Biol.* **2002**, *12*, 54–60.
- (129) Kiefhaber, T.; Bachmann, A.; Jensen, K. S. Dynamics and Mechanisms of Coupled Protein Folding and Binding Reactions. *Curr. Opin. Struct. Biol.* **2012**, *22*, 21–29.
- (130) Mollica, L.; Bessa, L. M.; Hanouille, X.; Jensen, M. R.; Blackledge, M.; Schneider, R. Binding Mechanisms of Intrinsically Disordered Proteins : Theory , Simulation , and Experiment. *Front. Mol. Biosci.* **2016**, *3*, 1–18.
- (131) Gianni, S.; Dogan, J.; Jemth, P. Coupled Binding and Folding of Intrinsically Disordered Proteins : What Can We Learn from Kinetics ? *Curr. Opin. Struct. Biol.* **2016**, *36*, 18–24.
- (132) Pang, X.; Zhou, H. Disorder-to-Order Transition of an Active-Site Loop Mediates the Allosteric Activation of Sortase A. *Biophys. J* **2015**, *109*, 1706–1715.
- (133) Tompa, P.; Fuxreiter, M. Fuzzy Complexes: Polymorphism and Structural Disorder in Protein-Protein Interactions. *Trends Biochem. Sci.* **2008**, *33*, 2–8.
- (134) Zhou, H.; Pang, X.; Lu, C. Rate Constants and Mechanisms of Intrinsically Disordered Proteins Binding to Structured Targets. *Phys. Chem. Chem. Phys.* **2012**, *14*, 10466–10476.
- (135) Iešmantavičius, V.; Dogan, J.; Jemth, P.; Teilum, K.; Kjaergaard, M. Helical Propensity in an Intrinsically Disordered Protein Accelerates Ligand Binding. *Angew. Chem. Int. Ed. Engl.* **2014**, *53* (6), 1548–1551.
- (136) Dogan, J.; Jemth, P. Only Kinetics Can Prove Conformational Selection. *Biophys. J.* **2014**, *107*, 1997–1998.
- (137) Gibbs, E. B.; Showalter, S. A. Quantitative Biophysical Characterization of Intrinsically Disordered Proteins. *Biochemistry* **2015**, *54*, 1314–1326.
- (138) Olson, S. T.; Srinivasan, K. R.; Bjork, I.; Shore, J. D. Binding of High Affinity Heparin to Antithrombin III - Stopped Flow Kinetic Studies of the Binding Interaction. *J. Biol. Chem.* **1981**, *256*, 11073–11079.
- (139) Rogers, J. M.; Steward, A.; Clarke, J. Folding and Binding of an Intrinsically Disordered Protein: Fast, but Not 'Diffusion-Limited.' *J. Am. Chem. Soc.* **2013**, *135*, 1415–1422.
- (140) Rangel, L.; Costa, D.; Vieira, T.; Silva, J. The Aggregation of Mutant P53 Produces Prion-Like Properties in Cancer. *Prion* **2014**, *8*, 75–84.

- (141) Iakoucheva, L.; Brown, C.; Lawson, J.; Obradovic, Z.; Dunker, A. Intrinsic Disorder in Cell-Signaling and Cancer-Associated Proteins. *J Mol Biol.* **2002**, *323*, 573–584.
- (142) Li, Y.; King, O.; Shorter, J.; Gitler, A. Stress Granules as Crucibles of ALS Pathogenesis. *J. Cell Biol.* **2013**, *201*, 361–372.
- (143) Tsafou, K.; Tiwari, P. B.; Metallo, S. J.; Toretsky, J. A. Targeting Intrinsically Disordered Transcription Factors : Changing the Paradigm. *J. Mol. Biol.* **2018**, *430* (16), 2321–2341.
- (144) Dunker, A. K.; Uversky, V. N. Drugs for ‘ Protein Clouds ’: Targeting Intrinsically Disordered Transcription Factors. *Curr. Opin. Pharmacol.* **2010**, *10* (6), 782–788.
- (145) Mol, E. De; Fenwick, R. B.; Phang, C. T. W.; Buzo, V.; Szulc, E.; Fuente, A. De; Escobedo, A.; Bertocini, C. W.; Este, E. EPI-001, A Compound Active against Castration-Resistant Prostate Cancer, Targets Transactivation Unit 5 of the Androgen Receptor. *ACS Chem. Biol.* **2016**, *11*, 2499–2505.
- (146) Vassilev, L. T.; Vu, B. T.; Graves, B.; Carvajal, D.; Podlaski, F.; Filipovic, Z.; Klein, C.; Fotouhi, N.; Liu, E. A. In Vivo Activation of the P53 Pathway by Small-Molecule Antagonists of MDM2. *Science (80-. )*. **2004**, *303*, 844–849.
- (147) Follis, A. V.; Hammoudeh, D. I.; Wang, H.; Prochownik, E. V.; Metallo, S. J. Structural Rationale for the Coupled Binding and Unfolding of the C-Myc Oncoprotein by Small Molecules. *Chem. Biol. Br. Commun.* **2008**, *15*, 1149–1155.
- (148) Ben-shimon, A.; Niv, M. Y.; Ben-shimon, A.; Niv, M. Y. AnchorDock : Blind and Flexible Anchor-Driven Peptide Docking Resource AnchorDock : Blind and Flexible Anchor-Driven Peptide Docking. *Structure* **2015**, *23*, 929–940.
- (149) Uversky, V. N. Unreported Intrinsic Disorder in Proteins: Building Connections to the Literature on IDPs. *Intrinsically Disord. Proteins* **2014**, *2* (1), 1–42.
- (150) Lukhele, S.; Bah, A.; Lin, H.; Sonenberg, N.; Forman-Kay, J. D. Interaction of the Eukaryotic Initiation Factor 4E with 4E-BP2 at a Dynamic Bipartite Interface. *Structure* **2013**, *21*, 2186–2196.
- (151) Uversky, V. N. The Multifaceted Roles of Intrinsic Disorder in Protein Complexes. *FEBS Lett.* **2015**, *589*, 2498–2506.
- (152) Tait, S.; Dutta, K.; Cowburn, D.; Warwicker, J.; Doig, A. J.; McCarthy, J. E. G. Local Control of a Disorder-Order Transition in 4E-BP1 Underpins Regulation of Translation via EIF4E. *Proc. Natl. Acad. Sci. U. S. A.* **2010**, *107* (41), 17627–17632.
- (153) Bah, A.; Vernon, R. M.; Siddiqui, Z.; Krzeminski, M.; Mhuandiram, R.; Zhao, C.; Sonenberg, N.; Kay, L. E.; Forman-Kay, J. D. Folding of an Intrinsically Disordered Protein by Phosphorylation as a Regulatory Switch. *Nature* **2015**, *519*, 106–109.
- (154) Gruner, S.; Peter, D.; Weber, R.; Wohlbold, L.; Chung, M.-Y.; Weichenrieder, O.; Valkov, E.; Igreja, C.; Izaurralde, E. The Structures of EIF4E-EIF4G Complexes Reveal an Extended Interface to Regulate Translation Initiation. *Mol. Cell* **2016**, *64*, 467–479.
- (155) Fletcher, C. M.; McGuire, A. M.; Gingras, A.; Li, H.; Matsuo, H.; Sonenberg, N.; Wagner, G. 4E Binding Proteins Inhibit the Translation Factor EIF4E without Folded Structure. *Biochemistry* **1998**, *37*, 9–15.
- (156) Abiko, F.; Tomoo, K.; Mizuno, A.; Morino, S.; Imataka, H.; Ishida, T. Binding

- Preference of EIF4E for 4E-Binding Protein Isoform and Function of EIF4E N-Terminal Flexible Region for Interaction, Studied by SPR Analysis. *Biochem. Biophys. Res. Commun.* **2007**, *355*, 667–672.
- (157) Igreja, C.; Peter, D.; Weiler, C.; Izaurrealde, E. 4E-BPs Require Non-Canonical 4E-Binding Motifs and a Lateral Surface of EIF4E to Repress Translation. *Nat. Commun.* **2014**, *5*, 1–14.
- (158) Kedersha, N.; Stoecklin, G.; Ayodele, M.; Yacono, P.; Lykke-andersen, J.; Fritzler, M. J.; Scheuner, D.; Kaufman, R. J.; Golan, D. E.; Anderson, P. Stress Granules and Processing Bodies Are Dynamically Linked Sites of MRNP Remodeling. *J. Cell Biol.* **2005**, *169* (6), 871–884.
- (159) Haney, C. M.; Horne, W. S. Receptor-Templated Stapling of Intrinsically Disordered Peptide Ligands. *Org. Biomol. Chem.* **2015**, *13*, 4183–4189.
- (160) Edery, I.; Altmann, M.; Sonenberg, N. High-Level Synthesis in Escherichia Coli of Functional Cap-Binding Eukaryotic Initiation Factor EIF-4E and Affinity Purification Using a Simplified Cap-Analog Resin. *Gene* **1988**, *74*, 517–525.
- (161) Muñoz, V.; Serrano, L. Analysis of  $i$ ,  $i + 5$  and  $i$ ,  $i + 8$  Hydrophobic Interactions in a Helical Model Peptide Bearing the Hydrophobic Staple Motif. *Biochemistry* **1995**, *34*, 15301–15306.
- (162) Aumelas, A.; Chiche, L.; Kubo, S.; Chino, N.; Watanabe, T. X.; Kobayashi, Y. The Chimeric Peptide [Lys(-2)-Arg(-1)]-Sarafotoxin-S6b, Composed of the Endothelin pro-Sequence and Sarafotoxin, Retains the Salt-Bridge Staple between Arg(-1) and Asp8 Previously Observed in [Lys(-2)-Arg(-1)]-Endothelin. *Eur. J. Biochem.* **1999**, *266*, 977–985.
- (163) Scholtz, M. J.; Qian, H.; Robbins, V. H.; Baldwin, R. L. The Energetics of Ion-Pair and Hydrogen-Bonding Interactions In. *Biochemistry* **1993**, *32*, 9668–9676.
- (164) Forood, B.; Reddy, H. K.; Nambiar, K. P. Extraordinary Helicity in Short Peptides via End Capping Design. *J. Am. Chem. Soc.* **1994**, No. 116, 6935–6936.
- (165) Zhou, H. X.; Lyu, P. C.; Wemmer, D. E.; Kallenbach, N. R. Structure of a C-Terminal  $\alpha$ -Helix Cap in a Synthetic Peptide. *J. Am. Chem. Soc.* **1994**, *116*, 1139–1140.
- (166) Albert, J. S.; Hamilton, A. D. Stabilization of Helical Domains in Short Peptides Using Hydrophobic Interactions. *Biochemistry* **1995**, *34*, 984–990.
- (167) Phelan, J. C.; Skelton, N. J.; Braisted, A. C.; McDowell, R. S. A General Method for Constraining Short Peptides to an A-Helical Conformation. *J. Am. Chem. Soc.* **1997**, *119* (3), 455–460.
- (168) Jackson, D. Y.; King, D. S.; Chmielewski, J.; Singh, S.; Schultz, P. G. General Approach to the Synthesis of Short A-Helical Peptides. *J. Am. Chem. Soc.* **1991**, *113*, 9391–9392.
- (169) Blackwell, H. E.; Grubbs, R. H. Highly Efficient Synthesis of Covalently Cross-Linked Peptide Helices by Ring-Closing Metathesis. *Angew. Chemie - Int. Ed.* **1998**, *37* (23), 3281–3284.
- (170) Schafmeister, C. E.; Po, J.; Verdine, G. L. An All-Hydrocarbon Cross-Linking System for Enhancing the Helicity and Metabolic Stability of Peptides. *J. Am. Chem. Soc.* **2000**, *122*, 5891–5892.
- (171) Stewart, M. L.; Fire, E.; Keating, A. E.; Walensky, L. D. The MCL-1 BH3 Helix Is an Exclusive MCL-1 Inhibitor and Apoptosis Sensitizer. *Nat. Chem. Biol.* **2010**, *6*

- (8), 595–601.
- (172) Walensky, L. D.; Kung, A. L.; Escher, I.; Malia, T. J.; Barbuto, S.; Wright, R. D.; Wagner, G.; Verdine, G. L.; Korsmeyer, S. J. Activation of Apoptosis in Vivo by a Hydrocarbon-Stapled BH3 Helix. *Science* **2004**, *305*, 1466–1470.
- (173) Bird, G. H.; Mazzola, E.; Opoku-nsiah, K.; Lammert, M. A.; Godes, M.; Neuberg, D. S.; Walensky, L. D. Biophysical Determinants for Cellular Uptake of Hydrocarbon-Stapled Peptide Helices. *Nat. Chem. Biol.* **2016**, *12*, 845–852.
- (174) Chu, Q.; Moellering, R. E.; Hilinski, G. J.; Kim, Y.-W.; Grossmann, T. N.; Yeh, J. T.-H.; Verdine, G. L. Towards Understanding Cell Penetration by Stapled Peptides. *Med. Chem. Commun.* **2015**, *6* (1), 111–119.
- (175) Walensky, L. D.; Bird, G. H. Hydrocarbon-Stapled Peptides: Principles, Practice, and Progress. *J. Med. Chem.* **2014**, *57*, 6275–6288.
- (176) Okamoto, T.; Zobel, K.; Fedorova, A.; Quan, C.; Yang, H.; Fairbrother, W. J.; Huang, D. C. S.; Smith, B. J.; Deshayes, K.; Czabotar, P. E. Stabilizing the Pro-Apoptotic BimBH3 Helix (BimSAHB) Does Not Necessarily Enhance Affinity or Biological Activity. *ACS Chem. Biol.* **2013**, *8* (2), 297–302.
- (177) Bernal, F.; Tyler, A. F.; Korsmeyer, S. J.; Walensky, L. D.; Verdine, G. L. Reactivation of the P53 Tumor Suppressor Pathway by a Stapled P53 Peptide. *J. Am. Chem. Soc. Commun.* **2007**, *129*, 2456–2457.
- (178) Felix, A. M.; Heimer, E. P.; Wang, C.; Lambros, T. J.; Fournier, A.; Mowles, T. F.; Maines, S.; Campbell, R. M.; Wegrzynski, B. B.; Toome, V.; Fry, D.; Madison, V. S. Synthesis, Biological Activity and Conformational Analysis of Cyclic GRF Analogs. *Int. J. Pept. Protein Res.* **1988**, *32*, 441–454.
- (179) Shepherd, N. E.; Hoang, H. N.; Abbenante, G.; Fairlie, D. P. Single Turn Peptide Alpha Helices with Exceptional Stability in Water. *J. Am. Chem. Soc.* **2005**, *127*, 2974–2983.
- (180) Lau, Y. H.; de Andrade, P.; Wu, Y.; Spring, D. R. Peptide Stapling Techniques Based on Different Macrocyclisation Chemistries. *Chem. Soc. Rev.* **2015**, *44*, 91–102.
- (181) Ko, S. Y.; Guo, H.; Barengo, N.; Naora, H. Inhibition of Ovarian Cancer Growth by a Tumor-Targeting Peptide That Binds Eukaryotic Translation Initiation Factor 4E. *Cancer Ther. Preclin.* **2009**, *15* (13), 4336–4348.
- (182) Gradi, A.; Imataka, H.; Svitkin, Y. V.; Rom, E.; Raught, B.; Morino, S.; Sonenberg, N.; Zions, N. A Novel Functional Human Eukaryotic Translation Initiation Factor 4G. *Mol. Cell. Biol.* **1998**, *18* (1), 334–342.
- (183) Peraro, L.; Deprey, K. L.; Moser, M. K.; Zou, Z.; Ball, H. L.; Levine, B.; Kritzer, J. A. Cell Penetration Profiling Using the Chloroalkane Penetration Assay. *J. Am. Chem. Soc.* **2018**, *140*, 11360–11369.
- (184) Klein, M. J.; Schmidt, S.; Wadhvani, P.; Bu, J.; Reichert, J.; Afonin, S.; Berditsch, M.; Schober, T.; Brock, R.; Kansy, M.; Ulrich, A. S. Lactam-Stapled Cell-Penetrating Peptides: Cell Uptake and Membrane Binding Properties. *J. Med. Chem.* **2017**, *60*, 8071–8082.
- (185) Keeling, K. L.; Cho, O.; Scanlon, D. B.; Booker, G. W.; Abell, A. D.; Wegener, K. L. The Key Position: Influence of Staple Location on Constrained Peptide Conformation and Binding. *Org. Biomol. Chem.* **2016**, *14*, 9731–9735.

- (186) De Araujo, A. D.; Hoang, H. N.; Kok, W. M.; Diness, F.; Gupta, P.; Hill, T. A.; Driver, R. W.; Price, D. A.; Liras, S.; Fairlie, D. P.; de Araujo, A. D.; Hoang, H. N.; Kok, W. M.; Diness, F.; Gupta, P.; Hill, T. A.; Driver, R. W.; Price, D. A.; Liras, S.; Fairlie, D. P. Comparative  $\alpha$ -Helicity of Cyclic Pentapeptides in Water. *Angew. Chemie Int. Ed.* **2014**, *53* (27), 6965–6969.
- (187) Houston, M. E.; Gannon, C. L.; Kay, C. M.; Hodges, R. S. Lactam Bridge Stabilization of  $\alpha$ -Helical Peptides : Ring Size , Orientation and Positional Effects. *J. Pept. Sci.* **1995**, *1*, 274–282.
- (188) Hedstrom, L.; Szilagyi, L.; Rutter, W. J. Converting Trypsin to Chymotrypsin : The Role of Surface Loops Author ( s ): Lizbeth Hedstrom , Laszlo Szilagyi and William J . Rutter Published by : American Association for the Advancement of Science Stable URL : <https://www.jstor.org/stable/2876543> Dig. *Science* (80-. ). **1992**, *255* (5049), 1249–1253.
- (189) Carone, F. A.; Peterson, D. R. Hydrolysis and Transport of Small Peptides by the Proximal Tubule. *Am. J. Physiol.* **1980**, *238* (3), F151–F158.
- (190) Katsila, T.; Siskos, A. P.; Tamvakopoulos, C. PEPTIDE AND PROTEIN DRUGS : THE STUDY OF THEIR METABOLISM AND CATABOLISM BY MASS SPECTROMETRY. *Mass Spectrom. Rev.* **2012**, *31*, 110–133.
- (191) Bottger, R.; Hoffmann, R.; Knappe, D. Differential Stability of Therapeutic Peptides with Different Proteolytic Cleavage Sites in Blood , Plasma and Serum. *PLoS One* **2017**, *12* (6), 1–15.